Terrestrial Carbon-isotope Stratigraphy: an Exploration of the Method from Miocene and Jurassic Examples

Linhao Fang

St Peter's College

University of Oxford

Submitted for the degree of Doctor of Philosophy

in the Department of Earth Sciences, University of Oxford

Michaelmas Term 2013

Terrestrial Carbon-isotope Stratigraphy:
an Exploration of the Method from Miocene and Jurassic Examples

D.Phil Thesis **Linhao Fang**

Michaelmas Term 2013 **St Peter's College**

Abstract

Terrestrial carbon-isotope stratigraphy has proven a promising tool for stratigraphic correlation between the different exchangeable carbon-isotope reservoirs, as well as a powerful approach to reconstructing the evolution of $\delta^{13}C$ of atmospheric CO_2, which is closely associated with the evolution of palaeoenvironment and palaeoclimate. However, the limited understanding of pitfalls in specific application potentially restricts the method's utility for stratigraphic correlation and palaeoenvironmental reconstruction. This thesis takes advantage of three case studies at two vital geological intervals which are both characterized by the significant carbon-isotope perturbation in the exchangeable reservoirs, to explore the nature of terrestrial carbon-isotope stratigraphy.

Two of the case studies focus on the late Early to Middle Miocene, the period of the so called Monterey Event that is marked by remarkable positive carbon-isotope excursions in benthic and pelagic marine carbonate records. There are few terrestrial carbon-isotope records for the Monterey Event. In the present study, shallow marine sediments were collected from boreholes in the New Jersey margin, USA (IODP, Expedition 313) and North Sea Basin, Denmark. Phytoclasts are concentrated from palynological residues as the basis for a terrestrial carbon-isotope stratigraphy from the two locations. The carbon-isotope curves obtained can be correlated in detail locally, and correlated crudely on a global scale. However, there are no definite positive carbon-isotope excursions observed in the terrestrial isotopic stratigraphic records through the biostratigraphically determined Langhian interval equivalent to the Monterey Event. The reasons for the absence of relatively positive carbon-isotope excursions in terrestrial carbon-isotope stratigraphy might be caused by the reworking deposits of woody phytoclasts from older strata or some other process related to reworking.

Another case study centres on the Triassic-Jurassic boundary and Early Jurassic fluvial and lacustrine succession in the Kuqa section, Tarim Basin, NW China. Macrofossil wood samples were collected to generate the terrestrial carbon-isotope stratigraphy. On the basis of the biostratigraphy and potential Stage/Age (sub-) boundaries implied by biological overturns, the terrestrial carbon-isotope stratigraphy in the Kuqa section can be well correlated with both terrestrial and marine carbon-isotope stratigraphic records from UK through the Early Jurassic. For the Triassic-Jurassic boundary, more precise correlation was made globally and an exact the position of Triassic-Jurassic boundary is proposed in the Kuqa section. In light of the biostratigraphy and the carbon-isotope stratigraphy obtained in the present study, an updated age assignment of the lithostratigraphic units is proposed to Age/Stage level in the Early Jurassic across the Northern Tarim Basin. The carbon-isotope stratigraphy thus significantly improves the terrestrial stratigraphic resolution.

Terrestrial carbon-isotope stratigraphy is a powerful tool for global stratigraphic correlation and unifies stratigraphic correlation over marine and non-marine strata in cases when potential biasing factors are excluded.

Terrestrial Carbon-isotope Stratigraphy:

an Exploration of the Method from Miocene and Jurassic Examples

D.Phil Thesis **Linhao Fang**

Michaelmas Term 2013 **St Peter's College**

Extended Abstract

The emergence and development of carbon-isotope stratigraphy is reviewed and the general historical lines of advancement in carbon-isotope stratigraphy described. After the fundamental basis of global correlation was confirmed by many empirical records derived from the inorganic marine reservoirs, the application of terrestrial carbon-isotope stratigraphy became possible, allowing a novel approach to establishing links between marine and non-marine time-equivalent strata. This integrated understanding of global carbon-isotope reservoirs is also significantly useful to reconstruct the $\delta^{13}C$ fluctuation of atmospheric CO_2, which is closely associated with the evolution of palaeoenvironment and palaeoclimate.

The primary aim of this thesis is to explore the strengths and weaknesses in specific application of terrestrial carbon-isotope stratigraphy and thus improve the practical utility in the stratigraphic correlation and palaeoenvironmental reconstruction. Three case studies were undertaken for two different geological ages, the late Early to Middle Miocene, and the Triassic-Jurassic boundary to the Early Jurassic, which are both characterized by the significant carbon-isotope perturbation of the exchangeable reservoirs.

The marine carbon-isotope stratigraphy during the late Early to Middle Miocene is marked by remarkable relatively positive carbon-isotope excursions, which have been unambiguously documented by foraminiferal carbonate in numerous oceanic settings. These records suggest a carbon-isotope fluctuation in the whole marine reservoirs and thus were inferred to represent changes in the atmospheric carbon-isotope reservoir that should also be evidenced by terrestrial carbon-isotope stratigraphic signals. However, very few terrestrial carbon-isotope stratigraphic records for the carbon-isotope fluctuation during the Monterey Event are reported. In the present thesis, the siliciclastic shallow marine sediments collected from boreholes in the New Jersey margin, USA (IODP Expedition 313) and North Sea Basin, Denmark are intensively investigated.

Through density separation applied to the raw woody palynological residues, phytoclasts were concentrated and separated from the mixed terrestrial and/or marine organic matter such as pollen, spores, dinoncysts and algae. Hand-picked individual woody phytoclasts were also obtained to generate the carbon-isotope stratigraphic data in high confidence. Coherent stratigraphic trends and

short-term isotopic excursions are observed consistently in palynological preparation residues, concentrated woody phytoclasts, and individually picked woody phytoclasts obtained from the New Jersey sediments. A bulk organic matter carbon-isotope curve shows somewhat different stratigraphic trends but, when corrected for mixing of marine-terrestrial components on the basis of measured C/N ratios, a high degree of conformity with the woody phytoclast record is observed. However, assuming that the correlations based on strontium-isotope values and biostratigraphy are correct, the carbon-isotope record from the New Jersey margin contrasts with that previously documented from oceanic settings (i.e. lack of positive excursion of carbon-isotope values in terrestrial organic matter through the Langhian Stage). Factors that may potentially bias local terrestrial carbon-isotope records include reworking from older deposits, degradation and diagenesis, as well as environmental factors affecting vegetation in the sediment source areas. These possible factors are assessed on the basis of pyrolysis data, SEM observations, and comparison to palynological indices of environmental change. Some evidence is found for localised degradation and/or reworking of older woody phytoclasts, but where such processes have occurred they do not readily explain the observed carbon-isotope values. It is concluded that the overall carbon-isotope signature for the exchangeable carbon reservoir is distorted, to the extent that the Monterey Event excursion is not easily identifiable. The most likely explanation is that phytoclast reworking has occurred in clinoform toe-of-slope facies, but the reason for the resulting relatively heavy carbon-isotope values produced remains obscure.

For the shallow marine sediments in the North Sea Basin, Denmark, the carbon-isotope stratigraphic data were generated both from the concentrated phytoclasts and the raw palynological residues. The potential influence of diagenetic alteration and of changes in ecosystem were examined and largely excluded. A carbon-isotope stratigraphy was obtained and consistent carbon-isotope stratigraphic trends were presented between two local boreholes on the basis of composite age control, including biostratigraphy, sequence stratigraphy and the strontium-isotope stratigraphy. The carbon-isotope stratigraphic records from New Jersey, USA and North Sea Basin, Denmark can be broadly correlated on the basis of biostratigraphy through the late Early to Middle Miocene. However, there are no definite relative positive carbon-isotope excursions observed through the biostratigraphically identified Langhian interval equivalent to the Monterey Event at either location. The precise reasons for the absence of relatively heavy carbon-isotope excursions during the Monterey Event in terrestrial carbon-isotope stratigraphic records in the two specific case studies remain obscure. According the data from these two case studies, a notable phenomenon of glauconite occurrence and associated abnormally heavy carbon-isotope values was consistently observed in both locations. The relatively low sedimentation rate (~26 to 33 mm/Kyr during the Aquitanian interval on the New Jersey margin and ~4 to 5 mm/Kyr during the Serravallian interval in the North Sea Basin, assuming no hiatus in the calibrated intervals) is closely related with the glauconite occurrence, both in the New Jersey and North Sea Basin records, and the intervals at such low sedimentation rate show the abnormally heavy carbon-isotope signals. The reworking of woody phytoclasts from older strata might account for the

abnormal carbon-isotope values, but this interpretation needs further verification and identification of the precise mechanism that leads to concentration of the phytoclasts with heavy values.

The third case study focused on the Triassic-Jurassic boundary and Early Jurassic fluvial and lacustrine sediments in the Kuqa section, Tarim Basin, NW China. The terrestrial carbon-isotope stratigraphic records are generated primarily on basis of macrofossil wood. The macrofossil wood samples were largely collected from alluvial conglomerate, associated braided-fluvial sandstone and siltstone. The samples comprising bulk organic matter were collected from coal seams, organic-rich mudstone and the laminated shales as supplements. All the available literature about the biostratigraphy and lithostratigraphy around the Kuqa section, N Tarim Basin and other relevant regions are reviewed. In light of the previous results, the present study combines newly compiled biostratigraphy and newly generated carbon-isotope stratigraphy. On the basis of the biostratigraphic age control and the potential Stage/Age (sub-) boundaries implied by biological overturns, the terrestrial carbon-isotope stratigraphy in the Kuqa section, N Tarim Basin can be coherently correlated with the carbon-isotope stratigraphic records based on the fossil wood in England, and also well correlated with the marine carbon-isotope records on the biological carbonates in mostly UK sections through the Early Jurassic. On the basis of the newly updated biostratigraphy and the carbon-isotope stratigraphy obtained in the present studies, an updated age assignment for the lithostratigraphic units in the Kuqa section is proposed. It is the first time that the lithostratigraphic division can be broken down into the Age/Stage level for the Early Jurassic across the Tarim Basin. The new age assignment identifies the Yangxia Fm as more than 10 Myr older than previously recognised. The ages for other formation involved in this study at the Kuqa section are updated as well, and the carbon-isotope stratigraphy thus significantly improves the resolution of stratigraphic correlations. Of course, it is likely that on a broad scale the formation will be diachronous. Further work could focus on this possibility.

For the Triassic-Jurassic boundary, more intensive and extensive carbon-isotope stratigraphic correlation is made between the Kuqa section and other various locations worldwide. The positive and negative carbon-isotope excursions at the Kuqa section through the Triassic-Jurassic boundary could be also found at those other nearly synchronous strata across the world. The accurate correlation among these positive and negative shifts around the Triassic-Jurassic boundary is attempted, although the biostratigraphic resolution is not sufficient to strongly support this correlation. An exact position of the Triassic-Jurassic boundary is discussed and suggested on the basis of the new results. A bed with the character of soft-sediment deformation and its occurrence at the Triassic–Jurassic boundary recalls the similar phenomena in NW Europe, where the strata are marked by the uniquely widespread (across > 250,000 km^2 in the shallow marginal marine strata in UK) seismites inferred by some authors as the evidence for bolide impacts.

The success of the stratigraphic correlation in these three case studies verifies that terrestrial carbon-isotope stratigraphy is a powerful tool for stratigraphic correlation in the local ranges, over a long distance, and particularly useful as a bridge to link marine and non-marine strata. However, caution needs to be exercised when the method is used in settings characterised by prolonged marine reworking, such as those containing abundant glauconite.

An extra method of carbon-isotope stratigraphy based on terrestrial-derived biomarkers has also been tried, but due to the availability of instruments and the contamination of samples, the experimental data were not useful. A theoretical discussion has been completed and included as one of the appendixes. The mechanism by which the individual biomarkers in high molecular weight can faithfully maintain the original carbon-isotope signals registered during plants' growth, regardless of the degree of degradation by bacteria, or other chemical or physical processes during diagenesis, is also described in Appendix A.

Preface

The research described in this thesis was carried out by the author in the Department of Earth Sciences at the University of Oxford between October 2009 and November 2013, under the supervision of Professor Stephen Hesselbo. No part of this thesis has been submitted or accepted for any other degree at this university or elsewhere.

Parts of this work have been published in peer reviewed papers and presented at international conferences as follows:

Scientific peer-reviewed papers and supplements

Fang, L., C. J. Bjerrum, S. P. Hesselbo*, U. Kotthoff, F. M. G. McCarthy, B. Huang, and P. W. Ditchfield (2013), Carbon-isotope stratigraphy from terrestrial organic matter through the Monterey event, Miocene, New Jersey margin (IODP Expedition 313), Geosphere, 9(5), 1303-1318, DOI 10.1130/ges00851.1.

Conference abstract

Fang L., Hesselbo SP., 2011. Atmospheric carbon-isotope fluctuations in the Early-Middle Miocene: evidence from terrestrial organic matter, New Jersey shallow shelf, USA (IODP Expedition 313), University of Southampton OCS, American Association of Stratigraphic Palynologists(AASP), Southampton (Conference abstract)

Fang L., Hesselbo SP., Deng Shenghui, 2010. Terrestrial carbon-isotope stratigraphy of the Triassic-Jurassic Boundary and Early/Middle Jurassic from Tarim Basin in Xinjiang, NW China: initial results. Earth Science Frontiers, vol. 17: 10 (Conference abstract)

Acknowledgements

This thesis would not have been possible without the support and encouragement from numerous individuals and various organizations over the past four years.

First, and foremost, I would like to thank my supervisor Professor Stephen Hesselbo, late-stage co-supervisor Dr. Stuart Robinson, and external advisor Dr. Shenghui Deng for all the help and support they have given. I am deeply indebted to Stephen for the scientific discussions, numerous corrections and guidance at all the stages over the four years, and to Shenghui helped with the sampling in the Kuqa section, northern Tarim basin, NW. China and his guidance in biostratigraphy and regional geological settings.

The teams from Department of Chemistry (Oxford) provide me numerous extra help with the part of lignin decomposition, isolation of lignin monomers. They are Dr. Jeremy Robinson, Dr. Boshen Wu and Dr. Lingbin Kong. Especially, Jeremy and Boshen, they were teaching me the basic chemistry operation, column chemistry, the ways of mass spectrometry and how to read NMR graphs. Lingbin was training me to use the HPLC independently. Another team from School of Chemistry (Bristol) also supplies a precious help with the carbon-isotope analysis of lignin-derived monomers. They are Dr. Ian Bull and Professor Richard Evershed.

I feel grateful to Stephen for providing me with the opportunity of working on such exciting and compelling subject. His constant enthusiasm whenever I present new data was always cheering. His prospective sense in Earth sciences and abilities of explicitly presenting science in spoken and written form provided me an excellent model to follow.

Much sincere appreciation also goes to the China Oxford Scholarship Fund (COSF) from Hong Kong, Burdett-Coutts Fund from Department of Earth Sciences and Graduate Student Award from St Peter's College, University of Oxford, Wing Yip Bursary from Wing Yip Fund, London, and Shell Mudrock Observation in the different stages of my four-year study for funding my research and living. I also would like to express many thanks to Dr. Hugh Jenkyns and Dr. Gregory Price for their examining this thesis.

Dr. Yuanzheng Lu helped and supported me tremendously with scientific chats, and advice to work in the field observation and importantly sampling in the Kuqa section, northern Tarim, NW. China. Shenhui Deng funded me and Yuanzheng sampling in the field work, Kuqa section and the field investigation of other coeval strata along other neighbouring terrestrial basin, NW China.

There are various other individuals who supplied key assistance during my time as a DPhil student in Oxford. Steve Wyatt merits immense appreciation for all the prevision of clean acid and furnace capabilities over the years. Many thanks go to Owen Green for his tireless help with all the details in microscopy work such as training me operating SEM, preparing permanent thin-section slides. I am grateful to Norman Charnley and Dr Babette Hoogakker for helping with foraminiferal cleaning and the carbon-isotope analyses.

I truly acknowledge Dr. Peter Ditchfield who is the stable isotope laboratory manager, at Research Laboratory for Archaeology and the History of Art, University of Oxford, for his constant help with generating high-quality organic carbon-isotope data, especially for the exploration and attempt on the hand-picked individual phytoclasts in tiny amounts.

There are many other Earth Scientists who have been integral to my sanity during the past four years and deserve profound appreciation and thanks. My lovely office mates: Mark Bourne, Richard Paulin, Julia Barrott and Tom O'Tool, etc.

St. Peter's College have definitely been a key part of keeping me going for past four years. All the times in MCR, seminar rooms or the peaceful count gifted me the best memory in Oxford. College staff, Ms. Mary Chalk, Ms. Olivia Henley, and friendly and helpful Porters, epscially Mr. Paul Irons are all the part of the best memory.

Finally I would like to thank my lovely and wise wife Xuan Du, my kind parents-in-law and my diligent parents, their persistent courage to life and complete trust in me always brings me the biggest mind power.

Table of Contents

List of Figures

Chapter 1

INTRODUCTION

1.1 The early history of carbon-isotope stratigraphy

1.1.1 Onset of carbon-isotope stratigraphy based on marine carbonates

From the work of Craig (1953, 1957), the routine experimental measurements of the stable carbon-isotope values for geological samples were possible in 1950s. However, it still took more than ten years for the knowledge of carbon isotopes to be applied to the stratigraphic realms. In brief, after the success of oxygen isotope stratigraphy (Emiliani, 1955, 1966), a number of works of oxygen isotope stratigraphy based on the planktonic and benthic foraminifera (Imbrie *et al.*, 1973; Shackleton and Opdyke, 1973; Emiliani and Shackleton, 1974) were completed. Nearly at the same time, pioneers launched carbon-isotope studies as well (Savin and Douglas, 1973). The fruitful results inspired more exploration of carbon-isotope records in strata and the concept of 'carbon-isotope stratigraphy' gradually emerged in the geological literature, making use of both 'radiocarbon' and stable carbon isotopes (e.g. Erlenkeuser *et al.*, 1974; Savin *et al.*, 1975; Berger *et al.*, 1978a, 1978b; Shackleton and Vincent, 1978).

At that time, the biggest debate focused on whether the carbon-isotope values represented equilibrium between biological carbonate skeletons and their environments, or was at least quantifiable on basis of empirical correction factors. This was a vital stage of research, as it set up the foundation of using carbon-isotope proxies to reconstruct palaeoenvironment and stratigraphic correlation globally.

Under simple chemical equilibrium, the temperature coefficient for carbon-isotope fractionation between calcite and dissolved bicarbonate ion was determined in the early days

(Emrich *et al.*, 1970). The chemical equilibrium experimental data and theoretical calculation were consistent and illustrated that ^{13}C is enriched in $CaCO_3$ (shell carbonate) by (1.85±0.23)‰ at 20°C with respect to HCO_3^- (seawater) and the degree of ^{13}C enrichment (equilibrium offset) only slightly affected by temperature at (0.035±0.013)‰/°C (Emrich *et al.*, 1970).

The variations of carbon-isotope values in sediments were witnessed in empirical data. According to the empirical data, a tentative conclusion was reached that the carbon-isotope variations were insensitive to changes in temperature and the $\delta^{13}C$ ($\delta^{13}C = [(\frac{^{13}C}{^{12}C})_{sample} / (\frac{^{13}C}{^{12}C})_{standard} - 1] \times 1000‰$) of foraminifera was largely determined by $\delta^{13}C$ of dissolved carbon in seawater, although biological (nonequilibrium) fractionations could occur during the secretion of the test (Savin and Douglas, 1973).

Foraminiferal tests precipitated from the seawater and were supposed to be in chemical equilibrium with the carbon-isotope composition of that reservoir. However, this turned out to be far from the case, since the so called 'vital effect' that favours the isotopically light carbon during metabolic processes (e.g. Williams *et al.*, 1977; Berger *et al.*, 1978a; Shackleton and Vincent, 1978). Coccoliths can be even farther from carbon isotopic equilibrium precipitation than foraminifers (Berger *et al.*, 1978b). Nevertheless, the carbon isotopic offsets derived from the physiological processes seemed to be consistent enough to largely document the values of $\delta^{13}C$ in seawater and thus the isotopic variations in oceanic carbon reservoir could be inferred in time series (Margolis *et al.*, 1975; Kroopnick *et al.*, 1977; Arthur 1979; Keigwin, Jr., 1979). Up to the early 1980s, some authors (Savin *et al.*, 1981, pp. 423) had unequivocally summarized: '*foraminiferal carbon-isotope ratios at most of the sites varied quasi-sympathetically throughout the Miocene and these variations must*

reflect comparable variations in the mean $^{13}C/^{12}C$ of marine HCO_3^- '. This conclusion can be also extended to other geological times under the principle of uniformitaranism. Since then, the utility of carbon-isotope stratigraphic records as a tool of stratigraphy with global significance has been established.

Later, the further detailed culture experiments confirmed the conclusions in the previous studies. Both carbon isotopic composition of seawater and physiological effects (Grazzini, 1976; Kahn, 1979; Erez and Honjo, 1981; Killingley *et al.*, 1981; Deuser, 1987) influence the $\delta^{13}C$ of foraminiferal calcite, but the physiological vital effect can be regressed by empirical correction factors derived from the systematic culture experiments (Erez, 1978; Zimmerman *et al.*, 1983; Spero and Williams, 1988; Spero *et al.*, 1991; Sepro, 1992; Spero and Lea, 1996).

1.1.2 A (very) brief review of the applications

At the early stage, carbon-isotope 'excursions' from 'background' values were observed in stratigraphic sequences, but it was poorly known whether these represented a local isotopic fluctuation or a global event (Savin *et al.*, 1975). The confidence in the utility of carbon-isotope stratigraphy was gradually established on the basis of marine biological carbonate shells (primarily foraminiferal tests) by the end of 1970s. Later, the variations of $\delta^{13}C$ from biological and non-biological carbonates were employed to interpret geological events, for instance, the tectonic event altering the conditions at one site of deep-water formation (Bender and Keigwin, Jr., 1979), upwelling intensity (Berger et al, 1987b), carbon-isotope difference in the different level of water column (Berger *et al.*, 1987a), the global events of carbon-isotope excursions (Haq *et al.*, 1980), and carbon-isotope fluctuations in the

Cretaceous pelagic limestones which were applied as a potential stratigraphic and petroleum exploration tool (Scholle and Arthur, 1980).

Furthermore, carbon-isotope stratigraphy was widely employed to address the paleoceanographic, paleoclimatologic and paleoecologic problems, such as collapse of the photosynthetic system in the oceans, so called 'Strangelove' at Ocean the Cretaceous/Tertiary boundary (Shackleton, 1986; Zachos et al, 1989; Kump, 1991), negative excursions close to the Paleocene/Eocene boundary (e.g. Shackleton, 1986; Aubry *et al.*, 1996), the records both in marine and continental carbon reservoirs at the Paleocene/Eocene boundary (Koch *et al.*, 1992), perturbations of carbon reservoirs at the end of Permian (e.g. Baud *et al.*, 1989), and Toarcian OAE (e.g. Jenkyns, 1985; Hermoso *et al.*, 2012). More importantly, these major carbon-isotope excursions further proved to be globally synchronous events and thus confirmed carbon-isotope stratigraphy as a fundamental tool for global stratigraphic correlation.

1.2 Terrestrial carbon-isotope stratigraphy

The confidence of marine carbon-isotope stratigraphy is established primarily on the basis of biological shell carbonates. Similarly, the major advancements of terrestrial carbon-isotope stratigraphy are based on terrestrial plant fossils, both as macrofossils and microfossils. This is because the specific proxies are relatively easy to look into from both empirical and theoretical approaches together. The discussion about terrestrial carbon-isotope stratigraphy in this section (also in whole thesis) will primarily focus on the materials derived from C3 plants.

The terrestrial plants uptake atmospheric carbon dioxide to compose their tissues and thus the changes in the carbon isotopic composition of atmosphere register in the plants, which can be employed to reconstruct the atmospheric $\delta^{13}C$ values through geological history. In addition, a relatively rapid atmospheric circulation provides the basis for synchronous global stratigraphic correlation in light of terrestrial carbon-isotope stratigraphy. However, interpretation of the terrestrial carbon-isotope stratigraphy has proven challenging in three primary aspects: 1) how to determine the quantifiable relationship between $\delta^{13}C$ value in a plant fossils (if without influence of diagenetic alteration) and that of the contemporary atmosphere, 2) how to decipher the potential influence of diagenetic alteration, and 3) how to situate the data in an accurate geological context.

1.2.1 Relationship between $\delta^{13}C$ values in plant fossils versus atmosphere

All discussions in the Section 1.2.1 assumed no effect of diagenetic alteration. The diagenetic factors will be separately discussed in the Section 1.2.2.

Carbon-isotope variations of C3 plants in nature and sampling representative

The relationship between the $\delta^{13}C$ value of atmospheric CO_2 and the $\delta^{13}C$ value of plant fossils is complicated by the multi-path nature of photosynthesis. The modern C3, C4 and CAM plants are characterized by the distinct ranges of carbon-isotope signatures, due to their different photosynthetic pathway (C3 plants: -23 to -34‰; C4 plants: -8 to -16‰; CAM plants have intermediate signatures but occur in a lower percentage in ecosystems; e.g. Bender 1971; Smith and Epstein 1971; Farquhar *et al.*, 1982, 1989). C4 plants have not been considered to primarily occupy biological niches in global significance unit the Late Miocene based on carbon-isotope data (Cerling *et al.*, 1997) and phylogenetic evidence (Edwards *et al.*, 2010), although some compound-specific carbon-isotope evidence from phytoplankton chlorophyll, leaf-wax and steranes (e.g. Kuypers *et al.*, 1999) is used to imply C4 plant temporarily booming around Cenomanian–Turonian boundary during the Late Cretaceous. Therefore, the systematic carbon-isotope stratigraphic variations led by vegetation ratio changes C3 and C4 plants in can be basically excluded, if the age of samples is older than the Late Miocene.

However, even if only C3 plants are focused on, the processes of carbon-isotope fractionation during CO_2 diffusion and fixation in plants are not yet fully understood (Schleser, 1999). It was thought that 'the basic fractionations take place at the leaf level which, in a broader sense, determines the carbon-isotope level within a tree' (Schleser, 1999, pp. 307). However, the empirical data show that this is far from true, because the carbon-isotope fractionations are not only taking place at leaves during the photosynthesis, but also any biochemical reaction (metabolic processes) commonly under the effect of enzymes. Actually, even without enzymes, the carbon-isotope fractionations occurs as well between reagents and products; and

the isotopic fractionation is not necessarily small (Clayden *et al.*, 2001). Therefore, it is no wonder that carbon isotopes commonly vary in quite large ranges (up to 4‰) in plant organs within a single C3 plant, between individuals, or between different species.

For example, leaves are consistently lighter than branches by about 3‰ (Leavitt and Long, 1991; Schleser, 1999). There is also carbon-isotope discrimination between twigs and branches (up to 2–3‰, Leavitt and Long, 1986; Schleser, 1999). For the trunk of trees, the rings in their radial direction shows annually recurring pattern of carbon isotopic variation up to 2.5‰ (Leavitt and Long, 1982; Loader *et al.*, 1995). Even tissues from single rings but at a different height document variable carbon isotopes by 0.5–4‰ (Schleser, 1999). These variations could be accounted for by changes in the relative humidity, temperature, vapour pressure or moisture and precipitation (Leavitt and Long, 1991; Ogle and McCormac, 1994; Loader *et al.*, 1995). Among the different species, deciduous trees are typically depleted by about 3‰ relative to coniferous trees at a site. Inter-tree variations in the same locations can shift by 2–3‰, among the same or between different species (Schleser, 1999).

Because of these isotopic variations exemplified above, the present thesis takes an approach advocated by some earlier authors (e.g. Schleser, 1999; Robinson and Hesselbo, 2004), that the reconstruction of atmospheric $\delta^{13}C$ and application of carbon-isotope stratigraphy should be based on consistent plant organs (trunk is preferred) and only the independently reproducible results can be in confidence of reflecting reliable geological records.

However, do those samples necessarily document the reliable geological information, if the identical plant organs are consistently sampled through a stratigraphic sequence? Unfortunately, it would be not true according to logical inference, because the even trunk

materials themselves show quite variable carbon-isotope ratios in a single tree, vertically and horizontally. Nevertheless, as the results from just random sampling through a stratigraphic sequence exhibit the comparable carbon-isotope curves with different locations (e.g. Hesselbo *et al.*, 2002; Gröcke *et al.*, 2005; Nunn *et al.*, 2010; Hesselbo and Pienkowski, 2011), even in the totally different carbon-isotope reservoirs, i.e. marine reservoirs, on both long-term scales (e.g. Gröcke *et al.*, 1999; Robinson and Hesselbo, 2004) and short-term scales (e.g. Hasegawa, 1997, 2003; Hesselbo *et al.*, 2000, 2002, 2007). These empirical data unambiguously illustrate that the results have a reliable geological signal. All these studies follow essentially a random sampling strategy. Why does random sampling so commonly faithfully represent the isotopic stratigraphy so well?

Most likely these results are due to some kind of statistical effect on the stratigraphic sampling, which remains unknown. It is common sense that the simple statistical effect is a fundamental principle of the natural world, but the boundary conditions for the carbon-isotope stratigraphic sampling remain poorly known. Up to now, the quantifiable relationship between the $\delta^{13}C$ value of atmospheric CO_2 and the $\delta^{13}C$ value of C3 plant fossils is established on an empirical basis.

Laboratory experiments and the meta-analysis of modern plants

The relationship between the $\delta^{13}C$ value of atmospheric CO_2 and the $\delta^{13}C$ value of C3 plants is quantified by laboratory experiments (Jahren *et al.*, 2008; Lomax *et al.*, 2012). These results illustrate an excellent quantifiable correlation between $\delta^{13}C$ value of C3 plants and that of atmospheric CO_2. However, Lomax *et al.*, (2012) pointed out that the environmental factors which alter stomatal opening (e.g. extreme aridity or high altitude) can critically

impact on this correlation and applying the correlation to interpret data should be done with caution. Jahren *et al.* (2008) contended that a few cubic centimetres of many terrestrial rocks comprised statistically adequate C3 plant materials for reconstructing the $\delta^{13}C$ value of atmospheric CO_2. Arens *et al.* (2000) argued that most organic matter was buried under mesic or seasonally moist conditions and so presumably reducing the variability from the environmental effects.

In addition, the meta-analysis of modern plants growing in natural environments also indicates a similar relationship as the laboratory experiments and an inverse prediction solution was proposed (Arens *et al.*, 2000). This empirical inverse prediction solution is thought to be more suitable for applying to geological records than experiments based on the individual model C3 plants such as *Raphanus sativus L.* (Jahren *et al.*, 2008) and *Arabidopsis thaliana* (Lomax *et al.*, 2012), because the meta-dataset better represents the average mixed assemblage of C3 plants, which is more likely to be sampled from sedimentary sequences.

Therefore, the quantifiable relationship has been established by empirical geological data and laboratory culture experiments. Terrestrial carbon-isotope stratigraphy based on C3 plants fossils has proven to reliably reconstruct the evolution of the palaeo-atmospheric $\delta^{13}C$ values and to correlate globally sedimentary sequences as a chemostratigraphic tool.

1.2.2 The influence of diagenetic alteration

The published data in the previous examples (cited in the Section 1.2.1) have already empirically demonstrated that the C3 fossil wood is resistant enough to variations in post-

depositional alternation that it can faithfully record the geological information over hundreds of millions of years. Below the more general situations about diagenetic alternation are discussed and tentatively go beyond the case-by-case basis.

When a piece of C3 fossil wood is collected as a geological sample, its initial fresh wood could have gone through one of two different routes to altering its carbon-isotope values: route A in the phase from A1 to A2, and route B (Figure1.1). Thus, the potential changes in carbon-isotope values relative to the initial wood are discussed below.

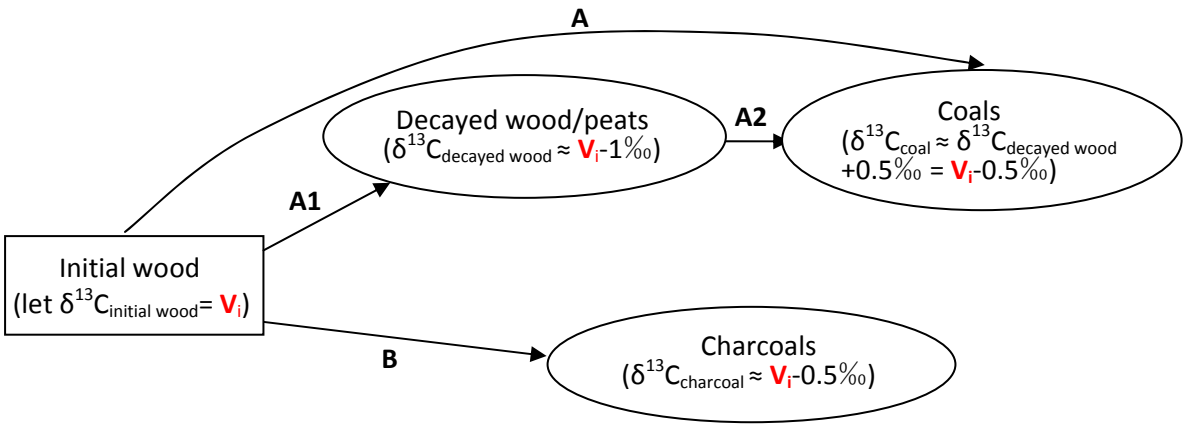

Figure 1.1. Schematic diagram on the alteration of carbon-isotope values in C3 plants relative to their initial values (V_i) during geological processes. There are two main routes to alteration of the initial carbon-isotope values in C3 woody plants when fossil wood is formed. The routes are represented by A1, A2 and B in the diagram. A1 = wood decayed or peat formed, A2 = coals formed in various advanced ranges, and B = charcoal yielded. In a summary, $\delta^{13}C_{decayed\ wood} \sim= \delta^{13}C_{coal} \sim= \delta^{13}C_{charcoal}$ (texts in Section 1.2.2 illustrate the values' origin) and hence there is no significant alteration against carbon-isotope values of fossil wood in the different preserved types.

Route A1 of A (Figure 1.1) is that the initial wood deposits in a normal setting in which the wood is mainly decomposed by bacteria and chemical solutions. All hemicelluloses, cellulose and lignin of the C3 wood simultaneously undergo the decomposition, but the hemicelluloses and cellulose are more easily decayed than lignin (Benner *et al.* 1987; Spiker and Hatcher

1987). Moreover, the wood lignin (accounting for 17–31% of the fresh biomoss) is depleted in ^{13}C by 2–3‰ relative to the whole plant $\delta^{13}C$ value, whereas cellulose and hemicelluloses (accounting for 57–76% of the fresh biomass) is enriched in ^{13}C by 1–2 ‰ relative to whole-plant tissue (Benner *et al.*, 1987) and proteins (accounting for little) are isotopically relatively heavy as well (Deines, 1980).

Integrated preferential preservation of lignin and the isotopic offset between hemicelluloses and cellulose, and lignin, the carbon-isotope alteration can be estimated as 1‰ lighter than that of initial wood (Figure 1.1). This estimation is also based on the statistically empirical data that initial wood is primarily composed by on average 2/3 cellulose and hemicelluloses, and 1/3 lignin (the ratio more or less subject to different plant species and plant organ) but after decomposition, the ratio of lignin to cellulose and hemicelluloses becomes around 2 to 1 (Benner *et al.*, 1987). The above selective preservation also involves bacterial decomposition. The bacterial reaction cannot much impact on the carbon-isotope ratios of the C3 plant tissues (see details in Appendix A).

Route A2 of A (Figure 1.1) is that the decayed wood after suffering preferential decomposition goes through coalification. Actually, there is not a distinct boundary between decayed wood and peat, or there is not a sharp starting point for coalification.

Coalification can be divided into three stages. First, aerobic degradation occurs on the ground surface and at a few centimetres depth. Active aerobic bacterial degradation significantly reduces wood volume, often as much as 50 % to 80 % (Harmon *et al.*, 2000). With continuous burial, the second stage is dominant in anaerobic degradation due to a rapid decline of oxygen level with increasing depth (little oxygen at a few centimetres depth, e.g. Greenwood and Goodman, 1967). These anaerobic bacteria go on decomposing wood and

reducing the volume, but they do not much change carbon-isotope values in the decayed wood (see details in Appendix A). Once depth is beyond ~1500 m (assumed geothermal gradient at 2.5°C /100 m), thermal alteration will take over, arriving at the third stage. With rising temperature, coals are yielded in an ascending range from peat, brown coals/lignite, bituminous coals to anthracite, and eventually graphite (not coal any more).

The carbon-isotope changes during the thermal alternation in coals has been intensively studied by modelling and empirical data (Berner *et al.*, 1992; Berner *et al.*, 1995; Cramer *et al.*, 1998; Cramer *et al.*, 2001). Cramer *et al.* (1998, 2001) used a mathematical model adapted from Berner (1992, 1995) that fundamentally relies on the first-order reaction kinetics for primary parallel reactions with a common preexponential factor. According to the model, carbon-isotope fractionation in any point can be indexed by thermal maturity expressed as vitrinite reflectance (Ro). In addition, Cramer's model fits very well with the experimental data that are obtained from Palaeozoic coal (Ro=0.72%), Mesozoic coal (Ro=0.43%) and Miocene coal (Ro=0.36%) (Cramer *et al.*, 2001). The pyrolyzed coals become slightly isotopically heavier, by <0.6‰, relative to the original value, with only one exception turning heavier by ~1.5‰, probably due to inhomogeneity of sampling. In other experiments (Cramer *et al.*, 1998), final coals become just 0.3‰ heavier relative to the initial peat.

In short, the carbon-isotope values become heavier, when coalification makes the decayed wood (or peat, as ratio of lignin to cellulose is broadly equal to peat) into coals in the various ranges. However, even if the wood reached the end of the extreme thermal alternation, the maximum alteration value is just about 0.6‰ (Cramer *et al.*, 2001).

Route B (Figure 1.1) is charcoalification. Charcoal is yielded by pyrolysis (charring) of plant material during the palaeo-wildfire without adequate oxygen. Although the precursor of charcoal can be from a range of vegetation materials, charcoal is commonly derived from wood. As mentioned above, the fresh wood is primarily composed by about 2/3 cellulose and hemicellulose, and 1/3 lignin. Interestingly, celluloses are preferentially removed during pyrolysis ahead of the lignin decomposition. This phenomenon is witnessed by SEM observation physically (Beall *et al.*, 1974, Cutter *et al.*, 1980; Jones and Chaloner, 1991) and the preference is inferred by the simulated experiments based on *Pinus sylvestris* (Phase 2, Table 1) and result in ≈0.5‰ isotopically lighter values relative to original wood samples. By around 1.0‰ isotopically lighter, if charcoal is yielded over about 340-600°C (Phase 3, Table1), however, the charcoal yielded at Phase 3 is fragile and hard to be preserved in pieces

Table 1. Physical and chemical parameters of pyrolysis of xylem tissue of (Jones and Chaloner, 1991)

Phase 1	**Phase 2**	**Phase 3**
Charred wood	Charcoal	Charcoal breaking-up
Experimental chars‘180-220°C ’	Experimental chars‘230-340°C’	Experimental chars‘340-600°C’
Internal cell wall structure seen	Cell walls apparently homogenised	Cracking along site of middle lamella
Preservation potential moderate, usually compressed	Preservation potential excellent. Anatomic preservation of high fidelity	Preservation potential poor. Very fragile, typically smashed to minute pieces.
Pit membranes intact	Pit membranes usually disappeared	Pit membrane disappeared
Attacked and oxidised by Schultze’s solution within a few hours	High resistant to oxidation by Schultze’s solution	Highly resistant to oxidation by Schultze’s solution
Reflectance $R_o \leq$ ‘0.4%’	Reflectance R_o = ‘0.4-1.2%’	Reflectance $R_o \geq$ ‘1.2%’
Stable carbon isotopes same as parent plant whole tissue	Stable carbon isotopes fractionated. In exp’ chars ≈ ‘0.5‰’ lighter	Stable carbon isotopes fractionated. In exp’ chars ≈ ‘1.0‰’ lighter
Seen in fossil record as semifusinite	Seen in fossil record as fusain, fusinite and semifusinite	Seen in fossil record as fusain, inertodetrinite

of block in sediments (Jones and Chaloner, 1991). This varying range of $\delta^{13}C$ values is consistent with laboratory charring data based on wood *Eucalyptus spp., Quercus robur and Pinus radiate* (Turney *et al.*, 2006). Thus, $\delta^{13}C$ values of the block charcoal samples collected in sediments is about 0.5‰ lighter than initial wood, i.e. $\delta^{13}C_{charcoal} \approx \mathbf{V}_i$-0.5‰ (Figure 1.1).

Table 1 summarizes the physical and carbon-isotope values of charcoalified wood. Moreover, a detailed pyrolysis experiment that quantitatively monitored the changes in composition has been reported (Yang *et al.*, 2007) and shown very good consistency with the critical points for pyrolysis of wood (process of charcoalification) in the work of Jones and Chaloner (1991). Above 230°C, hemicelluloses dramatically pyrolyze (Figure 1.2) and hence cell walls are apparently homogenised due to reduction of hemicelluloses and the wood becomes charcoal. Above 340°C, cellulose sharply loses its stability and dramatically pyrolyzes (Figure 1.2). This result leads to the charcoal becoming very fragile. Although the lignin is the most resistant composition in wood from the perspective of the whole pyrolysis, lignin begins to decompose as early as hemicelluloses and earlier than cellulose does (Figure 1.2). The composition of

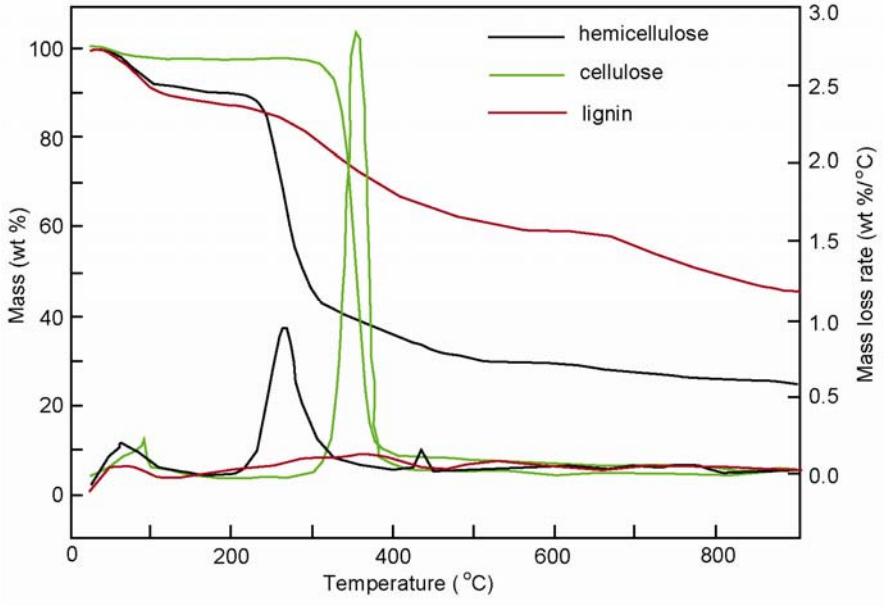

Figure 1.2. Pyrolysis curves of hemicellulose, cellulose and lignin in Thermogravimetric Analyzer (Yang *et al.*, 2007)

lignin at an early stage also contributes to the carbon-isotope changes. Therefore, carbon-isotope values in charcoal get heavier by about 0.5‰ (easily calculated from changes in ratio of cellulose/hemicelluloses to lignin, according to curves in Figure 1.2) relative to the decayed wood/peat, but lighter by about 0.5‰ relative to initial wood (Figure 1.2).

In conclusion, carbon-isotope values of the decayed wood, coals in various ranges, and charcoal are not significantly different. If the decayed wood, coal and charcoal are derived from the same fresh C3 plants in a consistent organ, their carbon-isotope values would be very similar (varying less than 1‰). These plant fossils preserved in different types can all be used for terrestrial carbon-isotope stratigraphy.

1.2.3 Age and Geological Context

Even where C3 fossil wood is concentrated, determination of the accurate geological contexts is still very necessary to interpret terrestrial carbon-isotope stratigraphy. This is because hiatuses can frequently occur in terrestrial or marginal marine sedimentary successions. In addition, a number of depositional processes (e.g. reworking), ecosystem changes, drainage changes, etc. could influence the interpretation of carbon isotopes generated from terrestrial strata. For instance, a significant proportion of terrestrial organic matter is reworked from older deposits along shallow-marine margins (e.g., McCarthy and Mudie, 1998) or lacustrine margins, during lowstand periods. All these potential pitfalls derived from geological contexts will be intensively discussed in the case studies in Chapter 2, Chapter 3 and Chapter4. Additionally it is necessary to know at least an approximate geological age in order to compare a terrestrial carbon-isotope stratigraphy with its marine equivalent.

1.3 Reviews and motivations for terrestrial carbon-isotope stratigraphy

1.3.1 Reviews

The scientific significance of terrestrial carbon-isotope stratigraphy is briefly generalized in Figure 1.3. Overall, the character of synchronous carbon-isotope shifts between the marine and terrestrial carbon-isotope stratigraphic curves is an essential key to the establishment of terrestrial carbon-isotope stratigraphy and raises further scientific topics.

Since the 1980s marine carbon-isotope stratigraphy based on biogenic carbonates has been established, owning to both the culture experiments in the laboratory and globally comparable stratigraphic data from deep and shallow oceans (see Section 1.1). Thus, the global signature is recognisable and generally well documented from marine carbonate carbon-isotope reservoirs. The major carbon-isotope fluctuations occurring in marine reservoirs are also documented synchronously by those of C3 plant fossils (e.g. Hasegawa, 1997, 2003; Gröcke *et al.*, 1999; Jahren *et al.*, 2001; Ando *et al.*, 2002; Heimhofer *et al.* 2003; Robinson and Hesselbo, 2004; Hesselbo *et al.*, 2000, 2002, 2003, 2007; Korte and Hesselbo, 2011). Importantly, the key breakthrough took place when it was observed that terrestrial carbon-isotope stratigraphic curves shifted synchronously with the well-studied marine carbon-isotope stratigraphic ones. This means the terrestrial carbon-isotope stratigraphic records register global signatures. The various factors that potentially bias the reliable stratigraphic records were primarily excluded in many studies published to date. These biasing factors for interpretation of the geological data include diagenesis, a relatively large range of carbon-isotope variations within an individual plant, between plants and between

species, changes in ecology, changes in aridity, unrepresentative sampling, and more (Figure 1.3, right charts).

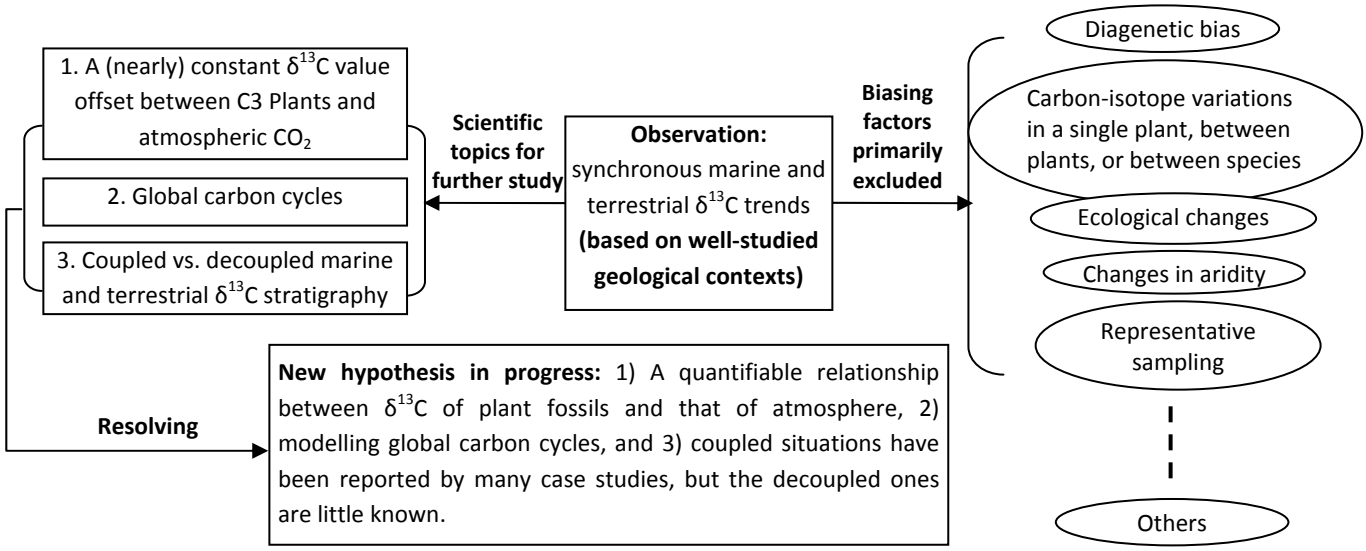

Figure 1.3. Schematic diagram of significance of terrestrial carbon-isotope stratigraphy based on the C3 plant fossils. The observation of synchronous carbon-isotope excursions from both marine and non-marine reservoirs raises questions in three important scientific areas (left charts) and can primarily exclude potential bias factors (right charts).

The observation that synchronous carbon-isotope shifts occur in both marine and terrestrial settings also raises scientific questions in three aspects: 1) why does $\delta^{13}C$ value retain a (nearly) constant offset between C3 Plants and atmospheric CO_2? 2) does terrestrial carbon-isotope perturbation at a global scale help to model global carbon cycling? and 3) does the atmosphere-ocean coupled carbon-isotope evolution always last over geological timescales and what are the dynamic mechanisms (Figure 1.3, left charts)?

The scientific topics above lead to the corresponding points of novel studies and hypotheses: 1) a quantifiable relationship between $\delta^{13}C$ of plant fossils and that of atmosphere are explored (Arens *et al.*, 2000; Jahren *et al.*, 2001, 2008); 2) the simulations of global carbon cycles are proposed (Hayes *et al.*, 1989; 1999; Kump, 1991; Hedges, 1992; Kump and Arthur,

1999); and 3) the coupled situations between terrestrial and marine carbon-isotope stratigraphic curves are reported by many case studies (e.g. Hasegawa, 1997; Gröcke *et al.*, 1999; Hesselbo *et al.*, 2000; Ando *et al.*, 2002; Robinson and Hesselbo, 2004; Korte and Hesselbo *et al.*, 2011), but the decoupled ones have been little investigated (Hasegawa *et al.*, 2003; Hasegawa, 2003).

1.3.2 Motivations

Terrestrial carbon-isotope stratigraphy is a promising approach to reconstruction of atmospheric $\delta^{13}C$ (Arens *et al.*, 2000; Gröcke, 2002; Jahren *et al.*, 2008) in time series, and thus it is particularly useful to study the evolution of atmospheric CO_2. The method also potentially allows correlation between coeval marine and non-marine carbon-cycle related paleoenvironmental events (Koch *et al.*, 1992; Hasegawa, 1997; Gröcke *et al.*, 1999; Gröcke, 2002; Hesselbo *et al.*, 2000, 2007; Hasegawa *et al.*, 2003; Bacon *et al.*, 2011; Hesselbo and Pienkowski, 2011).

The terrestrial carbon-isotope stratigraphy provides a promising chemostratigraphic tool that is potentially able to correlate between different terrestrial basins, between terrestrial and marine sedimentary successions, as well as marine sediments within the same or between different ocean basins which both contain the fossil wood or other terrestrial carbon-isotope proxies, e.g. terrestrial-derived biomarkers (Pancost and Boot, 2004). More promisingly, when the carbon-isotope stratigraphic correlations are applied constrained by a biostratigraphic or other chronostratigraphic framework, carbon-isotope stratigraphy can potentially permit much more accurate correlation than the biostratigraphy, because of the rapid atmospheric circulations and distinctive isotopic excursions.

Terrestrial carbon-isotope stratigraphy is critical to understanding of long-term global carbon cycling, because it provides a vital parameter to model global carbon cycles through Earth history. The geological records are often incomplete, whereas modelling can fill this gap and be helpful to explore the dynamic processes (Ridgwell *et al.*, 2007). In order to model global carbon cycles, both the organic and inorganic carbon-isotope reservoirs in nature need to be taken into account (Kump, 1991; Kump and Arthur, 1999). The coeval photosynthetic carbon fixation by marine and terrestrial organisms has to be studied, as this process involves a large carbon-isotope fractionation (Hayes *et al.*, 1989; 1999; Hedges, 1992). Therefore, to properly understand the global carbon cycle, it is logical to reconstruct the evolution of every carbon-isotope reservoir, e.g. both the organic and inorganic carbon reservoirs. The terrestrial carbon-isotope stratigraphy was pioneered by study of carbonate nodules in paleosol and mammal's teeth (Koch *et al.*, 1992). Furthermore, terrestrial carbon-isotope stratigraphy based on the C3 plants can be applied more broadly, as the fossil C3 plant materials (phytoclasts) are widely preserved in both non-marine and marine sediments.

1.4 Thesis outline

Chapter 1 has introduced the history of carbon-isotope stratigraphy and its developing trends including: the pioneering work primarily based on marine biological carbonates; the progress of terrestrial carbon-isotope stratigraphy; the associated three primary challenging aspects for successful application of terrestrial carbon-isotope stratigraphy; and the three major motivations for its development.

Chapter 2 investigates a case study on the Miocene terrestrial carbon-isotope stratigraphy from the Atlantic Ocean margin, offshore New Jersey, USA (IODP Expedition 313). This chapter presents the specific New Jersey depositional setting, sampling, carbon-isotope data, and discussion and interpretation to these data. In addition, the global correlations of carbon-isotope fluctuations in the atmosphere-ocean reservoirs during the Early to Middle Miocene will be discussed. However, assuming that the correlations based on strontium-isotope values and biostratigraphy are correct, the carbon-isotope records from the New Jersey margin lack a positive excursion of carbon-isotope values in terrestrial organic matter through the Langhian Stage. This contrasts with previous studies from oceanic settings. Factors that may potentially bias local terrestrial carbon-isotope records are assessed on the basis of pyrolysis data, scanning electron microscope observations, and comparison to palynological indices of environmental change. Finally, it is concluded that the overall carbon-isotope signature for the exchangeable carbon reservoir is distorted in this case study, to the extent that the mid-Miocene Monterey event excursion is not easily identifiable.

Chapter 3 investigates a case study of the Miocene terrestrial carbon-isotope stratigraphy from North Sea Basin, onshore Denmark. This chapter introduces the local geological settings and history of sedimentary evolution. Sampling strategy is discussed and carbon-isotope data are generated from the concentrated phytoclasts, and SEM images are used to investigate the diagenetic situation of the phytoclasts. Subsequently, the carbon-isotope data are interpreted in local and global geological contexts for the late Early to Middle Miocene. Finally, the long-distance correlations of terrestrial carbon-isotope stratigraphy between New Jersey and the North Sea Basin are tentatively made.

Chapter 4 investigates a case study of the Jurassic terrestrial carbon-isotope stratigraphy from the Kuqa section, Tarim Basin, NW China. This chapter introduces the Jurassic plate tectonic history in the study area and regional geological backgrounds, including a brief evolutionary history of other neighbouring terrestrial sedimentary basins. The Jurassic terrestrial carbon-isotope stratigraphy in fluvial and lacustrine deposits is described. Due to the lack of radiometric dating, the plant fossils and palynological stratigraphy are summarized to constrain the stratigraphic ages. Based on the composite biostratigraphy, the global correlations with both terrestrial and marine European carbon-isotope reservoirs are attempted. The time interval of global correlation goes through the Triassic-Jurassic boundary and Early Jurassic. An exact horizon of Triassic-Jurassic boundary is suggested by the new results. A bed with the character of soft-sediment deformation and its occurrence at the Triassic–Jurassic boundary is recognised and it recalls universal seismites interpreted to the huge bolide impacts in NW Europe. The correlation between the terrestrial carbon-isotope stratigraphy in the Tarim Basin and other coeval terrestrial and marine strata are first witnessed by both entire marine and terrestrial sedimentary successions in the Jurassic. Long-term coupled atmosphere-ocean reservoirs are hence inferred during that time. The negative

excursion that characterises the Toarcian OAE in other Early Jurassic successions is not recognised and it is concluded that the event is either missing or else represented by strata higher in the Kuqa section.

Chapter 5 summarizes the conclusions of the thesis and presents outlooks for terrestrial carbon-isotope stratigraphy.

Chapter 2

CARBON-ISOTOPE STRATIGRAPHY FROM TERRESTRIAL ORGANIC MATTER THROUGH THE MONTEREY EVENT, MIOCENE, NEW JERSEY MARGIN (IODP EXPEDITION 313)

A reformatted version of this chapter was published as: *Fang, L., C. J. Bjerrum, S. P. Hesselbo*, U. Kotthoff, F. M. G. McCarthy, B. Huang, and P. W. Ditchfield* (2013), Carbon-isotope stratigraphy from terrestrial organic matter through the Monterey event, Miocene, New Jersey margin (IODP Expedition 313), *Geosphere,* doi:10.1130/GES00851.1.

It is reproduced here in thesis format. This chapter includes the part of data and data interpretations contributed by co-authors as follows.

C. J. Bjerrum contributed the measurement of pyrolysis parameters, bulk organic matter and bulk C/N ratio, and the relevant data interpretation.

S. P. Hesselbo is corresponding author.

U. Kotthoff contributed the palynological analysis on the evolution of terrestrial ecosystems.

F. M. G. McCarthy contributed the palynological analysis on the T: M ratio (i.e. the ratio of terrestrial to marine material in each sample, based on the percentages of terrestrial and marine palynomorph).

B. Huang contributed part of carbon-isotope data from planktonic foraminifera, single species *Globigerina praebulloides*.

P. W. Ditchfield helped to accurately analyse the carbon-isotope derived from tiny amount of the individually hand-picked woody phytoclasts.

Abstract

The stratigraphic utility of carbon-isotope values from terrestrial organic matter is explored for Miocene siliciclastic sediments of the shallow shelf, New Jersey margin, USA (IODP Expedition 313). These shallow marine strata, rich in terrestrial organic matter, provide a record of deposition equivalent to the Monterey Event, a prolonged interval of time characterised by relatively positive carbon-isotope values recorded from foraminiferal carbonate in numerous oceanic settings. Coherent stratigraphic trends and short-term isotopic excursions are observed consistently in palynological preparation residues, concentrated woody phytoclasts, and individually picked woody phytoclasts obtained from the New Jersey sediments. A bulk organic matter carbon-isotope curve shows somewhat different stratigraphic trends but, when corrected for mixing of marine-terrestrial components on the basis of measured C/N ratios, a high degree of conformity with the woody phytoclast record is observed. However, assuming that the correlations based on strontium-isotope values and biostratigraphy are correct, the carbon-isotope record from the New Jersey margin contrasts with that previously documented from oceanic settings (i.e. lack of positive excursion of carbon-isotope values in terrestrial organic matter through the Langhian stage). Factors that may potentially bias local terrestrial carbon-isotope records include reworking from older deposits, degradation and diagenesis, as well as environmental factors affecting vegetation in the sediment source areas. These possible factors are assessed on the basis of pyrolysis data, SEM observations, and comparison to palynological indices of environmental change. Some evidence is found for localised degradation and/or reworking of older woody phytoclasts,

but where such processes have occurred they do not readily explain the observed carbon-isotope values. It is concluded that the overall carbon-isotope signature for the exchangeable carbon reservoir is distorted, to the extent that the Monterey Event excursion is not easily identifiable. The most likely explanation is that phytoclast reworking has occurred in clinoform toe-of-slope facies, but the reason for the resulting relatively heavy carbon-isotope values produced remains obscure.

2.1 Introduction

Correlation of sedimentary successions by carbon-isotope values of organic and carbonate components has become a routine method in stratigraphy (e.g. Scholle and Arthur 1980; Jenkyns *et al.*, 2002; Jarvis *et al.*, 2006). This method works on the basis that the measured carbon-isotope signature within a succession is representative of changes in the isotopic signature of the surface Earth carbon reservoirs through time. In particular, distinctive trends or excursions can be matched between sections, providing correlative time lines. In addition to simple analysis of bulk sedimentary organic matter or bulk carbonate, many studies have focussed on isolated fractions that are derived from individual materials making up the sedimentary carbon in order to minimise the overprinting or distorting effects of processes such as mixing of different sedimentary components with their own distinct isotopic signatures or diagenetic changes and additions (e.g. Veizer *et al.*, 1999 focusing on brachiopods and belemnites).

It is particularly useful that the carbon-isotope composition of terrestrial organic matter tracks that of atmospheric carbon dioxide (Aren *et al.*, 2000; Jahren *et al.*, 2008), and this commonly results in terrestrial carbon-isotope signatures identical to those from coeval marine materials, potentially allowing correlation between marine and non-marine palaeoenvironments. Such correlations allow consideration of carbon-cycle related environmental changes taking place on land at the same time as in the oceans (Koch *et al.*, 1992; Hasegawa 1997; Gröcke *et al.*, 1999; Hesselbo *et al.*, 2000, 2007; Gröcke, 2002; Hasegawa *et al.*, 2003; Bacon *et al.*, 2011; Hesselbo and Pienkowski, 2011).

Although the technique of terrestrial carbon-isotope stratigraphy has shown considerable promise, there are a number of potential pitfalls. One issue is the possibility that a significant proportions of the sedimentary organic matter is reworked from older deposits, a problem one might predict to be acute when sediments are resuspended from continental shelves and redeposited further down the margin during sea-level lowstands (e.g. McCarthy and Mudie, 1998). Additional complications arise because isotope discrimination during formation of terrestrial organic matter seems to be a function of temperature and soil moisture independent of pCO_2, whereas isotope fractionation during formation of marine organic matter is a function of pCO_2 for some photosynthetic species (e.g. Bowen *et al.* 2004; Jahren *et al.* 2008). In the present study these and other problems are explored with respect to sedimentary organic matter from Miocene sequences on the New Jersey margin drilled for IODP Expedition 313 (Figure 2.1).

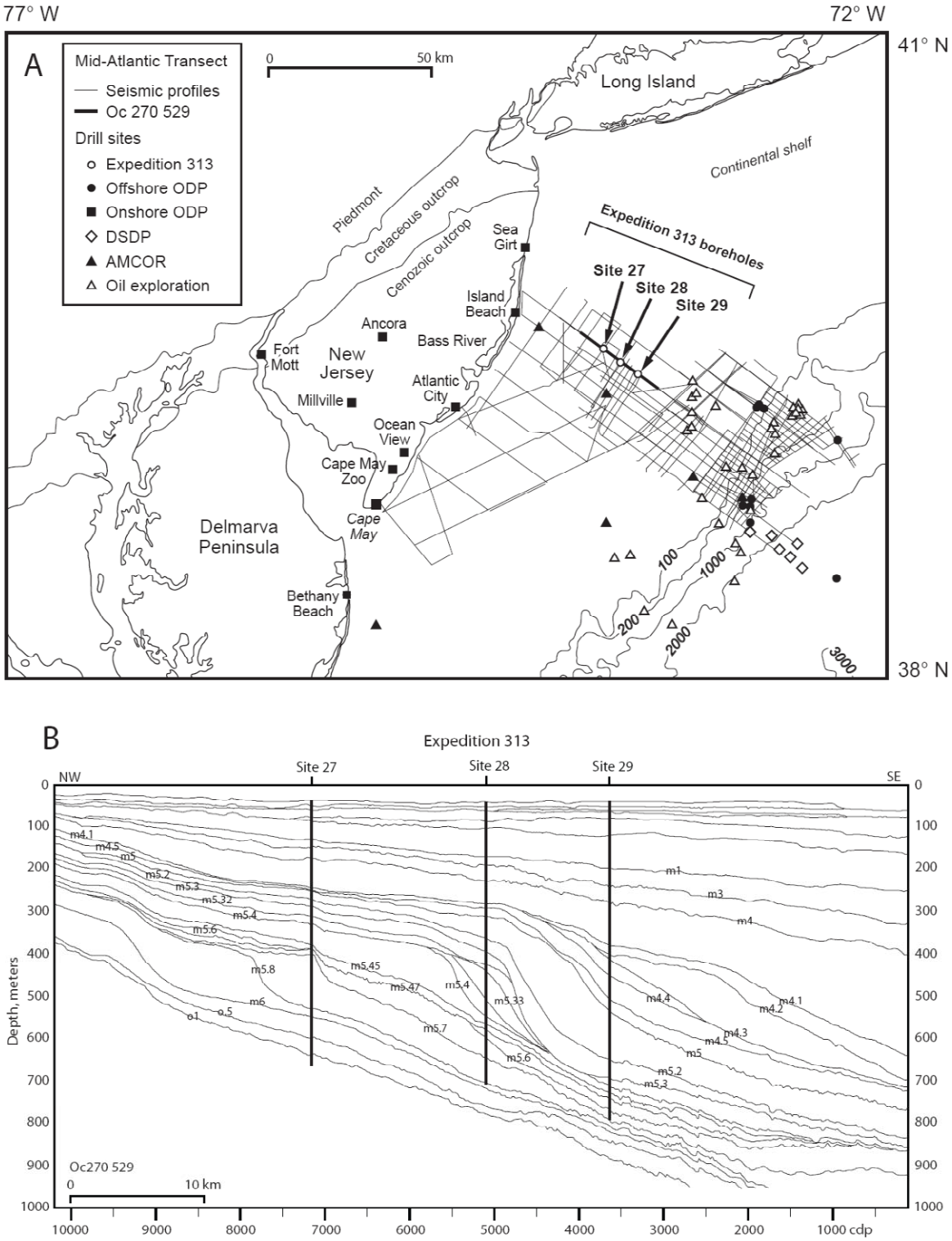

Figure 2.1. A. Location map. B. Depth-converted seismic stratigraphic framework Expedition 313 boreholes. (Modified from Mountain *et al.*, 2010)

Carbon-isotope signatures for the Neogene exchangeable carbon reservoirs are well known based on analysis of multiple oceanic carbonate records (Zachos *et al.*, 2001). For the Miocene in particular, the Monterey Event and its carbon-isotope signature is of some prominence (Figure 2.2; Vincent and Berger, 1985; Woodruff and Savin, 1985; Flower and Kennet, 1994; Zachos *et al.*, 2001; Abels *et al.*, 2005; Holbourn *et al.*, 2005, 2007; Diester-Haass *et al.*, 2009). This isotopic and palaeoenvironmental event was originally defined in the tropical Indian Ocean at DSDP Site 216 by Vincent and Berger (1985), and the positive carbon-isotope excursion ($\geqslant$+1.5‰), was documented for the benthic inorganic carbon reservoir. This event is thought to coincide with a time of extensive burial of organic matter (Vincent and Berger, 1985; Woodruff and Savin, 1991). Combined benthic and planktonic foraminiferal records of the Monterey Event have also been published, by Cheng *et al.* (2004), and these data provide substantial evidence of a whole ocean-atmosphere carbon cycle perturbation (Figure 2.2).

Studies at high-resolution from many pelagic and hemipelagic locations have shown the long-term carbon-isotope excursion of the Monterey Event to comprise a number of separate short, ~1 per mil positive excursions, superimposed on the overall positive carbon-isotope values (Woodruff and Savin, 1985; Woodruff and Savin, 1991; Figure 2.2). Integration with astronomical timescales has resulted in the recognition of nine of these short-term excursions, each identified as having a long eccentricity 400 ky periodicity, and allowing by fit to the La2004 astronomical model a refined dating for the whole Monterey Event from 16.9 to 13.5 Ma (Holbourn *et al.* 2007), i.e. latest Burdigalian, Langhian, and very earliest Serravalian. [It is noted that the definition of the

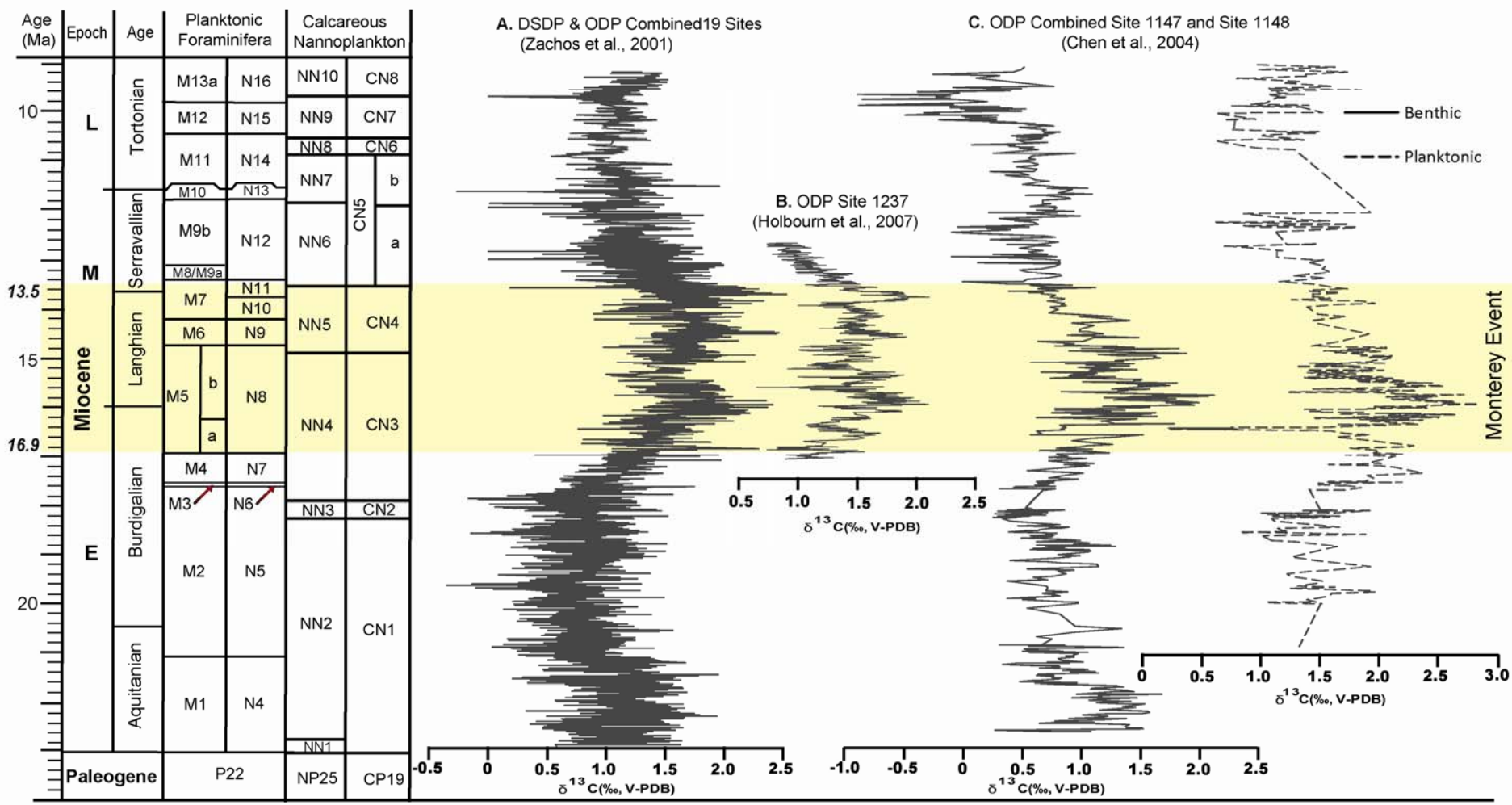

Figure 2.2. Published carbon-isotope curves for the Miocene interval illustrating the long-term changes in oceanic carbon-isotope values. All data recalibrated to Gradstein et al. (2004) timescale. A. Data compilation from multiple sites (Zachos et al., 2001). B. High-resolution data from benthic foraminifers (Holbourn et al., 2007), showing previously described individual excursions within the overall Monterey Event. C. Combined benthic and planktonic foraminifer dataset from the South China Sea (Cheng et al. 2004).

event changes by author, so Holbourn *et al.* (2007) do not include strata at the top of the event that were included by Woodruff and Savin (1991).]

The Miocene of the New Jersey margin makes for a particularly useful case study because the sedimentology, stratigraphy, and palaeontology of this marginal setting is now well characterised for the Cenozoic, including the interval that spans the Monterey Event (Browning *et al.* 2006, 2008, 2013; Monteverde *et al.*, 2008; Mountain *et al.*, 2010; Miller *et al.*, 2013; Proust, 2013, personal commun.). In the present study carbon-isotope curves generated from a variety of substrates are presented, comprising bulk organic matter, bulk concentrated phytoclasts, hand-picked phytoclasts, and planktonic foraminifers, and these data are compared with newly generated pyrolysis datasets of organic matter type, atomic C/N ratios, and relevant palynological analyses. The overall aim is to improve understanding of the strengths and weaknesses of using terrestrial materials as the basis for carbon-isotope stratigraphic correlation. In addition, the analysis sheds further light on the development of Miocene depositional sequences on the New Jersey margin.

2.2 Methods

Phytoclasts are components of a palynological preparation residue made up of recognizable fragments of plant cuticles and woody tissue (Tyson, 1995; Hasegawa *et al.*, 2003), and herein the woody tissue components of the phytoclast assemblages have been specifically studied.

2.2.1 Palynological preparation and analysis

Standard palynological techniques were used to extract organic matter from sediment samples. Preparation for the majority of samples was carried out at the National Oceanographic Centre, University of Southampton, UK (from 260 to 760 mbsf at Site 29 and from 200 to 450 mbsf at Site 28). A subordinate sample set was prepared at Brock University, Canada (from 600 to 760 mbsf at Site 29, from 400 to 660 mbsf at Site 28 and from 180 to 300 mbsf at Site 27).

At Southampton, a five gram sample was placed in a plastic beaker and cold hydrochloric acid (30%) added to remove carbonate. After decanting, the sample was washed with deionized water until the pH approached 7. Hydrofluoric acid (60%) was then added with regular stirring until the sample was wholly broken down, and then the sample was decant-washed with deionized water until the pH approached 7 again. Subsequently, the residue was sieved at 15 micrometers, and the coarse fraction separated into a glass beaker. With most water removed from the sample, hydrochloric acid (30%) was added

into the beaker and heated until it just boiled (to take neoformed fluorides into solution). The boiled sample in the beaker was rapidly diluted in 500 ml of water and was sieved at 15 micrometers; the remaining organic matter was put into vials after washing through with deionised water. For each sample one standard slide was made up in Elvacite 2044.

At Brock University, 5 cm^3 of sample (measured by liquid displacement) was placed in Nalgene test tube and a very weak (0.02%) Calgon solution was added. Samples were then placed in a warm (not boiling) water bath until clays were disaggregated, then they were washed in distilled water and centrifuged at 3000 rpm for 3 minutes. Samples were then sieved using distilled water through a 15 micron Nitex mesh to remove clays and subsequently returned to the test tubes. Weak hydrochloric acid (10%) was then added together with a *Lycopodium* tablet (Stockmarr, 1971) and samples were again placed in a warm water bath until reaction stops to remove carbonates. Samples were again washed in distilled water and centrifuged at 3000 rpm for 3 minutes, and hydrofluoric acid (60%) was added and test tubes returned to the warm water bath. Samples were stirred regularly over a period of approximately one hour, decanted and rinsed with distilled water until neutral. The residue was again sieved at 15 microns, and the residue was mounted on a glass slide using glycerine jelly.

2.2.2 Separation and concentration of palynological particulates, and the component monitoring after concentration

In order to concentrate the terrestrial organic fraction (mostly phytoclasts) from palynological particulates, a further separation procedure was carried out. The organic residues produced by standard palynological preparation techniques were suspended in alcohol, and the microfossils (e.g. dinoflagellates, acritarchs, spores and pollen) absorbed a sufficient amount of the alcohol to reduce their average density relative to those of phytoclasts (method of Hansen and Gudmundsson, 1977).

Deionized water was placed into the separating funnel and then 5 ml ethanol on to the water surface. A pipette was used to take and transfer the organic sample into the funnel. After leaving to stand for 10-15 minutes (depending on the size of the particles), the samples were divided into two parts as 'top' and 'bottom'. The 'bottom' part was collected into 10 ml Teflon tubes, while the 'top' part was collected into the 50 ml centrifuge tubes and reclaimed by centrifuge; finally, the top and bottom parts were dried out in 60 °C oven for 48 hours.

The technique of separation takes advantage of the difference in settling rate between the phytoclasts and the microfossils. After this separation, the marine fraction (dinoflagellate, zoomorphs and Chlorococcales) and the terrestrial pollen and spores, which tend to be hollow and very small, are largely excluded, leaving the phytoclasts concentrated. Furthermore, in order to monitor the components for the carbon-isotope measurements, a

quantitative palynofacies analysis was undertaken by identifying the components and counting their absolute number (N=300 per sample) under a transmitted-light microscope. Percentage of each component in organic matter was thus determined. The classification scheme (Table 2.1) for palynofacies analysis in this thesis follows Ross's scheme and classification protocol (Ross, 1999), but a bit of simplification is made, as the aim of present study is simply to monitor the accurate components for the carbon-isotope measurements rather than study of the detailed palaeoenvironmental changes (Ross, 1999).

Table 2.1. Classification scheme of particulate organic matter (simplified from Ross, 1999)

Phase 1	**Phase 2**	**Phase 3**	**Phase 4**
Palynomorphys	Sporomorphs	Pollen	Bisaccate Pollen
			Non Bisaccate Pollen
		Spores	
		Unidentified	
	Phytoplanton	Chlorococcales	Single Bodied (or Colonial)
		Prasinophytes	e.g. Tasmanitids, Leiospheres
		Dinoflagellatge cysts	
		Acritarchs	
	Zoomorphs	e.g. Foraminiferal linings	(lenticular slits)
	Fungal Bodies		
	Unidentified		
Discrete Fragments	Vita Fragments	Cuticle/ Epidermal Remains	
		Definite Wood	
		Vascular Bundles/tracheid	
		Resin	
		Plant Tissue	
	Non-Vita Fragments	Brown	
		Black	
Structureless Organic Matter (SOM)		Transparent-Yellow	
		Yellow-Brown	
		Brown-Black	

The various components of palynological particulates are identified under the transmitted-light microscope observation (Figure 2.3).

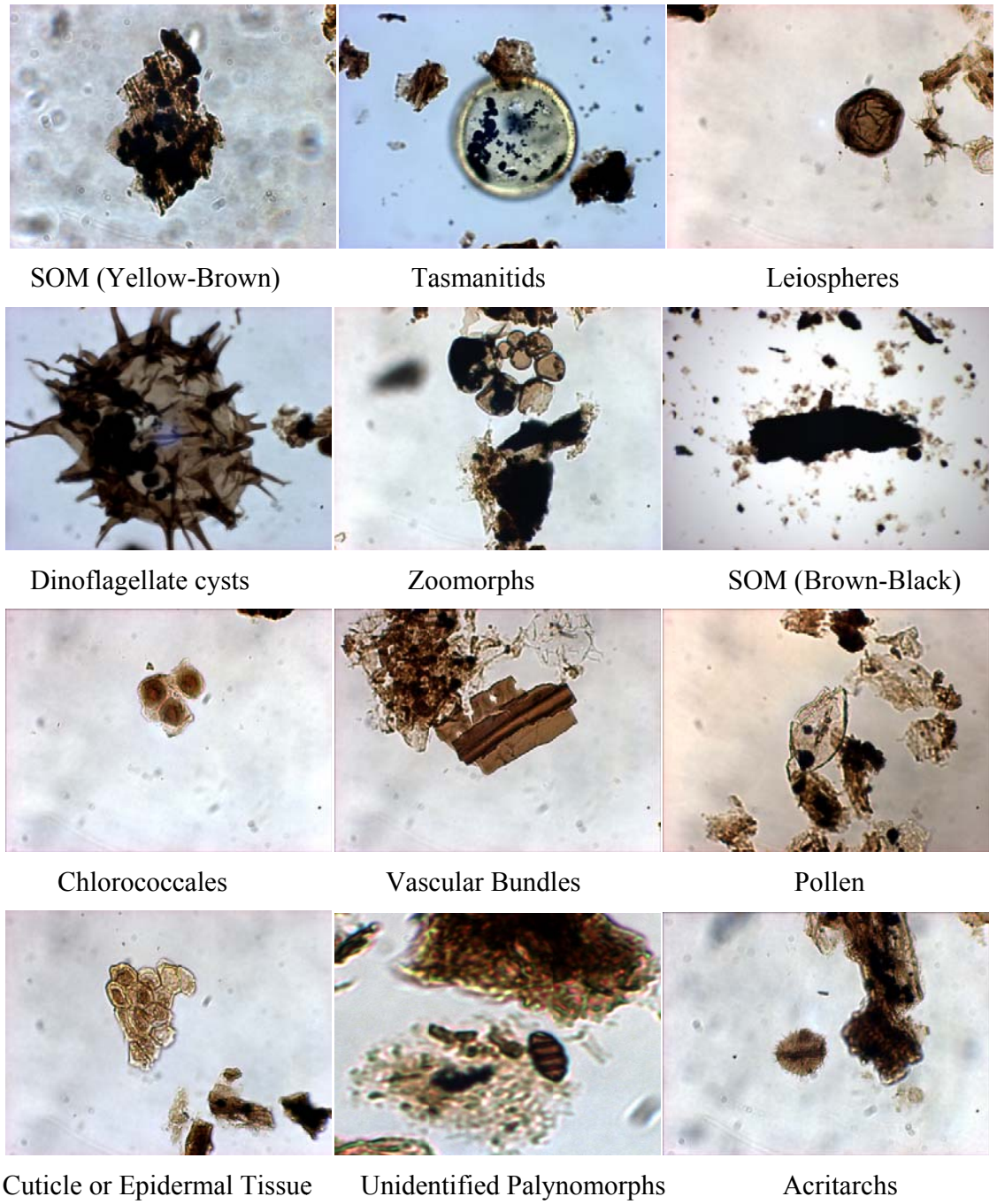

Figure 2.3. The various components of palynological sedimentary organic matter under observation of the microscope in transmitted white light

2.2.3 Carbon-isotope analysis and C/N ratios

Organic matter carbon

Bulk organic matter — Bulk organic C/N ratios and stable carbon isotope ratios were measured in the Stable Isotope Laboratory at Department of Geography and Geology, University of Copenhagen. Freeze dried samples were crushed with an agate mortar and pestle to <125 μm. Carbonate was removed by treating 1.2 g of sample with 30 ml 1% HCl, and heating on a hot plate for 1 hour. Acid treated sample was then transferred to a centrifuge tube, and washed with Milli-Q water and centrifuged. The sample was further washed until neutral pH, then freeze-dried and subsequently equilibrated to room temperature in eksikator. The equivalent of ~0.07 mg of pure carbon of the acid washed sample were weighed into a tin capsule. Stable carbon isotope composition and C/N ratio was measured on EuroVector elemental analyser coupled to an Isoprime dual inlet Stable Isotope Ratio Mass Spectrometer. Every tenth sample was run in duplicate and internal standards were interspersed throughout the batch of samples. Samples were single point calibrated toward a calibration curve made of 10 different weights of the internal laboratory standard, thus bracketing the pure carbon weights of the samples. The internal standard (AK of pure active carbon (-25.65 ‰) homogenized in mortar with clay sized pure quartz), has been calibrated to USGS-24 (-15.99‰), and tested by repeated random sampling of the homogenized mixture. Long-term reproducibility is ±0.1‰.

Phytoclasts — Isotope analyses of both bulk concentrated phytoclasts and hand-picked phytoclasts were carried out for this study. Hand-picked phytoclasts were manually separated from concentrated phytoclasts by using a needle under reflected-light microscope, and in this case only definite woody material was collected and accumulated to around 20–40 micrograms for each sample (quantities of hand picked phytoclasts were too small to yield valid C/N ratios). For bulk concentrated woody phytoclasts, dried sample weights ranged from 0.2 mg to 2 mg, depending on recovered quantity.

Phytoclast samples for analysis were dried, weighed and sealed in tin capsules. These samples were run on a Sercon Europa EA-GSL sample converter connected to a Sercon 20-22 Stable Isotope Ratio Mass Spectrometer running in continuous flow mode with a Helium carrier gas with a flow rate of 70 ml per min. Carbon isotope ratios were measured against an internal alanine standard ($\delta^{13}C_{alanine}$ = -26.9 ± 0.2‰ V-PDB) using a single point calibration at the Research Laboratory for Archaeology and History of Art (RLAHA), University of Oxford, UK. The in-house RLAHA alanine standard is checked weekly against USGS40, USGS41 and IAEA-CH6 international reference materials. Thus the reported results are traceable back to the V-PDB international standard.

Carbonate carbon

Carbon-isotope data were generated from planktonic foraminifers. Two sample sets were combined for the present study. One sample set was analysed in Oxford and comprised a subsample of planktonic foraminifers used for strontium isotope analyses (Browning *et al.*, 2013) originally picked by Mimi Katz (2013, personal commun.). A second set was

picked at Peking University and analysed at the University of California, Santa Cruz (UCSC).

The foraminiferal dataset comprises two parts, single species *Globigerina praebulloides* (surface dwelling, 43 samples, analysed at UCSC) and, due to lack of sufficient numbers of specimens, species mixtures analysed at Oxford comprising some or all of the following taxa: *Catapsydrax parvulus, Dentoglobigerina altispira altipira, Globigerinita glutinata, Globorotaloides suteri, Globigerina woodi, Globoquadrina baroemoenensis, Globoquadrina dehiscens, Globoquadrina. langhiana, Globorotalia (Menardella) archeomenardii, Globorotalia* (Neogloboquadrina) *continuosa, Globorotalia (Jenkinsella) mayeri, Globorotalia (Globigerinella) obesa, Globorotalia (Fohsella) peripheroronada, Globorotalia (Globoconella) praescitula, Globigerinoides obliquus, Globigerinoides sacculifer, Globigerinoides sicanus, Globigerinoides subquadratus, Globigerinoides triloba, Sphaeroidinellopsis disjuncta* (16 samples). At Oxford, species mixtures were gently crushed between small plastic plates to open the foraminifer chambers. A drop of methanol was added and each plate cleaned by ultrasonification for 30 minutes. Methanol was removed with a 2 ml syringe under a reflected-light microscope to ensure minimal inclusion of clay. Finally, the cleaned foraminifera were transferred by brush into vials and dried in an oven at 60°C. The typical sample weights were about 25-40 micrograms. Measurement was carried out on Thermo Scientific MAT 253 Stable Isotope Ratio Mass Spectrometer (online coupled to KIEL IV Carbonate Device) at the Department of Earth Sciences, University of Oxford. An overall external precision of 0.04 ‰ for $\delta^{13}C$ is reached for samples greater than 20 micrograms. All

carbon isotope ratios are expressed in per mil (‰) the internationally accepted standard notation, Vienna Pee Dee belemnite (VPDB).

Pyrolysis parameters

Total organic carbon (TOC, wt%) of each bulk organic matter sample was analysed by decarbonating the sample with HCl, whereafter 50 mg was combusted in a LECO CS-200 induction furnace. Hydrogen index of each sample was measured by pyrolysing 100 mg of de-carbonated sample in a Humble Instruments and Services source rock analyzer (SRA) system in the source rock laboratory at the Geological Survey of Denmark and Greenland. The SRA have been evaluated to give S1, S2, Tmax data comparable to the commonly used 'Rock-Eval' instrument (Espitalié *et al.*, 1977, 1985). Source rock screening data were quality checked and questionable data with TOC contents <0.5 wt.% and/or S2 pyrolysis yields <0.2 mg HC/g rock were omitted as organically lean samples give unreliable HI values (Peters, 1986).

2.3 Results

2.3.1 Palynofacies analysis to monitor the components of carbon-isotope measurements

After the procedure of density separation of the palynological particulates, the concentrated phytoclasts were obtained and checked by light microscope. The prevalence of woody phytoclasts was confirmed. Some of the larger cuticle fragments were also sedimented with the woody phytoclasts but do not dominate the assemblages (Figure 2.4).

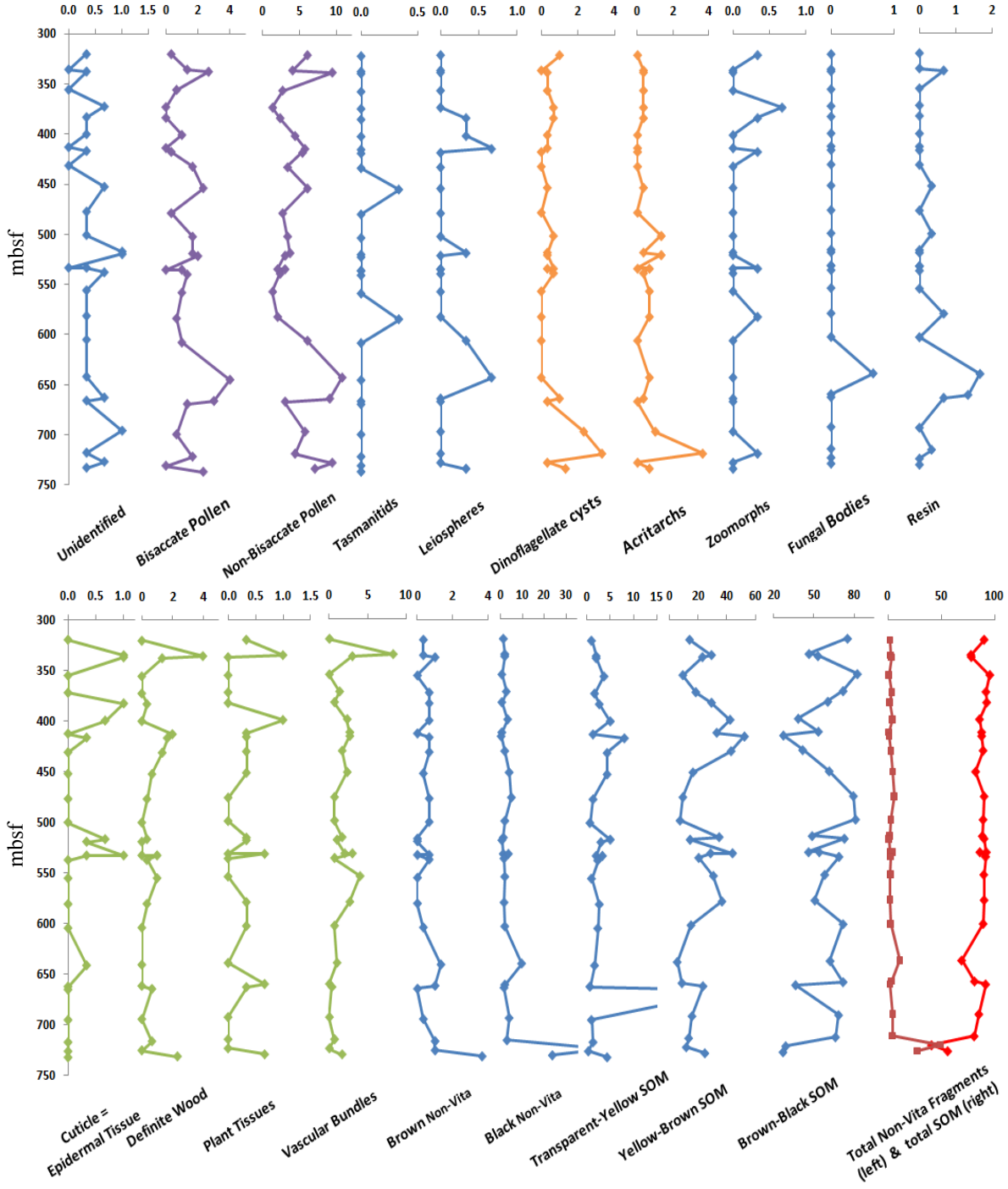

Figure 2.4. Percentage of the each palynological component against the depth (metres below seafloor - mbsf) at Site M0029 (28 samples for the palynofacies analysis). Y axis is the depth and X axis is relative percentage (%) of palynological particulates.

2.3.2 Carbon-isotope records

Carbon-isotope values for Site 29 are presented in Figure 2.5. The analyses are focussed at this site because, of the three Expedition 313 sites, initial expedition results indicated that succession at Site 29 provides the most complete and continuous sedimentary record over the interval of the Monterey Event (Mountain *et al.*, 2010; Browning *et al.*, 2013).

Column A in Figure 2.5 shows data from bulk organic matter, column B from planktonic foraminiferal carbonate, column C from phytoclast concentrates, and column D from individually picked phytoclasts. The following points for these data are most noteworthy:

1) The bulk organic matter data overall decrease from relatively heavy carbon-isotope values (-24 to -23 ‰) between 680 and 610 mbsf (Burdigalian) to lighter values up section. From 610 to 450 mbsf (Langhian to early Serravalian), carbon-isotope values are intermediate (-24 to -25‰) with small excursions within this range, each defined by several data points. Relatively light values (-26 to -25 ‰ occur above 450 mbsf (Serravalian). The majority of values are in the range -23 to -26 ‰. On average the bulk organic matter is enriched 0.5‰ relative to phytoclast measurements.

2) Data from planktonic foraminifers are quite variable and most range from 0-2 per mil. A few values exceed 2 per mil. They are basically pristine with being glassy cemented according to observation using reflected-light microscope and SEM (see images in

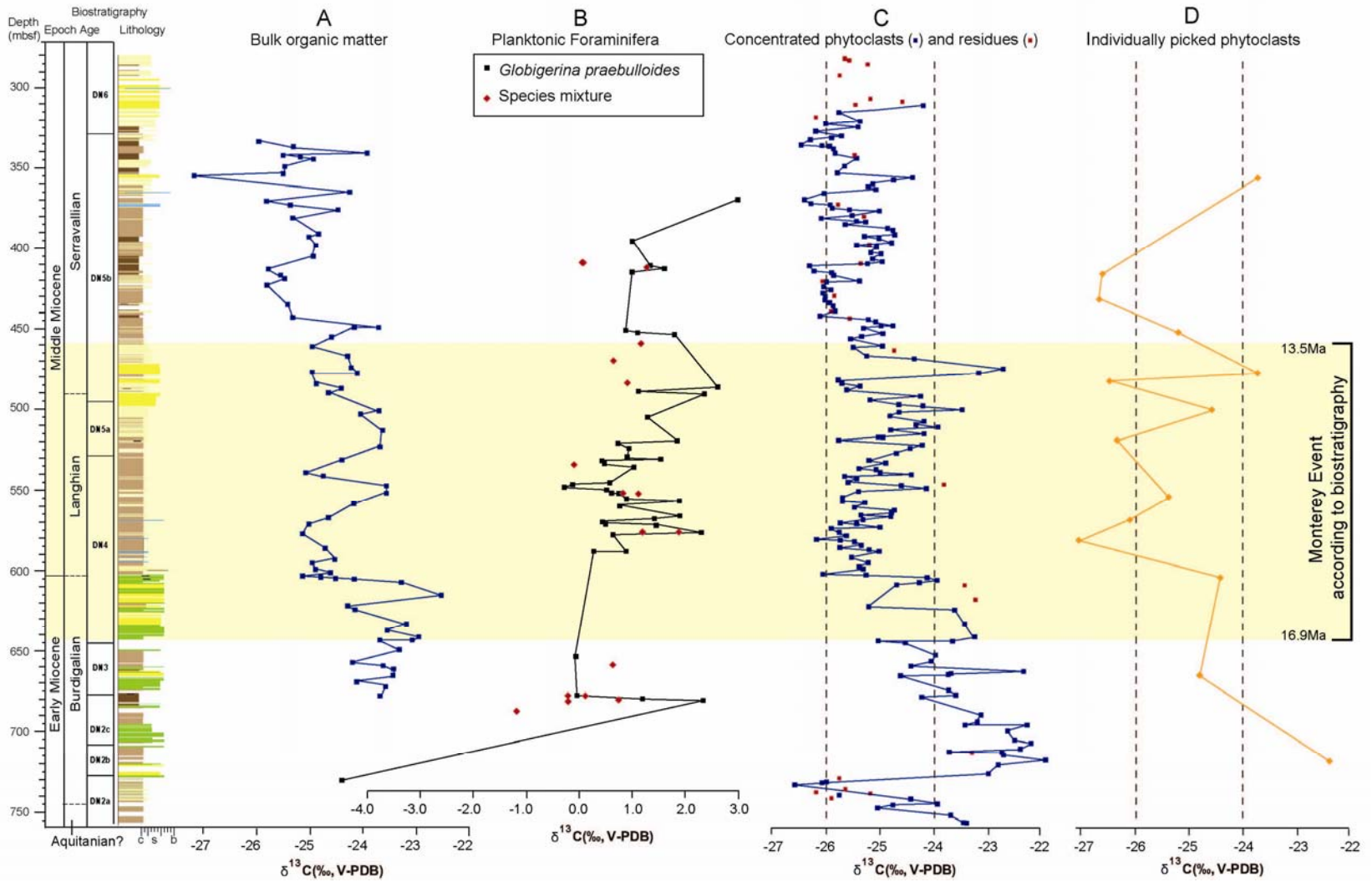

Figure 2.5. All carbon-isotope results for Site 29 set against lithological log. A. Bulk organic. B. Planktonic foraminifers, C. Concentrated phytoclasts and palynological residues. D. Picked phytoclasts (column D). Lithological log from Mountain et al. (2010), ages from Browning et al. (2013), and dinoflagellate cyst zonation from McCarthy et al. (2013). For key to graphic log refer to Figure 2.6.

Appendix B). Disregarding individual anomalous data points there is a very weak stratigraphic trend towards heavier carbon-isotope values up-section.

3). Data from the relatively low-resolution set of individually-picked phytoclasts show good conformity with data from phytoclast concentrates (as do analyses of raw palynological residues). Data from phytoclast concentrates show coherent stratigraphic trends. From 750 to 730 mbsf (?Aquitanian to early Burdigalian) carbon-isotope values become progressively lighter up-section (from -23.4 to -26.5‰). Between 730 and 610 mbsf (Burdigalian) carbon-isotope values are relatively heavy (-22 to -25‰). Above 610 mbsf (Langhian to Serravallian) carbon-isotope values are intermediate (-24 to -26‰) but also show coherent excursions within this approximate range. A notable positive excursion to -22.5‰ occurs at 475 mbsf, in the earliest Serravallian, which is not present in raw bulk organic matter. There is overall more isotopic variability in the phytoclast record relative to the bulk organic matter, as the standard deviations are 0.94 for phytoclast data and 0.85 for bulk data. However the overall trends are present in both records.

2.3.3 Correlation of phytoclast carbon-isotope curves between Expedition 313 Sites

In Figure 2.6 a correlation panel for all three Expedition 313 Sites in shown, including the more limited phytoclast data for sites 28 and 27. Correlation lines between sites are based on best-estimates of depths of key seismic stratigraphic surfaces, which take into account

all relevant geophysics, biostratigraphy and strontium-isotope stratigraphy (Miller *et al.*, 2013). Where data density is such that meaningful comparison is possible the same values and trends are apparent at different sites. This is particularly the case for Sites 28 and 29 for the Langhian to Seravallian interval. Where differences occur, as for example concerning the narrow positive excursion 475 mbsf in Site 29, the data can be explained by unconformity in the up-dip, more proximal location, an interpretation fully supported by the seismic stratigraphy (Proust, 2013, personal commun.).

Figure 2.7 shows the enlarged stratigraphic logs and carbon isotope curves from 615 m to 610 m at Site 28 and from 745 m to 725 m at Site 29 and the correlation line of sequence boundary m 5.7. The lithology dramatically changes across the sequence boundary. Below the boundary, lithologies are clay at Site 28 and Site 29; strata immediately above sequence boundary are glauconite sands at both sites, and upwards turn to less glauconitic sands. Carbon isotope curves from Site 28 and Site 29 show generally similar trends in this enlarged interval. Both rapidly change from light to heavy carbon isotope values through the boundary. The values for the lightest points are about -28‰ at Site 27 and about -27‰ at Site 29. It is concluded that the carbon-isotope signature of phytoclasts has value for correlation on at least the local scale of Expedition 313 sites.

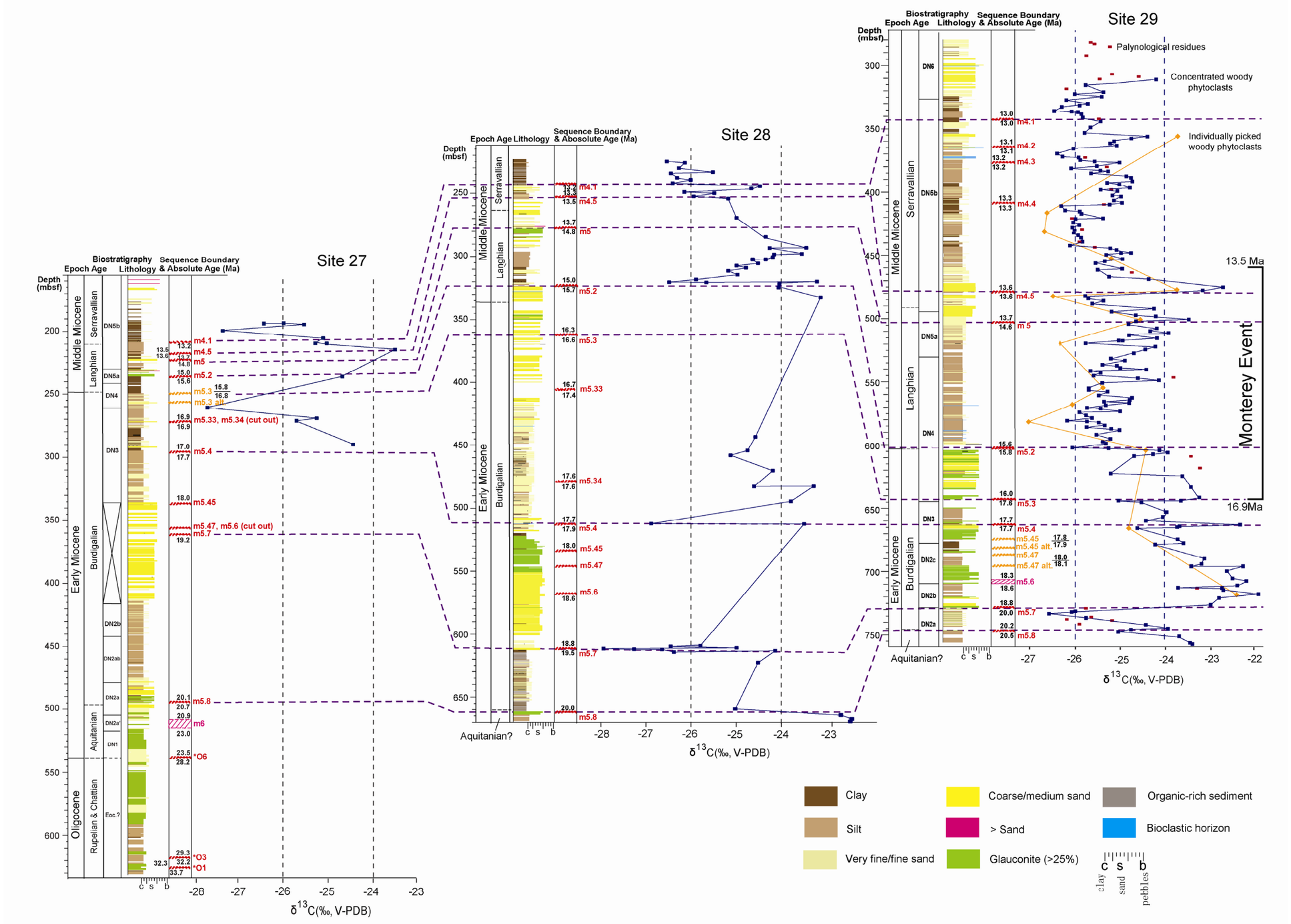

Figure 2.6. Correlation panel and concentrated phytoclast carbon-isotope records for Sites 27, 28 and 29. Correlations and ages from Browning et al., 2013 and Miller et al., 2013. Dinoflagellate cyst zonation from McCarthy et al., 2013. Oligocene sequence boundaries marked with an asterisk (*) are not resolvable on seismic reflection profiles (Browning et al., 2013).

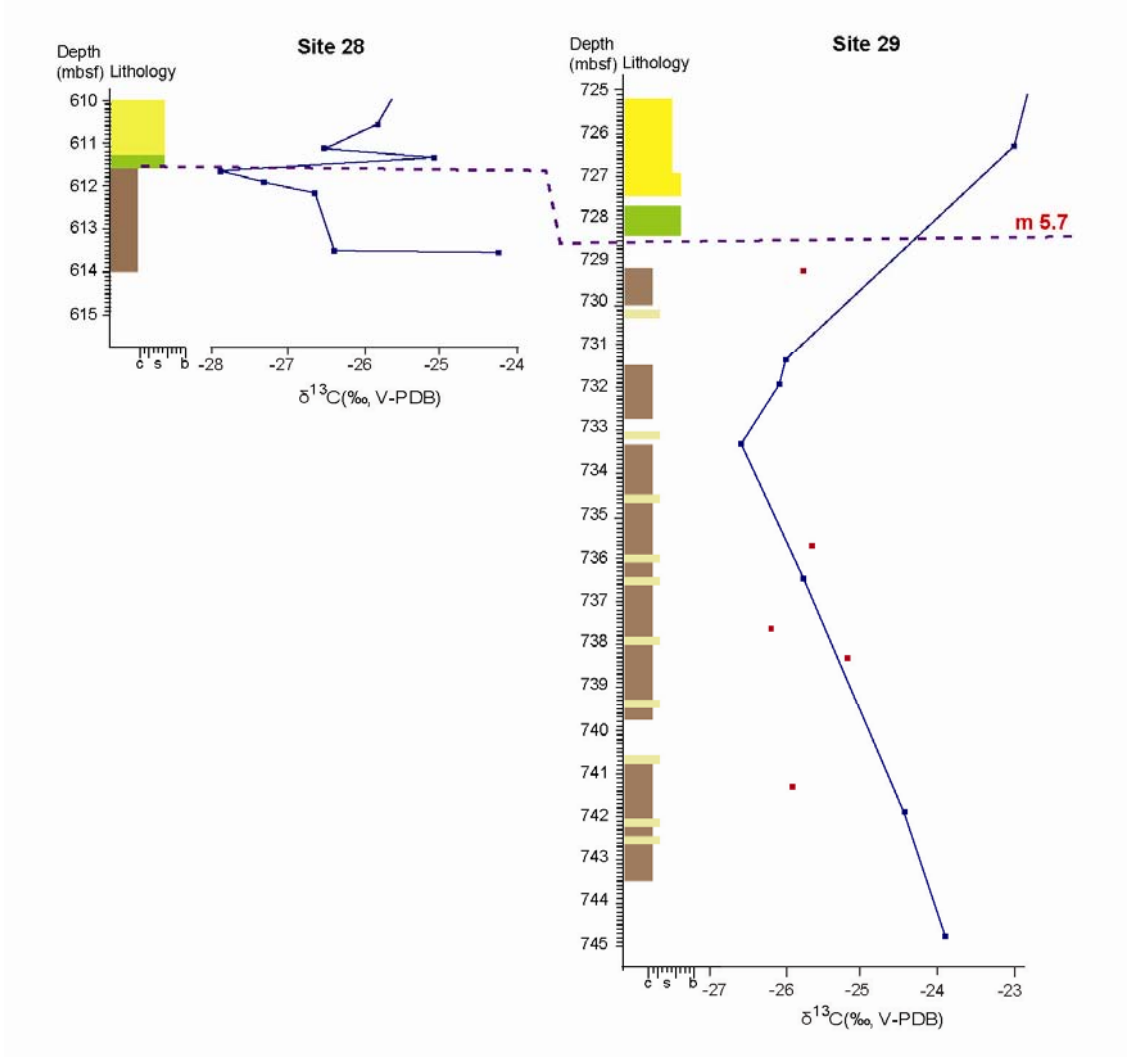

Figure 2.7. Enlarged stratigraphic logs and carbon isotope curves from 615 m to 610 m at Site 28 and from 745 m to 725 m at Site 29. Correlation line is sequence boundary m 5.7 based on the integrated stratigraphy (see text). See Figure 2.6 for key to graphic logs.

2.3.4 Pyrolysis data and C/N ratios

For pyrolysis, 27 samples were analysed from Site 27, 34 samples from Site 28, and 65 samples from Site 29. Pyrolysis data and C/N ratios show notable variation through the studied succession (Figure 2.8).

Hydrogen Index, Tmax, TOC and S2.

Pyrolysis data are included as Supplemental Data Files. Hydrogen index (HI) varies between 50 and 250 mg HC/g TOC (Figure 2.8), indicating the sediment is dominated by a type III kerogen, with some levels up to gas/oil prone (Peters, 1986, pp. 273). Tmax of ~420 °C with only a single samples with Tmax of 450 °C (at 597.5 mbsf) indicate that organic matter is still immature (Petersen *et al.*, 2011). Cross plot of TOC and the S2 peak indicates that the majority of the samples are below good/fair source rock potential, but that some of the more clay rich samples have good to excellent source rock potential because TOC > 2% and S2 > 6 mg HC/g rock (Peters, 1986; Petersen, *et al.*, 2011).

Stratigraphically the HI is highly variable up to 595 mbsf, and progressively increases from 180 to 230 mg HC/gTOC up to 502 m mbsf (Figure 2.8). HI is variable (50–200 mg HC/gTOC) between 500 and 460 mbsf and then shows steady values (150–170 mg HC/gTOC) up to 364 mbsf. Low values (~50 mg HC/gTOC) occur between 364 and 340 mbsf, but HI recovers to 100 mg HC/gTOC between 340 and 333 mbsf.

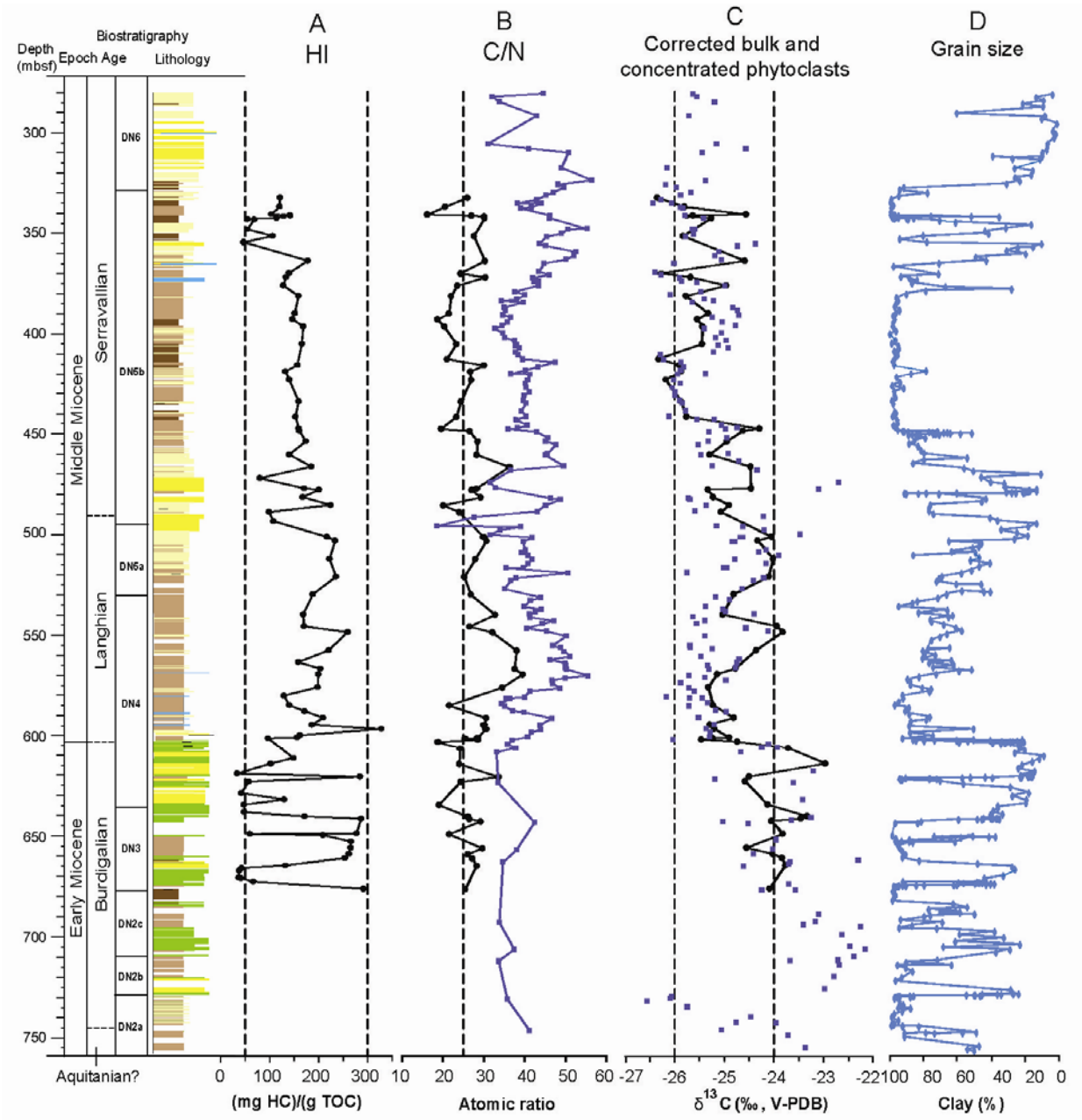

Figure 2.8. Comparison of relevant organic matter parameters for Site 29 (65 samples). A. Hydrogen index. B. C/N ratios of bulk organic carbon (black dots) and concentrated phytoclasts (blue dots). C. Adjusted (vascular plant matter equivalent) bulk organic carbon $\delta^{13}C$ (black dots), and concentrated phytoclast $\delta^{13}C$ (blue squares). D. Grain size expressed as % clay content (from Browning *et al.*, 2013). See Figure 2.6 for key to graphic log.

Only a weak correlation is present between HI and bulk organic C/N ratios. Only few samples have HI < 100 and have C/N ~20 ratios overlapping with general bulk organic C/N ratio. There is a tendency for high HI to be associated with enriched bulk $\delta^{13}C_{org}$ values. A few samples plot outside the general sample field in a crossplot of HI versus $\delta^{13}C$, these with HI <80 and heavy $\delta^{13}C$ values (-24 to -22.5‰) of both phytoclasts and bulk organic matter.

C/N ratios of bulk organic matter and separated phytoclasts

At Site 29, bulk organic matter C/N ratios (C/N_{bulk}) vary between 15 and 30, clearly distinguished from the C/N ratio of separated phytoclasts, which vary between 35 and 50 (Figure 2.8). (In the present study only C/N ratios of phytoclasts from samples processed in Southampton have been used to reduce the possibility of introducing artefacts related to processing method.) Stratigraphically, C/N_{bulk} ratios between 15 and 20 are related to coarse grain sizes (Figure 2.8). However, C/N_{bulk} ratios greater than 20 in some cases correspond to coarser grained sediment and in other cases they do not. The C/N_{bulk} ratios are relatively low in the sandy Burdigalian, increasing to high values in the Langhian strata where the sediments are fine grained. The Langhian/Serravallian boundary strata have variable C/N_{bulk} ratios, whilst the remaining Serravallian is characterized by low to moderate C/N_{bulk} ratios.

2.4 Discussion

If the dates assigned to strata from 640-725 mbsf (Browning *et al.*, 2013) are accepted then it appears that the Monterey carbon-isotope excursion, which is well established from diverse oceanic carbonate records, is not clearly developed in the organic-matter fractions analysed from the New Jersey Margin. The analysed terrestrial organic matter components have relatively heavy values in strata assigned to the Burdigalian, and relatively light values in the Serravallian, with intermediate values in the Langhian, somewhat contrary to expected trends of Monterey carbon-isotope excursion, especially with respect to the Burdigalian. In the following sections potential explanations for this observation are explored.

2.4.1 The $\delta^{13}C$ of bulk organic matter adjusted to vascular plant debris values

The $\delta^{13}C$ of bulk organic matter may be adjusted to represent the contemporaneous $\delta^{13}C$ of vascular plant debris (i.e. $\delta^{13}C_{vpc}$, where vpc refers to 'vascular plant, corrected'), a value that should in theory be very similar to the measured $\delta^{13}C$ of woody phytoclasts. A modest correlation is observed between phytoclast $\delta^{13}C_{phy}$ and $\delta^{13}C_{bulk}$ (slope = 0.8, r^2 = 0.5), suggesting that bulk organic matter is composed of a fraction of vascular plant debris (i.e. phytoclasts) (Figure 2.9A). In a cross-plot of organic $\delta^{13}C$ and C/N there is a clear spatial separation between bulk organic matter and phytoclasts, a pattern mimicking

that observed in modern deltaic/coastal-shelf sediments (Hedges *et al.* 1997; Figure 2.9B). Waterborne transport of particles from the land to the ocean combined with local marine production results in a mixing line between end-members of terrestrial vascular plant debris and marine organic matter (Hedges *et al.*, 1997). From this mixing relation it is common to calculate the fraction of vascular plant debris or marine organic carbon in the sediment. The observed C/N_{bulk} value between 20–30 suggests that between 60% and 80% of the organic matter is vascular plant debris. Further, using the mixing line concept, each sample $\delta^{13}C_{bulk}$ value is adjusted to a contemporaneous vascular plant debris $\delta^{13}C_{vpc}$ value using the measured $\delta^{13}C_{bulk}$ and C/N_{bulk}.

Isotope composition of end-members based on modern day organic matter cannot readily be applied to the Miocene. For example, Miocene marine organic matter has been reported with isotope composition of about -24 to -26‰, depending on location, relative to -22‰ today (Dieter-Haas *et al.*, 2009). However, it is no reason to suspect that C/N ratios of end-members have changed. In calculating an estimated vascular plant debris isotope composition on a point-by-point basis from bulk organic matter, the slope, α, of the mixing line between end-member mean compositions of vascular plant debris ($\overline{\delta^{13}C_{vpc}}$, $\overline{C/N_{vpc}}$) and bulk organic matter ($\overline{\delta^{13}C_{bulk}}$, $\overline{C/N_{bulk}}$) are first identified. (Eq 1; table 1; Figure 2.9B). Given the isotope composition of bulk organic matter at each point ($\delta^{13}C_{bulk}$), the isotope composition of the corresponding vascular plant debris ($\delta^{13}C_{vpc}$) can be calculated from the difference between C/N_{bulk} and the estimated mean vascular plant debris C/N composition ($\overline{C/N_{vpc}}$), assuming that linear mixing can be applied and that α is constant (Eq. 2, table 1). The best correlation between observed phytoclast $\delta^{13}C$

and estimated vascular plant debris composition ($\delta^{13}C_{vpd}$) is obtained with end-member mean compositions: $\overline{\delta^{13}C_{bulk}}$ = -24 ‰; $\overline{\delta^{13}C_{bulk}}$ = 25.3 ‰; $\overline{C/N_{bulk}}$ = 23; $\overline{C/N_{vpc}}$ = 42.

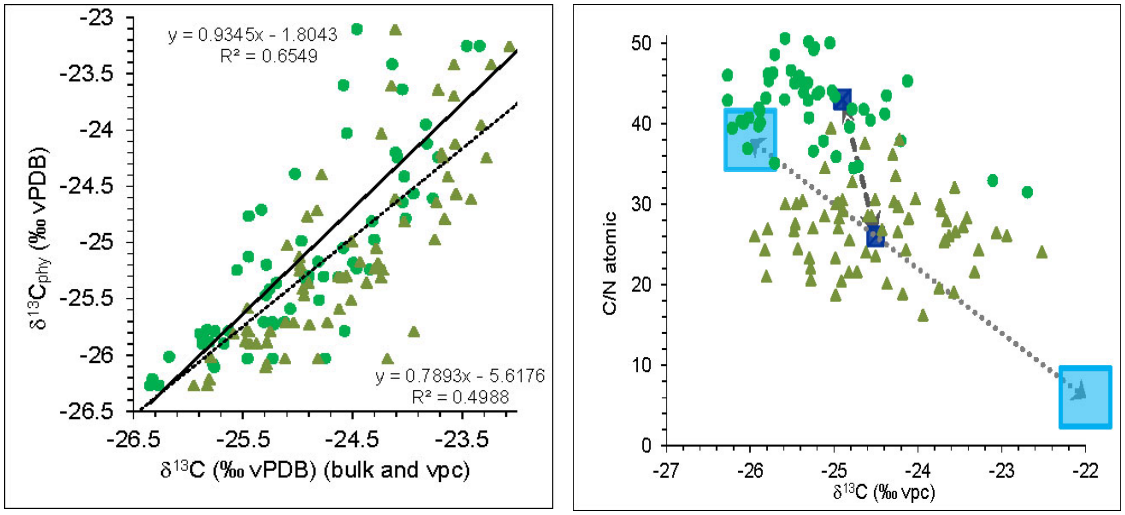

Figure 2.9. A. Carbon isotope composition of phytoclasts ($\delta^{13}C_{phy}$) versus bulk organic matter ($\delta^{13}C_{bulk}$, triangles) and calculated vascular plant debris end-members ($\delta^{13}C_{vpc}$, dots). Correlation between $\delta^{13}C_{phy}$ and $\delta^{13}C_{vpc}$ is stronger (slope=0.92, r^2=0.64) than between $\delta^{13}C_{phy}$ and $\delta^{13}C_{bulk}$ (slope = 0.78, r^2 = 0.49), showing that the bulk composition predominantly is a result of mixing between terrestrial and marine end-members. B. Atomic C/N ratios versus $\delta^{13}C$ of marine and terrestrial organic matter. Measured composition of phytoclasts (green dots) and bulk organic matter (green triangles) from marine sediments at Site 29. Light blue boxes represent modern end-members of vascular plant debris and marine organic matter, where shallow marine sediment samples exhibit a linear mixing between end-members (Hedges et. al., 1997). Model average mixing line between Miocene end-members (dark blue) resulting in the best fit between observed phytoclast composition and corrected bulk composition calculated from bulk organic matter. Model mixing line uses end-member composition of phytoclasts (C/N = 42, $\delta^{13}C$ = -25.3 ‰) and bulk organic matter (C/N = 23, $\delta^{13}C$ = -24.5 ‰) (see text for equations governing correction). The projected Miocene marine organic matter carbon-isotope value is inferred to have been significantly lighter than for the modern case.

The resulting correlation slope and r^2 between calculated vascular plant debris end-member and phytoclast composition is 0.9 and 0.7, respectively (Figure 2.9A). This correlation is better than the correlation between bulk organic matter and phytoclasts, suggesting that a mixing line indeed describes the bulk organic matter composition from two end-member compositions. The method is not perfect, because the mixing line is assumed to have a constant slope and fixed C/N ratio of the vascular plant debris end-member. C/N ratios can vary depending on the plant assemblage and average terrestrial degradation before the particles enter the marine realm. Bacterial decay of phytoclasts would result in relative N enrichment (Hedges *et al.*, 1997) impacting smaller particles more than the larger phytoclasts extracted and analysed here. Significant bacterial decay during transport and after deposition most likely would obscure the mixing line relation and the correction of bulk organic matter. Thus, the correlation between $\delta^{13}C_{phy}$ and $\delta^{13}C_{vpc}$ suggests that most of the primary stratigraphic trends in $\delta^{13}C$ of phytoclasts and bulk organic matter remain unobscured by transport and post-depositional bacterial degradation or diagenesis. These observations do not rule out significant alteration of chemical signatures over limited stratigraphic intervals.

2.4.2 Relationship between grain-size, glauconite content, and organic matter parameters

Stratigraphically there does seem to be a relationship between grain size and $\delta^{13}C_{phy}$ and $\delta^{13}C_{vpc}$ (Figure 2.8). Coarser grained sediments have organic matter more enriched in $\delta^{13}C$, while finer grained sediments tend to be relatively ^{13}C depleted. However, there are

fine-grained intervals with well-defined intermediate $\delta^{13}C_{phy}$ values, and stratigraphic trends in $\delta^{13}C_{phy}$ that are not reflected in grain-size trends (e.g. 380–410 mbsf).

Coarser grained sediments with HI = 50–100, in general have the most positive $\delta^{13}C_{phy}$ (473, 491–500, 602–617, 625–637, 649, 665–672 mbsf). These low HI values are associated with low C/N_{bulk} ratios, both potentially a result of bacterial degradation, with accompanying N enrichment at discrete stratigraphic horizons (e.g. Meyers, 1997, and references therein). It is particularly noteworthy that these low HI, low C/N_{bulk} values occur in strongly glauconitic sediments, the glauconite pointing towards prolonged reworking close to the seafloor prior to final burial. On the other hand, it is also noteworthy that intercalated muddy horizons have heavy carbon-isotope values that are combined with high HI (e.g. 650–665 mbsf). Thus, although terrestrial organic matter in the glauconitic sands may be strongly degraded by bacterial processes, this does not seem to have affected the carbon isotopic composition and, in any case as discussed below, degradation would not be expected to lead to heavier carbon-isotope values.

2.4.3 Degradation and diagenesis - general considerations

Because the various plant biopolymer components have different carbon-isotope values, change of the overall carbon-isotope values of terrestrial organic matter may take place during transport and deposition as chemical alteration takes place. Specifically, plant lipids and lignin (accounting for 22–36% of fresh biomass) are depleted in $\delta^{13}C$ by 2–5 ‰ relative to the whole plant $\delta^{13}C$ value, whereas cellulose and hemicelluloses (accounting

for 57–77% of the fresh biomass) are enriched in $\delta^{13}C$ by 1–2 ‰ relative to whole-plant tissue (Benner *et al.*, 1987), and proteins, accounting for a very small proportion of the biomass, are also isotopically relatively heavy (Deines, 1980). Compositional changes of plant matter continuously occur during transport from the source terrestrial plants through to eventual burial.

Generally, the biopolymer components in order of increasing degree of preservation potential are: proteins, cellulose, lipids, and lignin, in which the cellulose and lignin take up a large percentage, although depositional environment and history influence this order in some extent (Meyers, 1997; Gröcke, 1998, and references therein). Thus lignin is preferably preserved in sediments after undergoing early degradation and diagenesis (Stout *et al.*, 1988; Hatcher *et al.*, 1989a, 1989b). As a result of loss of cellulose, degradation and diagenesis will lead to a two- to three-fold increase in lignin content (Tyson, 1995, and references therein). As a result, the original $\delta^{13}C$ values of fresh wood undergo alteration towards lighter carbon-isotope values.

Alteration in $\delta^{13}C$ values seems to occur mostly at very shallow burial depths of < 1–4 m (Hatcher *et al.*, 1983; Spiker and Hatcher, 1984). Consistent shifts in $\delta^{13}C$ values are not commonly observed in thermally immature organic matter subject to deeper burial (Sackett, 1964; 1989; Hunt 1970; Dean *et al.*, 1986; Jasper and Gagosian, 1990).

In the present case it is observed that isotopically heavy phytoclast carbon-isotope values occur preferentially in the coarser (i.e. sandy) strata. It is in these coarser sediments that

stronger oxidation of organic matter might be predicted (e.g. Meyers, 1997) and, as discussed above, likely reflected in the low HI and low C/N_{bulk}. Therefore, if degradation and early diagenesis were responsible for the observed stratigraphic patterns in carbon-isotope values, these sandy sediments should contain isotopically lighter rather than heavier phytoclasts. In other words, the observed positive carbon-isotope excursions where it would be expected negative excursions if degradation were the principal control on isotopic values.

Preservation state of woody phytoclasts

Observation with a light microscope (both reflected and transmitted) reveals no significant difference in the appearance of phytoclasts recovered from different lithologies, such as sand versus mud (associated with the heavy and light carbon-isotope signature, respectively).

However, scanning electron microscope (SEM) observations do reveal some structural differences. A suite of samples from a range of lithologies at Site 29 were selected from the Early Miocene to Middle Miocene. The samples were chosen from lithologies representing lowstand and highstand (or transgressive) depositional environments. For each sample, three to four phytoclasts were randomly chosen and consistent ultrastructure were observed for these different pieces within each sample.

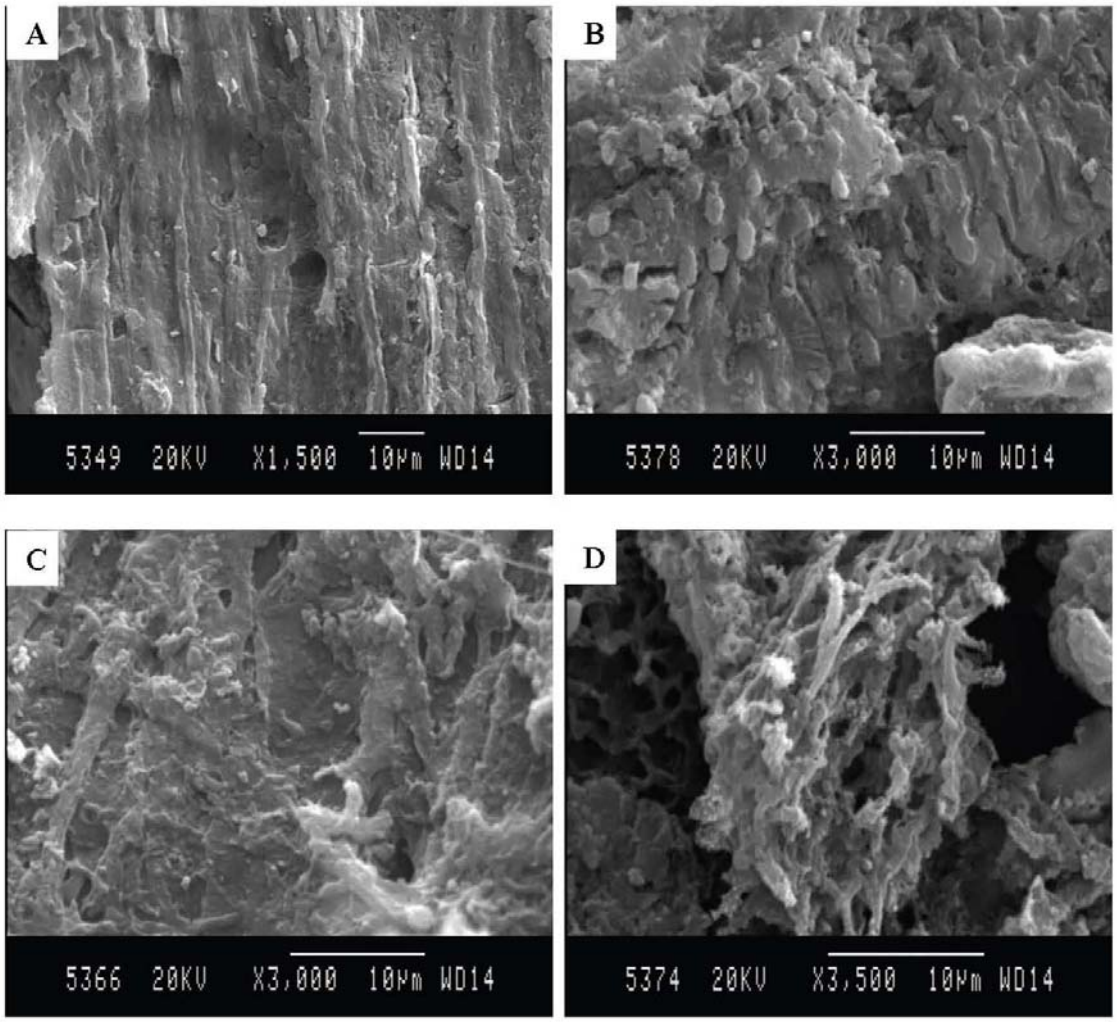

Figure 2.10. Scanning electron micrographs of selected woody phytoclasts. Some 10-20 phytoclast pieces were randomly selected from each sample. The fragments illustrated here are representative of those assemblages examined. A. Phytoclast showing good wood ultrastructural preservation, from mud 581.45 mbsf, $\delta^{13}C$ = -26.16. B. Phytoclast showing good ultrastructural preservation, from mud at 666.00 mbsf, $\delta^{13}C$ = -24.61. C. Phytoclast showing poor ultrastructural preservation, from sand at 500.71 mbsf, $\delta^{13}C$ = -23.47. D. Phytoclast showing poor ultrastructural preservation, from sand at 663.00 mbsf, $\delta^{13}C$ = -22.30. According to palynological analysis (Figure 2.11) the type of wood in the hinterland has not changed significantly through this stratigraphic interval and so the SE micrographs likely (but not definitively) show differences in preservation state for different species of wood.

Phytoclasts in the mud retain more structure than those in sand (Figure 2.10A, B), but eroded and coarse surfaces are dominant in the phytoclasts obtained from the sand (Figure 2.10C, D). This kind of selective preservation goes through the Early Miocene and the Middle Miocene, although there are obviously different sedimentary environments for the Early Miocene and the Middle Miocene in Site 29. The contrasting appearances of phytoclasts may be interpreted as reflecting differential degradation prior to burial.

However, the difference of preservation does not necessarily lead a bias of carbon-isotope values in phytoclasts if all the observed phytoclasts have lost most of their cellulose components. Furthermore, again, selective degradation of cellulose should lead to systematically lighter isotope values rather than the heavier values observed in the sands.

2.4.4 Carbonate carbon-isotope records in comparison to organic carbon isotope records

Whilst the carbon-isotope data for single species analyses and multiple species analysis are in close agreement, the overall dataset shows considerable scatter at closely adjacent stratigraphic levels. The scatter, taken together with the uneven stratigraphic distribution of data points, means that comparisons to the detailed structure of the organic carbon-isotope record is difficult (Figure 2.5). It is noted that throughout the Langhian interval the carbon-isotope values are similar but slightly lighter to those for the Monterey Event reported by Cheng *et al.* (2004) from the South China Sea. One apparently anomalous

isotopically light data point occurs at 730 mbsf (Figure 2.5). Although this value is < -4 ‰, and could therefore be entirely the result of diagenetic alteration, it corresponds stratigraphically to isotopically light values in the concentrated phytoclast fraction as well. Thus, this stratigraphic horizon may indeed also be recording an interval of isotopically light carbon in the whole exchangeable atmosphere-ocean reservoir.

2.4.5 Relation of carbon-isotope values to palynological indicators of environmental change

Changes in hinterland vegetation

Changes in hinterland vegetation might have occurred due to climate change. If different biomes were established through the Miocene interval in the sediment source areas, and these plant communities occupied environments that differed in key attributes such as soil moisture (e.g. Poole *et al.*, 2004), then contrasting carbon-isotope compositions might have resulted. As well as influencing the carbon-isotope compositions of organic matter from the same taxa, such environmental changes may also be characterised by changing dominance of plant groups with intrinsically different isotopic values such as gymnosperms (relatively heavy) versus angiosperms (relatively light) (e.g. Bechtel *et al.*, 2007; Holdgate *et al.*, 2009), or ferns with their even lighter carbon isotope values (e.g. Watkins *et al.*, 2007; Brearley, 2010). Contrasts in carbon-isotope compositions can also be caused by changes in the ratio between C3 and C4 plants with their different

photosynthetic systems, the latter mainly consisting of members of the Cyperaceae and Poacea families of sedge and grass.

The hypothesis of shifting biomes can be tested by analysis of palynological components throughout the interval in question with taxonomic composition translated into environmental preference (Figure 2.11). In this section any possible relationships between carbon-isotope values and palynological indices are examined according to the studies of Kotthoff (see Supplemental Data File) and McCarthy *et al.* (2013). Note that the data in Figure 2.11 are particle counts and are not equivalent to mass ratios; most mass is represented by the phytoclasts and on this basis mass ratios would be expected to be greater than indicated. However, some finer marine organic matter particulates may have been lost during sieving. Therefore T:M ratios derived from palynological counts cannot be linearly compared to mixing ratios derived from isotope and C/N values.

Eventual alteration of the pollen record through transport effects (e.g., over-representation of bisaccate pollen) can to a high degree be identified via the content of marine components (dinoflagellate cysts and foraminifer test linings) within the palynological samples: higher values of marine components indicate a longer site to shoreline distance and thus stronger over-representation of bisaccate taxa. In light of this, the high values of conifer forest pollen (dominated by bisaccate pollen) in the lowermost part of the examined interval from ~500 to ~740 mbsf at Site 29 are probably partly caused by transport effects, while other increases and the decrease at ~400 mbsf are true signals of vegetation change (Figure 2.11; McCarthy *et al.*, 2013).

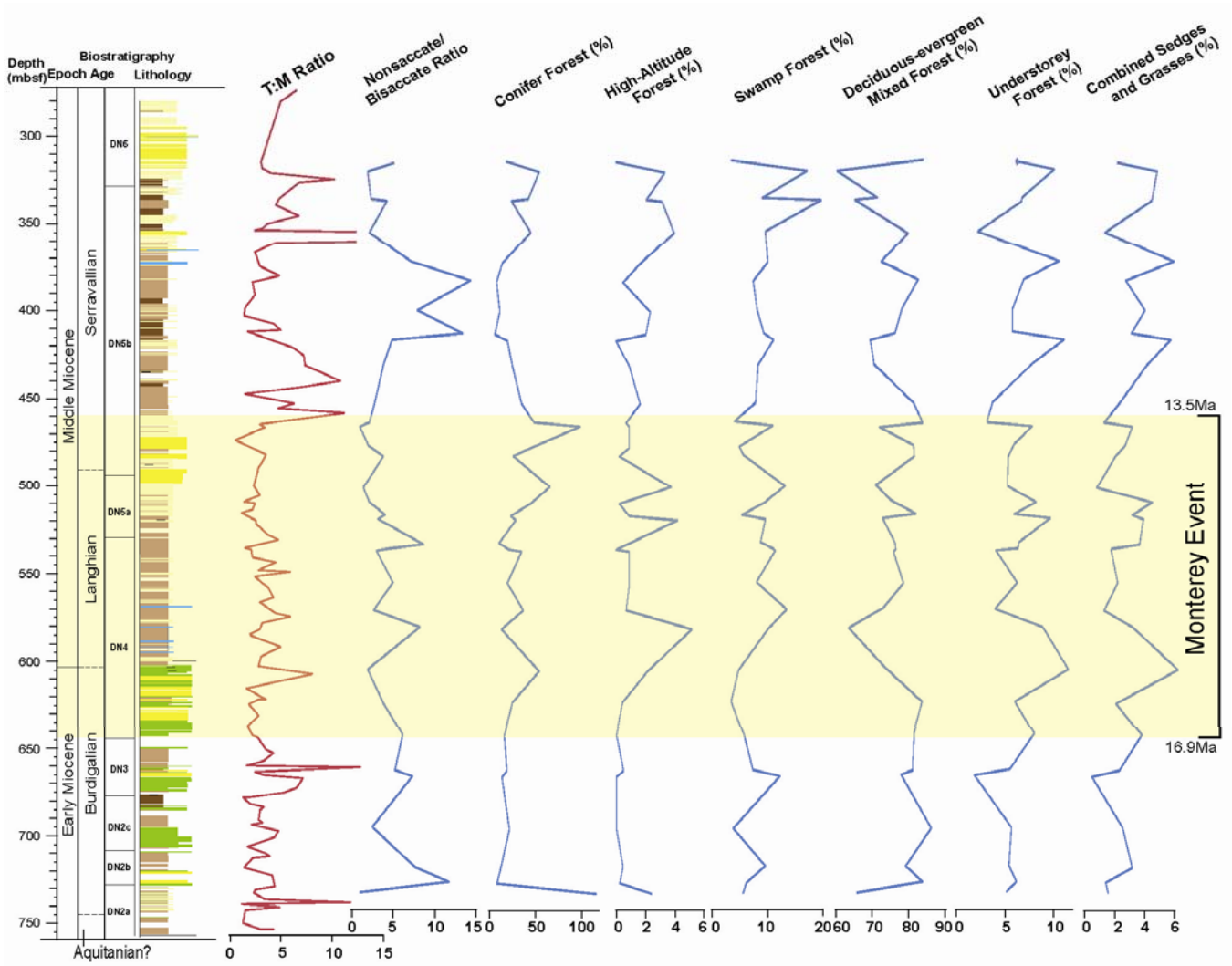

Figure 2.11. Key palynological indices for Site 29 (35 samples for palynological analysis, and 112 samples for T:M ratio). T:M is the ratio of terrestrial to marine components (McCarthy et al., this volume). Nonsaccate/Bisaccate ratio: ratio between pollen without sacci and with sacci (thus more effective airborne and/or floating transport). Pollen-percentages for conifer forest taxa (including bisaccate pollen), high-altitude forest taxa, swamp forest taxa, deciduous-evergreen mixed forest taxa, understorey plants, and combined sedges and grasses, are based on the total amount of nonsaccate pollen. See Supplemental data file for taxa and counts included in the respective

The non-saccate pollen percentages reveal no significant change in the hinterland vegetation: in some cases, deciduous-evergreen mixed forest pollen (dominated by oak and hickory) show small decreases which are paired with increases in swamp and/or understory vegetation (Figure 2.11). These environmental changes, as well as a notable expansion of conifer forests may be tied to climate changes but, if so, these are probably not of major impact.

Spores are very rare in most of the samples, generally less than 1.5 % of combined spores and pollen grains, except for two samples from ~733 and ~605 mbsf which have spores reaching ~5% of the terrestrial palynomorphs. This indicates that ferns and other spore-producing plants played a very minor role in the hinterland vegetation for the interval analysed, and phytoclasts analysed in this study must have been only rarely derived from ferns.

Percentages of Cyperaceae remain relatively stable over the whole interval, and Poacea pollen is virtually absent (combined as 'sedges and grasses' in Figure 2.11). Therefore, it can be excluded that changes in the carbon isotope values are mainly altered by changes in the C3/C4 plant ratio.

In summary, there are no overwhelming changes in palynomorph content that could explain the observed carbon-isotope ratios through major environmental changes in the sediment source areas.

Reworking of terrestrial organic matter from older deposits

Seismic stratigraphic evidence shows that there has been considerable erosion and re-deposition of siliciclastic sediments through successive relative sea-level cycles, and this may particularly have been the case during the Burdigalian (Figure 2.1). Both seismic stratigraphy and core sedimentology indicate a period of strong erosional degradation of recently deposited clinoform sediment bodies from about 19-18 Myr ago (Proust, 2013, personal commun.). The possibility therefore needs to be considered that older phytoclasts with heavier isotopic values have been reworked into sediments deposited at this time.

If reworking were a significant factor in explaining the observed carbon-isotope profiles, then it follows that Burdigalian deposits contain phytoclasts reworked from a period of overall relatively heavy carbon-isotope values, and/or that Langhian sediments contain phytoclasts reworked from a period of overall relatively light carbon-isotope values.

If it is assumed that reworking of recently deposited sediments then Langhian sediments may be predicted to contain an abundance of reworked Burdigalian pollen and spores, and Burdigalian sediments may be predicted to contain an abundance of reworked Aquitanian pollen and spores. Unfortunately there is little stratigraphic discrimination possible for Early to Middle Miocene pollen and spores, but at some horizons there is evidence from corroded palynomorphs that points to some degree of reworking, particularly in the interval between ~696 and ~642 mbsf (Burdigalian), with some samples showing relatively high rates of broken/corroded pollen grains. The thick mud-

dominated Langhian succession at Site 29 from 600-500 mbsf shows no similar direct evidence of incorporation for reworked terrestrial palynomorphs. Indeed, reworking during these times of relative sea-level rise and transgression, leading to a mud-dominated succession, would be very unlikely (cf. McCarthy *et al.*, 2003). It is concluded that reworking is unlikely to explain the observed stratigraphic patterns in phytoclast carbon-isotope values in the Langhian strata, although the possibility remains that reworked phytoclasts concentrated in the clinoform toe-of-slope facies may be affecting the Burdigalian carbon-isotope record.

2.5 Conclusions

Coherent stratigraphic trends and excursions in carbon isotope values are observed for a variety of sedimentary organic matter components of the Miocene from the New Jersey Margin, specifically: concentrated phytoclast separates, individually picked woody phytoclasts, and bulk organic matter adjusted on the basis of C/N ratios to be equivalent to vascular plant debris.

Assuming that the ages assigned to the analysed strata are correct, the terrestrial carbon-isotope stratigraphy for the New Jersey margin does not match well that previously described for the mid-Miocene Monterey Event, a positive carbon-isotope excursion, based on mainly benthic foraminifers from oceanic settings. Notably the Burdigalian sediments of the New Jersey margin yield a relatively heavy isotopic signature compared to Langhian sediments.

Explanations for the observed patterns of stratigraphic change may lie with reworking, degradation or diagenetic alteration, or floral change in the hinterland. However, there is little or no observational support for these explanations. Although degradation can be demonstrated on the basis of HI and SEM observation at certain limited horizons (especially characterised by the occurrence of glauconitic sand), these levels are notable for their relatively heavy carbon-isotope values, the opposite of what would normally be expected from selective removal of labile biopolymers. The most likely explanation for the observations is that phytoclast reworking has occurred in clinoform toe-of-slope

facies, but the reason for the resulting relatively heavy carbon-isotope values produced remains obscure.

2.6 Acknowledgments

Stephen Hesselbo acknowledges support from NERC (NE/F001428/1 - Miocene sea-level change and carbon cycling: New Jersey shallow shelf Expedition 313). Linhao Fang sincerely thanks the China Oxford Scholarship Fund (COSF), Burdett-Coutts Fund, and Wing Yip Bursary. Ulrich Kotthoff thanks the German Research Foundation for funding (DFG project KO 3944/3-1). Francine McCarthy acknowledges NSERC fellowships awarded to R. Zanatta and M. Drljepan who processed the palynological samples at Brock University. Christian Bjerrum acknowledges financial support from the Danish Natural Science Research Council (FNU) and Danish National Research Foundation (grant number DNRF53). We thank Mimi Katz and Jim Browning for making available planktonic foraminifer samples and grain size data. Discussion with Ken Miller and insightful comments from the referees are gratefully acknowledged.

Chapter 3

CARBON-ISOTOPE STRATIGRAPHY FROM TERRESTRIAL ORGANIC MATTER THROUGH THE EARLY TO MIDDLE MIOCENE, NORTH SEA BASIN AND ITS CORRELATION WITH COUNTERPARTS IN AGE, NEW JERSEY MARGIN (IODP EXPEDITION 313)

3.1 Introduction

The late Early to Middle Miocene is a vital step in the climatic transition from greenhouse into the icehouse during the Cenozoic (Flower and Kennett, 1994; Zachos *et al.*, 2001). This climatic transition is associated with a series of geological events, including: multiple global cooling events indicated by oxygen-isotope records derived from benthic foraminifera (Miller and Katz, 1987; Miller *et al.*, 1991; 2005) and the inferred East Antarctic ice sheet variations (Flower and Kennett, 1994; Kocsis *et al.*, 2009); closure of the eastern Tethys Ocean (Hsü, 1978) and restriction of the Indonesian Seaway (Kennet *et al.*, 1985); deep ocean circulation changes (Woodruff and Savin, 1989, 1991; Wright *et al.*, 1992); the Monterey Carbon Excursion Event (or the Monterey Event, in Zone N8-N11, 16.9-13.5 Ma) (Vincent and Berger, 1985; Woodruff and Savin, 1985; Flower and Kennet, 1994; Holbourn *et al.*, 2005, 2007; also see Section 2.1); Middle Miocene Climatic Optimum (MMCO) (in Zone N8, ~17.0-15.0 Ma) (Cifelli, 1969; Jenkins, 1973; Buchardt 1987; Miller *et al.*, 1987; Zachos *et al.*, 2001) and its influence on the evolution of Neogene terrestrial environments and biota (Flower and Kennet, 1994, and therein; Utescher *et al.*, 2000; Turco *et al.*, 2001).

In addition, a significant global redistribution of biogenic silica and carbonate deposition between ~18 Ma and ~12 Ma took place in the North Atlantic Ocean, the North Pacific, and Indian Oceans, so called 'silica switch' (Keller and Barron, 1983; Woodruff and Savin, 1989; Barron and Baldauf, 1990). The silica deposits significantly decreased in the North Atlantic Ocean but enhanced in the North Pacific and Indian Oceans, and the critical phase of this redistribution occurred in the Zone N8-11 (Flower and Kennett, 1994) equivalent to the period of the Monterey Event.

The Columbia River flood basalt province (CRB) represents the latest large continental flood basalt events in the Phanerozoic and coincides with a number of geological events, as previously stated. The huge volcanic episode yielded approximately 230,000 cubic kilometres of total eruptive volume through the late Early to Middle Miocene. Three primary eruption phases occurred from 16.6 Ma to 15.0 Ma, and two secondary eruptions took place about 14.5 Ma (Reidel and Hooper, 1989; Hooper et al, 2007). The large igneous provinces (LIPs) could have enormous potential environmental and climatic influences in Earth's history (Coffin and Eldholm, 1994; Olsen, 1999; Wignall, 2001). Therefore, the CRB likely played an important role in impacting environments and climate during the Early to Middle Miocene, although it is a relatively small LIP in term of total volume and emplacement rate (Coffin and Eldholm, 1994).

Given the geological background, can carbon-isotope stratigraphy based on terrestrial organic components be used for a stratigraphic correlation at both local and global scale? To address this question, the present chapter is a case study to explore the method of terrestrial carbon-isotope stratigraphy and to test correlation on the basis of terrestrial carbon-isotope curves from North Sea Basin with those from the New Jersey margin during the equivalent time intervals. A high-resolution biostratigraphy of the Miocene succession has recently become available (Dybkjær & Piasecki, 2010), primarily based on dinocyst zones but also combined with foraminifera zones and nanoplankton zones. In addition, absolute ages for these biostratigraphic subdivisions were proposed, in light of correlation from international zonations, and partly based on the strontium-isotope stratigraphy of mollusc shells (Dybkjear & Piasecki, 2010).

Moreover, climatic evolution during the Early to Middle Miocene has been recently investigated on the basis of palynological analysis of the materials derived from the Sønder Vium borehole (Larsson *et al.*, 2011). The results provide a good constraint on the source input which potentially influences interpretation of carbon-isotope data mainly derived from either palynological residues or the concentrated phytoclasts that are dominated by the fragments of terrestrial woody higher plants.

3.2 Geological setting in the North Sea Basin

3.2.1 Tectonic history

The North Sea Basin was initially formed by active rifting in the Triassic (Ziegler, 1990; Vejbæk, 1997). The active rifting resumed during the Middle-Late Jurassic and Early Cretaceous but then died down, leaving the North Sea Basin as a failed rift-system (Ziegler *et al.*, 1995; Møller and Rasmussen, 2003). During the Late Cretaceous and Palaeogene, basin inversion took place and the previous grabens were elevated. The tectonic inversion and present framework of the basin were led by two primary drives: 1) collisions between the African and the European tectonic plates characterized by the rise of Alpine Orogeny and numerous large structural changes around the North Sea Basin (e.g. Ziegler, 1990), and 2) the opening of the North Atlantic marked by increasing spreading rates of both the Aegir Ridge and the Kolbeinsey Ridge (Mosar *et al.*, 2002; Rasmussen, 2004a, 2009; Doré *et al.*, 2008). Subsequently, the subsidence of the northern North Sea chiefly resulted from relaxation due to a following rifting (Donato and Tully, 1981; Dimitropoulos and Donato, 1982).

Since 22 Ma the North Sea has been a silled basin connected with the Atlantic Ocean only by a narrow strait between Shetland and Norway (Figure 3.1). Thus the North Sea Basin became an epicontinental basin surrounded by landmasses, including the Fenno-Scandian Shield around the north-east, the Rheinish- Bohemian Massif to the south, and landmasses probably covering most or all of present day England, Scotland, Northern Ireland and the Shetland Isles, towards the west (Ziegler, 1990; Knox *et al.*, 2010) (Figure 3.1).

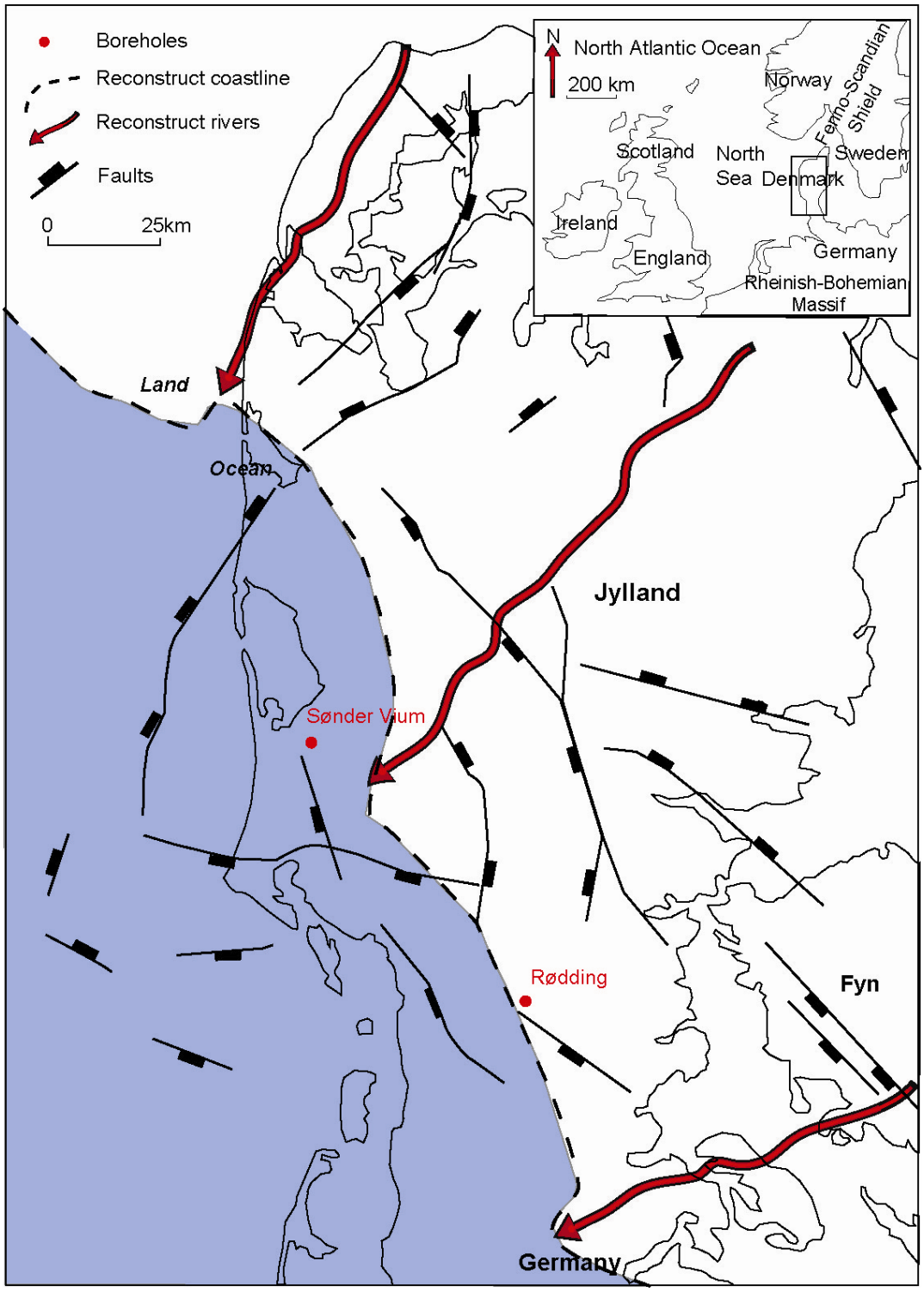

Figure 3.1. Location of the onshore Rødding and Sønder Vium wells in Jylland, Denmark and the reconstruction of the Early to Middle Miocene coastline and rivers (compiled from Rasmussen, 2004b; Rasmussen *et al.*, 2010) and the reconstructed palaeo-coastline and faults (simplified from Michelsen *et al.*, 2003; Dybkjær and Rasmussen, 2007; and Rasmussen et al, 2010, pp. 80-87).

3.2.2 Sedimentology and stratigraphy

Both worldwide and local tectonism influenced the Miocene sedimentation succession in the North Sea Basin (Rasmussen, 2004a, 2009; Potter and Szatmari, 2009). During the Miocene, fluvio-deltaic depositional system dominated at the study area in the vicinity of Jylland. Based on a combination of seismic data, geophysical logs, sedimentary facies analysis and biostratigraphy (primarily on dinocysts) from both onshore and offshore materials, the Miocene succession is divided into six sequences, A to F (Rasmussen, 2004b) (Figure 3.2) .

From the topographically elevated Fennoscandian Shield sediments were shed southward into the eastern North Sea Basin. Marked uplift of modern Norway commenced in the late Tertiary and thus formed an important source area for the eastern North Sea Basin during the Miocene. The margins of the Fennoscandian Shield noticeably uplifted during the early Neogene based on apatite fission track dating (Rasmussen, 2009). Sediments were transported to the North Sea Basin from the present Norway. The large rivers and delta systems of the earliest Miocene developed around northern and central present Jylland (e.g. Rasmussen, 2009; Rasmussen *et al.*, 2010). The depositional sources were supplied by the two or three major river systems in the study area through the Early to Middle Miocene. There rivers were running generally from the NNE to SSW (Figure 3.1). The sedimentary architecture of the fluvial-delta system was built up around the coast which was aligned northwest-southeast.

The enhanced sediment supply was partly caused by the tectonic uplift on the Fennoscandian Shield margins and subsidence around the basin central area, and partly by the warm climate,

i.e. the MMCO (Zachos *et al.*, 2001), although there were at least two high-frequency cooling events in period of the MMCO.

The Miocene succession in the study area comprises several transgrassive and regressive cycles, resolved into five depositional sequences which were driven by effects of both global sea level change and local tectonic activity. These sedimentary sequences are presented in Figure 3.2. The earliest Miocene deposits are transgressed by organic-rich, restricted marine clays (Larsen and Dinesen, 1957; Sorgenfrei, 1958; Rasmussen *et al.*, 2010) and then fluvio-deltaic sands in the Aquitanian (Rasmussen, 2004a, b; Rasmussen *et al.*, 2010). Afterwards, a minor transgression accumulated the Aquitanian marine clay and prodelta sediments (Rasmussen, 1961; Rasmussen *et al.*, 2010) and followed sedimentary wedge (Rasmussen *et al.*, 2010), which represents a second progradation of a delta complex in the Early Miocene. This sequence was overlain by the marine, clay-rich deposits in the Burdigalian (Sorgenfrei, 1958; Rasmussen *et al.*, 2010). The third and final prograding shoreline led by uplifting the hinterland took place at the Early to Middle Miocene transition (boundary between the Burdigalian and the Langhian) and is characterized by coal-bearing strata (Rasmussen, 1961; Koch, 1989; Rasmussen *et al.*, 2010).

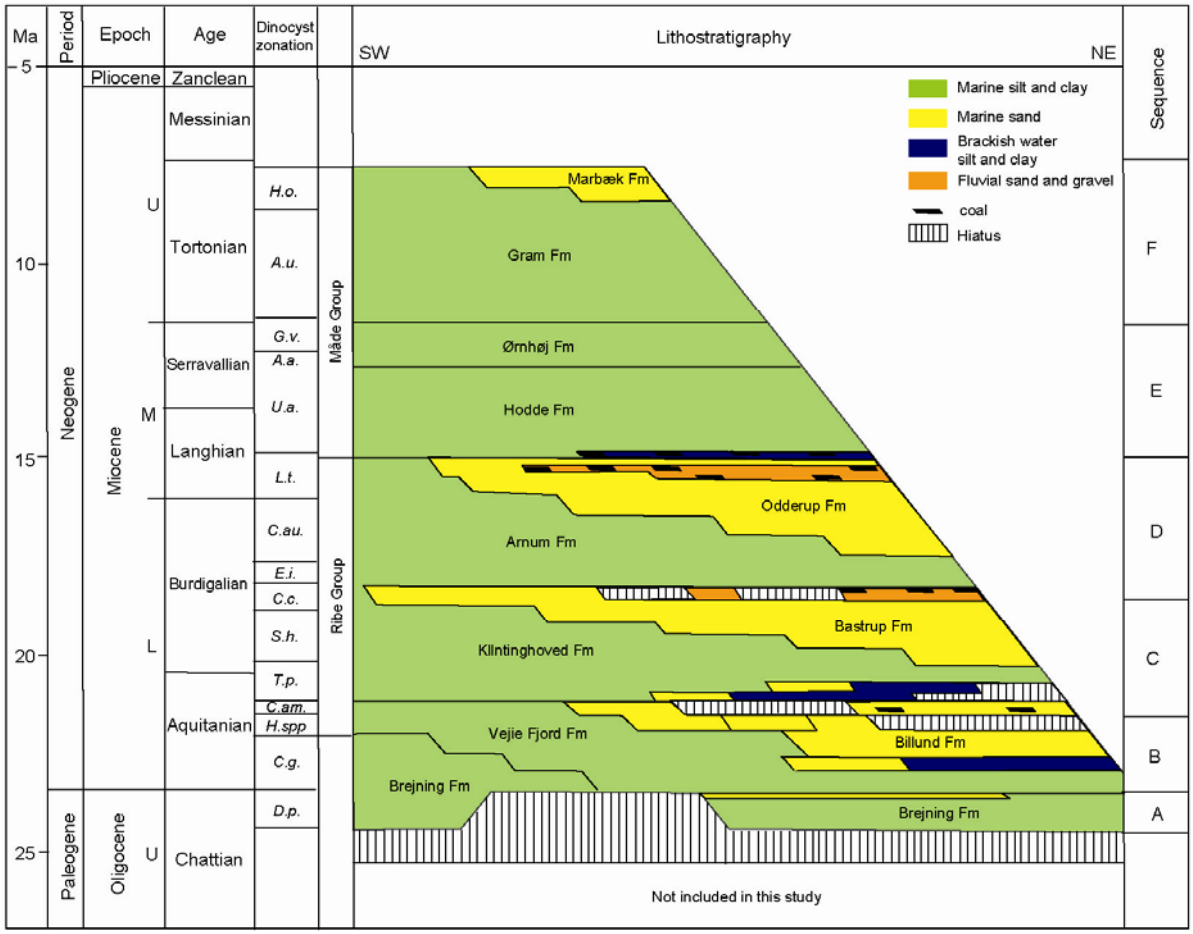

Figure 3.2. Lithostratigraphy of the onshore Danish Miocene succession. The age of the succession is indicated at the left and the sequence stratigraphy is shown at the right (after Rasmussen *et al.*, 2010).

Large areas of the North Sea Basin underwent an increased subsidence (Koch 1989; Ziegler 1990; Clausen *et al.*, 1999; Rasmussen, 2005) during the middle Middle Miocene to early Late Miocene (the late Langhian to Tortonian), and thus fully marine deposition dominated by clays widely occurred (Rasmussen, 1961; Piasecki, 1980, 2005; Rasmussen, 2004a, 2005; Rasmussen *et al.*, 2010). Synsedimentary normal faults were associated with tectonic subsidence and these normal faults largely controlled the sedimentary architecture along the Jylland coast in the North Sea Basin. Specifically, sediments are thinned in the footwall of synsedimentary normal faults, while thickened in the hanging wall (Figure 3.1 and Figure 3.8). Both the Rødding and Sønder Vium wells are located on the footwall of synsedimentary

normal faults (summarized form Figure 3.1 and correlation panel in Plate 1 to Plate 8, in Rasmussen *et al.*, 2010). Therefore, the sediments in the late Langhian to Tortonian are conformable but very condensed in both the Rødding and Sønder Vium wells.

3.2.3 Rødding and Sønder Vium wells

The locations of the Rødding and Sønder Vium wells during the Miocene varied in the marine or marginal-marine environment through time, but the Rødding well has a relatively proximal setting. The palaeocoastline is inferred to be north of Jylland and south of the present Norwegian coast (Figure 3.1; Michelsen *et al.*, 2003; Dybkjær and Rasmussen, 2007; and Rasmussen et al, 2010, pp. 80-87). Marine clay and clayey silt occurs in the latest Oligocene (the late Chattian). In the overlying strata, Aquitanian sediments are also dominantly clay and clayey silt, but with intermittent interbeds of fine-grained sand and rare medium-grained sand. Upwards, the Burdigalian sediments are primarily clay and clayey silt in the lower parts and medium-grained sand, gravel and coal in the upper parts. In the Langhian, the regressive facies succeeded from former very shallow deposits. The sediments are fine-grained sand and upwardly coarsen into the gravel and medium-grained sand. At the upper most parts of the Burdigalian, sediments turn into transgressive marine clays and clayey silt from gravel and fine-grained sand. From the Serrevallian onwards, the study area was located in the footwall of synsedimentary normal faults when undergoing a regional reactive subsidence. Although global eustatic sea level was rapidly falling during this epoch, relative sea level was rising in the Rødding well area due to regional subsidence, and thus marine clay and clayey silt was deposited. However, deposits in the Rødding well during the Serrevallian and Tortonian tended to bypass, because of the footwall setting. Therefore,

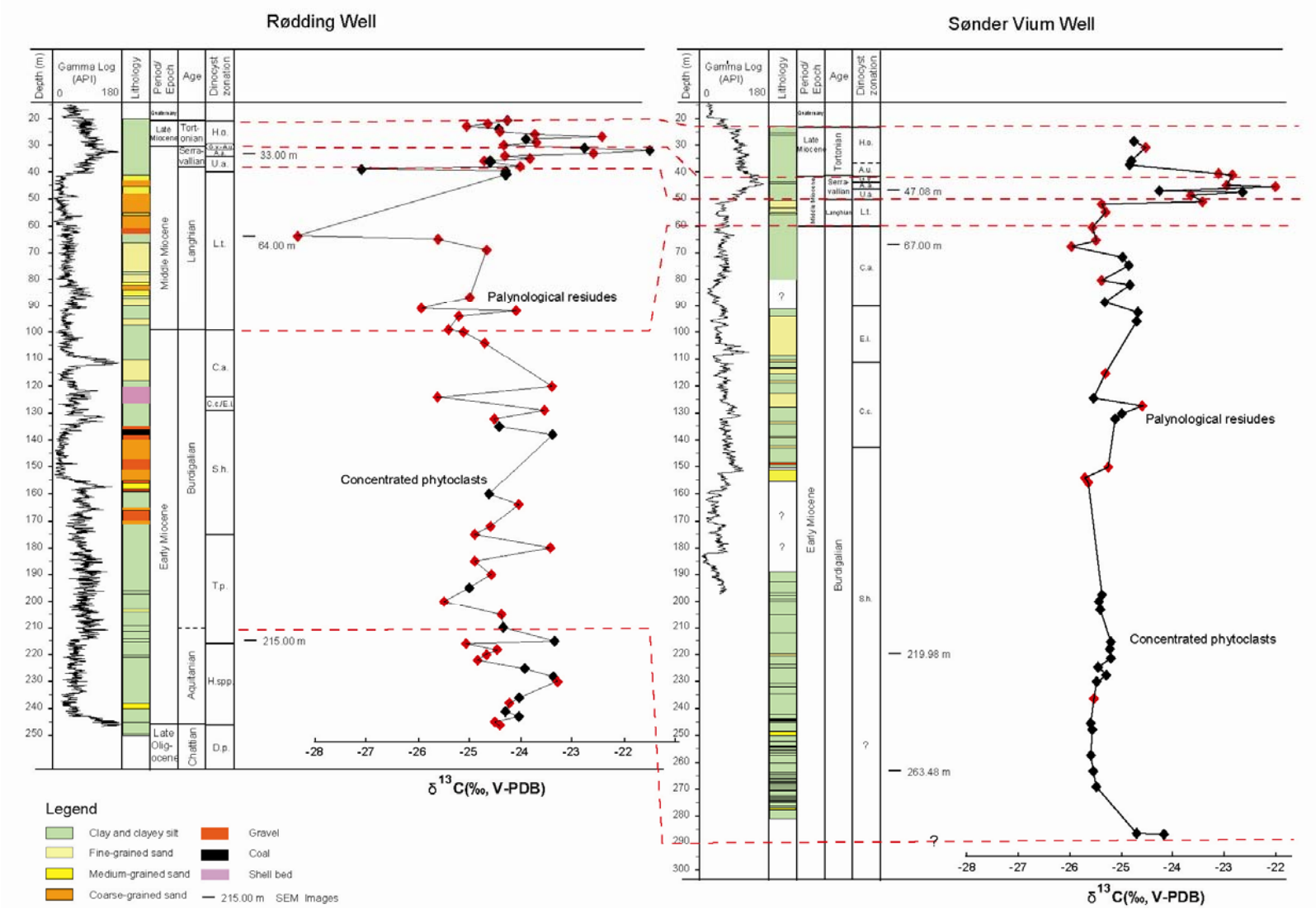

Figure 3.3. Local correlation of carbon-isotope stratigraphy between the Rødding and Sønder Vium wells, based on biostratigraphy (primarily on the well established dinocysts zonation)

sediments in the Serrevallian and Tortonian both are very condensed marine clay and clayey silt (Figure 3.3).

The Sønder Vium well is also located in a proximal part of the basin, but more distal than the Rødding well (Figure 3.1). The Burdigalian sediments are primarily clay and clayey silt in the lower parts with common inter-bedded fine-grained sand, and grading into fine-grained sand in the upper part. In the upper most Burdigalian, sediments are transgressive marine clay and clayey silt. In the Langhian, Serrevallian and Tortonian, the Sønder Vium well was located in the footwall of synsedimentary normal faults due to the regional tectonics. Therefore, the sediments in the Langhian are condensed marine clay and clayey silt in the lower parts and fine-grained sand in the upper parts; while the Serrevallian and Tortonian both are characterized by very condensed marine clay and clayey silt (Figure 3.3).

3.3 Biostratigraphy

The Miocene dinocyst biostratigraphy in the North Sea Basin has recently been intensively refined and correlated with the North Atlantic and revised Northwest European zonations, based on a combination of new data from onshore boreholes, offshore boreholes and outcrops around the eastern North Sea Basin, Denmark (Dybkjær and Rasmussen,2007; Dybkjær and Piasecki, 2010). The refined zonations have been also independently calibrated with foraminifer and nannoplankton biostratigraphy (Dybkjær and Piasecki, 2010).

The biostratigraphy and chronology of the Rødding and Sønder Vium wells in this study are provided and examined by our collaborator Karen Dybkjær who is following the most updated biostratigraphic work for the Danish Miocene successions (Dybkjær and Piasecki, 2010). Therefore, the carbon-isotope stratigraphic correlations in this chapter are referred to the most updated chronologic and biostratigraphic schemes.

3.4 Materials and palynological methods

3.4.1 Materials

The samples studied here were collected from the onshore Rødding and Sønder Vium wells on the Danish peninsula of Jylland (Figure 3.1). A total of the 62 core samples from the Rødding well were processed. The 19 samples concentrated by the density separation from raw palynological residues (Figure 3.3, black diamond) and the 43 samples of raw palynological residues (Figure 3.3, red diamond) were analysed. A total of 49 core samples from the Sønder Vium well were analysed, comprising the 30 samples of concentrated phytoclasts (Figure 3.3, black diamond) processed by density separation from raw palynological residues, and the 19 samples (Figure 3.3, red diamond) of raw palynological residues (see the detailed procedures of density separation in Section 2.2).

The phytoclasts are components of palynological preparation residues made up of recognizable fragments of plant cuticles and woody tissue (Tyson, 1995; Hasegawa *et al.*, 2003), and herein the concentrated phytoclasts primarily consist of woody tissue components (also called woody phytoclasts) derived from the raw palynological assemblages. The technique of separation takes advantage of the difference in settling rate between the phytoclasts and the microfossils. After this concentration, the marine fraction (dinoflagellate, zoomorphs and chlorococcales) and the terrestrial pollen and spores, which tend to be hollow and very small, are largely excluded, leaving the terrestrial phytoclasts (more see Section 2.2.2).

3.4.2 Palynological preparation

Samples were prepared at the Geological Survey of Denmark and Greenland (GEUS) by Karen Dypkjaer in Copenhagen, Denmark. Standard palynological techniques were used to extract organic matter from sediment samples, including treatment HF (60%) and HCL (30%) to dissolve silicates and heavy liquid separation to remove the undissolved mineral matter. The residues were sieved using an 11 μm mesh, and mild oxidation with dilute nitric acid was carried out (method in Larsson *et al.*, 2010).

3.4.3 Carbon-isotope measurement

Phytoclast samples for analyse were dried, weighed and sealed in tin capsules 5 x 8 mm. These samples were run on a Sercon Europa EA-GSL sample converter connected to a Sercon 20-22 Stable Isotope Ratio Mass Spectrometer running in continuous flow mode with a Helium carrier gas with a flow rate of 70 ml per min. Carbon isotope ratios were measured against an internal alanine standard ($\delta^{13}C_{alanine}$ = -26.9 ± 0.2‰ V-PDB) using a single point calibration at the Research Laboratory for Archaeology and History of Art (RLAHA), University of Oxford, UK. The in-house RLAHA alanine standard is checked weekly against USGS40, USGS41 and IAEA-CH6 international reference materials. Thus the reported results are traceable back to the V-PDB international standard.

3.5 Results

Carbon-isotope analyses of the present study are summarized in Figure 3.3 where they are set against the lithological and downhole geophysical log data from the Log Report of Rødding Well and the Log Report of Sønder Vium Well, GEUS, Copenhagen. In addition, the long-distance correlation between the North Sea Basin and New Jersey are presented in the Figure 3.4, the trends of carbon-isotope stratigraphy are marked by arrows, and the intervals rich in glauconite occurrence are highlighted by the green shadows.

3.5.1 Local correlation in the North Sea Basin

In Figure 3.3, the dashed correlation lines follow boundaries of biostratigraphy, primarily based on dinocysts. The carbon-isotope stratigraphy from the two boreholes shows basically coherent trends and similar characters: 1) carbon-isotope values in the Langhian are lighter than those in the Burdigalian in the Rødding Well and the only two points in the Sønder Vium Well during the Langhian are not heavier than the average values in the Burdigalian; 2) in the Serravallian and Tortonian intervals, the carbon-isotope values are relatively heavy and the maximum $\delta^{13}C$ values of approximate by -22‰ in the Rødding and Sønder Vium wells both occurring in the Serravallian; and 3) the maximum heavy carbon-isotope values in both wells coincide with the peak of high gamma values and both occur in the condensed interval during the Serravallian.

By contrast, some differences between two boreholes are observed as well. The lightest $\delta^{13}C$ value from Rødding is about -28‰ in the L.t. dinocysts zones, but the counterpart records in Sønder Vium are absent probably because of only two data points. In the local context, the

carbon-isotope stratigraphy from two boreholes shows basically correlatable characteristics. However, for the Early Miocene Burdigalian interval, the $\delta^{13}C$ values from Rødding are consistently heavier than those in Sønder Vium by about 1-2‰. Additionally, in this interval, the systematic fluctuation (probably cyclostratigraphic cycles) of carbon-isotope values is documented on the higher frequency and amplitude in Rødding than in Sønder Vium.

3.5.2 Correlation between the North Sea Basin and New Jersey

The long-distance correlations are principally based on biostratigraphy (Dybkjær and Piasecki, 2010), which has been already calibrated to the seismic stratigraphy and strontium-isotope stratigraphy. Although correlations are based on the integrated dataset, in practice the priority order of correlation lines is as follows: the defined Epoch boundaries, biostratigraphic zone boundaries and local sequence boundaries. Therefore, the long-distance correlation between boreholes from New Jersey and North Sea Basin are established based on their Series and Stage boundaries with the highest priority. That is why some inconsistency can be seen, if correlation lines are only examined by biostratigraphic zone boundaries or sequence boundaries. This kind of discrepancy often derives from the of biostratigraphic correlation over large area based on comparable biozonation but not on the exactly same fossil species.

In the Aquitanian strata, $\delta^{13}C$ values from all the studied boreholes rapidly fall approximately from -23‰ to -25‰ when approaching the Aquitanian-Burdigalian boundary (red arrows, Figure 3.4). The intervals through the entire Burdigalian in Site 28, Rødding, and Sønder Vium wells, all show a broad trend to become isotopically heavier upwards; about two or three cycles of isotopic fluctuation can be recognized (purple arrows, Figure 3.4).

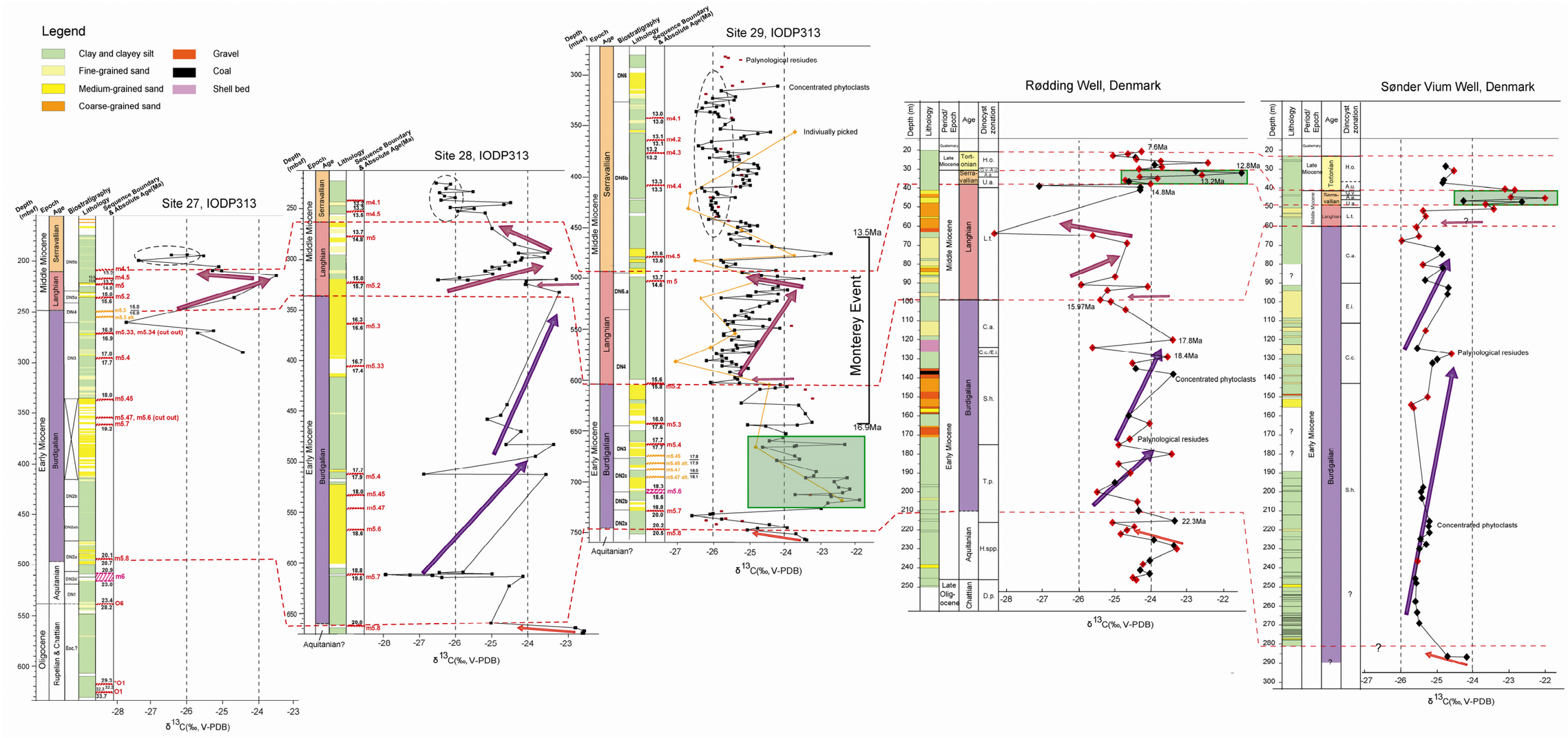

Figure 3.4. Long-distance correlation of carbon-isotope stratigraphy with counterpart of sedimentary sequence from New Jersey margin, USA, IODP Expedition 313. See more detailed legends of Site 27, Site 28 and Site 29 in Figure 2.5 and Figure 2.6. The green shades on Site 29, Rødding and Sønder Vium indicate the glauconite intervals with notably heavy carbon-isotope values.

Immediately above the Burdigalian-Langhian boundary, the distinct stratigraphic signals drop down to around -26‰ in almost all boreholes (horizontal pink arrows, Figure 3.4). Although there are no adequate data from Site27 or Sønder Vium, the limited data still suggest the same trends as other three boreholes with a negative excursion. Subsequently, $\delta^{13}C$ values present a carbon-isotope trend of gradually becoming relative heavy to around -24‰, and then turning back to relative light $\delta^{13}C$ values passing upwards (pink arrows, Figure 3.4).

The Langhian corresponds largely to the period of the Monterey Event, which is defined by the remarkably positive carbon-isotope excursions derived from benthic foraminifera as fully described in Chapter 2 (Figure 2.2). However, records from all the five boreholes seem not show more significant positive carbon-isotope records in the Langhian than those in the Burdigalian interval (Figure 3.4).

The Serravallian interval in the Site 27, Site 28 and Site 29 boreholes is characterized by remarkably light carbon-isotope values (highlighted by the dashed line circles, Figure 3.4). The isotopic signature shows a good and consistent correlation among the three New Jersey boreholes in the Serravallian. However, the Serravallian intervals from both Danish boreholes are characterized by significantly heavy $\delta^{13}C$ values, as much as -22‰. Interestingly, this interval is associated with occurrence of noticeable glauconite reflected by high gamma records (Figure 3.3). More interestingly, at the Burdigalian interval from Site 29, the similar phenomenon that the notably heavy $\delta^{13}C$ values are associated with much glauconite (highlighted by green shadows, Figure 3.4) is observed once more. Actually, the carbon-isotope stratigraphic trend of the Burdigalian interval from Site 29 unambiguously differs from all other data from available boreholes time equivalent parts in Site 28, Rødding, and Sønder Vium, where their isotopes turn heavy periodically up-section (purple arrows, Figure 3.4). The Burdigalian of Site 29 neither resembles the inorganic carbon-isotope reservoir where presents definitely relative light isotopic signatures during that interval (see Figure 2.2).

3.6 Discussion

3.6.1 Diagenesis examined by Scanning Electron Microscope (SEM)

Diagenesis often occurs in phytoclasts of sedimentary organic matter during transport or deposition. Potentially, diagenesis can influence $\delta^{13}C$ values of phytoclasts. Therefore, the preservation state of phytoclasts has been examined.

Two sets of samples (3 samples in the Rødding well and 4 samples in the Sønder Vium well) were collected for SEM observation (Figure 3.5 and Figure 3.6). These were selected to be representative of both heavy and light extremes of carbon-isotope values and also average values in each well (see sampling horizons in Figure 3.3).

For the Rødding well, broadly similar preservation of phytoclasts is observed at 64.00 m and 215.00 m where they show quite different carbon-isotope values. Samples at these two depths show the preserved original biological structures of the plants (Figure 3.5). However, at 64.00 m, the preservation of the original structure is especially good. This observation suggests a good preservation potential for organic matter, for example phytoclasts, under a rapid deposition and/or reduced depositional environment. The sample at 33.00 m is associated with heavy carbon-isotope values and its original biological structure is rather ambiguous.

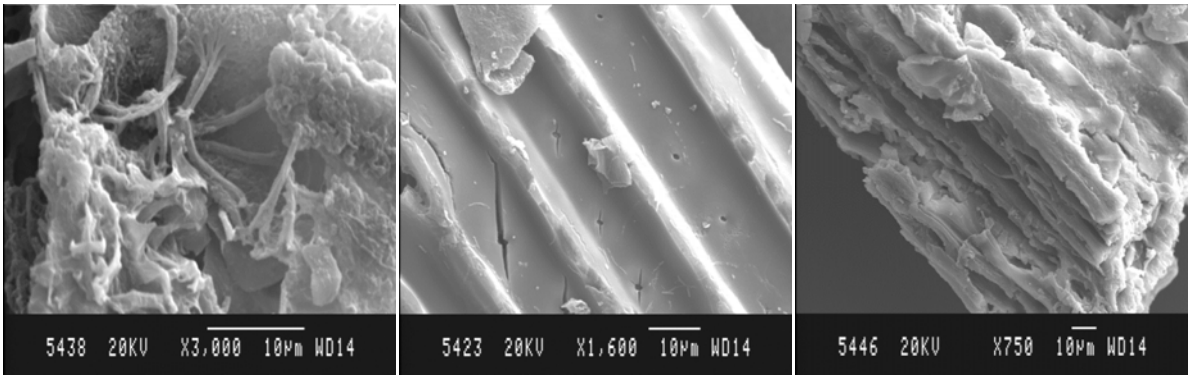

33.00m 64.00m 215.00m

Figure 3.5. SEM images of phytoclasts from the Rødding Well

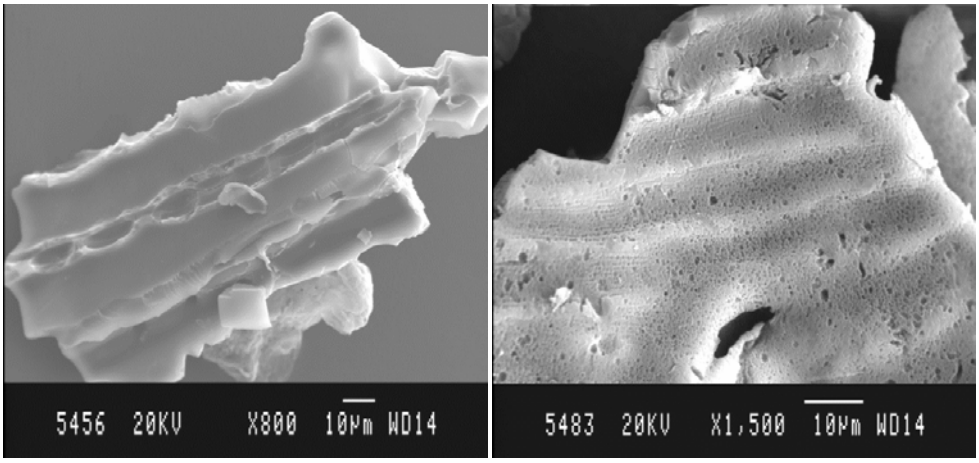

47.08m 67.00m

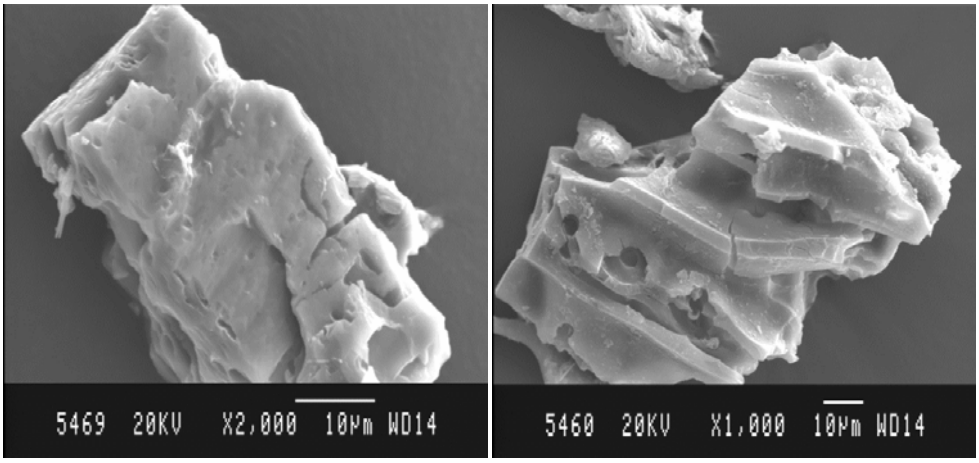

219.98m 263.48m

Figure 3.6. SEM images of phytoclasts from the Sønder Vium Well

Similarly, although carbon-isotope values vary through the Sønder Vium well, a broadly similar preservation of phytoclasts is observed. All SEM images from the Sønder Vium well reveal a preserved original biological structure of plants (Figure 3.6). In general, the best preservation is observed at 64.00m in the Rødding well and at 263.48m in the Sønder Vium well. Samples at other depths show an intermediate quality of preservation.

Enough pieces of phytoclasts from palynological materials were randomly selected to observe under SEM for each depth to enable an overview of preservation quality. At 33.00 m at Rødding and 47.08 m at Sønder Vium with the heavy extremes of $\delta^{13}C$ values, poorly preserved structure in the woody phytoclasts are associated with glauconite enrichment, although some small pieces of organic matter in a good preservation (e.g. the selected pieces at 47.08 m in Figure 3.7).

3.6.2 Carbon-isotope values vs. changes of input sources

As discussed in Chapter 2, significant changes in terrestrial source input by evolution of river systems or fluctuations of vegetation types can potentially lead to changes in carbon-isotope values in stratigraphy, such as gymnosperms (relatively heavy) versus angiosperms (relatively light) (e.g. Bechtel *et al.*, 2007; Holdgate *et al.*, 2009), ferns with their even lighter $\delta^{13}C$ values (e.g. Brearley, 2010; Watkins *et al.*, 2012), or changes in a ratio between C3 (relatively light) and C4 (relatively heavy) plants that are characterized by distinctively different carbon isotopes. Around the study area, evolution of river systems and climate changes did take place during the Miocene. However, in light of palynological analysis, the Miocene coast around the study area was consistently dominated by swamp forests, associated with a deciduous-evergreen mixed forest e.g. a hard-wood forest (Larsson *et al.*,

2011). The source of woody phytoclasts deposited at Sønder Vium did not fundamentally change, even though the rivers evolved (Rasmussen *et al.*, 2010) and climate underwent warming or cooling (Larsson *et al.*, 2011). In addition, there is no evidence for significant changes in the source of woody phytoclasts deposited at Rødding. Therefore, carbon-isotope records derived from terrestrial woody phytoclasts from Rødding and Sønder Vium represent carbon-isotope stratigraphic signatures that were not affected by changing source vegetation.

3.6.3 Glauconite and abnormal carbon-isotope values – caused by reworking of terrestrial organic matter from older deposits?

The occurrence of glauconite, with high gamma values, typically indicates a slow sedimentary rate due to relative sea level rise or sedimentary starvation due to some reasons, e.g. eustatic sea level rising, or tectonic subsidence in the basin (Amorosi, 1997; Hesselbo and Huggett, 2001).

In the case study of the North Sea Basin the Rødding and Sønder Vium wells are both located on the footwalls of synsedimentary normal faults which were active during the late Middle Miocene regional subsidence (during the Serravallian and Tortonian) (Figure 3.1). The deposits in the footwall of a synsedimentary normal fault tend to bypass and then ultimately accumulate in the hanging wall of the fault where subsidence is greater (Figure 3.7). Therefore, sediments in the Rødding and Sønder Vium locations accumulated at very low sedimentary rates during the Serrevallian and Tortonian.

In the case study of IODP 313, New Jersey, Site 29 exhibits low sedimentary rates during the Burdigalian, when that location was a distal end of the sediment transport path according to

seismic profile and sequence stratigraphy (Browning *et al.*, 2013). This interval is associated with the notable glauconite and high gamma-ray signatures (Miller *et al.*, 2013).

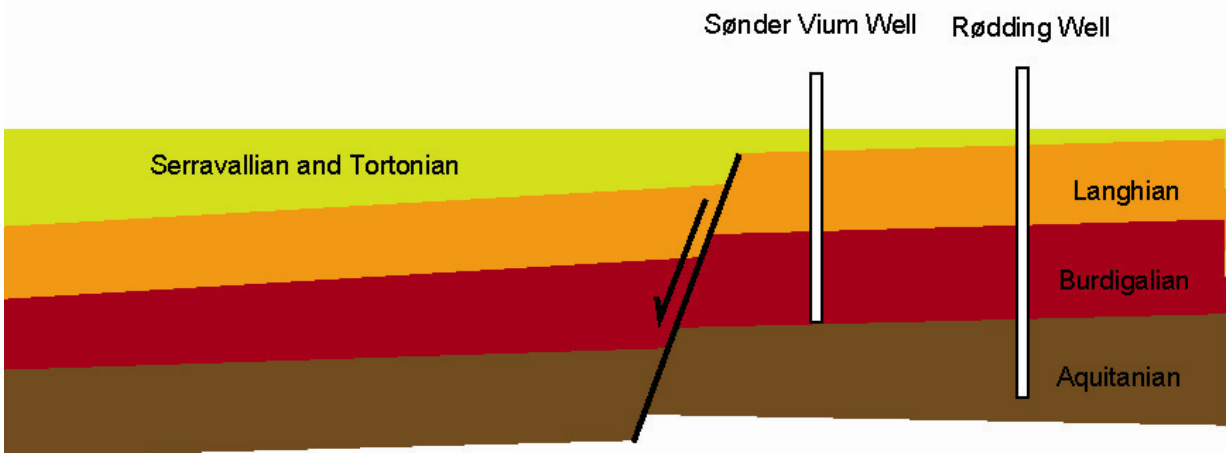

Figure 3.7. A schematic diagram of the synsedimentary normal faults and the relevant locations of the Rødding and Sønder Vium well

During a period of very low sedimentary rates, sediments tend to accumulate reworked materials because of inadequate sedimentary supplies. Therefore, there are four potential origins of the notably heavy carbon-isotope values during the period of low sedimentary rates: 1) isotope values changed by bacterial effects, 2) selective preservation due to the different resistance of lignin and cellulose, 3) mixture with the marine components which with light carbon-isotope values, and 4) carbon-isotope signatures from reworked sources.

Indeed, we can see relatively poor preservation at the interval associated with the notably heavy carbon-isotope values, but reason 1), reason 2) and reason 3) can be excluded. Plant lignin are depleted in ^{13}C by 2–5% relative to the whole plant $\delta^{13}C$ values but cellulose and hemicelluloses-structural carbohydrates is enriched in ^{13}C by 1–2 ‰ relative to whole-plant tissue (Benner *et al.*, 1987). Thus, the different degradation of lignin to cellulose

characterized by different $\delta^{13}C$ signatures could impact the $\delta^{13}C$ values documented in the terrestrial organic matter. The significant bacterial decay during transport and after deposition most likely would be accompanied with the selective preservation of lignin over cellulose (Kirk and Cowling, 1984; Benner *et al.*, 1984; Kirk, 1987). Therefore, bacterial effects and/or selective degradation of cellulose could enable systematically lighter isotope values rather than the heavier values observed in the glauconite intervals. With regard to possible reason 3, the data from the hand-picked individual woody phytoclasts in Site 29 (Figure 2.5), also show consistent anomalously heavy isotope values. Thus, it can be excluded that the abnormally heavy carbon-isotope values originated from mixture with marine components.

In summary, the possible reason 4, that these abnormally heavy carbon-isotope values represent the carbon-isotope signature from the reworked sources is most likely explanation for the observations. However, potential reasons for the origin of notably heavy carbon-isotope values should still be critically tested by more work in future. For example, the carbon-isotope stratigraphic records from single pollen in a given species, which can provide certain age constraints, could be used to compare with the results obtained from current methods. The carbon-isotope records from the compound-specific molecules is also useful to further test the selective preservation; and the Rock Eval parameters can be used to test the whether these phytoclast underwent thermal alteration, which could indicate reworked deposits from weathered older sedimentary rocks.

3.6.4 Assessment of long-distance correlation

The terrestrial carbon-isotope stratigraphic correlation over the North Sea Basin and New Jersey shows a good result at the Aquitanian-Burdigalian boundary, because the trends and

values are both consistent in all data available from boreholes (i.e. Site 28, Site 29, Rødding and Sønder Vium). The correlation at the Burdiganlian–Langhian boundary gives a fair confidence as well, although the boundary values are not perfectly correlated, as the carbon-isotope values and trends around the Burdiganlian–Langhian boundary are generally coherent (also see Section 3.5.2). The correlation at Langhian–Serravallian boundary is placed with relatively less confidence, since the depositional records at low sedimentation rate from North Sea Basin do not permit adequate records of sedimentary sequences due to structural activities and depositional effects of synsedimentary normal faulting.

3.6.5 The Monterey Event

Not matching correlation of carbon-isotope stratigraphic records from Mediterranean

The recent work (Brandano *et al.*, 2010) compares several carbon-isotope stratigraphic curves dated to the period of the Early to Middle Miocene (~21 to ~11 Ma). These curves are from four successions around the Mediterranean, where sedimentary processes tend to be influenced by local tectonic (Lustrino *et al.*, 2009) or volcanic activities (Beccaluva *et al.*, 2005). Therefore, some of these carbon-isotopic curves that look unusual if correlated to global curves of the classic Monterey Carbon Isotope Excursion (MCIE) (Zachos *et al.*, 2001; Holbourn *et al.*, 2007) are attributed to regional controlling factors by the authors (Brandano *et al.*, 2010).

However, the explanation of attribution to regional factors for these inorganic carbon-isotope curves is questionable. First, the basic character of the MCIE is the inorganic positive carbon-isotope excursion of ~1.5‰ with superposed nine eccentricity 400 ky cycles (Holbourn *et al.*,

2007) with periodic positive and negative peaks. However, the authors (Brandano *et al.*, 2010) cited a very low resolution mean curve after Zachos *et al.* (2001) and missed the significantly important carbon-isotope stratigraphic information of periodic peaks during the MCIE. Obviously, the authors (Brandano *et al.*, 2010) failed to point out that the carbon-isotope curves derived from bulk carbonate in the Malta section (Jacob *et al.*, 1996; John *et al.*, 2003) can be well correlated with those from benthic foraminifers in the deep ocean (Zachos *et al.*, 2001; Holbourn *et al.*, 2007) when plotted against the age axis. In particular, there are three well-correlated positive carbon-isotope peaks at ~16.3 Ma, ~14.5 Ma and 13.7 Ma (Zachos *et al.*, 2001; Holbourn *et al.*, 2007), and one well-correlated negative carbon-isotope peak at ~15.3 Ma (Zachos *et al.*, 2001) or ~ 15.1 Ma (Holbourn *et al.*, 2007) where the slight age difference is likely a result of a homogenizing effect during the combination of 19 global sites in the work of Zachos *et al.*(2001). Additionally, John *et al.*, (2003) undertook a detailed and necessary estimation of sedimentation rate, which is important for the carbon-isotope stratigraphic correlation. Thus, the carbon-isotope curves from Malta against age are supposed to be reliable. This indicates that the global character of MCIE is documented in the section in Malta, Mediterranean.

Secondly, the Northern Apennies (Italy) section shows a carbon-isotope stratigraphy that can be basically correlated to those from Malta and thus correlated to the MCIE. The Northern Apennies (Italy) are 50 – 60 Km away from Maiella and Pietrasecca, Central Apennines (Italy). The remarkable difference in the maximum δ13C shift between the Central Apennines (Maiella and Pietrasecca) and Northern Apennines is hard to explain by the dramatically different depositional environment suggested by Brandano *et al.*, (2010). Therefore, Northern Apennies and Central Apennines (Maiella and Pietrasecca) dominated by similar regional controlling factors cannot be definitely excluded until the convincing evidence that

conditions for Maiella and Pietrasecca are isolated from Northern Apennies (Italy) is provided.

Thirdly, the authors (Brandano *et al.*, 2010) falsely indicated the stratigraphic age in Pietrasecca, Central Apennines (Italy) to be reliable just because of its consistent stratigraphic correlation with Maiella. The age model in Maiella is on basis of the Sr isotope stratigraphic age and microfossils (Mutti *et al.*, 1997). The correlation of stratigraphic age between Maiella and Pietrasecca is far from being independent, in that the stratigraphic age itself in Pietrasecca, Central Apennines (Italy) (Brandano and Corda, 2002) is based on Sr isotopic ratios from the similar restricted sea water as that of Maiella, and adjacent regional areas (Garminati *et al.*, 2007). For the succession in Maiella, the age of Lithothamnium Limestone in the upper part is poorly constrained, as both biostratigraphic data and strontium-isotope ages are inconsistent because of reworking of older microfossils (Mutti *et al.*, 2006). No chemostratigraphically significant events can be recognized based on the bulk $\delta^{18}O$ record through the entire Decontra section in Maiella (Mutti *et al.*, 2006). Therefore, the absolute ages alone derived from Sr isotopic ratios for this succession remain debatable. Moreover, the regional correlation is primarily based on the lithostratigraphy (see Garminati *et al.*, 2007) and this kind of stratigraphic correlation could be diachronous.

Fourthly, even if it is assumed that the stratigraphic age model is correct, the authors (Brandano *et al.*, 2010) did not provide any estimation of sedimentation rate when transforming the depth axis into the time axis, with just a simple linear sedimentation rate. The apparent geometric characters of carbon-isotope stratigraphic curves are significantly influenced by the sedimentation rate. Until the sedimentation rates in different stratigraphic

interval are properly estimated, the depth-time transforming is variable and thus the correlation of carbon-isotope stratigraphic curves needs great care.

It has to be admitted that any single carbon-isotope stratigraphic curve is influenced by both regional and global signatures, and that the climax of the igneous activity was taking place during ~22 – 18 Ma around the Mediterranean (Lustrino *et al.*, 2009) and is roughly coeval with the maximum angular velocity of the Sardinia-Corsica block counter-clockwise rotation during ~21.5 –17 Ma (Gattacceca *et al.*, 2007). However, until more critical age constraints are provided, the explanation that the carbon-isotope signature of the carbonate platform successions of Central Italy is overwhelmingly controlled by the regional rather than global factors in Mediterranean between 20 and 15 Ma should not be accepted. The most likely explanation for the positive $\delta^{13}C$ shift maximum apparently not matching MCIE is the inaccurate stratigraphic age model in Maiella and Pietrasecca, Central Apennines (Italy).

The partial presence of positive carbon-isotope excursions in terrestrial records

As discussed in Chapter 2 the Monterey Event (16.9-13.5 Ma) is characterized by a noticeable positive carbon-isotope excursion (≥+1.5‰) which was originally defined in the tropical Indian Ocean at DSDP Site 216 by Vincent and Berger (1985), has been widely registered in the benthic inorganic carbon reservoir (see Figure 2.2; Vincent and Berger, 1985; Woodruff and Savin, 1985; Flower and Kennet, 1994; Zachos *et al.*, 2001; Abels *et al.*, 2005; Holbourn *et al.*, 2005, 2007; Diester-Haass *et al.*, 2009). The Monterey Event is thought to coincide with the extensive burial of organic matter around the margins of the northern Pacific; and the Monterey Formation containing the organic-rich sediments in California is

regarded as a typical example (Vincent and Berger, 1985; Woodruff and Savin, 1991), although recent intensive study shows the Monterey Formation is not as organic-rich as previously thought (Föllmi *et al.*, 2005). The detailed stratigraphic studies indicate a lag of starting time between the positive $\delta^{13}C$ excursions and the Monterey Formation in that the Monterey Formation started within planktic foraminiferal zone N6 and calcareous nannofossil zone CN2, before the distinct positive shifts of $\delta^{13}C$ values (DePaolo and Finger, 1991). However, in the $\delta^{13}C$ curves in Zachos' complied data (Zachos *et al.*, 2001), the beginning horizon of the $\delta^{13}C$ positive excursions of the Monterey Event can be either the zone N6 and CN2 or the zone N8 and CN3 (see Chapter 2, Figure 2.2). The difference is due to how the 'beginning of the pronounced $\delta^{13}C$ positive excursions' is defined.

In light of the accumulated evidence, the Monterey Event is thought to a global event with several eventual positive carbon-isotope peaks. On the basis of integrated correlation with synchronous global $\delta^{13}C_{inorg}$ records in 15 pelagic or deep sea sites (DSDP/ODP), Woodruff and Savin (1991) identified 7 carbon-isotope maxima (CM, labelled as CM1 to CM7) within the relatively heavy $\delta^{13}C$ of the so-called Monterey Event during the late Early Miocene to Middle Miocene. The tuning of astronomical timescales based on the carbon-isotope data has revealed nine of these short-term excursions, each identified as an eccentricity 400 ky periodicity, and allowing fit to the La2004 astronomical model to give a refined dating for the whole Monterey Event from 16.9 to 13.5 Ma (Holbourn *et al.* 2007).

The combined benthic and planktonic foraminiferal records through the time corresponding to the Monterey Event (Cheng *et al.*, 2004) provide the evidence for the whole ocean of carbon-isotope fluctuation and even it is inferred to the perturbation of entire ocean-atmosphere carbon-isotope reservoirs (see Figure 2.2).

However, in terms of the local and long-distance correlation of the terrestrial carbon-isotope stratigraphy, the Monterey Event is just partly observed in terrestrial carbon-isotope records both from the North Sea Basin and the New Jersey (Figure 3.3).

The CRB and potential impacts (A hypothesis)

The CRB province represents the latest large continental flood basalt events in the Phanerozoic and went through the late Burdigalian and early Langhian over about 1.5 million years. The hypothesis of CRB's origin include a mantle plume (Brando and Goles 1988; Wolff *et al.*, 2008; Smith *et al.*, 2009), back-arc processes (Christiansen *et al.*, 2002; Hales *et al.*, 2005), or the rupture of the Farallon slab (Liu and Stegman, 2012). Although the origin of CRB has remained controversial, the huge volcanism did suggest a potential cause-effect relationship to a couple of remarkable impacts on climate and environment around the transition period from the Early Miocene to the Middle Miocene such as mass extinction, perturbation of carbon reservoirs, and the prolonged warm climate MMCO.

The CRB took place on land and thus the voluminous gases originated from the eruption released into the atmosphere directly (Coffin and Eldholm, 1994). The huge volcanism of CRB during the Early to Middle Miocene resulted in an increased pCO_2 in atmosphere. A high-frequency increase in pCO_2 during the Middle Miocene is also supported by independent evidence (Pearson and Palmer, 2000; Kürschner *et al.*, 2008). The enhanced greenhouse effect superimposed by the astronomical long-term eccentricity periods forced a prolonged warm climate, so that the MMCO coincidently occurred. The most significant effect of MMCO is the prolonged rising temperature on the Earth's surface, and hence allows

a greatly increased primary production over the entire ocean, involving both the surface and the benthic ocean ecological groups. The results of increased oceanic primary production led to a positive carbon-isotope excursion in the whole ocean carbon reservoir (Berger and Vincent. 1986) and thus the new carbon-isotope balance between oceanic and atmospheric reservoirs would be establishing. However, the positive $\delta^{13}C$ excursions in the ocean carbon reservoir could not easily impact on the $\delta^{13}C$ in atmosphere during the period of MMCO, assuming the ocean-atmosphere equilibrium simply follow carbon-isotope kinetic nmechanism (Zeebe and Wolf-Gladrow, 2001, pp. 9–11, pp. 170–175), because the atmosphere was undergoing the increased pCO_2. Under the geological contexts above, a long-term well coupled situation of $\delta^{13}C$ values between atmosphere's and ocean's reservoirs might be temporarily broken and this could be one of the possible explanations for the positive carbon-isotope excursions only partly observed in the terrestrial records during Monterey Event.

3.7 Conclusions

1) Carbon-isotope data predominantly derived from terrestrial phytoclasts in two boreholes in the area of Jylland, North Sea Basin, show systematic stratigraphic signatures, from the Early Miocene to early Late Miocene. The carbon-isotope stratigraphic correlation between two local boreholes generally shows a good consistency. One major exception is in the Burdigalian interval; $\delta^{13}C$ values from Rødding are consistently heavier than those from Sønder Vium during the Burdigalian.

2) A tentative long-distance carbon-isotope stratigraphic correlation between Danish North Sea Basin and New Jersey margin, USA is proposed, with support from biostratigraphy and integration of other available chronological approaches. The long-distance stratigraphic correlation presents a basic consistency. It is concluded that terrestrial carbon-isotope stratigraphy is a promising stratigraphic correlation tool at long-distance or even global scale, if the correlated strata are well preserved and formed at a normal sedimentary rate.

3) The reliable carbon-isotope stratigraphic signatures seem not to be documented in the intervals which are associated with occurrence of abundant glauconite, suggesting a relatively low sedimentation rate (~4 to 5 mm/Kyr during the Serravallian, assuming no hiatus in the calibrated intervals). These intervals with slow sedimentary rate present notably heavy carbon-isotope values. These carbon-isotope stratigraphic signatures may be inherited and reworked from the older strata of sedimentary organic matter.

4) In the strata time equivalent to Monterey Event (the Langhian), the carbon-isotope stratigraphic values are consistently not heavier than those in the earlier (the Burdigalian) or

later (the Serravallian) strata. The Monterey Event is thus consistently absent in terrestrial carbon-isotope records both from the North Sea Basin and the New Jersey margin.

5) A possible explanation to the partial presence of Monterey Event in the carbon-isotope stratigraphy based on the terrestrial sedimentary organic matter has been proposed that the increasing atmospheric CO_2 concentration derived from CRB might delay the ocean-atmospheric equilibrium, which was driven by the oceanic primary production during MMCO. Nevertheless, the hypothesis still should be verified by more studies.

3.8 Acknowledgements

I would like to sincerely thank Karen Dybkjær for her providing samples of palynological residues from the two wells, and for her helping with biostratigraphic and chronological identification. I also truly acknowledge Erik Skovbjerg Rasmussen for his helping with the newly defined lithostratigraphy and downhole geophysical log data.

Chapter 4

TERRESTRIAL CARBON-ISOTOPE STRATIGRAPHY THROUGH THE LATEST TRIASSIC TO EARLY JURASSIC, NORTH TARIM BASIN, NW CHINA

4.1 Introduction

In the latest Triassic to Early Jurassic period (~ 201 Ma to ~174 Ma; based on GTS 2012, Gradstein *et al.*, 2012), the Earth system underwent a series of significant global geological events. The major end-Triassic mass extinction is documented both on land and in the sea (Raup and Sepkoski, 1982; Sepkoski, 1996; Tanner *et al.*, 2004; Kiessling *et al.*, 2007; Alroy, 2010; Kiessling and Simpson, 2011), associated with nearly synchronous eruption of the Central Atlantic Magmatic Province (CAMP) (Manspeizer, 1988; Holbrook and Kelemen, 1993; Oh *et al.*, 1995; McHone, 1996, 2000; Marzoli *et al.*, 2004; Deenen *et al.*, 2010) and with CO_2 injection into the atmospheric reservoir (Whiteside *et al.*, 2010; Ruhl *et al.*, 2011). The perturbation of carbon reservoirs through the latest Triassic, Triassic–Jurassic boundary, and Early Jurassic are witnessed by the short-term and long-term carbon-isotope excursions in both marine and terrestrial depositional sequences (e.g. Hesselbo *et al.*, 2002, 2007; Van Schootbrugge *et al.*, 2005; Williford *et al.*, 2007). The Early Jurassic is, however, also marked by multiple smaller events of carbon-cycle fluctuation such as in the late Sinemurian (Riding *et al.*, 2012), at the Sinemurian-Pliensbachian boundary and in the late Pliensbachian (Korte *et al.*, 2011). Subsequently, the early Toarcian Oceanic Anoxic Event (T-OAE) linked with the huge light carbon emission from geological reservoirs (Hesselbo *et al.*, 2000, 2007; McElwain *et al.*, 2005) was coincident with the nearly synchronous eruption of Ferrar/Karoo LIP at ~183 Ma to ~175 Ma (Pálfy and Smith, 2000; Svensen *et al.*, 2007), and with the first opening of central Atlantic Ocean related to the Pangaea break-up (Cox, 1992; Storey *et al.*, 1992).

Long-lasting continuous records of carbon-isotope stratigraphy through the latest Triassic, Triassic–Jurassic boundary, and Early Jurassic were reported from marine sequences (Katz *et*

al., 2005; the most recent dataset complied by Dera *et al.*, 2011). However, very few long-term continuous carbon-isotope records have been reported from the entirely terrestrial successions. The Tarim Basin located in NW China as an inland basin since the Mesozoic provides an exceptional opportunity to explore terrestrial carbon-isotope stratigraphy through the latest Triassic, Triassic–Jurassic boundary, and Early Jurassic.

4.2 Geological setting - a brief tectonic and sedimentary history

The Tarim block has merged into Eurasia since the Early Permian and was sutured by the Tian Shan Range and the Late Palaeozoic Aibi–Xingxing suture (or the Southern Tian Shan) (Windley *et al.*, 1990; Allen *et al.*, 1991; Yin *et al.*, 1996; Metcalfe, 2006). Therefore, the northern margin of the Tarim block accumulated terrestrial continental sediments in the Permian after the collision of Tarim with the Tian Shan/Kazakhstan.

The Tian Shan is the largest intracontinetal orogenic belt in the Central Asia and its multiple-phase accretions resulted from collisions of different blocks in the Late Palaeozoic (Coleman, 1989; Carroll *et al.*, 1990, 1995; Sengör *et al.*, 1993; Windley *et al.*, 1990, 2007). The South Tian Suture and North Tian Suture are identified on the basis of ophiolite melanges with the Tian Shan area (Gao *et al.*, 1998). The Tarim Basin and the Junggar Basin are situated along the south and north of Tian Shan, respectively (Figure 4.1). The Tian Shan definitely stood as a positive physiographic feature throughout Mesozoic and Cenozoic time (Hendrix *et al.*, 1992), and supplied the source of terrestrial sediments. The paleolatitude of North Tarim was about 55-60°N from the Late Triassic to the Middle Jurassic (Yin *et al.*, 1996; Metcalfe, 2006), but the climate was warmer than at the same latitude today. The southern margin of the Tarim Basin directly bordered the north of Tethys Ocean in that the Tibet block had not collided with the Tarim block either the Pamir-Kunlun Shan-Altyn Shan range had not originated (Figure 4.2).

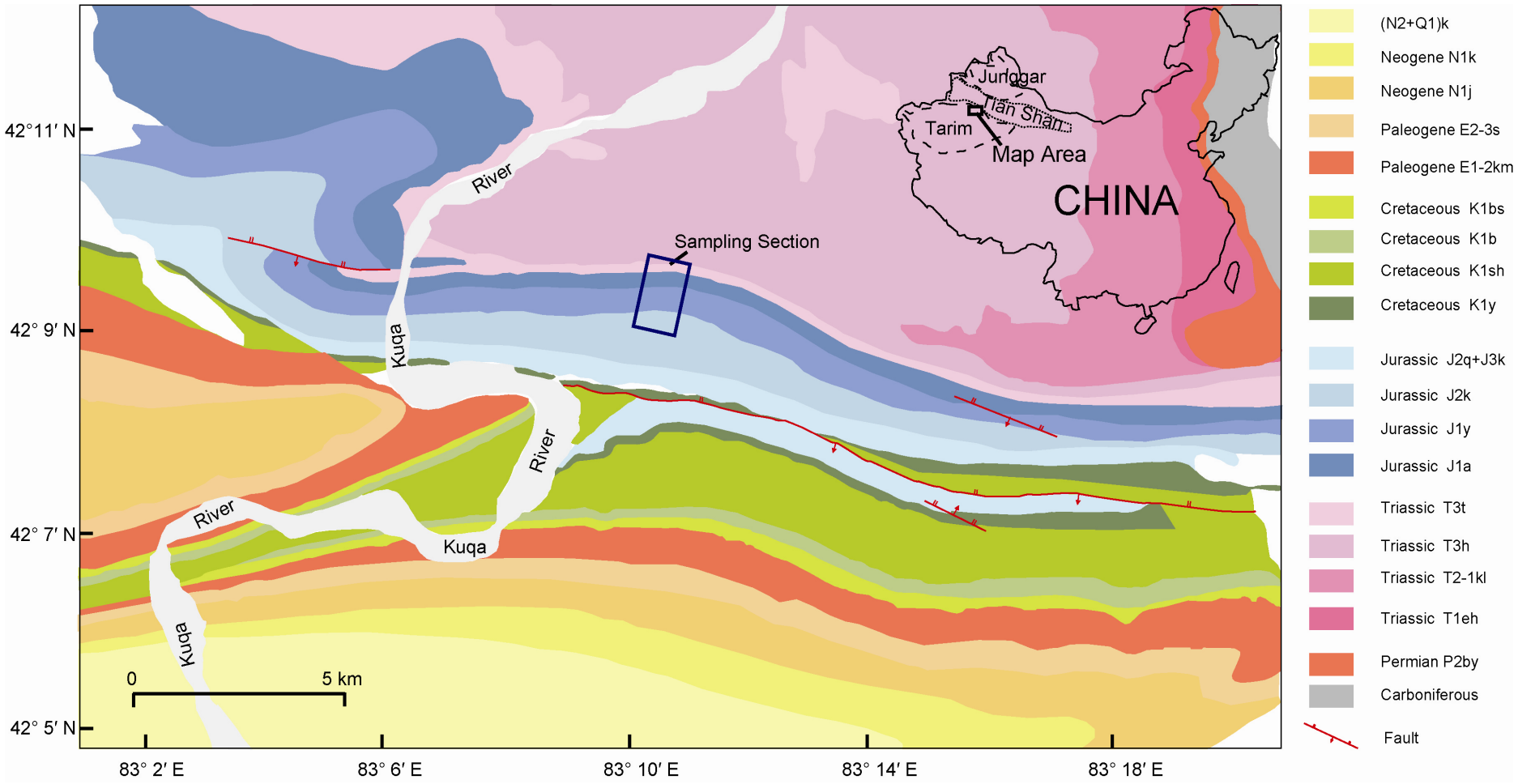

Figure 4.1. Geological maps of the Kuqa section (modified from the Regional Geological Map of the Kuqa Depression, 1997 - Tarim Division, Institute of Oil Exploration and Development)

The Tarim Basin was a foreland basin yielding an asymmetrical sedimentary distribution basinwide and foreland-style subsidence profiles throughout the Mesozoic and Cenozoic (Figures in Li *et al.*, 2004). The identification of the Tarim foreland basin is also evidenced by a number of outcrop and subsurface facies data (Hendrix *et al.*, 1992). However, some authors (Carroll *et al.*, 2010) recently proposed a new descriptive term 'walled basin' to highlight the unique features of a basin surrounded by dominantly contractional orogenic uplifts, but whose peripheral orogenies are relatively undeformed and maintained over relatively long geological time scales. According to these characteristics, the authors are pointing out that the Tarim Basin differs from conventional foreland settings.

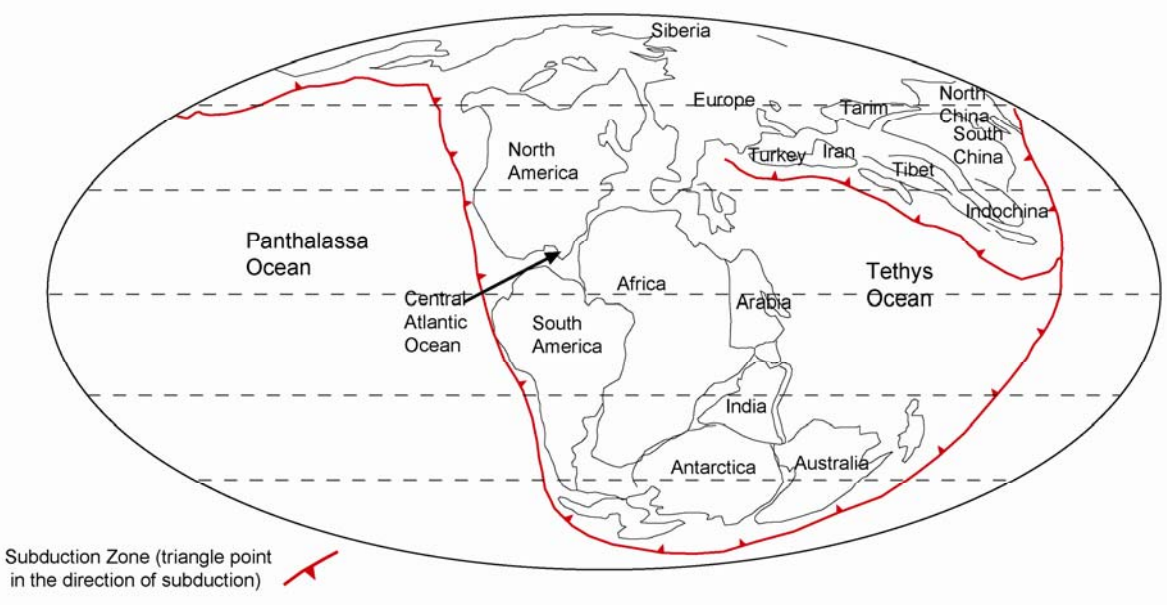

Figure 4.2. Palaeogeographic maps (adapted on the basis of combination from Cohen *et al.*, 2007; Izumi *et al.*, 2012 and http://www.scotese.com/jurassic.htm)

The study area, the Kuqa section in the Kuqa depression (i.e. the Kuqa subbasin and the 'Kuqa' also spelled as 'Kuche' following Chinese phonetic symbols in some previous literature) is located around the Yangxia River, in the north of the Tarim Basin. Under compressive tectonic loading and gravitational loading, the Kuqa depression is part of an

intra-continental foreland basin. The cross-section of the depression is asymmetric and the sedimentary thickness thins south towards the Tarim craton (Li *et al.*, 2004). In the Mesozoic, the entirely terrestrial deposition occurs reaching a thickness of 6000–8000 m in the Kuqa depression (Li and Peng, 2010). The whole Tarim Basin is interpreted to have subsided at a quite steady rate during the Jurassic (Hendrix *et al.*, 1992) and thus the lacustrine and associated alluvial deposits are likewise thought to record relatively continuous deposition. The oldest definite terrestrial deposits date back to the Late Permian (Carroll *et al.*, 2010).

4.3. Stratigraphy and chronological control

4.3.1 Lithostratigraphy

Generally, the Upper Triassic in the northern Tarim Basin consists of alluvial conglomerate and associated braided-fluvial sandstone and siltstone. Upward into the Lower and Middle Jurassic, meandering-fluvial and lacustrine strata broadly occur and very organic-rich strata locally occur. The Upper Jurassic comprises braided-fluvial red beds. A distinct pulse of alluvial conglomerate occurs in the uppermost Jurassic, and Cretaceous strata overly in a parallel unconformity over a large area, but with a pronounced angular unconformity in a restricted area (Xiao et al, 2005).

The lithostratigraphic division of the Jurassic System along the northern Tarim Basin has undergone a series of evolutionary steps, which are generalized below (Table 4.1). In the present study, the most recent lithostratigraphic division is followed (Wang *et al.*, 2004), but without complete agreement with the associated chronological identity (Table 4.1). The updated chronological identity is fully discussed below (see Section 4.3.3 and Section 4.6.1).

Combining all data in literature that can be found, there is not any direct evidence for specifically placing the Triassic–Jurassic boundary at a particular horizon in the Kuqa section. Two candidate horizons of the Triassic–Jurassic boundary, between Bed 35 and Bed 37 in the Taliqike Fm (Fig. 3), are proposed on basis of the field observation of distinct lithostratigraphic boundaries in this study and the most recent regional lithostratigraphic division (Wang *et al.*, 2004); the age identification lied on the composite biostratigraphy (Wang *et al.*, 2004; Deng *et al.*, 2010).

Table 4.1. Brief evolution of the Jurassic lithostratigraphic division, northern Tarim basin (after Wang et al., 2004)

Huang, 1943		Soviet Remote Survey Team, 1952-1953		Yao et al., (1956)		Xinjiang Petroleum Adiminstration Bureau, 1957		Xinjiang Petroleum Adiminstration Bureau, 1960-1962		Regional Stratigraphic Chart of Xinjiang, 1981		Northwest Petroleum Adiminstration Bureau, 1984		Tarim Oil Company, PetroChina, 1994		Wang et al., 2004	
Shuixigou Series J	Qiakemake Strata J_7	Red Rocks Series J_{2-3}		Qiakemake Series J_{2-3}		Zamikela Group	Red Conglomerate Strata J_{2-3}	Zamishentake Group	Red Conglomerate Fm J_3	Kalaza Fm J_3		Kalaza Fm J_2		Qigu Fm J_3		J_3	Kalaza Fm J_3k
							Red Mudstone Strata J_{2-3}		Red Mudstone Fm J_3	Qigu Fm J_3		Qigu Fm J_2					Qigu Fm J_3q
	Upper Green Strata J_6	Sand-Shale Coal-bearing Series J_2		Kelasu Series	Kezilenuer Strata J_{1+2}		Oil Shale Strata J_{2-3}		Oil Shale Fm J_3	Qiakemake Fm J_2		Kelasu Group	Qiketai Fm J_2	Qiakemake Fm J_2		J_2	Qiakemake Fm J_2q
	Upper Coal Strata J_5					Kelasu Group	Kezilenuer Strata J_2	Kelasu Group	Kezilenuer Fm J_2	Kezilenuer Fm J_2			Kezilenuer Fm J_2	Kelasu Group	Kezilenuer Fm J_2		Kezilenuer Fm J_2k
	Grey Strata J_4	Sandstone Series J_{1-2}			Sandstone Strata J_{1+2}		Sandstone Strata J_2		Standard Sandstone Fm J_1 Upper Member	Kelasu Group	Yangxia Fm J_1		Yangxia Fm J_1		Yangxia Fm J_1	J_1	Yangxia Fm J_1y
	Standard Sandstone Strata J_3								Standard Sandstone Fm J_1 Lower Member		Ahe Fm J_1		Ahe Fm J_1		Ahe Fm J_1		Ahe Fm J_1a
	Lower Coal Strata J_2	Coaly Shale-mudstone Series	Upper Layer		Taliqike Strata J_{1+2}	Misibulake Group	Taliqike Strata J_1	Misibulake Group	Taliqike Fm J_1	Taliqike Fm T_3		Taliqike Fm T_3		Taliqike Fm T_3 - J_1		T_3	Taliqike Fm T_3t
	Lower Green Strata J_1		Low Layer	Misibulake Series	Upper sub-strata T_3		Coaly Shale Strata J_1		Coaly Shale Fm T_3	Huangshanjie Fm T_3		Huangshanjie Fm T_3		Huangshanjie Fm T_3			Huangshanjie Fm T_3h

In order to correlate the chronological units of Junggar Basin, a regional correlation chart of lithostratigraphic division between the southern Junggar Basin and northern Tarim Basin is summarised (Table 4.2). The lithostratigraphic divisions are tentatively identified to Stage level on the basis of all available published literature (Wang *et al.*, 2004; Deng *et al.*, 2010), but this identification is revised in the present chapter based on new carbon isotope data (see Section 4.3.3).

Table 4.2. The correlation chart of regional Jurassic lithostratigraphical division between the southern Junggar Basin and northern Tarim Basin (Wang *et al.*, 2004 and Bian *et al.*, 2010)

<table>
<tr><th colspan="2">Period</th><th>Stage</th><th>S. Junggar Basin,
N. Tian Shan</th><th>N Tarim Basin,
S. Tian Shan</th></tr>
<tr><td colspan="2">Lower Cretaceous</td><td></td><td>Tugulu Gr (K_1t)</td><td></td></tr>
<tr><td rowspan="3">Upper Jurassic</td><td>Tithonian</td><td></td><td></td><td></td></tr>
<tr><td>Kimmeridgian</td><td></td><td>Kalazha Fm</td><td>Kalaza Fm</td></tr>
<tr><td>Oxfordian</td><td></td><td>Qigu Fm</td><td>Qigu Fm</td></tr>
<tr><td rowspan="5">Middle Jurassic</td><td>Callovian</td><td rowspan="2">Tugunhe Fm</td><td rowspan="2">Qiakemake Fm</td></tr>
<tr><td>Bathonian</td></tr>
<tr><td>Bajocian</td><td rowspan="2">Xishanyao Fm</td><td rowspan="3">Kezilenuer Fm</td></tr>
<tr><td>Aalenian</td></tr>
<tr><td rowspan="4">Lower Jurassic</td><td>Toarcian</td><td rowspan="2">Sangonghe Fm</td></tr>
<tr><td>Pliensbachian</td><td rowspan="3">Yangxia Fm</td></tr>
<tr><td>Sinemurian</td><td rowspan="2">Badaowan Fm</td></tr>
<tr><td>Hettangian</td><td>Ahe Fm</td></tr>
<tr><td colspan="2" rowspan="2">Upper Triassic</td><td rowspan="2">Haojiagou Fm
(or Baijiantan Fm)</td><td rowspan="2">Taliqike Fm</td></tr>
<tr><td>Huangshanjie Fm</td><td>Huangshanjie Fm</td></tr>
</table>

The southern Junggar Basin

Throughout the Jurassic, the southern Junggar Basin behaved as an entire intracontinental basin and accumulated only terrestrial sediments. The depositional environment was similar to that of the northern Tarim Basin. The alluvial conglomerate, meandering rivers, braided

rivers and lacustrine deposits are widely dominant. Specifically, the alluvial facies include alluvial fan and fan delta facies, as well as fluvial and flood-plain facies in the southern Junggar basin (Hendrix, 2000; Eberth *et al.*, 2001; Ashraf *et al.*, 2010).

The northern Tarim Basin

According to all available previous literature and observation in field for this study, the base of the Jurassic is conformable with the underlying Triassic and all the formation boundaries are conformable through the Jurassic sediments. The uppermost Jurassic strata are in a parallel unconformity with the overlying Cretaceous strata, which start with thick conglomerate layers.

The Ahe Fm and the Yangxia Fm (spelled as 'Yengisar Fm' in Hendrix *et al.*, 1992) around the Kuqa depression are major reservoirs. The Ahe Fm is characterized by alluvial conglomerates, meandering fluvial river sandstones or siltstones, and braided river sandstones (Hendrix *et al.*, 1992). The lower Yangxia Fm shows similar features to the Ahe Fm, but a lacustrine laminated mudstone occurs abruptly at the top of the Yangxia Fm. The Kezilernuer Fm is mainly shallow lacustrine facies. The Qiakemake Fm is of lacustrine facies in remarkable red strata, where the hematite among total heavy minerals, can be up to 95.4% and reaches 71.2% on average (Li S. J., *et al.*, 2005).

4.3.2 A brief review of the chronological control in the N Tarim Basin

Few studies obtained a precise dating for the Triassic and Jurassic terrestrial alluvial conglomerate, fluvial sandstone, and siltstone deposits in the N Tarim Basin, because that age interval around the region lacks interbedded volcanic units which can be used to provide absolute ages and the other approaches (e.g. biostratigraphic, magnetostratigraphic) do not readily yield a high-resolution age control. Chemostratigraphy is completely absent. However, the previous studies do give a general age control and they are summarized in Table 4.3.

4.3.3 Biostratigraphy of the Kuqa section

The precise age of the sediments in the Kuqa section, Kuqa depression, N Tarim Basin has been long debatable just based on the biostratigraphic profiles. This is because terrestrial biostratigraphy is limited in its time resolution and there is no absolute age control from the autogenetic radioactive minerals discovered around the study area. However, in the present chapter, the detailed biostratigraphy in the Kuqa section is investigated on the basis of the independently compiled dataset from Wang *et al.*, (2004) and combined with the most updated literature.

Table 4.3. A brief review on the chronological control in the N Tarim basin

System	Lithostratigraphic units	Magnetostratigraphic units (age, Ma)	Biostratigraphic units
Cretaceous	Bashijiqike Fm.	Early Cretaceous (133-125.7) (Li *et al.*, 2004, based on the Kuqa section)	Early-Late Cretaceous (Bureau of Geology and Mineral Resources of Xinjiang Uygur Autonomous region, 1993; Wang *et al.*, 2004)
	Baxigai Fm.	Early Cretaceous (138-133) (Li *et al.*, 2006, based on the Kuqa section)	Early Cretaceous (Bureau of Geology and Mineral Resources of Xinjiang Uygur Autonomous region, 1993; Wang *et al.*, 2004)
	Shushanhe Fm.	Early Cretaceous (144.2-138) (Li *et al.*, 2006, based on the Kuqa section)	
	Yageliemu Fm.	(? ~ 144.2) (Li *et al.*,2006; based on the Kuqa section)	
	Unconformity		
Jurassic	Kalaza Fm.	No data	Late Jurassic (Bureau of Geology and Mineral Resources of Xinjiang Uygur Autonomous region, 1993; Wang *et al.*, 2004)
	Qigu Fm.	No data	
	Qiakemake Fm.	No data	Middle Jurassic (Liu, 1990, based on conchostracans, Baicheng, N Tarim; Zhang W. P. and Li Y. A., 1990 palynology, Baicheng, N Tarim; Liu 1998, palynology primarily based on the Kuqa section and combined N Tarim; Liu *et al.*, 1999b, palynology, borehole, Kuqa area; Wang *et al.*, 2004)
	Kezilenuer Fm.	No data	
	Yangxia Fm.	No data	Early Jurassic (Wu, 1990, based on plant fossils, N Tarim; Liu 1998, palynology primarily based on the Kuqa section and combined N Tarim; Liu, 1999c based on palynology, primarily based on Kuqa section and combined N Tarim; Wang *et al.*, 2004)
	Ahe Fm.	No data	
Triassic	Taliqike Fm.	No data	Late Triassic (Peng, 1983; Wu, 1990; and Hu and Gu, 1987, based on plant fossils, N Tarim; Liu, 1999c based on palynology, primarily based on the Kuqa section and combined N Tarim; Liu 1999a, combined conchostracons and plants, N Tarim; Wang *et al.*, 2004)
	Huangshanjie Fm.	No data	
			Middle Triassic
Late Permian-Triassic		Triassic- Late Permian (McFadden et al, 1988, based on section of the Kuqa area)	

4.3.3.1 Plant fossils

The North Tarim Basin

For the Taliqike Fm, a dataset combined from several sections (no detailed locality provided) in the North Tarim Basin includes plant fossils: *Annulariopsis inopinata, Asterotheca szeiana, Cladophlebis cf. asiatica, Cl. raciborskii, Cl. cf. tsaidamensis, Dictyophyllum cf. nilssonii, Clathropteris sp., Ginkgo huttonii, Podozamites lanceolatus, Yuccites spathulata, Glossophyllum shensiensis, Hausmannia ussuriensis, Neocalamites hoerensis, N. carrerei, N. spp., Pityophyllum cf. nordenshioldi, Thinnfeldia nordenskioldi* (the table 2 in Wu *et al.*, 1990).

Hausmannia ussuriensis, Neocalamites carrerei are the abundant plant fossils in the Triassic (Wu, 1990), but the controversial point is that *Neocalamites carrerei* has been discovered in the Yangxia Fm (i.e. within inferred Jurassic strata) in the North Tarim Basin. The *Neocalamites hoerensis* and *Dictyophyllum cf. nilssonii* in the Taliqike Fm, North Tarim Basin are comparable with the Late Triassic flora in Eastern England (Wu, 1990), whereas the author pointed out that '*Neocalamites hoerensis, Dictyophyllum cf. nilssonii*' were also discovered in some early Jurassic strata in China, e.g. Junggar Basin, Northern Xinjiang Province, Western Hubei Province, and Western Jiangxi Province. Therefore, the author concluded that the Taliqike Fm in the northern Tarim is in the range from the Late Triassic to Early Jurassic. However, two vital flaws on the correlations were: 1) on the basis of lithostratigraphic chronological division, and 2) on the basis of the combined data from multiple sections in the North Tarim Basin. Until further solid evidence is provided, the inferences are far from conclusive.

The present chapter takes a general profile of age constraints on the lithostratigraphic divisions for the Triassic–Jurassic boundary, according to the available dataset of plant fossils. In order to identify the boundaries of Triassic and Jurassic and further a specific Stage assignment (e.g. the Sinemurian or Pliensbachian), the identification must be based on a certain continuous section (e.g. the Kuqa section) or well-documented overlapping multiple sections.

Stratigraphically upward, on the basis of combined data from several sections (no specific location provided) in the North Tarim, the Ahe Fm includes the plant fossils: *Equisetites sarrani, Sphenopteris sp., Cladophlebis asistica, Cl. cf. tsaidamensis, Cl. raciborskii, Ginkgo huttoni, Czekanowskia rigida, Phoenicopsis sp., Podozamites laceolatus, Pityophyllum cf. nordenskioldii* (Wu, 1990); passing up-section, the Yangxia Fm contains the plant fossils: *Equisetites cf. ferganensis, E. sarrani, Neocalamites carcinoides, N. hoerensis, N. carrerei, Rhizomopteris sinensis, Coniopteris hymenophylloides, Cladophlebis denticulala, Ginkgoites sp., Czekanowskia sp., Phoenicopsis cf. angustifolia, Baiera longifolia, Pityophyllum nordenskioldii* (Wu, 1990).

Very recently, the plant fossil records have been intensively studied in the Junggar Basin and the Late Triassic–Middle Jurassic floras consist of the four assemblages as follows (Sun *et al.*, 2010). I. *Danaeopsis–Nanzhangophyllum* assemblage (Carnian–Norian florule); II. *Glossophyllum–Cycadocarpidium* assemblage (Norian–Rhaetian florule); III. *Neocalamites–Marattiopsis* assemblage (Early Jurassic florule); and IV. *Coniopteris–Raphaelia* assemblage (early Middle Jurassic flora). These four assemblages constrain the age of the strata in the southern Junggar Basin. Owing to the studies on regional basin, these data also provide a general age control when correlated with data from the N Tarim Basin (Wu, 1990).

The Kuqa section

Based on the dataset of plant macrofossils from the Kuqa section (Wang *et al.*, 2004), three stratigraphic boundaries can be identified broadly: between the Bed 34 and Bed 46 (from ~ -10 m to ~55 m), around Bed 75 (~ 280 m), and the base of Bed 139 (~ 576 m) (Figure 4.3).

The interval between Bed 34 and Bed 46 is identified as a transitional zone of the Triassic–Jurassic boundary (Figure 4.3). This conclusion is supported by the last occurrence of *Taeniopteris sp*. which commonly occurs from the Permian to Triassic. *Neocalamites nathorstii* is a rare species in the flora from Yorkshire NE England (van Konijnenburg-van Cittert, 2008) which only occurs in strata younger than late Pliensbachian and mainly age (Harris, 1961). The only finding in Bed 34 in the Kuqa section may not suggest the last occurrence but a rare occurrence.

The first occurrence of *Sphenobaiera sp*. in the Kuqa section might suggest a boundary which is marked by a slight climatic perturbation (see pollen data in Section 4.3.3.2 and Figure 4.5). The last occurrence *Cladophlebis haiburensis* and *Cladophlebis sulcala* (?), and the first occurrence of *Equisetites cf. multidentatus, Vittifoliolum sp., Radicites sp., Equisetites sp., Cladophlebis suluktensis, Coniopteris sp*. could clearly define a boundary of biostratigraphic break at around Bed 75 to Bed 77 (~280 m) (Figure 4.3).

A relatively broad range of the last occurrence of *Vittifoliolum sp., Desmiophyllum sp., Coniopteris sp., Sphenobaiera cf. spectabilis* and the first occurrence of *Cladophlebis cf. tsaidamensis, Nilssoniopteris cf. nittata, Phoenicopsis cf. angustifolia* define a boundary biostratigraphic break at the base of Bed 139 (~576 m) (Figure 4.3).

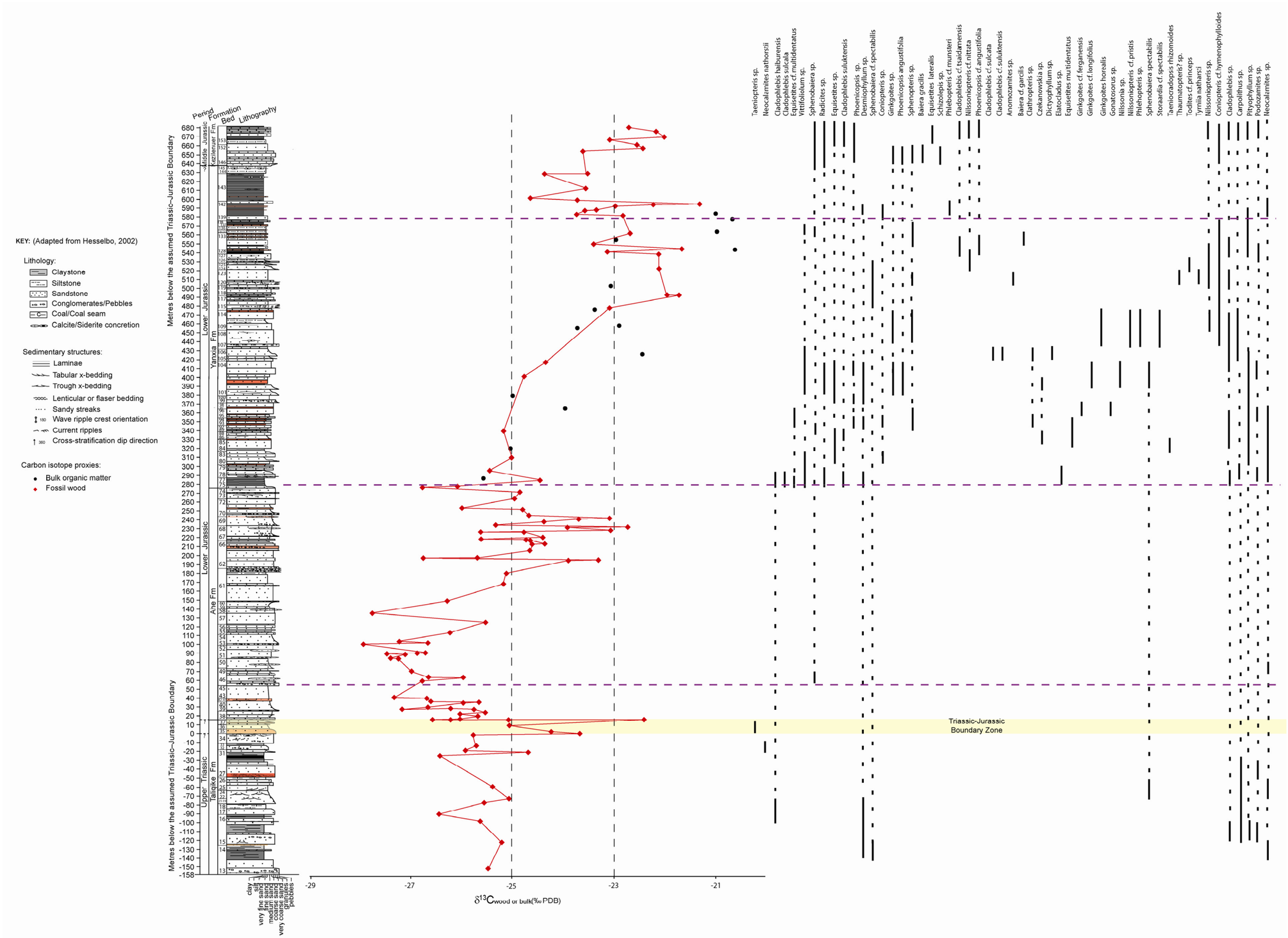

Figure 4.3. Lithography, carbon-isotope stratigraphy and the stratigraphic ranges of plant macrofossils in the Kuqa section, N Tarim Basin, NW China. Four biostratigraphic boundaries can be identified (the data of plant macrofossils compiled from Wang et al., 2004).

In light of the data from the Kuqa section, from the Bed 75 to Bed 122 in the Yangxia Fm (Fig 4.3), *Coniopteris hymenophylloides* begins to occur commonly and is associated with the presence of *Eboracia*; *Cladophlebis* is still present but lessens its diversity as compared with the underlying strata. In addition, *the Ginkgoacea* are dominant in the gymnosperms, including: *Ginkgo, Ginkgoites, Phoenicopsis, Baiera, Sphenobaiera and Vittifoliolum.* Coniferales and Cycdales place in the secondary position (Wang *et al.*, 2004).

In the middle-upper Yangxia Fm, there are plant macrofossils including: *Coniopteris* cf. *hymenophylloides*, *Pityophyllum* sp., *Nilssonia* sp., *Anomozamites* sp., *Nilssoniopteris vittata*, *N. major*, *Taeniopteris* sp., *Ginkgoites* sp., *Baiera concinna*, *B. furcata*, *B.* sp., *Phoenicopsis angustifolia* and *Czekanowskia rigida*, around the Bed 128 to Bed 138 (around 540 m to 570 m) (Figure 4.5) (Deng *et al.*, 2003). These are the usual species in the Jurassic flora and the genus of *Coniopteris* gives particular significance in terms of age constraint.

Although only one species, *Coniopteris* cf. *hymenophylloides,* has been discovered in the middle-upper Yangxia Fm, Kuqa section, Tarim Basin, it is quite abundant and characterized by the advanced frond and rachis. *Coniopteris* in Europe do not first occur in the *Thaumathopteris* Zone, which is the early stage of the Early Jurassic (i.e. *Coniopteris* first emerge in the Toarcian Stage in European flora). However, this genus appears much earlier than the Toarcian Age in China, where the earliest *Coniopteris* composing two species, *Coniopteris gaojiatianensis* and *C. microlepioides* are discovered in the Guanyin Fm, SW Hunan Province (i.e. located in the South China Block). These two species are both characterized by the tender frond and rachis, which reflect the primitive features of *Coniopteris.* In spite of no direct ammonite fossils in the Guanyin Fm, the discovered ammonites in nearby region constrain the Guanyin Fm at around the Hettangian and

Sinemurian Stage (Zhou, 1984). *Coniopteris* in the Yangxia Fm, Kuqa section is more advanced than those in the Guanyin Fm, and thus is inferred to be in the younger strata. The primitive types of *Coniopteris* have not been reported in the lower part of the Kuqa section, probably due to the few studies there.

However, the *Coniopteris* fossils from the middle-upper Yangxia Fm are also clearly distinct from the types in the early Middle Jurassic. The early Middle Jurassic is a peak stage of *Coniopteris*, which occur in very high diversity and abundance, and are usually dominant in the flora. The peak of diversity and abundance can only be observed upto the upper coal beds (Bed 168) in the overlying Kezilenuer Fm, Kuqa section.

Coniopteris gaojiatianensis, a species reported from the Hettangian and Sinemurian Stage of SW Hunan Province (Zhou, 1984), has been also discovered in the upper part of the Badaowan Fm, Junggar Basin (Deng *et al.*, 2003, 2010), although it is not found in the Kuqa section, Tarim Basin, indicating that the Badaowan Fm. is correlated with the Hettangian and Sinemurian Stage of Hunan Province, South China. The Badaowan Fm was previously correlated with the Ahe Fm, Tarim Basin (Deng *et al.*, 2003), but notably, the Ahe Fm comprises deposits of thick-bedded fluvial medium/coarse sandstone and interbedded conglomerate, which suggests a relative high sedimentary rate and relative short time span. Therefore, the Badaowan Fm in the Junggar Basin can possibly be correlated with the Ahe Fm and the middle-lower part of the Yangxia Fm, and the middle-upper part of the Yangxia Fm should be of Pliensbachian age.

Generally, plant macrofossils can be helpful to define stratigraphy in a broad profile, but less helpful in identifying very specific boundaries. Obviously, as lithostratigraphic boundaries

are not always synchronous, the correlation of plant fossils based on the profile of the lithostratigraphic unit cannot unambiguously illustrate an Epoch boundary.

4. 3.3.2 Palynological stratigraphy

Megaspore

The palynological data presented here are primarily compiled from Wang *et al.*, (2004). According to the megaspore occurrence and extinction, five stratigraphic boundaries can be identified: in the Bed 35 to Bed 37 interval (~0 m to ~18 m), the base of Bed 43 (~40 m), Bed 69 to Bed 70 (~ 245 m), the base of Bed 95 (~ 355 m), and the base of Bed 139 (~ 576 m). Triassic–Jurassic Boundary can be recognized around the top of Bed 37 (~18 m height), on the basis of last occurrence of *Aneuletes sp., Bacutriletes tylotus, Bothriotriletes conicus (Bothriolepis), Dijkstraisporites beutleri, Echitriletes latispinosus, E. hispidus, Nathorstisporites invenustus, Triangulatisporites sp., Trileites vulgaris, T. pinguis, T. sp.*(Figure 4.4).

Dijkstraisporites beutleri is an important Triassic component (Kozur, 2003; Traverse, 2007) and also discovered in the definite Triassic strata, the Karmay Fm (the definite Middle or Lower Triassic), Junggar Basin. *Trileites vulgaris is* characteristic for the Lower Triassic in Poland (Fuglewicz, 1973) and *Trileites pinguis* occurs in Triassic strata around South Australia (Dettmann, 1961) as well as Poland (Fuglewicz, 1973). They are consistent in the last occurrence at bed 37, which suggests the end of the Triassic and defines the Triassic–Jurassic boundary. However, *Hughesisporites sp*. is a common species in the Triassic, and thus the rare occurrence stratigraphically higher than this boundary could be reworked from older strata.

In addition, a secondary boundary could be suggested around the base of the Bed 43 (~ 40 m), on the basis of the first occurrence of *Hughesisporites kendollis, Trileites pullus, Horstisporites harrisi, Verrutriletes minutes* (Figure 4.4).

Besides, another three subdivisions can be distinctly defined on the basis of megaspore data. A boundary at about 245 m is recognized by the first occurrence of *Kuqaia quadrata, K. radiate, K. sp.*. A boundary at about 355 m is recognized by the last occurrence of *Calamospra rhaeticus, Hughesisporites kendollis, Trileites pullus.* At about 576 m, a boundary is recognized by the last occurrence of *Horstisporites harrisi, Kuqaia quadrata, K. radiate, K. sp., Verrutriletes minutes, Erlansonisporites sparassis, Bacutriletes lavatus*, and is also coincident with a broad range of the first occurrence of *Bacutriletes sp. Minerisporites institus, M. richardsoni, M. sp., Paxillitriletes phyllicus, P. sp.*.

In particular, the first occurrence of *Paxillitriletes phyllicus* and *Minerisporites institus* is in the late Pliensbachian age (Marcinkiewicz, 1988; Pieñkowski, 2004, summarized according to Marcinkiewicz, 1971; Kopik and Marcinkiewicz, 1997). Besides, *Minerisporites institus* is also documented as a marker for the Pliensbachian around the Polish swampy-lacustrine and swampy-lagoonal sub-systems (Anna Feldman-Olszewska, 1997). Therefore, stratigraphic age at the height ~520 m to ~ 570 m (Figure 4) can be identified as around the late Pliensbachian age.

Paxillitriletes phyllicus (Marcinkiewicz, 1988; Anna Feldman-Olszewska, 1997) and *Minerisporites richardsoni* (Anna Feldman-Olszewska, 1997) is applied to constrain stratigraphic age as Toarcian age, owing to their abundance at that stratigraphic interval.

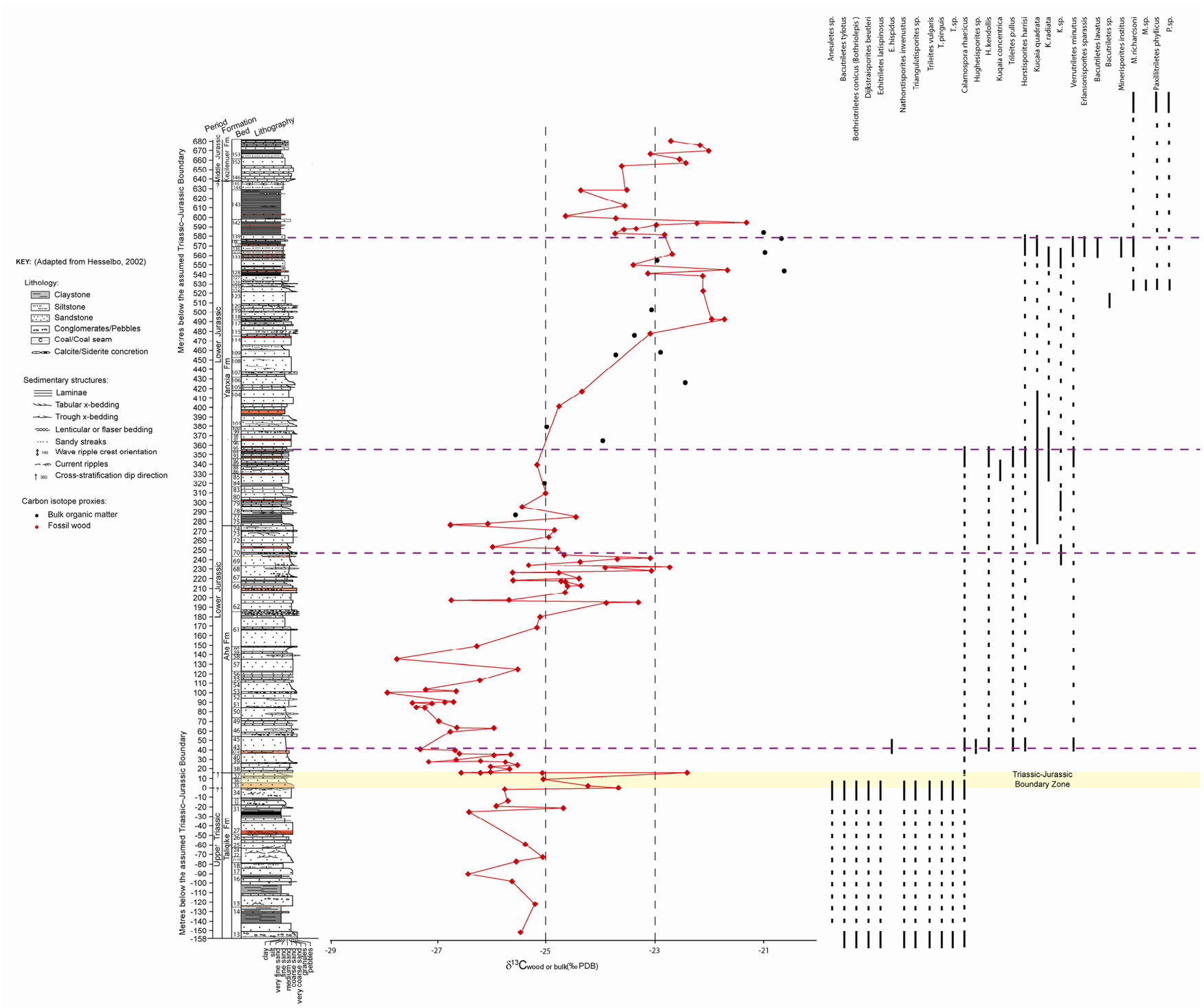

Figure 4.4. Lithostratigraphy, carbon-isotope stratigraphy and the biostratigraphic ranges of megaspore in the Kuqa section, N Tarim Basin, NW China. Five biostratigraphic boundaries can be identified (the megaspore data compiled from Wang et al., 2004).

Moreover, *Kuqaia* is an important stratigraphic marker which is widely found during the Sinemurian-Pliensbachian around the Europe (Morris *et al.*, 2009). *Kuqaia quadrata Zone (Sinemurian - Lower Pliensbachian)* is defined on the presence of the *Kuqaia quadrata* without *Horstisporites areolatus.* The lower boundary identified here coincides with the first common/abundant occurrence of the miospore *Cerebropollenites thiergartii* and the upper with the first common occurrence of the dinoflagellate cyst *Nannoceratopsis gracilis/senex* (Morris *et al.*, 2009), as discussed in more detail below. Moreover, the *Nannoceratopsis gracilis/senex* occurs early in the Early Toarcian in sections defined by ammonite stratigraphy (Poulsen and Riding, 2003).

In summary, combining all the previous megaspore data, the lowest horizon of the Pliensbachian age should be above the boundary at ~ 245 m. The horizon of ~ 576 m should be the boundary between the Early Pliensbachian and the Late Pliensbachian.

Pollen and miospores

According to the pollen occurrence and extinction, five stratigraphic boundaries can be identified between Bed 35 and Bed 37 (~0 m to ~18 m), about the top of the Bed 45 (~50 m), around Bed 73 to Bed 74 (~270 m), around Bed 92 (~345 m) and the base of Bed 139 (~576 m) (Figure 4.5).

The Triassic–Jurassic boundary can be identified at the interval of ~0 m to ~18 m, based on the last occurrence of *Alisporites minutisaccus, Alisporites parvus, Baculatisporites sp., Podocarpidites mutesimus, Osmundacidites alpines, Minotossaccus fusiformis, Minutasaccus parvus, Alisporites auritus, Alisporites australis*, and based on the first occurrence of *Cyathidites minor, Deltoidospora sp.* and *D. spp., Osmundacidites sp.* and *O. spp.,*

Quadraeculina minor, Quadraeculina anellaeformis, Quadraeculina enigmata, Osmundacidites elegans, Chasmatosporites sp. and *C. spp., Asseretospora sp.* and *A. spp., Podocarpidites proximus, Pseudopius sp., Podocarpidites miniculus, Protopicea sp.* and *P. spp., Piceaepollenites omoriciformis, Piceaepollenites exlioides*, although these pollen do not abruptly disappear or appear at the same horizons (Figure 4.5).

Minutasaccus parvus is reported in Triassic strata from India (Tripathi *et al.*, 2005). *Alisporites parvus* occurs in the Triassic to Jurassic boundary zones in New Zealand (Raine *et al.*, 2011), and in the Upper Triassic strata, northern Middle Siberia (Ilyina and Egorov, 2008) and in the Moenave Formation on the southern Colorado Plateau, USA (Lucas, *et al.*, 2011). *Alisporites parvus* is also reported as the last occurrence just below the Triassic–Jurassic boundary, which is constrained by the age of the Central Atlantic Magmatic Province (CAMP) volcanism in the Fundy Basin (Nova Scotia) and by the associated radiometric age constrains (Cirilli *et al.*, 2009). *Alisporites australis* occurs in the Upper Triassic strata, northern Middle Siberia (Ilyina and Egorov, 2008).

Additional pollen data are archived without specific stratigraphic position in the Kuqa section, but they also provide important age constrains. Specifically, they are combined as follows: *Aratrisporites granulates, A. fischeri, Limatulasporites limatulus (=Nevesisporites), and Jugasporites sp.*1 occur in the Taliqike Fm (Liu, 1999a) and their last occurrence is below the top of the Taliqike Fm (combined data from Liu, 1999a and Liu, 1999c) (Figure 4.5). *Zebrasporites* and *Parataeniaesporites* (Liu, 1999c) (*Zebrasporites corneolus* and *Parataeniaesporites pseudostriatus* involved in this study) importantly constrain the age ranges for the Triassic strata and *Zebrasporites corneolus* is also widely discovered in the Late Triassic around Europe (Klaus, 1960). *Aratrisporites* (*Aratrisporites granulates* and *A.*

fischeri involved in this study) are reported from the strata in the Junggar Basin where the strata are identified as the latest Late Triassic (Lu and Deng, 2005; Sha *et al.*, 2011).

Cerebropollenites thiergartii is a good marker for the Triassic–Jurassic boundary and its first occurrence is above the Triassic–Jurassic boundary (Gómez *et al.*, 2007; Hillebrandt *et al.*, 2007; Kürschner *et al.*, 2007; Lucas and Tanner, 2007; Ruhl *et al.*, 2009; Bonis *et al.*, 2010; Ruhl and Kürschner 2011) where it coincided with the starting horizon of the 'main negative excursion' (Ruhl and Kürschner 2011). This kind of pollen is documented in the southern Junggar Basin as the Triassic–Jurassic boundary marker (Sha *et al.*, 2011), but has not been reported in the Kuqa section, Tarim Basin.

On the basis of the pollen assemblage *Dictyohyllidites-Aratrisporites-Parataeniaesporites*, the top of the Triassic was identified around the top of Bed 37 (~18 m, see lithostratigraphy) by some authors (e.g. Liu, 1999c).

The palynological data from the Ahe Fm, Yangxia Fm, and Kezilernuer Fm in the Baicheng area (NW Tarim Basin, approximately 60 km away, west of the Kuqa section) are consistent in general features compared with these from the Kuqa section (Zhang W. P., 1990), but there are differences in the Ahe Fm. The difference could be derived from an error in identifying the regional lithostratigraphic boundary of the base of the Ahe Fm or from the improper definition of regional lithostratigraphy. For example, the ratio of gymnosperm pollen to fern spores becomes overwhelming above the basal Ahe Fm, in the Kuqa section, but the so called 'base of Ahe Fm' in the Baicheng area is still dominated by the fern spores (fern spore : gymnosperm Pollen = 7 : 4) (Zhang L. J., 1983; Zhang W. P. and Li Y. A., 1990). This flora is distinctly contrasted with that in the Kuqa section (Wu [1990] thought that Zhang L. J.

[1983] probably sampled from the incorrect strata). Additionally, the palynological data indicate a break of floral occurrence between Bed 37 and Bed 44 (Lu 2010, unpublished palynological data) in the Kuqa section.

In conclusion, according to the composite pollen data, the Triassic–Jurassic boundary is located at around the boundary between the Taliqike Fm and the Ahe Fm. For the very exact boundary, there are two candidate horizons, at the base of Bed 35 (~0 m) or top of Bed 37 (~18 m).

Going up-section, the last occurrence of *Alisporites australis* and *Podocarpidites proximus,* and the first occurrence of *Piceaepollenites exlioides, Piceaepollenites omoriciformis, Protopicea sp.* and *P. spp. Podocarpidites miniculus, Pseudopius sp.* define a boundary at the top of Bed 45 (~50 m).

The initial records of *Calamospora sp., Asophosphaera sp.* and *A. spp., Cerebropollenites sp.* suggest a possible boundary around Bed 73 to Bed 74 (~270 m).

The first occurrence of *Cyathea australis, Peripollenites sp.* and *P. spp., Concentrisporites sp.* and *C. spp., Calamospora sp., Protopinus sp., Cerebropollenites sp., Asophosphaera sp.* and *A. spp., Pseudopicea variabiliformis, Paleoconiferus sp., Chasmatosporites apertus, Callialasporites sp., Dictyophyllidites harrisii, Dictyophyllidites mortonii, Klukisporites pseudoreticulatus, Neoraistrickia sp., Lunzisporites lunzensis,* and *Chasmatosporites hians* can define a bio-event boundary and thus a stratigraphic boundary around Bed 92 (~345 m).

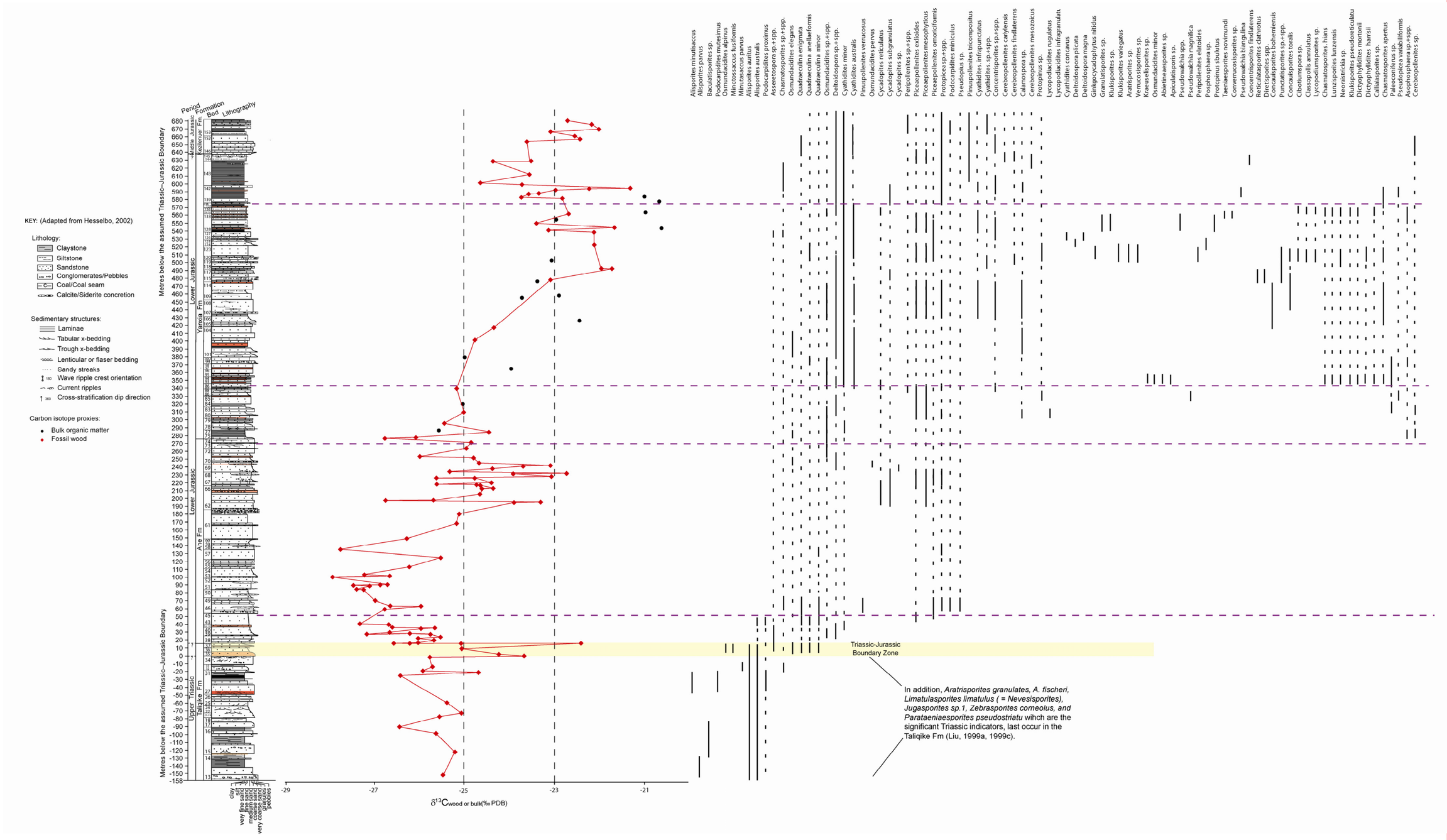

Figure 4.5. Lithostratigraphy, carbon-isotope stratigraphy and the biostratigraphic ranges of pollen and misospores in the Kuqa section, N. Tarim Basin, NW China. Five biostratigraphic boundaries can be identified (the pollen and miospore data compiled from Wang et al., 2004). Additional important information with stratigraphic significance from other independent resources is included as well (Liu 1999a, 1999c).

The last occurrence of *Podocarpidites proximus, Cycadopites reticulates, Cycadopites subgranulatus, Cibotiumspora sp., Classopollis annulatus, Lycopodiumsporites sp., Chasmatosporites. Hians, Lunzisporites lunzensis, Neoraistrickia sp., Klukisporites pseudoreticulatus, Dictyophyllidites mortonii, Callialasporites sp., Chasmatosporites apertus, Pseudopicea variabiliformis, Asophosphaera sp.* and *A. spp.* can define a bio-event boundary and thus a stratigraphic boundary around the base of Bed 139 (~576 m).

Notably, the first occurrence of *Cerebropollenites mesozoicus* indicates an age no older than the Sinemurian Age (Morbey, 1978), independently supported by evidence from offshore well, Norway (Millioud *et al.*, 1980).

The *genus Classopollis* is distributed across the world in the Upper Triassic-Upper Cretaceous (Turonian) strata (Reyre 1970; Srivastava, 1976). The first increase of the genus *Classopollis* in strata is reported as a marker around the latest Early Jurassic (Vakhrameyev, 1991). This first increase had also been documented occurring at the passage of Pliensbachian and the Toarcian and referred to the Early Toarcian thermal event (Vakhrameyev, 1982, 1991). In the Kuqa section, the first increasing *Classopollis* was independently reported in the Kezilernuer Fm by different authors (Zhang W. P., 1990; Liu 1999a). Zhang W. P. illustrated the top of Kezilernuer Fm, Bed 59 in the Section II around Baicheng area and the top of Kezilernuer Fm in the Kuqa section. However, Liu (1999a) did not point out the specific beds in the Kuqa section. Therefore, the top horizon of our sampling in the lower part of the Kezilernuer Fm, Kuqa section (Figure 4.5) is likely earlier than the Early Toarcian Age.

Trilobosporites antiques was discovered in the bottom part of the Kezilernuer Fm around the Kuqa section (Liu, 1999b). This kind of pollen was also reported in the Lower Jurassic

around the Surat Basin, Australia (Reiser and Williams, 1969). In addition, Liu, (1999b) correlated the pollen data in the Kuqa section with those from the Surat Basin. He placed the Kezilenuer Fm into the Middle Jurassic without giving any further explanation or citation. A logic gap is overlooked in this reasoning, probably because Liu, (1999b) did not combine all the available pollen data in the Jurassic Kuqa section, and thus did not notice that the occurrence of *Trilobosporites antiques* at the bottom of Kezilernuer Fm is the first occurrence. Therefore, the author (Liu, 1999b) just follows previous lithostratigraphic divisions in the official Regional Geological Survey Report. In summary, the first occurrence of *Trilobosporites antiques* indicates that the bottom of Kezilernuer Fm unambiguously belongs in the Lower Jurassic rather than into the boundary between Lower and Middle Jurassic as otherwise thought (see lithostratigraphic divisions and references therein, Table 4.1).

In the Figure 4.5, the pollen and miospores which exist constantly through the whole study strata from -158 m to 680 m are not presented, because they have no stratigraphic significance (see dataset, Appendix D). These Pollen and miospores are: *Araucariacites. sp., Piceites expositus, Piceites podocarpoides, Densoisporites scanicus, Classopollis sp., Osmundacidites wellmanii, Psophosphaera sp.* and *P. spp., Piceaepollenites complanatiformis, Podocarpidites multicinus, Podocarpidites sp.* and *P. spp., Quadraeculina limbata, Quadraeculina sp.* and *Q. spp., Abietineaepollenites sp.* and *A. spp., Piceaepollenites sp.* and *P. spp., Piceites sp.* and *P. spp., Pinuspollenites divulgatus, Pinuspollenites sp.* and *P. spp., Cyclogranisporites sp.* and *C. spp., Pinuspollenites pernobilis, Cadargasporites sp.* and *C. spp., Chordasporites sp.* and *C. spp., Protoconiferus sp.* and *P. spp., Araucariacites australis, Alisporites sp.* and *A. spp.*.

4.4 Sampling and method

4.4.1 Sampling

The samples were collected from the Triassic–Jurassic sequences at the Kuqa section around the Kuqa River area, Kuqa County, North Tarim Basin, Xinjiang Province, China. GPS location: 42°9'10.20'N, 83°10'34.10'E (Figure 2). In the Kuqa section, two days' field work was carried out in 2004 by Stephen Hesselbo, Shenhui Deng and Yuanzheng Lu, and three days' field work was carried out by Linhao Fang and Yuanzheng Lu in 2010. Linhao Fang made the field observations, lithological descriptions and photographs, generated the detailed lithostratigraphic log in field notebooks, and collected part of the samples. Yuanzheng Lu guided identification of the lithostratigraphic units and then aided labelling and sampling. To the best of our understanding, there is no major hiatus through the whole working outcrop in the Kuqa section.

When the samples were collected in the field, the sampling materials were concentrated on fossil wood, including charcoal and coalified wood. For the strata without wood fossils, the carbon-rich mudstone or the coal was collected for bulk organic carbon-isotope analysis.

Isolated wood macrofossils can be readily recognized. For fossil wood preserved in coal seams required more care in identification. Each sample was examined by naked eye in the field and under microscope in the laboratory (see the detailed description and the examined results in Appendix D.3 and Appendix D.4). Selected samples, which ranged from typical fossil wood to ambiguous or definite non-wood, were observed using scanning electronic microscopy (SEM) (see Appendix D.4).

4.4.2 Method

4.4.2.1 Pre-treatment and preparation

Samples were prepared in the Wet Chemistry Laboratory, Department of Earth Sciences, University of Oxford, UK.

With regard to fossil wood, a 0.5 to 1 g sample was placed into the 15 ml centrifuge tube and deionized water added. The tube was placed into an ultrasonic bath for 10 minutes to clean the surface dust and then dirty water removed. This procedure was repeated 2 to 3 times until the deionized water remained clear after ultrasonic washing. Subsequently, hydrochloric acid (30%) was added to remove carbonate and sulphur while placing the centrifuge tube into the 55°C water bath on a magnetic-stirrer. The cap of the centrifuge tube was released, in order to release the CO_2 and gaseous sulphur. After 2 or 3 hours, after yellowing of the hydrochloric acid (part of the elemental sulphur dissolves into the acid) the acid was replaced by new hydrochloric acid (30%). This water bath procedure under hydrochloric acid was repeated for 5 to 10 times until the acid remained clear at the end of a 2 or 3-hour reaction. After decanting, the sample was washed with deionized water until the pH approached 7. The fossil wood was dried at 55 °C in an oven for 48 hours ready for weighing out.

With regard to the bulk organic matter, a 3 to 5 g sample was placed in a glass beaker and deionized water added. The ultrasonic surface-washing procedure was the same as that of fossil wood. After the surface was cleaned up, the organic matter sample was dried at 55 °C in an oven for 48 hours. The dried organic matter sample was then powdered by silica mortar and collected into 50 ml centrifuge tube. Hydrochloric acid (30%) was slowly added into the centrifuge tube to remove carbonate and sulphur in a 55 °C water bath on the magnetic-stirrer

for 2 or 3 hours. Subsequently, the following procedures are the same as that for fossil wood above, except for the acid or water removal. Due to the bulk organic matter being in powder state, before the liquid poured out from the 50 ml centrifuge tube, the samples were centrifuged to firmly deposit solid matter at the bottom of centrifuge tube.

4.4.2.2 Carbon-isotope measurement

The samples for analysis were weighed out and sealed in 5 x 8 mm tin capsules. These samples were run on a Sercon Europa EA-GSL sample converter connected to a Sercon 20-22 Stable Isotope Ratio Mass Spectrometer running in continuous flow mode with a Helium carrier gas with a flow rate of 70 ml per min. Carbon isotope ratios were measured against an internal alanine standard ($\delta^{13}C_{alanine}$ = -26.9 ± 0.2‰ V-PDB) using a single point calibration at the Research Laboratory for Archaeology and History of Art (RLAHA), University of Oxford, UK. The in-house RLAHA alanine standard is checked weekly against USGS40, USGS41 and IAEA-CH6 international reference materials. Thus the reported results are traceable back to the V-PDB international standard.

4.5 Results

4.5.1 Stratigraphic boundaries based on biological turnovers

The stratigraphic boundaries that are defined by the biological events are synthetically presented in Figure 4.6. The Triassic–Jurassic boundary zone (marked as Boundary A, see Figure 4.6) is constrained around Bed 35 to Bed 37 (~0 m to ~18 m) by the three kinds of biological records consistently (also see Section 3.3). The boundary (marked as Boundary B, see Figure 4.6) at Bed 43 to Bed 46 (~42 m to ~55 m) shows consistency across different datasets, although the megaspores exhibits turnover a bit earlier. The boundary (marked as Boundary D, see Figure 4.6) at the base of Bed 139 (~580 m) is the most consistent, as the three boundaries of plant macrofossil, pollen and megaspore events occur closely in the same horizon. The boundary (marked as Boundary C, see Figure 4.6) at a relatively broad range from Bed 70 to Bed 75 (~246 m to ~278 m), is defined by the three kinds of biostratigraphy. Besides, the plant macrofossil and pollen boundaries are fairly close and narrowed to Bed 74 to Bed 75 (~270 m to ~278 m). At the horizon (marked as Boundary C', see Figure 4.6) about Bed 89 to Bed 94 (~340 m to ~355 m), only plant macrofossils and megaspores indicate biological event boundaries, whereas plant macrofossils seem not to be distinctly influenced at interval. Interestingly, the pollen event boundaries appear always slightly earlier than the boundaries defined by the plant macrofossils.

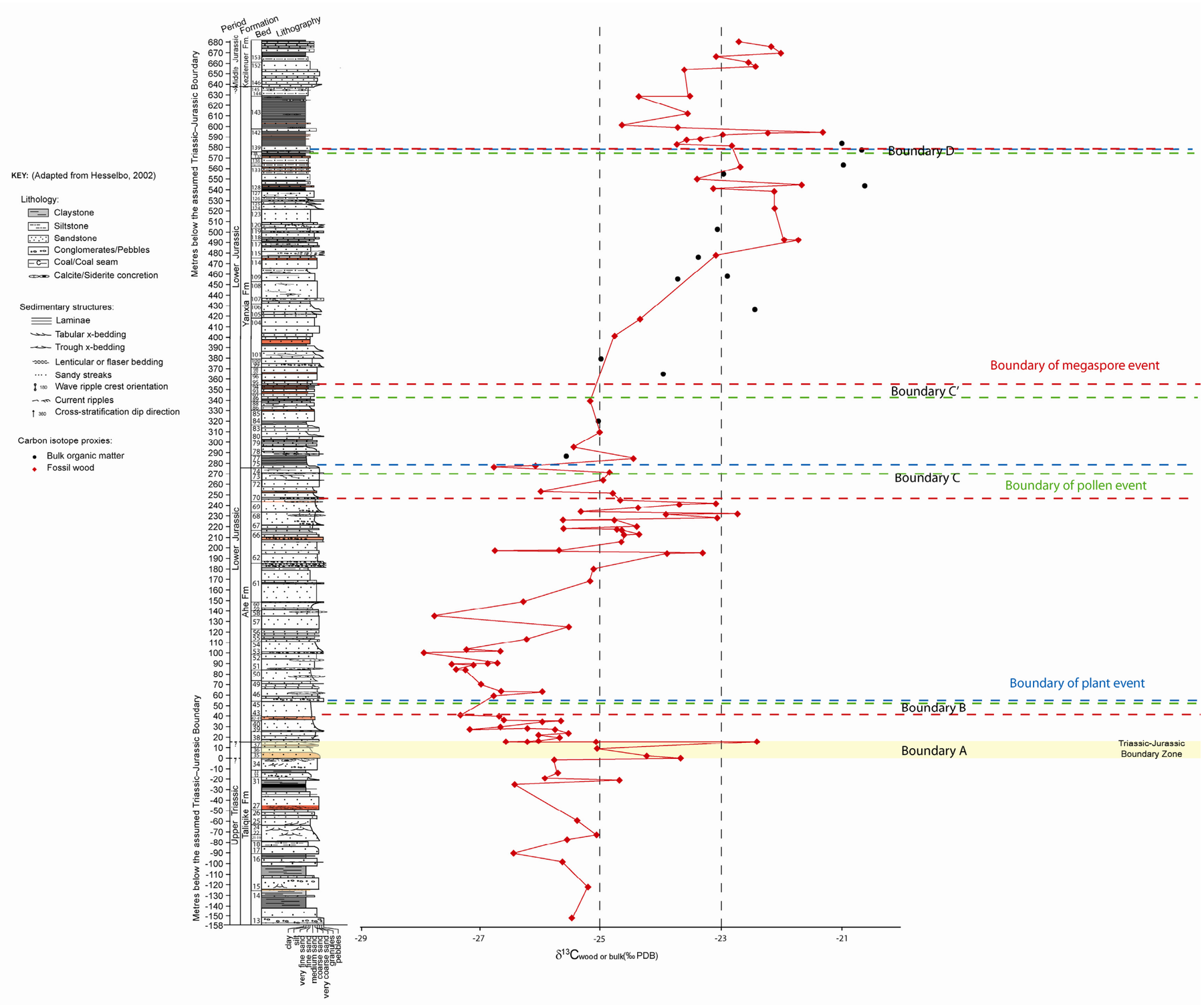

Figure 4.6. A synthesis of biostratigraphic boundaries. Red dashed line = boundary of megaspore event, green dashed line = boundary of pollen event, and blue dashed line = boundary of plant macrofossil event. Yellow shadow = Triassic-Jurassic boundary zone. Boundary A, B, C, C' D are marked for the identified boundaries of biological events.

These abrupt changes in floras documented in the Kuqa section should reflect the real biotic turnover due to fluctuation in the ecosystems rather than indicate the presence of a hiatus. There are two lines of evidence supporting this inference. First, the hiatuses tend to occur in the conglomerate beds of fluvial channel facies, but no remarkable erosional surfaces have been observed on the base of the base of conglomerate beds in field of this study. In addition to the observation and analysis of sedimentary facies, there are no major hiatuses identified on basis of carbon-isotope stratigraphy, as no abrupt changes in carbon-isotope values took place through the whole working section.

4.5.2 Carbon-isotope stratigraphy in the Kuqa section

The 114 carbon-isotope data from fossil wood and 15 data from bulk organic matters were generated. Carbon-isotope stratigraphy plotted against the lithological succession in the Kuqa section is presented in Column A (Figure 4.7). Some of the most notable points are as follows:

1) The red diamonds represent fossil wood and the black dots represent bulk organic matter. The bulk organic matter is generated as a supplement when the fossil wood is rare or absent in the horizons. Thus, there are only a few close horizons with data of both bulk organic matter and fossil wood. However, for these points, the carbon isotope values of fossil wood are similar to that of the bulk organic matter. The trend of the carbon-isotope curve of fossil wood is broadly consistent with that of the bulk organic matter. From ~270 m to ~585 m, carbon-isotope curves of fossil wood and bulk organic matter both exhibit a trend towards heavier values.

2) The carbon-isotope values present systematic positive and negative fluctuations against the lithostratigraphy through the latest Triassic to the Early Jurassic (Figure 4.6). The majority of adjacent points fluctuate commonly within the amplitude of 2 per mil. A good carbon-isotope stratigraphic character is documented.

Looking at the general trends of carbon-isotope profiles, overall there is an increase from relatively light carbon-isotope values (-28‰ to -25 ‰) below Boundary A and around Boundary B to heavier values (-23‰ to -21 ‰) around Boundary D (Figure 4.6). Before the Triassic (i.e. below Boundary A), carbon-isotope values are generally relatively light, but they are heavier than those of interval ~18 m to ~150 m. Through the whole section, the maximum points appear in the bulk organic matter at ~543 m (at about -20‰) and in the fossil wood at ~595 m (at about -21‰). The minimum points are present at ~100 m (at about -28‰) in the fossil wood but there is no carbon isotope of bulk organic matter from this level.
3) As introduced previously, most excursions between two adjacent points are limited within a 2‰ range; thus the points that vary more than 2‰ amplitude are noticeable. These points are

respectively at ~18 m associated with the Triassic–Jurassic boundary zone, ~198 m associated with the top of thick-bedded conglomerate strata, ~230 m associated with the base of a conglomerate bed, and ~598 m associated with the top of a sandstone bed (relatively coarse to the black shales upward). Noticeably, except for the two points at 0 m and 10 m around Boundary A, all other points with larger adjacent excursions are turning from heavy into light carbon-isotope values (see Section 4.6.2).

4) The horizons at ~ 0 m, and 10 m to 18 m are unusual in that carbon-isotope values at these horizons rapidly increase with the amplitude of more than 2‰, and then promptly descend

into lower values. The abnormal intervals suggest a dramatic carbon-isotope fluctuation and infer a remarkable perturbation in the exchangeable carbon reservoirs.

5) The lowest horizons of laminated mudstones tend to have relatively light carbon isotope values, for example, at the base of Bed 75 (~275 m) and at the base of Bed 143 (~598 m). All boundaries in Figure 4.6 except for Boundary C' (probably due to low-resolution records in this boundary), are associated to some extent with negative excursions of 1‰ to 2‰.

4.5.3 Global correlations

The tentative global correlation of the carbon-isotope stratigraphy is presented in Figure 7, supported by the integrated biostratigraphy as previously discussed (see Section 4.3). Column A represents carbon-isotope stratigraphy as documented in fossil wood, which is through the Late Sinemurian to Early Toarcian and collected from Robin Hood's Bay, Yorkshire, England (Korte and Hesselbo 2011). Column B represents the carbon-isotope stratigraphy derived from fossil wood and terrestrial bulk organic matter from the Kuqa section. Column C represents the carbon-isotope stratigraphy against the time axis documented in the inorganic carbonate, which is derived from the belemnite (blue diamond) or bivalves (red square) around the Tethys realm, UK and Portugal (compiled and succeeded by Dera *et al.*, 2011 from published literature). Carbon-isotope stratigraphic records in the Column A and Column C are well defined by ammonite zones.

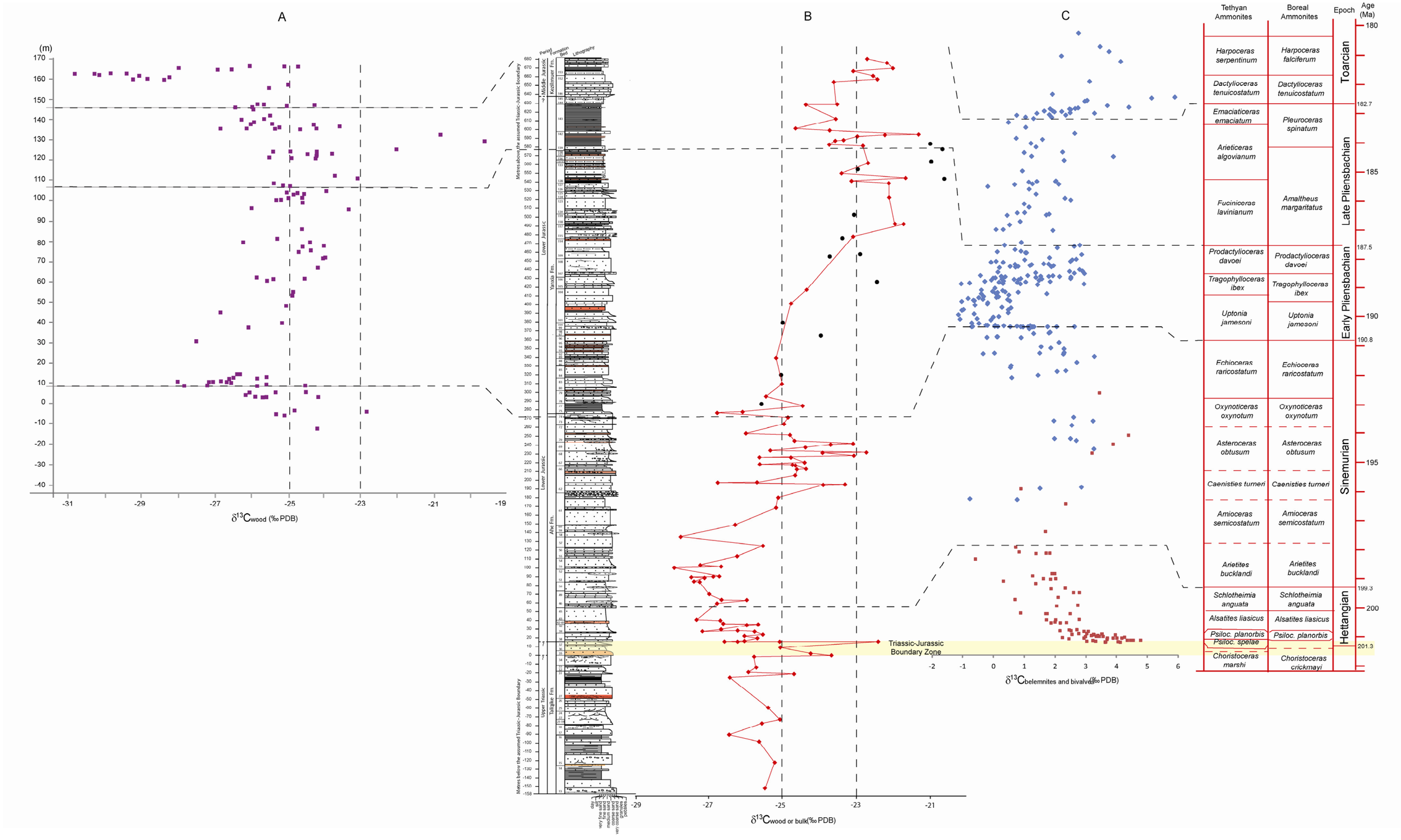

Figure 4.7. Global correlation of the carbon-isotope stratigraphy from both terrestrial (/atmosphere) and marine reservoirs. Column A is generated from fossil wood in England (Korte and Hesselbo 2011); Column B is generated from fossil wood in the Kuqa section N Tarim Basin, NW China; and Column C presents the carbon-isotope stratigraphy from inorganic carbonate of mostly UK sections (Jenkyns et al., 2002; Korte et al., 2011). All data have been calibrated to the GTS 2012, and the correlation is based on biostratigraphy.

On the basis of biostratigraphy, the carbon-isotope stratigraphy documented in fossil wood from England can be coherently correlated with entirely terrestrial carbon-isotope stratigraphy in Column B from the Kuqa section. During the same age interval, overall trends with positive or negative excursions are present in both records, from the Late Sinemurian to Late Pliensbachian (Figure 4.7).

Comparing the two curves, the Early Pliensbachian to Late Pliensbachian shows a positive excursion of ~5‰ both in fossil wood in England (Column A, from ~28‰ to ~23‰) and fossil wood in the Kuqa section (Column B, from ~27‰ to ~22‰). The negative excursion through the boundary between the latest Late Sinemurian and earliest Early Pliensbachian reaches ~4‰ both in Column A (from ~28‰ to ~24‰) and Column B (from ~27‰ to ~23‰), if only one point heavier than -23‰ is ignored in Column A. It is noted that there seems to be an offset by ~1‰ between curves of Column A and Column B, in which the carbon-isotope stratigraphy is derived from the fossil wood.

In terms of biostratigraphy, the carbon-isotope stratigraphy documented in belemnites or bivalves from UK and Portugal, Column C can be correlated with Column B very well. The isotopically positive or negative carbon-isotope excursions are consistently present in both Column B and Column C from the earliest Triassic to the Late Pliensbachian (Figure 4.7).

Specifically, a long-term negative carbon-isotope excursion is well documented in the both terrestrial fossil wood and marine carbonates (belemnites and bivalves) in the Sinemurian. This long-term negative excursion starts with a rapid negative shift and then maintains the relatively light carbon-isotope values through the entire Sinemurian. Through the Sinemurian, the overall trends start with light carbon-isotope values evolving into relatively heavy isotope

values, then returning to relatively light values again before the end of the Sinemurian. Upwards in the section, the Early Pliensbachian interval continues to show strong similarities between Column A and Column B: here is an unambiguous trend towards isotopically heavy values from the Early Pliensbachian to the Late Pliensbachian both in Column A (from ~28‰ to ~23‰) and Column C (from ~-1 to ~3‰).

In the Late Pliensbachian interval, fossil wood in Column A documents abnormally heavy carbon-isotope values, and the belemnites (or bivalves) from UK and Portugal in Column C just exhibits a trend towards to heavier values without abnormally heavy isotopes. In the Kuqa dataset Column B, there is a general increasingly heavy isotope trend in the Late Pliensbachian. However, the carbon-isotope stratigraphy presented in Column B seems to be far from the entire Late Pliensbachian, assuming the sedimentation rate would not dramatically vary without any noteworthy tectonic movement. The Early Pliensbachian strata are ~300 m thick, whereas Late Pliensbachian strata here are just logged as ~100 m thick: the Early Pliensbachian ~3.3 Myr but the Late Pliensbachian lasted for ~4.8 Myr (according to GST 2012).

4.6 Discussion

4.6.1 A tentative proposal on revising the chronologic division in the Kuqa section, N Tarim, NW China

A revised chronology of the Kuqa section is proposed in the present chapter, based on a combination of the traditional lithostratigraphy, magnetostratigraphy, newly compiled and analysed biostratigraphic dataset (including plant macrofossils, pollen and misosproes, and megaspores), and carbon-isotope stratigraphy.

According to previous authors, the boundary between the Early Jurassic and Middle Jurassic is recognized at the end of Yangxia Fm in the Kuqa section and also around the whole N Tarim region (Wang *et al.*, 2004; and see Section 4.3.1 and Table 4.1). The new results in the present chapter clearly illustrate that the upper part of Yangxia Fm still stay in the Late Pliensbachian (even in the early Late Pliensbachian). As the duration of Toarcian and the Late Pliensbachian are respectively 8.6 Myr and 4.8 Myr (according to GTS2012), the age of Yangxia Fm should be at least ~10 Myr earlier than conventional chronologic schemes, as long as the field observation and inference of lack of major hiatus is correct. The regional chronological division in the N Tarim could also be largely revised, although it is admitted that further independent evidence and tests are necessary.

The establishing 'floating' astronomical time scales in the Jurassic provide much of improved age duration for the Jurassic system (GTS 2012, Chapter 26). The duration of the Hettangian is shortened to 2.0 Myr, but the Sinemurian, Pliensbachian, and Toarcian is extended to 8.5 Myr, 8.1 Myr, and 8.6 Myr, respectively (GTS 2012, Chapter 26). This revision should be

paid attention when the sedimentation rates are estimated in study of the regional chronological schemes.

4.6.2 The exact position of the Triassic–Jurassic boundary in the Kuqa section, N Tarim Basin

Based on the integrated biostratigraphic data, the Triassic–Jurassic boundary is located at a transitional zone between the Taliqike Fm and the Ahe Fm. However, it is difficult to work out whether the definite boundary horizon should be identified on the top surface of Bed 37, or around 18 metres lower, on the top surface of Bed 34. Because the basal deposits of the Bed 38 are conglomerates, the top surface of Bed 37 has previously been considered as the Triassic–Jurassic boundary (Zhang L. J., 1980; Liu, 1999b, 1999c; Wang *et al.*, 2004) due to its being the boundary of the lithostratigraphic units (Figure 4.7).

Interestingly, the top surface of Bed 34 is characterized by distinct deformation structures (convolute bedding), which seem to be the structure of seismites (field notes of S.P. Hesselbo, 2004). Both the character of the structure and the occurrence at the Triassic–Jurassic boundary recall similar phenomena in NW Europe (Mayall, 1983). The unique seismite from the latest Triassic are extensively documented around the United Kingdom (across > 250,000 km^2) and they are inferred as the evidence for bolide impact occurring at the end of Triassic (Simms, 2003). Deformation depositional structures coincide with the abrupt (> 2‰ at two adjacent points, see Section 4.5.2) carbon isotope positive excursions at ~ 0 m in the Kuqa section. This synchronous coincidence might suggest a cause-effect relationship, by which the bolide impact might trigger the sharp atmospheric carbon-isotope fluctuations due to an abrupt influence on ecosystems and synchronously yield soft-sediment deformation.

More interestingly, looking into the details of Figure 4.4, the 10 megaspore species sharply disappear at a same horizon above 0 m but below 18 m. This observation clearly suggests that a rapid disturbance in ecological system is presented below 18 m in the Kuqa section. Therefore, this evidence supports placement of the Triassic–Jurassic boundary at the 0 m. In the St Audries Bay section, the Triassic–Jurassic boundary is now placed at the top of the Langport Member - i.e. above the deformed bed ('seismite') and below the subsequent positive excursion (Korte *et al.*, 2009). Moreover, palynological extinctions are abrupt and synchronous throughout the Newark Supergroup, USA (Fowell and Olsen, 1993) and the Eiberg basin, Austria (Bonis *et al.*, 2009) going across the Triassic–Jurassic Boundary.

Therefore, the present evidence and correlation suggest that the boundary should be placed at top of Bed 34 (~0 m). It is admitted that this identification is not conclusive and more lines of convincing evidence and intensive studies are still required in the future.

4.6.3 Negative and positive excursions around the Triassic–Jurassic boundary

The various analysis of materials around the Triassic–Jurassic boundary have been reported, including marine bulk carbonate (Galli *et al.*, 2005; Galli *et al.*, 2007; Van de Schootbruge *et al.*, 2008), marine bulk organic matter (Ward *et al.*, 2001; Pálfy *et al.*, 2001; Hesselbo *et al.*, 2002; Galli *et al.*, 2005; Ward *et al.*, 2007; Williford *et al.*, 2007; Kuerschner *et al.*, 2007; Quan *et al.*, 2008, Ruhl *et al.*, 2009; Bonis *et al.*, 2009, 2010), and the entire terrestrial organic matter, such as fossil wood (Hesselbo *et al.*, 2002), bulk leaf cuticles (Bacon *et al.*, 2011) and terrestrially derived organic compounds (Whiteside *et al.*, 2010; Ruhl *et al.*, 2011).

Negative carbon-isotope excursions are reported by several authors (Pálfy *et al.*, 2001; Hesselbo *et al.*, 2002; Quan *et al.*, 2008; Korte *et al.*, 2009; Bonis *et al.*, 2009, 2010; Ruhl *et al.*, 2009, 2011; Bacon *et al.*, 2011) across and above the palaeontologically defined Triassic–Jurassic boundary. On the other hand, positive carbon-isotope excursions are also reported (Ward *et al.*, 2001, 2007; Williford *et al.*, 2007) above the palaeontologically defined boundary. These positive carbon-isotope excursions are highlighted by distinctly heavy $\delta^{13}C$ values relative to their 'baseline value'. The observation of both positive and negative excursions around the Triassic–Jurassic boundary reported by the different authors from various locations appears to be a paradox. However, the so called 'positive' or 'negative' is relative to the 'observed baseline value' rather than to a fixed baseline value. If this argument can be accepted, when the published results are re-examined, it is readily found that some kind of relative positive excursion exists (located above the Triassic–Jurassic boundary but below the main negative isotope excursion) in the literature, where the authors emphasize the negative excursions (Hesselbo *et al.*, 2002; Quan *et al.*, 2008; Korte *et al.*, 2009; Ruhl *et al.*, 2009, 2011; Bonis *et al.*, 2009, 2010): in the specific contexts, the different authors emphasised different points.

As pointed out in Section 4.5.2, around the Triassic–Jurassic boundary in the Kuqa section, there are positive and negative carbon-isotope fluctuations (Figure 4.7, Column B). Below the main negative isotope excursion starting in the earliest Jurassic section, there is a distinct positive excursion interval (~0 to ~18 m) in the Kuqa section. This positive excursion interval comprises two peaks at ~0 m and ~18 m. Although the upper positive peak (at ~18 m) is just defined by one point, if the one point is ignored, the positive excursion interval (~0 to ~18 m) still exists. Similarly, a positive peak interval at ~ 12 m below the earliest Jurassic main negative excursion is witnessed by the fossil wood from East Greenland despite a minor

hiatus (Hesselbo *et al.*, 2002). In the marine bulk organic matter, similar positive carbon-isotope fluctuations before the main negative carbon-isotope excursions are clearly observed in St. Audrie's Bay, SW England with the positive peak ranging over ~5 m of strata (Hesselbo *et al.*, 2002), in Kennecott Point, Western Canada with the positive peak ranging over ~50 m of strata (Williford *et al.*, 2007), and in Muller Canyon, Nevada, USA with the positive peak ranging over ~20 m of strata (Guex *et al.*, 2004; Ward *et al.*, 2007). A positive carbon-isotope peak is observed in belemnites and bivalves in the earliest Jurassic (Figure 4.7, Column C). In addition, although the resolution of correlation between the terrestrial Kuqa section and marine European sections is not adequate for much comparative detail, the clear heavy carbon-isotope values at the very earliest Jurassic in the marine deposits do suggest that the positive peak interval (~0 m to ~18 m) at the Kuqa section is a reliable stratigraphic record rather than a record of local signals. In summary, the interval above the palaeontologically defined Triassic–Jurassic Boundary but below the main negative carbon-isotope excursion consistently and widely shows relative positive carbon-isotope excursions at the Kuqa section and other locations across the world.

However, it is difficult to conclude whether these positive $\delta^{13}C$ excursions reported from various locations are synchronous or not, due to lack of sufficient age resolutions in the biostratigraphy. In order to make a robust correlation of carbon-isotope curves between the different locations, the same/similar time scales should be followed. The traditional basis of biostratigraphy provides not only an age tie-point constraint, in an alternative perspective, but naturally also a time-scale standard (e.g. in a scale of 10^5-10^6 years rather than in a scale of 10^2-10^3 years). For instance, the carbon-isotope stratigraphic correlation over a long distance (e.g. from Europe to America) can be based on the biostratigraphy over a relatively long-time scale (e.g. over the whole Early Jurassic or across even longer time); nonetheless, the

biostratigraphic constraint for the correlation in a short-time scale (e.g. around the transitional zone of Triassic–Jurassic boundary which may be within ~1-2 Myr) may not work due to being insufficient stratigraphic resolution. In the latter case, biostratigraphy commonly provides a tie point rather than an internally calibrated ruler, as the resolution of biostratigraphy itself is commonly lower than that of chemostratigraphy. Moreover, when the correlation interval deviates further from the biostratigraphic tie points, the carbon-isotope stratigraphic correlation over a long distance becomes less and less certain. The problem is exacerbated when the correlation tie points are based on correlatable but not exactly the same fossil zones. Therefore keeping to the same/similar time scale or biostratigraphic scheme is an important premise for detailed chemstratigraphic correlation, as the resolution of biostratigraphy is commonly insufficient to give intensive chemstratigraphic correlation in detail.

In conclusion, given the baseline values below the Triassic–Jurassic boundary the negative and positive excursions around the Triassic–Jurassic boundary might be not a paradox from a local chaos, but rather suggest global events of carbon-isotope perturbations.

4.6.4 Perturbation of the atmospheric carbon cycle in a global scale and coupled ocean-atmospheric carbon-isotope reservoirs

As the results presented in this chapter (see Figure 4.7 and Section 4.5.3), the carbon-isotope stratigraphy of fossil wood from the Kuqa section, N Tarim Basin can be coherently correlated with other fossil wood records from European locations across the Triassic–Jurassic boundary (Hesselbo *et al.*, 2002; Bacon *et al.*, 2011) and through the Late Sinemurian and the Pliensbachian (Korte and Hesselbo, 2011). This nearly synchronous $\delta^{13}C$

excursion record from fossil wood indicates that the carbon-isotope stratigraphy from the Kuqa section registers global rather than only local characters. Moreover, the carbon-isotope stratigraphy derived from fossil wood documents $\delta^{13}C$ fluctuations in atmospheric CO_2 (Farquhar *et al.*, 1989; Arens and Jahren., 2000; Gröcke, 2002; Jahren *et al.*, 2008), which can be used to infer perturbation of the carbon cycle in the atmospheric reservoir. Thus, an important perturbation of the atmospheric carbon cycle is reflected by the rapid negative and positive $\delta^{13}C$ excursions around the Triassic–Jurassic boundary; and a relatively steady long-term atmospheric evolution through the Early Jurassic is inferred by a relative steady $\delta^{13}C$ trend (Figure 4.7).

Furthermore, the terrestrial carbon-isotope stratigraphy from the Kuqa section can be also broadly correlated with the $\delta^{13}C$ records derived from marine carbonates around the Triassic–Jurassic boundary and through the Early Jurassic (Figure 4.7, Column C). The nearly synchronous $\delta^{13}C$ fluctuations in the atmospheric and marine reservoirs suggest that ocean-atmosphere carbon reservoirs are in a coupled situation both at the long term scale (inter-Age scale) evolutions, and at the short-term scale (within 1 Myr or even shorter) when dramatic carbon perturbations are taking place. Thus, the Triassic–Jurassic boundary and the Early Jurassic could undergo a co-evolution of ocean-atmospheric carbon reservoirs on a global scale.

4.7 Conclusions

1) The carbon-isotope stratigraphy from the Kuqa section, N Tarim can be coherently correlated with both terrestrial and marine records globally, on the basis of biostratigraphy. Specifically, the overall trends of positive and negative isotope excursions are closely synchronous and similar in contemporary intervals across various locations worldwide.

2) A revised chronological division of the lithostratigraphic units in the Kuqa section is proposed on the basis of the newly compiled biostratigraphy and newly generated carbon-isotope stratigraphy. The division of the Hettangian, Sinemurian and Early Pliensbachian stage are identified in the Kuqa section, N Tarim. The Yangxia Fm is more than 10 Myr older than previously identified, according to this new age assignment. The ages of other corresponding formations are updated as well.

3) The success of stratigraphic correlation further verifies that carbon-isotope stratigraphy is a powerful tool for stratigraphic correlation over long distances, and particularly useful as a bridge between the marine and terrestrial strata. In addition, carbon-isotope stratigraphy can greatly improve the resolution of stratigraphic correlations.

4) The exact horizon of the Triassic–Jurassic boundary has been disputed and suggested, on the basis of the new results in the present chapter. The available lines of evidence prefer that the boundary be placed at the top of Bed 34 (~0 m). This differs with the traditional ideas that are primarily based on the boundary of lithostratigraphic units.

5) The soft-sediment deformation bed immediately below the Triassic–Jurassic boundary in the Kuqa section clearly resembles those in NW Europe. The similar features, such as positions just below the Triassic–Jurassic boundary, rapid carbon-isotope disturbance, and a dramatic change in biostratigraphic records, suggest a potentially common origin, which may be associated with a huge bolide impact.

6) As the carbon-isotope stratigraphy from the Kuqa section correlate globally very well, the synchronous carbon-isotope excursions suggest that the carbon-cycle perturbations on a global scale occurred across the Triassic–Jurassic boundary on the short term and through the Early Jurassic on the long term. The results imply that the atmosphere and ocean carbon reservoirs were coupled during this interval.

7) Palynological overturns, especially for megaspores, are unambiguously documented in the Kuqa section across the Triassic–Jurassic boundary. This biological disturbance can be correlated with the terrestrial ecological system in the Newark basin, USA and Eiberg basin, Austria through the same time interval. This long spatial distance suggests a significant crisis in terrestrial ecosystems globally occurring during the same time.

Chapter 5

CONCLUSIONS AND OUTLOOK

5.1 Conclusions

The work presented in this thesis made use of the three case studies to explore terrestrial carbon-isotope stratigraphy, which recorded the fluctuations of exchangeable carbon reservoirs in the Early to Middle Miocene and Triassic-Jurassic boundary to the Early Jurassic.

For the case study in the New Jersey margin, coherent stratigraphic trends and excursions in carbon-isotope values are observed for a variety of sedimentary organic matter components, specifically including: concentrated phytoclast separates, individually picked woody phytoclasts, and bulk organic matter adjusted on the basis of C/N ratios to be equivalent to vascular plant debris. The raw bulk carbon-isotope values from the shallow-marine deposits are based on mixed marine-terrestrial components resulting in quite ‘noisy’ signals. The carbon-isotope stratigraphic correlation among the three New Jersey margin boreholes shows good consistency. With important exceptions, there is little or no observational support for significant reworking, degradation or diagenetic alteration, or floral change in the hinterland. The terrestrial carbon-isotope stratigraphy for the New Jersey margin does not match well with the positive carbon-isotope excursions based on benthic and planktonic foraminifers from oceanic settings during the mid-Miocene (Langhian) Monterey Event. The terrestrial carbon-isotope stratigraphic records in the Burdigalian from Site 29 yield a relatively heavy isotopic signature compared to Langhian. This Burdigalian interval from Site 29 underwent relatively low sedimentation rate and is notably associated with glauconite occurrence. The most likely explanation for notably heavy carbon-isotope records in the Burdigalian interval is that reworking deposition of phytoclast from older strata has occurred in clinoform toe-of-slope facies.

For the case study in the Danish North Sea Basin shallow shelf, coherent terrestrial carbon-isotope stratigraphic signatures are observed in both concentrated phytoclast separates and raw palynological residues in each borehole. Consistent carbon-isotope stratigraphy is observed in the two local boreholes. There are no distant positive carbon-isotope excursions observed in the terrestrial carbon-isotope stratigraphy for the depositional interval equivalent to the mid-Miocene (Langhian) Monterey Event. The sediments with abundant glauconite occurrence that resemble those in the New Jersey case study coincide with relatively heavy carbon-isotope values and were associated with low sedimentation rate, but the notable interval in the two boreholes from the Danish North Sea is in the Serravallian; in contrast to the heavy values in the Burdigalian at Site 29, New Jersey margin. The terrestrial carbon-isotope stratigraphy of New Jersey shelf can be broadly correlated with the terrestrial carbon-isotope stratigraphic records in time-equivalent strata in North Sea Basin, except for the glauconitic interval with notably heavy carbon-isotope values in respective strata.

The case study of the Triassic-Jurassic boundary to the Early Jurassic involves the entire fluvial and lacustrine sediments in the Kuqa section, N Tarim Basin, NW China. The terrestrial carbon-isotope stratigraphy mainly based on fossil wood from the Kuqa section can be consistently correlated with both terrestrial and marine records globally. In light of the composite biostratigraphy and globally correlatable carbon-isotope stratigraphy established in this work the stratigraphic resolution is significantly improved and the Hettangian, Sinemurian and Early Pliensbachian stage are identified in the Kuqa section for the first time. An exact horizon of Triassic-Jurassic boundary in the Kuqa section is suggested. A remarkable soft-sediment deformation bed that resembles European examples in age equivalent strata is reported. A coupled situation of atmosphere-ocean carbon reservoirs is inferred across the Triassic–Jurassic boundary in the short term and through the Early

Jurassic in the long term. Palynological turnovers in the Kuqa section across the Triassic-Jurassic boundary coincide with other terrestrial ecosystems such as in the Newark Basin, USA and Eiberg Basin, Austria, and support the idea of a global biological crisis on land at that interval of geological time.

Overall, a series of potential pitfalls for utility of the terrestrial carbon-isotope stratigraphy as a chemostratigraphic tool have been investigated in the present thesis. A range of biases for reliable carbon-isotope stratigraphy mainly include: reworking from older deposits, changes in drainage and/or river input, environmental factors affecting vegetation in the sediment source areas, changes in the ratio of marine to terrestrial organic matter derived from shallow-marine margins, reduced sedimentation rate associated with glauconite occurrence, and diagenesis during and after deposition (e.g. due to selective degradation and oxygen availability during taphonomy). These possible biases were assessed in each specific study. The knowledge acquired in this thesis is useful to improve future terrestrial carbon-isotope stratigraphic application to regional and global stratigraphic correlation and palaoenvironmental reconstruction.

With the major potentially biased influence excluded, the success of stratigraphic correlation in the three case studies indicates that carbon-isotope stratigraphy based on woody materials is a powerful tool for the stratigraphic correlation locally and globally. It can be particularly useful to link marine and terrestrial strata and significantly improve chronostratigraphic resolution in both marine and terrestrial strata.

5.2 Outlook

Carbon-isotope stratigraphy has proved a powerful tool for stratigraphic correlation. The future technological development of terrestrial carbon-isotope stratigraphy can be seen in perspective as follows:

1) If the wood-derived biomarkers could be recovered from deep marine sediments and measured isotopically, this would facilitate a new realm of 'deep ocean terrestrial carbon-isotope stratigraphy'. As the deep ocean sediments tend to deposit continuously so that they potentially permit a high-resolution and continuous terrestrial carbon-isotope stratigraphy in the deep marine sedimentary sequences. Moreover, most deep ocean basins accumulate the terrestrial-derived biomarkers with mixed sources from various continents. Thus, this kind of carbon-isotope stratigraphic curve may be more complete and better suited for establishing a standard for a global terrestrial carbon-isotope stratigraphic correlation and more representative of terrestrial carbon-isotope stratigraphic records for global carbon cycling.

Some terrestrially derived biomarkers could faithfully archive the original carbon-isotope signals registered during plant growth, regardless of the degree of degradation by bacteria, or other chemical or physical processes during diagenesis (see details in Appendix A).

2) Pollen can document reliable carbon-isotope values as well as fossil wood (Jahren, 2004; Loader and Hemming, 2004). Pollen containing certain age information thus can provide some age constraint when carbon-isotope stratigraphy is based on pollen carbon-isotope values. With the advancement of technology in future, carbon-isotope stratigraphy based on the mixed pieces of pollen or a single piece of pollen could be possible. Single-pollen carbon-

isotope stratigraphy could be promising for both shallow marine and terrestrial sediments in various lithologies even in red mudstone strata.

These newly exploring realms can allow us to resolve Earth science questions on a scale as large as the Earth itself.

REFERENCES

Abels, H. A., F. J. Hilgen, W. Krijgsman, R. W. Kruk, I. Raffi, E. Turco, and W. J. Zachariasse (2005), Long-period orbital control on middle Miocene global cooling: Integrated stratigraphy and astronomical tuning of the Blue Clay Formation on Malta, *Paleoceanography*, *vol. 20*, PA 4012.

Allen, M. B., B. F. Windley, Z. Chi, Z. Zhong-Yan, and W. Guang-Rei (1991), Basin evolution within and adjacent to the Tien Shan Range, NW China, *Journal of the Geological Society*, *148*(2), 369–378.

Alroy, J. (2010), The Shifting Balance of Diversity Among Major Marine Animal Groups, *Science*, *329*(5996), 1191–1194.

Amorosi, A. (1997), Detecting compositional, spatial, and temporal attributes of glaucony: a tool for provenance research, *Sedimentary Geology, 109*(1–2), 135–153.

Ando, A. (2002), New perspective on Aptian carbon isotope stratigraphy: data from $\delta^{13}C$ records of terrestrial organic matter, *Geology*, *30*(3), 227–230.

Anna, F-O. (1997), Depositional systems and cyclicity in the intracratonic Early Jurassic basin in Poland, *Geological Quarterly, 41*(4), 475–490.

Arens, N. C., A. H. Jahren, and R. Amundson (2000), Can C3 plants faithfully record the carbon isotopic composition of atmospheric carbon dioxide?, *Paleobiology*, *26*(1), 137–164.

Arthur, M. A. (1979), Paleoceanographic events-recognition, resolution, and reconsideration, *Reviews of Geophysics and Space Physics, 17*(7), 1474–1494.

Ashraf, A. R., Y. Sun, G. Sun, D. Uhl, V. Mosbrugger, J. Li, and M. Herrmann (2010), Triassic and Jurassic palaeoclimate development in the Junggar Basin, Xinjiang, Northwest China—a review and additional lithological data, *Palaeobiodiversity and Palaeoenvironments*, *90*(3), 187–201.

Aubry, M.-P., W. A. Berggren, L. Stott, and A. Sinha (1996), The upper Paleocene-lower Eocene stratigraphic record and the Paleocene-Eocene boundary carbon isotope excursion: implications for geochronology, *Geological Society, London, Special Publications*, *101*(1), 353–380.

Bacon, k. L., C. M. Belcher, S. P. Hesselbo, and J. C. McElwain (2011), The Triassic-Jurassic boundary carbon-isotope excursions expressed in taxonomically identified leaf cuticles, *Palaios*, *26*(8), 461–469.

Baud, A., M. Magaritz, and W. T. Holser (1989), Permian-Triassic of the Tethys: Carbon isotope studies, *Geologische Rundschau*, *78*(2), 649–677.

Beall, F., P. Blankenhorn, and G. Moore (1974), Carbonized wood-physical properties and use as an SEM preparation, *Wood Science*, *6*, 212–219.

Beccaluva, L., G. Bianchini, M. Coltorti, F. Siena and M. Verde (2005), Cenozoic tectono-magmatic evolution of the central-western Mediterranean: migration of an arc-interarc basin system and variations in the mode of subduction, *CROP Project: Deep seismic exploration of the central Mediterranean and Italy*. Elsevier, pp. 623–639.

Bechtel, A., D. Reischenbacher, R. F. Sachsenhofer, R. Gratzer, and A. Lücke (2007), Paleogeography and paleoecology of the upper Miocene Zillingdorf lignite deposit (Austria), *International journal of coal geology*, *69*(3), 119–143.

Bender, M. L., and L. D. Keigwin Jr (1979), Speculations about the Upper Miocene change in abyssal Pacific dissolved bicarbonate $\delta^{13}C$, *Earth and Planetary Science Letters*, *45*(2), 383–393.

Bender, M. M. (1971), Variations in the $^{13}C/^{12}C$ ratios of plants in relation to the pathway of photosynthetic carbon dioxide fixation, *Phytochemistry*, *10*(6), 1239–1244.

Benner, R., M. L. Fogel, E. K. Sprague, and R. E. Hodson (1987), Depletion of ^{13}C in lignin and its implications for stable carbon isotope studies, *Nature*, *329*(6141), 708–710, doi:10.1038 /329708a0.

Benner, R., S. Y. Newell, A. E. Maccubbin, and R. E. Hodson (1984), Relative Contributions of Bacteria and Fungi to Rates of Degradation of Lignocellulosic Detritus in Salt-Marsh Sediments, *Applied and environmental microbiology, 48*(1), 36–40.

Berger, W. H., J. S. Killingley, and E. Vincent (1978a), Sable isotopes in deep-sea carbonates-box core erdc-92, west equatorial pacific, *Oceanologica Acta, 1*(2): 203–216.

Berger, W., and E. Vincent (1986), Deep-sea carbonates: Reading the carbon-isotope signal, *Geologische Rundschau, 75*(1), 249–269.

Berger, W., L. Diesterhaass, and J. Killingley (1978b), Upwelling off northwest Africa-Holocene decrease as seen in carbon isotopes and sedimentological indicators, *Oceanologica Acta*, *1*(1), 3–7.

Berner, U. (1995), Primary cracking of algal and land plant kerogens: kinetic models of isotope variations in methane, ethane and propane, *Chemical geology*, *126*(3–4), 233.

Berner, U., E. Faber, and W. Stahl (1992), Mathematical simulation of the carbon isotopic fractionation between huminitic coals and related methane, *Chemical Geology: Isotope Geoscience section*, *94*(4), 315–319.

Bian, W., J. Hornung, Z. Liu, P. Wang, and M. Hinderer (2010), Sedimentary and palaeoenvironmental evolution of the Junggar Basin, Xinjiang, Northwest China, *Palaeobiodiversity and Palaeoenvironments, 90*(3), 175–186.

Bonis, N. R., M. Ruhl, and W. M. Kürschner (2010), Climate change driven black shale deposition during the end-Triassic in the western Tethys, *Palaeogeography, Palaeoclimatology, Palaeoecology*, *290*(1–4), 151–159.

Bonis, N. R., W. M. Kürschner, and L. Krystyn (2009), A detailed palynological study of the Triassic–Jurassic transition in key sections of the Eiberg Basin (Northern Calcareous Alps, Austria), *Review of Palaeobotany and Palynology*, *156*(3–4), 376–400.

Bowen, G. J., D. J. Beerling, P. L. Koch, J. C. Zachos, and T. Quattlebaum (2004), A humid climate state during the Palaeocene/Eocene thermal maximum, *Nature*, *432*(7016), 495–499.

Brandano, M., and L. Corda (2002), Nutrients, sea level and tectonics: constrains for the facies architecture of a Miocene carbonate ramp in central Italy, *Terra Nova*, *14(4),* 257–262.

Brandano, M., M. Brilli, L. Corda, and M. Lustrino (2010), Miocene C-isotope signature from the central Apennine successions (Italy): Monterey vs. regional controlling factors, *Terra Nova*, *22*(2), 125–130.

Brandon, A. D., and G. G. Goles (1988), A Miocene subcontinental plume in the Pacific Northwest: geochemical evidence, *Earth and Planetary Science Letters*, *88*(3–4), 273–283.

Brearley, F. Q. (2010), Carbon Isotope ($\delta^{13}C$) Signatures of Rheophytic Dipteris lobbiana, *American Fern Journal*, *100*(1), 66–69.

Browning, J. V., K. G. Miller, P. P. McLaughlin, M. A. Kominz, P. J. Sugarman, D. Monteverde, M. D. Feigenson, and J. C. Hernandez (2006), Quantification of the effects of eustasy, subsidence, and sediment supply on Miocene sequences, mid-Atlantic margin of the United States, *Geological Society of America Bulletin*, *118*(5–6), 567–588.

Browning, J. V., K. G. Miller, P. J. Sugarman, M. A. Kominz, P. P. McLaughlin, A. A. Kulpecz, and M. D. Feigenson (2008), 100 Myr record of sequences, sedimentary facies and sea level change from Ocean Drilling Program onshore coreholes, US Mid-Atlantic coastal plain, *Basin Research*, *20*(2), 227–248.

Browning, J. V., K. G. Miller, P. J. Sugarman, J. Barron, F. M. G. McCarthy, D. K. Kulhanek, M. E. Katz, and M. D. Feigenson (2013), Chronology of Eocene-Miocene sequences on the New Jersey shallow shelf: Implications for regional, interregional, and global correlations, *Geosphere,* doi: 10.1130/ GES00857.1.

Buchardt, B. (1978), Oxygen isotope palaeotemperatures from the Tertiary period in the North Sea area, *Nature, 275*(5676), 121–123.

Carminati, E., L. Corda, G. Mariotti, and M. Brandano (2007), Tectonic control on the architecture of a Miocene carbonate ramp in the Central Apennines (Italy): insights from facies and backstripping analyses, *Sedimentary Geology, 198(3),* 233–253.

Carroll, A. R., L. Yunhai, S. A. Graham, X. Xuchang, M. S. Hendrix, C. Jinchi, and C. L. McKnight (1990), Junggar basin, northwest China: trapped Late Paleozoic ocean, *Tectonophysics*, *181*(1–4), 1–14.

Carroll, A. R., S. A. Graham, M. S. Hendrix, D. Ying, and D. Zhou (1995), Late Paleozoic tectonic amalgamation of northwestern China: Sedimentary record of the northern Tarim, northwestern Turpan, and southern Junggar Basins, *Geological Society of America Bulletin*, *107*(5), 571–594.

Carroll, A. R., S. A. Graham, and M. E. Smith (2010), Walled sedimentary basins of China, *Basin Research*, *22*(1), 17–32.

Cerling, T. E., J. M. Harris, B. J. MacFadden, M. G. Leakey, J. Quade, V. Eisenmann, and J. R. Ehleringer (1997), Global vegetation change through the Miocene/Pliocene boundary, *Nature*, *389*(6647), 153–158.

Cheng, X., Q. Zhao, J. Wang, Z. Jian, P. Xia, B. Huang, D. Fang, J. Xu, Z. Zhou, and P. Wang (2004), Data report : Stable Isotopes from Sites 1147 and 1148, In Prell, W.L., P. Wang, P. Blum, D. K. Rea, and S. C Clemens (Eds.), Proceedings of the Ocean Drilling Program, Scientific Results, 184, 1-12. [Online] Available from http://www-odp.tamu.edu/publications /184_SR/ VOLUME/CHAPTERS/223.PD.

Christiansen, R. L., G. R. Foulger, and J. R. Evans (2002), Upper-mantle origin of the Yellowstone hotspot, *Geological Society of America Bulletin*, *114*(10), 1245–1256.

Cifelli, R. (1969), Radiation of Cenozoic Planktonic Foraminifera, *Systematic Biology*, *18*(2), 154–168.

Cirilli, S., A. Marzoli, L. Tanner, H. Bertrand, N. Buratti, F. Jourdan, G. Bellieni, D. Kontak, and P. R. Renne (2009), Latest Triassic onset of the Central Atlantic Magmatic Province (CAMP) volcanism in the Fundy Basin (Nova Scotia): New stratigraphic constraints, *Earth and Planetary Science Letters*, *286*(3–4), 514-525.

Clausen, O. R., U. Gregersen, O. Michelsen, and J. C. Sørensen (1999), Factors controlling the Cenozoic sequence development in the eastern parts of the North Sea, *Journal of the Geological Society*, *156*(4), 809–816.

Clayden, J., N. Greeves, S. Warren, and P. Worthers (2001), *Organic Chemistry,* vol. 1. Oxford University Press, Oxford.

Coffin, M. F., and O. Eldholm (1994), Large igneous provinces: crustal structure, dimensions, and external consequences, *Reviews of Geophysics, 32*(1), 1–36.

Cohen, A. S., A. L. Coe, and D. B. Kemp (2007), The Late Palaeocene–Early Eocene and Toarcian (Early Jurassic) carbon isotope excursions: a comparison of their time scales, associated environmental changes, causes and consequences, *Journal of the Geological Society*, *164*(6), 1093–1108.

Coleman, R. G. (1989), Continental growth of northwest China, *Tectonics*, *8*(3), 621–635.

Cox, K. G. (1992), Karoo igneous activity, and the early stages of the break-up of Gondwanaland, *Geological Society, London, Special Publications*, *68*(1), 137–148.

Craig, H. (1953), The geochemistry of the stable carbon isotopes, *Geochimica et Cosmochimica Acta, 3*(2), 53–92.

Craig, H. (1957), Isotopic standards for carbon and oxygen and correction factors for mass-spectrometric analysis of carbon dioxide, *Geochimica et Cosmochimica Acta, 12*(1-2), 133–149.

Cramer, B. (1998), Modelling isotope fractionation during primary cracking of natural gas: a reaction kinetic approach, *Chemical Geology*, *149*(3-4), 235–250.

Cramer, B. (2001), Reaction kinetics of stable carbon isotopes in natural gas insights from dry, open system pyrolysis experiments, *Energy and Fuels*, *15*(3), 517–532.

Cutter, B. E., B. Cumbie, and E. McGinnes Jr (1980), SEM and shrinkage analyses of southern pine wood following pyrolysis, *Wood Science and Technology*, *14*(2), 115–130.

Dean, W. E., M. A. Arthur, and G. E. Claypool (1986), Depletion of ^{13}C in Cretaceous marine organic matter: Source, diagenetic, or environmental signal?, *Marine Geology*, *70*(1–2), 119–157.

Deenen, M. H. L., M. Ruhl, N. R. Bonis, W. Krijgsman, W. M. Kuerschner, M. Reitsma, and M. J. van Bergen (2010), A new chronology for the end-Triassic mass extinction, *Earth and Planetary Science Letters*, *291*(1–4), 113–125.

Deines, P. (1980), The isotopic composition of reduced organic carbon, In: Fritz P., and Fontes, J.Ch. (Eds.), *Handbook of Environmental Isotope Geochemistry*, vol. 1. Elsevier, New York, pp. 329–406.

Deng S. H., Y. M. Yao and D. Q. Ye (2003), Cretaceous Strata of Northern China (I): *Strata Division and Correlation*, Petroleum Press, Beijing.

Deng, S. H., Y. Z. Lu, R. Fan, Y. H. Pan, X. S. Cheng, G. B. Fu, C. K. Jia, W. Z. Duan, Y. Q. Wang, and L. H. Fang (2010), The Jurassic System of Northern Xinjiang. Press of University of Science and Technology of China, Hefei. (In Chinese and English)

Depaolo, D. J., and K. L. Finger (1991), High-resolution strontium-isotope stratigraphy and biostratigraphy of the Miocene Monterey Formation, central California, *Geological Society of America Bulletin, 103*(1), 112–124.

Dera, G., B. Brigaud, F. Monna, R. Laffont, E. Pucéat, J.-F. Deconinck, P. Pellenard, M. M. Joachimski, and C. Durlet (2011), Climatic ups and downs in a disturbed Jurassic world, *Geology*, *39*(3), 215–218.

Dettmann, M. E. (1961), Lower Mesozoic Megaspores from Tasmania and South Australia, *Micropaleontology*, *7*(1), 71–86

Deuser, W. (1987), Seasonal variations in isotopic composition and deep-water fluxes of the tests of perennially abundant planktonic foraminifera of the Sargasso Sea; results from sediment-trap collections and their paleoceanographic significance, *The Journal of Foraminiferal Research*, *17*(1), 14–27.

Diester-Haass, L., K. Billups, D. R. Gröcke, L. François, V. Lefebvre, and K. C. Emeis (2009), Mid-Miocene paleoproductivity in the Atlantic Ocean and implications for the global carbon cycle, *Paleoceanography*, *24*(1), PA1209, doi:10.1029/2008PA001605.

Dimitropoulos, K., and J. A. Donato (1981), The Inner Moray Firth central ridge, a geophysical interpretation, *Scottish Journal of Geology,* 17(1): 27–38.

Donato, J., and M. Tully (1981), A regional interpretation of North Sea gravity data, *Petroleum Geology of the Continental Shelf of North-West Europe*, 65–75.

Doré, A. G., E. R. Lundin, N. J. Kusznir, and C. Pascal (2008), Potential mechanisms for the genesis of Cenozoic domal structures on the NE Atlantic margin: pros, cons and some new ideas, *Geological Society, London, Special Publications*, *306*(1), 1–26.

Dybkjær, K., E. S. Rasmussen, (2007), Dinocyst stratigraphy in an expanded Oligocene-Miocene boundary section in the eastern North Sea Basin (the Frida-1 well, Denmark) and correlation from basinal to marginal areas, *Journal of Micropalaeontology,* 26, 1–17

Dybkjær, K., S. Piasecki, (2010), Neogene dinocyst zonation for the eastern North Sea Basin, Denmark, *Review of Palaeobotany and Palynology,* 161, 1–29.

Eberth, D. A., D. B. Brinkman, P. J. Chen, F. T. Yuan, S. Z. Wu, G. Li, and X. S. Cheng (2001), Sequence stratigraphy, paleoclimate patterns, and vertebrate fossil preservation in Jurassic–Cretaceous strata of the Junggar Basin, Xinjiang Autonomous Region, People's Republic of China, *Canadian Journal of Earth Sciences*, *38*(12), 1627–1644.

Edwards, E. J., C. P. Osborne, C. A. Strömberg, and S. A. Smith (2010), The origins of C4 grasslands: integrating evolutionary and ecosystem science, *Science*, *328*(5978), 587–591.

Emiliani, C. (1955), Pleistocene temperatures, *The Journal of Geology*, *63*(6), 538–578.

Emiliani, C. (1966), Paleotemperature analysis of Caribbean cores P6304-8 and P6304-9 and a generalized temperature curve for the past 425,000 years, *The Journal of Geology*, *74*(2), 109–124.

Emrich, K., D. H. Ehhalt, and J. C. Vogel (1970), Carbon isotope fractionation during the precipitation of calcium carbonate, *Earth and Planetary Science Letters*, *8*(5), 363–371.

Emiliani, C., and N. J. Shackleton (1974), The Brunhes epoch: isotopic paleotemperatures and geochronology, *Science*, *183*(4124), 511–514.

.

Erez, J. (1978), The influence of differential production and dissolution on the stable isotope composition of planktonic foraminifera, *Diss. Massachusetts Institute of Technology and Woods Hole Oceanographic Institution*.

Erez, J., and S. Honjo (1981), Comparison of isotopic composition of planktonic foraminifera in plankton tows, sediment traps and sediments, *Palaeogeography, Palaeoclimatology, Palaeoecology*, *33*(1), 129–156.

Erlenkeuser, H., E. Suess, and H. Willkomm (1974), Industrialization affects heavy metal and carbon isotope concentrations in recent Baltic Sea sediments, *Geochimica et Cosmochimica Acta*, *38*(6), 823–842.

Espitalié, J., J. L. Laporte, M. Madec, F. Marquis, P. Leplat, J. Paulet, and A. Boutefeu (1977), Méthode rapide de caractérisation des roches mères, de leur potentiel pétrolier et de leur degré d'évolution, *Revue de l'Institut Français du Pétrole, 32*(1), 23–42.

Espitalié J., G. Deroo, and F. Marquis (1985), La pyrolyse Rock-Eval et ses applications, *Part 1. Revue de l'Institut Français du Pétrole*, 40 (6), 563–579.

Farquhar, G. D., M. O'leary, and J. Berry (1982), On the relationship between carbon isotope discrimination and the intercellular carbon dioxide concentration in leaves, *Functional Plant Biology*, *9*(2), 121–137.

Farquhar, G. D., J. R. Ehleringer, and K. T. Hubick (1989), Carbon isotope discrimination and photosynthesis, *Annual review of plant biology*, *40*(1), 503–537.

Flower, B. P., and J. P. Kennett (1994), The middle Miocene climatic transition: East Antarctic ice sheet development, deep ocean circulation and global carbon cycling, *Palaeogeography, Palaeoclimatology, Palaeoecology*, *108*(3–4), 537–555, doi:10.1016/0031–0182(94) 90251–8.

Föllmi, K. B., C. Badertscher, E. de Kaenel, P. Stille, C. M. John, T. Adatte, and P. Steinmann (2005), Phosphogenesis and organic-carbon preservation in the Miocene Monterey Formation at Naples Beach, California-The Monterey hypothesis revisited, *Geological Society of America Bulletin*, *117*(5–6), 589–619.

Fowell, S. J., and P. E. Olsen (1993), Time calibration of Triassic/Jurassic microfloral turnover, eastern North America, *Tectonophysics*, *222*(3–4), 361–369.

Fuglewicz, R. (1973), Megaspores of Polish Buntersandstein and their stratigraphical significance, *Acta Palaeontologica Polonica*, *18*(4), 401–451.

Galli, M. T., F. Jadoul, S. M. Bernasconi, and H. Weissert (2005), Anomalies in global carbon cycling and extinction at the Triassic/Jurassic boundary: evidence from a marine C-isotope record, *Palaeogeography, Palaeoclimatology, Palaeoecology*, *216*(3–4), 203–214.

Galli, M. T., F. Jadoul, S. M. Bernasconi, S. Cirilli, and H. Weissert (2007), Stratigraphy and palaeoenvironmental analysis of the Triassic–Jurassic transition in the western Southern Alps (Northern Italy), *Palaeogeography, Palaeoclimatology, Palaeoecology*, *244*(1–4), 52–70.

Gao, J., M. S. Li, X. C. Xiao, Y. Q. Tian, and G. Q. He (1998), Paleozoic tectonic evolution of the Tianshan Orogen, northwestern China, *Tectonophysics*, *287*(1–4), 213–231.

Gattacceca, J., A. Deino, R. Rizzo, D. S. Jones, B. Henry, B. Beaudoin, and F. Vadeboin (2007), Miocene rotation of Sardinia: New paleomagnetic and geochronological constraints and geodynamic implications, *Earth and Planetary Science Letters*, *258(3)*, 359–377.

Gómez, J. J., A. Goy, and E. Barrón (2007), Events around the Triassic–Jurassic boundary in northern and eastern Spain: A review, *Palaeogeography, Palaeoclimatology, Palaeoecology*, *244*(1–4), 89–110.

Gradstein, F.M., Ogg, J.G., and Smith, A.G. (Eds.), (2004), A Geologic Time Scale 2004, Cambridge University Press, Cambridge, pp. 589.

Gradstein, F. M., J. G. Ogg, and M. Schmitz (Eds.), (2012), *The Geologic Time Scale 2012,* vol. 2. Elsevier.

Greenwood, D., and D. Goodman (1967), Direct measurements of the distribution of oxygen in soil aggregates and in columns of fine soil crumbs, *Journal of Soil Science*, *18*(1), 182–196.

Gröcke, D. R. (1998), Carbon-isotope analyses of fossil plants as a chemostratigraphic and palaeoenvironmental tool, *Lethaia*, *31*(1), 1–13.

Gröcke, D. R., S. P. Hesselbo, and H. C. Jenkyns (1999), Carbon isotope composition of Lower Cretaceous fossil wood: ocean-atmosphere chemistry and relation to sea-level change, *Geology, 27*(2), 155–158.

Grocke, D. R. (2002), The carbon isotope composition of ancient CO_2 based on higher-plant organic matter, *Philosophical Transactions of the Royal Society of London. Series A, Mathematical, Physical and Engineering Sciences*, *360*(1793), 633–658.

Gröcke, D. R., G. D. Price, S. A. Robinson, E. Y. Baraboshkin, J. Mutterlose, and A. H. Ruffell (2005), The Upper Valanginian (Early Cretaceous) positive carbon–isotope event recorded in terrestrial plants, *Earth and Planetary Science Letters*, *240*(2), 495–509.

Guex, J., A. Bartolini, V. Atudorei, and D. Taylor (2004), High-resolution ammonite and carbon isotope stratigraphy across the Triassic–Jurassic boundary at New York Canyon (Nevada), *Earth and Planetary Science Letters*, *225*(1–2), 29–41.

Hales, T. C., D. L. Abt, E. D. Humphreys, and J. J. Roering (2005), A lithospheric instability origin for Columbia River flood basalts and Wallowa Mountains uplift in northeast Oregon, *Nature*, *438*(7069), 842-845.

Hansen, J. M., and L. Gudmundsson (1979), A method for separating acid-insoluble microfossils from organic debris, *Micropaleontology, 25*(2), 113–117.

Haq, B. U., T. R. Worsley, L. H. Burckle, R. G. Douglas, L. D. Keigwin, N. D. Opdyke, S. M. Savin, M. A. Sommer, E. Vincent, and F. Woodruff (1980), Late Miocene marine carbon-isotopic shift and synchroneity of some phytoplanktonic biostratigraphic events, *Geology*, *8*(9), 427–431.

Harmon, M. E., O. N. Krankina, and J. Sexton (2000), Decomposition vectors: a new approach to estimating woody detritus decomposition dynamics, *Canadian Journal of Forest Research*, *30*(1), 76–84.

Harris, T. M. (1961), On Otozamites bechei from the Irish Rhaetic, *Proceedings of the Royal Irish Academy, B61*, 339–344.

Hasegawa, T. (1997), Cenomanian-Turonian carbon isotope events recorded in terrestrial organic matter from northern Japan, *Palaeogeography, Palaeoclimatology, Palaeoecology*, *130*(1–4), 251–273

Hasegawa, T. (2003), Cretaceous terrestrial paleoenvironments of northeastern Asia suggested from carbon isotope stratigraphy: Increased atmospheric pCO_2-induced climate, *Journal of Asian Earth Sciences*, *21*(8), 849–859.

Hasegawa, T., L. M. Pratt, H. Maeda, Y. Shigeta, T. Okamoto, T. Kase, and K. Uemura (2003), Upper Cretaceous stable carbon isotope stratigraphy of terrestrial organic matter from Sakhalin, Russian Far East: a proxy for the isotopic composition of paleoatmospheric CO_2, *Palaeogeography, Palaeoclimatology, Palaeoecology*, *189*(1–2), 97–115.

Hatcher, P. G., E. C. Spiker, N. M. Szeverenyi, and G. E. Maciel (1983), Selective preservation and origin of petroleum-forming aquatic kerogen, *Nature*, *305*(5934), 498–501.

Hatcher, P. G., H. E. Lerch Iii, and T. Vincent Verheyen (1989a), Organic geochemical studies of the transformation of gymnospermous xylem during peatification and coalification to subbituminous coal, *International journal of coal geology*, *13*(1–4), 65–97.

Hatcher, P. G., M. A. Wilson, A. M. Vassallo, and H. E. Lerch Iii (1989b), Studies of angiospermous wood in Australian brown coal by nuclear magnetic resonance and analytical pyrolysis: new insights into the early coalification process, *International journal of coal geology*, *13*(1–4), 99–126.

Hayes, J., B. N. Popp, R. Takigiku, and M. W. Johnson (1989), An isotopic study of biogeochemical relationships between carbonates and organic carbon in the Greenhorn Formation, *Geochimica et Cosmochimica Acta*, *53*(11), 2961–2972.

Hayes, J. M., H. Strauss, and A. J. Kaufman (1999), The abundance of ^{13}C in marine organic matter and isotopic fractionation in the global biogeochemical cycle of carbon during the past 800 Ma, *Chemical geology*, *161*(1–3), 103–125.

Hedges, J. I. (1992), Global biogeochemical cycles: progress and problems, *Marine Chemistry*, *39*(1), 67–93.

Hedges, J. I., R. G. Keil, and R. Benner (1997), What happens to terrestrial organic matter in the ocean?, *Organic geochemistry*, *27*(5–6), 195–212.

Heimhofer, U., P. A. Hochuli, S. Burla, N. Andersen, and H. Weissert (2003), Terrestrial carbon-isotope records from coastal deposits (Algarve, Portugal): a tool for chemostratigraphic correlation on an intrabasinal and global scale, *Terra Nova*, *15*(1), 8–13.

Hendrix, M. S., S. A. Graham, A. R. Carroll, E. R. Sobel, C. L. Mcknight, B. J. Schulein, And Z. Wang (1992), Sedimentary record and climatic implications of recurrent deformation in the Tian Shan: Evidence from Mesozoic strata of the north Tarim, south Junggar, and Turpan basins, northwest China, *Geological Society of America Bulletin*, *104*(1), 53–79.

Hendrix, M. S. (2000), Evolution of Mesozoic Sandstone Compositions, Southern Junggar, Northern Tarim, and Western Turpan Basins, Northwest China: A Detrital Record of the Ancestral Tian Shan, *Journal of Sedimentary Research*, *70*(3), 520–532.

Hermoso, M., F. Minoletti, R. E. M. Rickaby, S. P. Hesselbo, F. Baudin, and H. C. Jenkyns (2012), Dynamics of a stepped carbon-isotope excursion: Ultra high-resolution study of Early Toarcian environmental change, *Earth and Planetary Science Letters*, *319–320*(0), 45–54.

Hesselbo, S. P., D. R. Gröcke, H. C. Jenkyns, C. J. Bjerrum, P. Farrimond, H. S. Morgans Bell, and O. R. Green (2000), Massive dissociation of gas hydrate during a Jurassic oceanic anoxic event, *Nature*, *406*(6794), 392–395.

Hesselbo, S. P., and J. M. Huggett (2001), Glaucony in ocean-margin sequence stratigraphy (Oligocene-Pliocene, offshore New Jersey, USA; ODP Leg 174A), *Journal of Sedimentary Research 71* (4): 599–607.

Hesselbo, S. P., S. A. Robinson, F. Surlyk, and S. Piasecki (2002), Terrestrial and marine extinction at the Triassic-Jurassic boundary synchronized with major carbon-cycle perturbation: A link to initiation of massive volcanism?, *Geology*, *30*(3), 251–254.

Hesselbo, S. P., H. C. Jenkyns, L. V. Duarte, and L. C. V. Oliveira (2007), Carbon-isotope record of the Early Jurassic (Toarcian) Oceanic Anoxic Event from fossil wood and marine carbonate (Lusitanian Basin, Portugal), *Earth and Planetary Science Letters*, *253*(3–4), 455–470.

Hesselbo, S. P., and G. Pieńkowski (2011), Stepwise atmospheric carbon-isotope excursion during the Toarcian Oceanic Anoxic Event (Early Jurassic, Polish Basin), *Earth and Planetary Science Letters*, *301*(1–2), 365–372.

Holbourn, A., W. Kuhnt, M. Schulz, and H. Erlenkeuser (2005), Impacts of orbital forcing and atmospheric carbon dioxide on Miocene ice-sheet expansion, *Nature*, *438*(7067), 483–487, doi:10.1038/nature04123.

Holbourn, A., W. Kuhnt, M. Schulz, J.-A. Flores, and N. Andersen (2007), Orbitally-paced climate evolution during the middle Miocene 'Monterey' carbon-isotope excursion, *Earth and Planetary Science Letters*, *261*(3–4), 534–550, doi:10.1016/j.epsl.2007.07.02.

Holbrook, W. S., and P. B. Kelemen (1993), Large igneous province on the US Atlantic margin and implications for magmatism during continental breakup, *Nature*, *364*(6436), 433–436.

Holdgate, G. R., B. McGowran, T. Fromhold, B. E. Wagstaff, S. J. Gallagher, M. W. Wallace, I. R. K. Sluiter, and M. Whitelaw (2009), Eocene–Miocene carbon-isotope and floral record from brown coal seams in the Gippsland Basin of southeast Australia, *Global and Planetary Change*, *65*(1–2), 89–103.

Hooper, P. R., V. E. Camp, S. P. Reidel, and M. E. Ross (2007), The origin of the Columbia River flood basalt province: Plume versus nonplume models, *Geological Society of America Special Papers*, *430*, 635–668.

Hsü., K. J., 1987, Tectonic evolution of the Mediterranean basins, A. E. M. Nairn et al. (Eds.), *The Ocean Basins and Margins.* Plenum Press, New York, pp. 29–75.

Hunt, J. M. (1970), The significance of carbon isotope variations in marine sediments, in G. D. Hobson and G. C. Spears (Eds.), *Advances in Organic Geochemistr*. Pergamon, Oxford, pp. 27–35.

Ilyina, N. V., and A. Y. Egorov (2008), The Upper Triassic of northern Middle Siberia: stratigraphy and palynology, *Polar Research*, *27*(3), 372–392.

Imbrie, J., J. van Donk, and N. G. Kipp (1973), Paleoclimatic investigation of a late Pleistocene Caribbean deep-sea core: Comparison of isotopic and faunal methods, *Quaternary research*, *3*(1), 10–38.

Izumi, K., T. Miyaji, and K. Tanabe (2012), Early Toarcian (Early Jurassic) oceanic anoxic event recorded in the shelf deposits in the northwestern Panthalassa: Evidence from the Nishinakayama Formation in the Toyora area, west Japan, *Palaeogeography, Palaeoclimatology, Palaeoecology*, *315–316*(0), 100–108.

Jacobs, E., H. Weissert, G. Shields, and P. Stille (1996), The Monterey event in the Mediterranean: A record from shelf sediments of Malta, *Paleoceanography*, *11*(6), 717–728.

Jahren, A. H., N. C. Arens, and S. A. Harbeson (2008), Prediction of atmospheric $\delta^{13}CO_2$ using fossil plant tissues, *Reviews of geophysics*, *46*(1), RG1002, doi:10.1029/2006RG000219.

Jarvis, I., A. S. Gale, H. C. Jenkyns, and M. A. Pearce (2006), Secular variation in Late Cretaceous carbon isotopes: a new $\delta^{13}C$ carbonate reference curve for the Cenomanian-Campanian (99.6–70.6 Ma), Geological Magazine, *143*(5), 561.

Jasper, J. P., and R. B. Gagosian (1990), The sources and deposition of organic matter in the Late Quaternary Pigmy Basin, Gulf of Mexico, *Geochimica et Cosmochimica Acta*, *54*(4), 1117–1132.

Jenkins, D. G. (1973), Diversity changes in the New Zealand Cenozoic planktonic foraminifera, *The Journal of Foraminiferal Research*, *3*(2), 78–88.

Jenkyns, H. C. (1988), The early Toarcian (Jurassic) anoxic event: stratigraphic, sedimentary and geochemical evidence, *American Journal of Science, 288*(2), 101–151.

Jenkyns, H. C., C. E. Jones, D. R. Gröcke, S. P. Hesselbo, and D. N. Parkinson (2002), Chemostratigraphy of the Jurassic System: applications, limitations and implications for palaeoceanography, *Journal of the Geological Society*, *159*(4), 351-378, doi: 10.1144 /0016-764901–130.

John, C. M., M. Mutti, and T. Adatte (2003), Mixed carbonate-siliciclastic record on the North African margin (Malta)—coupling of weathering processes and mid Miocene climate, *Geological Society of America Bulletin*, *115*(2), 217–229.

Jones, T. P., and W. G. Chaloner (1991), Fossil charcoal, its recognition and palaeoatmospheric significance, *Palaeogeography, Palaeoclimatology, Palaeoecology,* 97(1), 39–50.

Kahn, M. (1979), Non-equilibrium oxygen and carbon isotopic fractionation in tests of living planktonic-foraminifera, *Oceanologica Acta*, *2*(2), 195–208.

Katz, M. E., J. D. Wright, K. G. Miller, B. S. Cramer, K. Fennel, and P. G. Falkowski (2005), Biological overprint of the geological carbon cycle, *Marine Geology*, *217*(3–4), 323–338.

Keigwin Jr, L. D., and R. C. Thunell (1979), Middle Pliocene climatic change in the western Mediterranean from faunal and oxygen isotopic trends, *Nature*, *282*(5736), 294–296.

Keller, G., and J. A. Barron (1983), Paleoceanographic implications of Miocene deep-sea hiatuses, *Geological Society of America Bulletin*, *94*(5), 590–613.

Kennett, J. P., G. Keller, and M. S. Srinivasan (1985), Miocene planktonic foraminiferal biogeography and paleoceanographic development of the Indo-Pacific Region, pp. 197–236 in J. P. Kennett, (Eds.), The Miocene Ocean: Paleoceanography and Biogeography, *Geological Society of America Memoir, 163.*

Kiessling, W., M. Aberhan, B. Brenneis, and P. J. Wagner (2007), Extinction trajectories of benthic organisms across the Triassic–Jurassic boundary, *Palaeogeography, Palaeoclimatology, Palaeoecology*, *244*(1–4), 201–222.

Kiessling, W., and C. Simpson (2011), On the potential for ocean acidification to be a general cause of ancient reef crises, *Global Change Biology*, *17*(1), 56–67.

Killingley, J. S., R. F. Johnson, and W. H. Berger (1981), Oxygen and carbon isotopes of individual shells of planktonic foraminifera from Ontong-Java plateau, equatorial pacific, *Palaeogeography, Palaeoclimatology, Palaeoecology*, *33*(1–3), 193–204.

Kirk T, K., and B. Cowling Ellis (1984), Biological Decomposition of Solid Wood, in *The Chemistry of Solid Wood*, (Eds.), American Chemical Society, pp. 455–487.

Kirk, T. K., and R. L. Farrell (1987), Enzymatic 'combustion': the microbial degradation of lignin, *Annual review of microbiology*, *41*(1), 465–505.

Klaus W, (1960), Sporen der Karnischen Stufe der ostalpinen Trias, *J b. Geol. Bundesanst*, pp. 107–184.

Knox, R., A. Bosch, E. Rassmusen, C. Heilman-Clausen, M. Hiss, I. De Lugt, ... and N. Vandenberghe (2010), Cenozoic. In: Doornenbal, J.C. & Stevenson, A.G. (Eds.), Petroleum geological atlas of the southern Permian Basin area. Print + DVD. Houten, The Netherlands: EAGE Publications b.v.

Koch, B. E. (1989), Geology of the Søby-Fasterholt area. Danmarks Geologiske Undersøgelse Serie A 22, pp. 171 and atlas.

Koch, P. L., J. C. Zachos, P. D. Gingerich (1992), Correlation between isotope records in marine and continental carbon reservoirs near the Paleocene Eocene boundary, *Nature 358*(6384): 319–322, doi:10.1038/358319a0.

Kopik, J., & Marcinkiewicz, T. (1997). Jura dolna: Biostratygrafia. *S. Marek and M. Pajchlowa*, 196–205.

Kocsis, L., T. W. Vennemann, E. Hegner, D. Fontignie, and T. Tütken (2009), Constraints on Miocene oceanography and climate in the Western and Central Paratethys: O-, Sr-, and Nd-isotope compositions of marine fish and mammal remains, *Palaeogeography, Palaeoclimatology, Palaeoecology*, *271*(1–2), 117–129.

Korte, C., S. P. Hesselbo, H. C. Jenkyns, R. E. M. Rickaby, and C. Spötl (2009), Palaeoenvironmental significance of carbon- and oxygen-isotope stratigraphy of marine Triassic–Jurassic boundary sections in SW Britain, *Journal of the Geological Society*, *166*(3), 431–445.

Korte, C., and S. P. Hesselbo (2011), Shallow marine carbon and oxygen isotope and elemental records indicate icehouse-greenhouse cycles during the Early Jurassic, *Paleoceanography*, *26*(4), PA4219.

Kozur, H. W. (2003), Dating of the event succession in marine and continental beds around the Permian–Triassic boundary (PTB), *Permophiles Issue*, *43*, 32–37.

Kroopnick, P. M., S. V. Margolis, and C. S. Wong (1977), $\delta\ ^{13}C$ variations in marine carbonate sediments as indicators of the CO_2 balance between the atmosphere and oceans, In: Andersen N. R. and A. Malahoff (eds) *The fate of fossil CO_2 in the oceans*. Plenum, New York, pp. 295–321.

Kuerschner, W. M., N. R. Bonis, and L. Krystyn (2007), Carbon-isotope stratigraphy and palynostratigraphy of the Triassic–Jurassic transition in the Tiefengraben section — Northern Calcareous Alps (Austria), *Palaeogeography, Palaeoclimatology, Palaeoecology*, *244*(1–4), 257–280.

Kürschner, W. M., Z. Kvaček, and D. L. Dilcher (2008), The impact of Miocene atmospheric carbon dioxide fluctuations on climate and the evolution of terrestrial ecosystems, *Proceedings of the National Academy of Sciences*, *105*(2), 449–453.

Kump, L. R. (1991), Interpreting carbon-isotope excursions: Strangelove oceans, *Geology*, *19*(4), 299–302.

Kump, L. R., and M. A. Arthur (1999), Interpreting carbon-isotope excursions: carbonates and organic matter, *Chemical geology*, *161*(1–3), 181–198.

Kuypers, M. M., R. D. Pancost, and J. S. S. Damsté (1999), A large and abrupt fall in atmospheric CO_2 concentration during Cretaceous times, *Nature*, *399*(6734), 342–345.

Larsen, G., A. Dinesen (1957), Vejle Fjord Formationen ved Brejning, Sedimenterneog foraminiferfaunan (Oligocene–Miocene), *Danmarks Geologiske Undersøgelse*, 79, 1–503.

Larsson, L. M., K. Dybkjær, E. S. Rasmussen, S. Piasecki, T. Utescher, and V. Vajda (2011), Miocene climate evolution of northern Europe: A palynological investigation from Denmark, *Palaeogeography, Palaeoclimatology, Palaeoecology*, *309*(3–4), 161–175.

Leavitt, S. W., and A. Long (1982), Evidence for $^{13}C/^{12}C$ fractionation between tree leaves and wood, *Nature*, *298*(5876), 742–744.

Leavitt, S. W., and A. Long (1986), Stable-Carbon Isotope Variability in Tree Foliage and Wood, *Ecology*, *67*(4), 1002–1010.

Leavitt, S. W., and A. Long (1991), Seasonal stable-carbon isotope variability in tree rings: possible paleoenvironmental signals, *Chemical Geology: Isotope Geoscience section*, *87*(1), 59–70.

Leschik G, (1955), Die Keuperflora von Neuewelt bei Basel. Schweiz. Palaeont. A bh. , 72: 9–70

Li S. J., Q. C. Wang, and Z. Li (2005), Characteristics of Mesozoic and Cenozoic heavy minerals from Kuche River section in Kuche depression and their geological implications, *Acta Petrologica et Mineralogica*, *24*(1), 53–61. (in Chinese with English abstract)

Li, Z., Q. Wang, D. Wang, W. Lin, and Q. C. Wang (2003), Depositional record constraints on Late Cenozoic uplift of Tian Shan and tectonic transformation in Kuqa Subbasin, West China, *Acta Sedimentologica Sinica*, *21*(1), 38–45. (in Chinese with English abstract)

Li, Z., W. Song, S. Peng, D. Wang, and Z. Zhang (2004), Mesozoic–Cenozoic tectonic relationships between the Kuqa subbasin and Tian Shan, northwest China: constraints from depositional records, *Sedimentary Geology*, *172*(3–4), 223–249.

Li, Z., and S. Peng (2010), Detrital zircon geochronology and its provenance implications: responses to Jurassic through Neogene basin-range interactions along northern margin of the Tarim Basin, Northwest China, *Basin Research*, *22*(1), 126–138.

Liu Z. S. (1999a), Triassic palynological assemblages from the northern margin in Tarim Basin of Xinjiang, NW China, *Acta Palaeontologica Sinica*, *38*(4), 474–504. (in Chinese with English abstract)

Liu Z. S. (1999b), Palynological assemblage of a drilling-section (basal part of the Kizilnuer Formation) from the Yaha, Kuqa, Xinjiang, NW China, *Acta Micropalaeontologica Sinica*, *16*(1), 82–88. (in Chinese with English abstract)

Liu Z. S. (1999c), Palynological Assemblage of the Late Triassic Tariqike Fm and Triassic-Jurassic Boundary on the Northern Margin of the Tarim Basin, Xinjiang, *Journal of Stratigraphy*, *23*(2), 96–106. (in Chinese with English abstract)

Liu, L., and D. R. Stegman (2012), Origin of Columbia River flood basalt controlled by propagating rupture of the Farallon slab, *Nature*, *482*(7385), 386–389.

Loader, N. J., V. R. Switsur, and E. M. Field (1995), High-resolution stable isotope analysis of tree rings: implications of 'microdendroclimatology' for palaeoenvironmental research, *The Holocene*, *5*(4), 457–460.

Lomax, B. H., C. A. Knight, and J. A. Lake (2012), An experimental evaluation of the use of C3 $\delta^{13}C$ plant tissue as a proxy for the paleoatmospheric $\delta^{13}CO_2$ signature of air, *Geochemistry, Geophysics, Geosystems*, *13*(9), Q0AI03.

Lu, Y. Z., and S. H. Deng (2005), Triassic-Jurassic sporopollen assemblages on the southern margin of the Junggar Basin, Xinjiang and the T-J boundary, *Acta Geologica Sinica, 79*(1), 15–27. (in Chinese with English abstract)

Lucas, S. G., and L. H. Tanner (2007), The nonmarine Triassic–Jurassic boundary in the Newark Supergroup of eastern North America, *Earth-Science Reviews*, *84*(1–2), 1–20.

Lucas, S. G., L. H. Tanner, L. L. Donohoo-Hurley, J. W. Geissman, H. W. Kozur, A. B. Heckert, and R. E. Weems (2011), Position of the Triassic–Jurassic boundary and timing of the end-Triassic extinctions on land: Data from the Moenave Formation on the southern Colorado Plateau, USA, *Palaeogeography, Palaeoclimatology, Palaeoecology*, *302*(3–4), 194–205.

Luo, Z. J., R. Wang, J. H. Zhao, and L. Y. Ai (2007), Late Permian-middle Jurassic megaspores assemblages in the north-west area, Junggar Basin, *Xinjiang Geology, 25*(3), 243–247. (in Chinese with English abstract)

Lustrino, M., V. Morra, L. Fedele, and L. Franciosi (2009), Beginning of the Apennine subduction system in central western Mediterranean: Constraints from Cenozoic "orogenic" magmatic activity of Sardinia, Italy, *Tectonics*, *28(5),* TC5061.

Manspeizer, W. (1988), Triassic-Jurassic rifting and opening of the Atlantic: An overview, *Triassic-Jurassic rifting, continental breakup, and the formation of the Atlantic Ocean and passive margins, Part A: Amsterdam, Netherlands.* Elsevier, pp. 41–79.

Marcinkiewicz, T. (1988), Lower Jurassic Megaspores, *Geology of Poland, Atlas of Guide and Characteristic Fossils (ed. L. Malinowska), III, 2b*, 64–70.

Margolis, S. V. (1975), Oxygen and carbon isotopes from calcareous nannofossils as paleoceanographic indicators, *Science*, *189*(4202), 555–557.

Marzoli, A., et al. (2004), Synchrony of the Central Atlantic magmatic province and the Triassic–Jurassic boundary climatic and biotic crisis, *Geology*, *32*(11), 973–976.

Mayall, M. J. (1983), An earthquake origin for synsedimentary deformation in a late Triassic (Rhaetian) lagoonal sequence, southwest Britain, *Geological Magazine*, *120*(06), 613–622.

McCarthy, F. M., and P. J. Mudie (1998), Oceanic pollen transport and pollen: dinocyst ratios as markers of late Cenozoic sea level change and sediment transport, *Palaeogeography, Palaeoclimatology, Palaeoecology*, *138*(1), 187-206, doi:10.1016/S0031-0182(97)00135–1.

McCarthy, F.M.G., Gostlin, K.E., Mudie, P.J., and Hopkins, J. (2003), Terrestrial and marine palynomorphs as sea-level proxies: an example from Quaternary sediments on the New Jersey margin, in Olson, H.C. and Leckie, M. (Eds.), *Micropaleontologic Proxies for Sea-Level Change and Stratigraphic Discontinuities: SEPM Special Publication* no. 75, pp. 119–129.

McCarthy, F. M. G., M. E. Katz, U. Kotthoff, M. Drljepan, R. Zanatta, R. H. Williams, J. V. Browning, S. P. Hesselbo, C. J. Bjerrum, K. G. Miller, G. S. Mountain (2013), Eustatic control of New Jersey margin architecture: palynological evidence from IODP Expedition 313, *Geosphere*, 9(6), 1–31.

McElwain, J. C., J. Wade-Murphy, and S. P. Hesselbo (2005), Changes in carbon dioxide during an oceanic anoxic event linked to intrusion into Gondwana coals, *Nature*, *435*(7041), 479–482.

McHone, J. G. (1996), Broad-terrane Jurassic flood basalts across northeastern North America, *Geology*, *24*(4), 319–322.

McHone, J. G. (2000), Non-plume magmatism and rifting during the opening of the central Atlantic Ocean, *Tectonophysics*, *316*(3–4), 287–296.

Metcalfe, I. (2006), Palaeozoic and Mesozoic tectonic evolution and palaeogeography of East Asian crustal fragments: The Korean Peninsula in context, *Gondwana Research, 9*(1–2), 24-46

Meyers, P. A. (1997), Organic geochemical proxies of paleoceanographic, paleolimnologic, and paleoclimatic processes, *Organic geochemistry*, *27*(5–6), 213–250.

Miller, K. G., and M. E. Katz (1987), Oligocene to Miocene benthic foraminiferal and abyssal circulation changes in the North Atlantic, *Micropaleontology*, 33(2), 97–149.

Miller, K. G., J. D. Wright, and R. G. Fairbanks (1991), Unlocking the Ice House: Oligocene-Miocene oxygen isotopes, eustasy, and margin erosion, *Journal of Geophysical Research: Solid Earth*, *96*(B4), 6829–6848.

Miller, K. G., M. A. Kominz, J. V. Browning, J. D. Wright, G. S. Mountain, M. E. Katz, P. J. Sugarman, B. S. Cramer, N. Christie-Blick, and S. F. Pekar (2005), The Phanerozoic Record of Global Sea-Level Change, *Science*, *310*(5752), 1293–1298.

Miller, K. G., J. V. Browning, G. S. Mountain, M. A. Bassetti, D. Monteverde, M. E. Katz, J. Inwood, J. Lofi, and J.-N. Proust (2013), Sequence boundaries are impedance contrasts: Core-seismic-log integration of Oligocene–Miocene sequences, New Jersey shallow shelf, *Geosphere*, *9*(5), 1257–1285.

Millioud M. E., J. P. Colin, and M. Pons, (1980), Paleontological Study of the Stratoil 34/10–4, Offshore Norway Well, *Log I Report of Stratoil 34/10–4*.

Møller, J. J., and E. S. Rasmussen, (2003), Middle Jurassic–Early Cretaceous rifting of the Danish Central Graben, In: Inoson, J.R., Surlyk, F. (Eds.), The Jurassic of Denmark and Greenland, *Geological Survey of Denmark and Greenland*, Bulletin, vol. 1, pp. 247–264.

Monteverde, D. H., G. S. Mountain, and K. G. Miller (2008), Early Miocene sequence development across the New Jersey margin, *Basin Research*, *20*(2), 249–267.

Morbey, S. J. (1978), Late Triassic and Early Jurassic subsurface palynostratigraphy in northwestern Europe, *Palinologia,* 1, 355–365.

Morris, P. H., A. Cullum, M. A. Peace, and D. J. Batten (2009), Megaspore assemblages from the Åre Formation (Rhaetian–Pliensbachian) offshore mid-Norway, and their value as field and regional stratigraphical markers, *Journal of Micropalaeontology*, *28*(2), 161–181.

Mosar, J., G. Lewis, and T. H. Torsvik (2002), North Atlantic Sea-Floor Spreading Rates: Implications for the Tertiary Development of Inversion Structures of the Norwegian-Greenland Sea, *Journal of the Geological Society (London), 159* (5), 503–515.

Mountain, G., J.-N. Proust, D. McInroy, C. Cotterill, and the Expedition 313 Scientists (2010), Proceedings of the Ocean Drilling Program, Scientific Results, 313, Tokyo (Integrated Ocean Drilling Program Management International, Inc.), doi:10.2204/iodp.proc.313.101. 2010.

Mutti, M., D. Bernoulli, and P. Stille (1997), Temperate carbonate platform drowning linked to Miocene oceanographic events: Maiella platform margin, Italy, *Terra Nova*, *9(3),* 122–125.

Mutti, M., C. M. John, and A. C. Knoerich (2006), Chemostratigraphy in Miocene heterozoan carbonate settings: applications, limitations and perspectives, *Geological Society, London, Special Publications*, *255(1),* 307–322.

Nunn, E. V., G. D. Price, D. R. Gröcke, E. Y. Baraboshkin, M. J. Leng, and M. B. Hart (2010), The Valanginian positive carbon isotope event in Arctic Russia: Evidence from terrestrial and marine isotope records and implications for global carbon cycling, *Cretaceous Research*, *31*(6), 577–592.

Ogle, Neil, and F. G. McCormac (1994), High-resolution $\delta^{13}C$ measurements of oak show a previously unobserved spring depletion. *Geophysical Research Letters*, *21*(22), 2373–2375.

Oh, J., J. A. Austin, J. D. Phillips, M. F. Coffin, and P. L. Stoffa (1995), Seaward-dipping reflectors offshore the southeastern United States: Seismic evidence for extensive volcanism accompanying sequential formation of the Carolina trough and Blake Plateau basin, *Geology*, *23*(1), 9–12.

Pagani, M., K. Caldeira, R. Berner, and D. J. Beerling (2009), The role of terrestrial plants in limiting atmospheric CO_2 decline over the past 24million years, *Nature, 460*(7251), 85–88.

Pálfy, J., and P. L. Smith (2000), Synchrony between Early Jurassic extinction, oceanic anoxic event, and the Karoo-Ferrar flood basalt volcanism, *Geology*, *28*(8), 747–750.

Pálfy, J., A. Demény, J. Haas, M. Hetényi, M. J. Orchard, and I. Veto (2001), Carbon isotope anomaly and other geochemical changes at the Triassic-Jurassic boundary from a marine section in Hungary, *Geology*, *29*(11), 1047–1050.

Pearson, P. N., and M. R. Palmer (2000), Atmospheric carbon dioxide concentrations over the past 60 million years, *Nature*, *406*(6797), 695–699.

Pancost, R. D., and C. S. Boot (2004), The palaeoclimatic utility of terrestrial biomarkers in marine sediments, *Marine Chemistry*, *92*(1–4), 239–261.

Peters, K. E. (1986), Guidelines for evaluating petroleum source rock using programmed pyrolysis, *American Association of Petroleum Geologists Bulletin*, *70*(3), 318–329.

Petersen, H. I., A. C. Holme, E. Thomsen, M. F. Whitaker, T. Brekke, J. A. Bojesen-Koefoed, K. H. Hansen, and B. T. Larsen (2011), Hydrocarbon potential of Middle Jurassic coaly and lacustrine and Upper Jurassic–lowermost Cretaceous marine source rocks in the Søgne Basin, North Sea, *Journal of Petroleum Geology*, *34*(3), 277–304

Piasecki, S. (1980), *Dinoflagellate cyst stratigraphy of the Miocene Hodde and Gram Formations*, *Denmark*, *Bulletin of the Geological Society of Denmark,* vol.29, 53–76

Piasecki, S. (2005), Dinoflagellate cysts of the Middle–Upper Miocene Gram Formation, Denmark. In: Roth, F., Hoedemakers, K. (Eds.), The Marine Gram Formation at Gram, Denmark: Late Miocene Geology and Palaeontology, *Palaeontos,* vol. 7, pp. 29–45.

Pieñkowski G. (2004), The epicontinental Lower Jurassic of Poland, *Polish Geological Institute Special Papers, 12*, 1–152.

Poole, I., P. F. van Bergen, J. Kool, S. Schouten, and D. J. Cantrill (2004), Molecular isotopic heterogeneity of fossil organic matter: implications for $\delta^{13}C_{biomass}$ and $\delta^{13}C_{palaeoatmosphere}$ proxies, *Organic geochemistry*, *35*(11–12), 1261–1274.

Potter, P. E., and P. Szatmari (2009), Global Miocene tectonics and the modern world, *Earth-Science Reviews, 96*(4), 279–295.

Poulsen, N. E., and J. B. Riding (2003), The Jurassic dinoflagellate cyst zonation of subboreal Northwest Europe, *Geological Survey of Denmark and Greenland Bulletin*, vol.1, pp. 115–144.

Quan, T. M., B. van de Schootbrugge, M. P. Field, Y. Rosenthal, and P. G. Falkowski (2008), Nitrogen isotope and trace metal analyses from the Mingolsheim core (Germany): Evidence for redox variations across the Triassic-Jurassic boundary, *Global biogeochemical cycles*, *22*(2), GB2014.

Raine, J. I., D. C. Mildenhall, E. M. Kennedy (2011), New Zealand fossil spores and pollen: an illustrated catalogue, 4th edition, GNS Science miscellaneous series no. 4, from http://data.gns.cri.nz/ sporepollen /index.htm.

Rasmussen, E. S. (2004a), The interplay between true eustatic sea-level changes, tectonics, and climatic changes: what is the dominating factor in sequence formation of the Upper Oligocene–Miocene succession in the eastern North Sea Basin, Denmark?, *Global and Planetary Change*, *41*(1), 15–30.

Rasmussen, E. S. (2004b), Stratigraphy and depositional evolution of the uppermost Oligocene–Miocene succession in Denmark, *Bulletin of the Geological Society of Denmark,* vol.51, 89–109.

Rasmussen, E. S., O. V. Vejbæk, T. Bidstrup, S. Piasecki, and K. Dybkjær (2005), Late Cenozoic depositional history of the Danish North Sea Basin: implications for the petroleum systems in the Kraka, Halfdan, Siri and Nini fields, *Geological Society, London, Petroleum Geology Conference series*, *6*, 1347–1358.

Rasmussen, E. S. (2009), Neogene inversion of the Central Graben and Ringkøbing-Fyn High, Denmark, *Tectonophysics*, *465*(1–4), 84–97.

Rasmussen, E. S., K. Dybkjær, and S. Piasecki (2010), Lithostratigraphy of the Upper Oligocene- Miocene succession of Denmark, *Geological Survey of Denmark and Greenland Bulletin*, vol. 22, pp. 92.

Rasmussen, L.B., 1961, De Miocaene formationer i Danmark, DGU, IV Række, vol. 5, pp. 45.

Raup, D. M., and J. J. Sepkoski (1982), Mass extinctions in the marine fossil record, *Science*, *215*(4539), 1501–1503.

Reiser, R. F., and A. J. Williams (1969), *Palynology of the Lower Jurassic sediments of the northern Surat Basin, Queensland*, SG Reid, Government Printer, pp. 24.

Reyre, Y. (1970), Stereoscan observations on the pollen genus Classopollis Pflug 1953. *Palaeontology*, *13*(2), 303–322.

Ridgwell, A. (2007), Interpreting transient carbonate compensation depth changes by marine sediment core modeling, *Paleoceanography*, *22*(4), PA4102.

Riding, J. B., M. J. Leng, S. Kender, S. P. Hesselbo, and S. Feist-Burkhardt (2013), Isotopic and palynological evidence for a new Early Jurassic environmental perturbation, *Palaeogeography, Palaeoclimatology, Palaeoecology*, *374*(0), 16–27.

Robinson, S. A., and S. P. Hesselbo (2004), Fossil-wood carbon-isotope stratigraphy of the non-marine Wealden Group (Lower Cretaceous, southern England), *Journal of the Geological Society*, *161*(1), 133–145.

Ruhl, M., W. M. Kürschner, and L. Krystyn (2009), Triassic–Jurassic organic carbon isotope stratigraphy of key sections in the western Tethys realm (Austria), *Earth and Planetary Science Letters*, *281*(3–4), 169–187.

Ruhl, M., and W. M. Kürschner (2011), Multiple phases of carbon cycle disturbance from large igneous province formation at the Triassic-Jurassic transition, *Geology*, *39*(5), 431–434.

Ruhl, M., N. R. Bonis, G.-J. Reichart, J. S. S. Damsté, and W. M. Kürschner (2011), Atmospheric Carbon Injection Linked to End-Triassic Mass Extinction, *Science*, *333*(6041), 430–434.

Sackett, W. M. (1964), The depositional history and isotopic organic carbon composition of marine sediments, *Marine Geology*, *2*(3), 173–185.

Sackett, W. M. (1989), Stable carbon isotope studies on organic matter in the marine environment. In: Fritz, P., and Fontes, J.C. (Eds.), *Handbook of Environmental Isotope Geochemistry (Vol. 3), The Marine Environment, A, Amsterdam.* Elsevier, pp. 139–169.

Saltzman, M. R., and E. Thomas (2012), Carbon-isotope stratigraphy, in: Gradstein, F. M., J. G. Ogg, and M. Schmitz (Eds.), *The Geologic Time Scale*, pp. 207–232.

Savin, S. M., and R. G. Douglas (1973), Stable Isotope and Magnesium Geochemistry of Recent Planktonic Foraminifera from the South Pacific, *Geological Society of America Bulletin*, *84*(7), 2327–2342.

Savin, S. M., R. G. Douglas, and F. G. Stehli (1975), Tertiary marine paleotemperatures, *Geological Society of America Bulletin*, *86*(11), 1499–1510.

Savin, S. M., R. G. Douglas, G. Keller, J. S. Killingley, L. Shaughnessy, M. A. Sommer, E. Vincent, and F. Woodruff (1981), Miocene benthic foraminiferal isotope records: A synthesis, *Marine Micropaleontology*, *6*(4), 423–450.

Schleser, G. (1999), $^{13}C/^{12}C$ in growth rings and leaves: carbon distribution in trees, in: T. P. Jones and N. P. Rowe (Eds.), *Fossil Plants and Spores: Modern Techniques,* Geological Society, London, pp. 306–309.

Scholle P. A., and M. A. Arthur (1980), Carbon isotope fluctuations in Cretaceous pelagic limestones potential stratigraphic and petroleum exploration tool, *American Association of Petroleum Geologists, Bulletin, 64*(1), 67–87.

Schootbrugge, B. v. d., T. R. Bailey, Y. Rosenthal, M. E. Katz, J. D. Wright, K. G. Miller, S. Feist-Burkhardt, and P. G. Falkowski (2005), Early Jurassic Climate Change and the Radiation of Organic-Walled Phytoplankton in the Tethys Ocean, *Paleobiology, 31*(1), 73–97.

Sengör, A. M. C., B. A. Natal'in, and V. S. Burtman (1993), Evolution of the Altaid tectonic collage and Palaeozoic crustal growth in Eurasia, *Nature*, *364*(6435), 299–307.

Sepkoski Jr., J. J. (1996), Patterns of Phanerozoic Extinction: a Perspective from Global Data Bases, in *Global Events and Event Stratigraphy in the Phanerozoic*, edited by O. Walliser, Springer Berlin Heidelberg, pp. 35–51.

Sha, J. G., V. Vajda, Y. H. Pan, L. Linda, X. G. Yao, X. L. Zhang, Y. Q. Wang, X. S. Cheng, B. Y. Jiang, S. H. Deng, S. W. Chen, and B. Peng (2011), Stratigraphy of the Triassic–Jurassic Boundary Successions of the Southern Margin of the Junggar Basin, Northwestern China, *Acta Geologica Sinica-English Edition*, *85*(2), 421–436.

Shackleton, N. J., and N. D. Opdyke (1973), Oxygen isotope and palaeomagnetic stratigraphy of Equatorial Pacific core V28-238: Oxygen isotope temperatures and ice volumes on a 105 year and 106 year scale, *Quaternary research, 3*(1), 39–55.

Shackleton, N. J. (1977), Tertiary oxygen and carbon-isotope stratigraphy, Site 357 (mid-latitude South Atlantic), *Initial Reports of the Deep Sea Drilling Project* 39, 911–924.

Shackleton, N. J., and E. Vincent (1978), Oxygen and carbon isotope studies in recent foraminifera from the southwest Indian Ocean, *Marine Micropaleontology,* 3(1), 1–13.

Shackleton, N. J. (1986), Paleogene stable isotope events, *Palaeogeography, Palaeoclimatology, Palaeoecology*, *57*(1), 91–102

Simms, M. J. (2003), Uniquely extensive seismite from the latest Triassic of the United Kingdom: Evidence for bolide impact?, *Geology*, *31*(6), 557–560.

Smith, A. D. (1992), Back-arc convection model for Columbia river basalt genesis, *Tectonophysics*, *207*(3–4), 269–285.

Smith, A. D. (2003), Critical evaluation of Re–Os and Pt–Os isotopic evidence on the origin of intraplate volcanism, *Journal of Geodynamics*, *36*(4), 469–484.

Smith, B. N., and S. Epstein (1971), Two categories of $^{13}C/^{12}C$ ratios for higher plants, *Plant Physiology,* 47(3), 380–384.

Smith, R. B., M. Jordan, B. Steinberger, C. M. Puskas, J. Farrell, G. P. Waite, S. Husen, W.-L. Chang, and R. O'Connell, 2009, Geodynamics of the Yellowstone hotspot and mantle plume: Seismic and GPS imaging, kinematics, and mantle flow, *Journal of Volcanology and Geothermal Research, 188*(1–3), 26–56.

Sorgenfrei, T. (1958), Molluscan assemblages from the marine Middle Miocene of South Jutland and their environments, *Danmarks Geologiske Undersøgelse II, Pække 79*, pp. 503.

Spero, H. J., and D. F. Williams (1988), Extracting environmental information from planktonic foraminiferal $\delta^{13}C$ data, *Nature*, *335*(6192), 717–719.

Spero, H. J., I. Lerche, and D. F. Williams (1991), Opening the carbon isotope vital effect black box 2, Quantitative model for interpreting foraminiferal carbon isotope data, *Paleoceanography,* 6 (6), 639–655.

Spero, H. J. (1992), Do planktic foraminifera accurately record shifts in the carbon isotopic composition of seawater ΣCO_2?, *Marine Micropaleontology*, *19*(4), 275–285.

Spero, H. J., and D. W. Lea (1996), Experimental determination of stable isotope variability in Globigerina bulloides: implications for paleoceanographic reconstructions, *Marine Micropaleontology*, *28*(3–4), 231–246.

Spiker, E. C. (1984), Carbon isotope fractionation of sapropelic organic matter during early diagenesis, *Organic geochemistry*, *5*(4), 283–290.

Spiker, E. C. (1987), The effects of early diagenesis on the chemical and stable carbon isotopic composition of wood, *Geochimica et Cosmochimica Acta*, *51*(6), 1385.

Srivastava, S. K. (1976), The fossil pollen genus Classopollis, *Lethaia*, *9*(4), 437–457.

Stockmarr, J., (1971), Tablets with Spores used in absolute pollen analysis, *Pollen et Spores, 13*(4), 615–621.

Storey, B. C., T. Alabaster, M. J. Hole, R. J. Pankhurst, and H. E. Wever (1992), Role of subduction-plate boundary forces during the initial stages of Gondwana break-up: evidence from the proto-Pacific margin of Antarctica, *Geological Society, London, Special Publications*, *68*(1), 149–163.

Stout, S. A., J. J. Boon, and W. Spackman (1988), Molecular aspects of the peatification and early coalification of angiosperm and gymnosperm woods, *Geochimica et Cosmochimica Acta*, *52*(2), 405–414.

Sun, G., Y. Miao, V. Mosbrugger, and A. R. Ashraf (2010), The Upper Triassic to Middle Jurassic strata and floras of the Junggar Basin, Xinjiang, Northwest China. *Palaeobiodiversity and Palaeoenvironments*, *90*(3), 203–214.

Svensen, H., S. Planke, L. Chevallier, A. Malthe-Sørenssen, F. Corfu, and B. Jamtveit (2007), Hydrothermal venting of greenhouse gases triggering Early Jurassic global warming, *Earth and Planetary Science Letters*, *256*(3–4), 554–566.

Tanner, L. H., S. G. Lucas, and M. G. Chapman (2004), Assessing the record and causes of Late Triassic extinctions, *Earth-Science Reviews*, *65*(1–2), 103–139.

Traverse, A. (2007), *Paleopalynology (Vol. 28)*, Springer.

Tripathi, A., and A. K. Raychowdhuri (2005), Triassic Palynoflora from the Mahuli-Mahersop Area, Singrauli Coalfield (Southern Extension), Sarguja District, Chhattisgarh, India, *Journal of the Palaeontological Society of India*, *50*(2), 77–99.

Turco, E., F. J. Hilgen, L. J. Lourens, N. J. Shackleton, W. J. Zachariasse, (2001), Punctuated evolution of global climate cooling during the late Middle to early Late Miocene: high-resolution planktonic foraminiferal and oxygen isotope records from the Mediterranean, *Paleoceanography, 16*(4), 405–423.

Tyson, R.V. (1995), Sedimentary Organic Matter: Organic Facies and Palynofacies, *Chapman and Hall, London,* pp. 615.

Utescher, T., V. Mosbrugger, and A. R. Ashraf (2000), Terrestrial Climate Evolution in Northwest Germany Over the Last 25 Million Years, *Palaios, 15*(5), 430–449.

Vakhrameyev, V. A. (1982), Classopollis pollen as an indicator of Jurassic and Cretaceous climate, *International Geology Review*, *24*(10), 1190-1196, DOI:10.1080/00206818209451058.

Vakhrameyev, V. A. (1991), *Jurassic and Cretaceous floras and climates of the Earth*, Cambridge University Press.

van de Schootbrugge, B., J. M. McArthur, T. R. Bailey, Y. Rosenthal, J. D. Wright, and K. G. Miller (2005), Toarcian oceanic anoxic event: An assessment of global causes using belemnite C isotope records, *Paleoceanography*, *20*(3), PA3008.

van de Schootbrugge, B., J. L. Payne, A. Tomasovych, J. Pross, J. Fiebig, M. Benbrahim, K. B. Föllmi, and T. M. Quan (2008), Carbon cycle perturbation and stabilization in the wake of the Triassic-Jurassic boundary mass-extinction event, *Geochemistry, geophysics, geosystems*, *9*(4), Q04028.

van Konijnenburg-van Cittert, J. H. A. (2008), The Jurassic fossil plant record of the UK area, *Proceedings of the Geologists' Association*, *119*(1), 59–72.

Veizer, J., D. Ala, K. Azmy, P. Bruckschen, D. Buhl, F. Bruhn, G. A. F. Carden, A. Diener, S. Ebneth, Y. Godderis, T. Jasper, C. Korte, F. Pawellek, O. G. Podlaha, and H. Strauss (1999), $^{87}Sr/^{86}Sr$, $\delta^{13}C$ and $\delta^{18}O$ evolution of Phanerozoic seawater, *Chemical geology*, *161*(1–3), 59–88, doi:10.1016/ S0009-2541(99)00081–9.

Vejbæk, O. V. (1997), Dybe strukturer I danske sedimentære basiner, *Geologisk Tidsskrift, 4,* 1–31.

Vergnaud Grazzini, C. (1976), Non-equilibrium isotopic compositions of shells of planktonic foraminifera in the Mediterranean sea, *Palaeogeography, Palaeoclimatology, Palaeoecology*, *20*(4), 263–276.

Vincent, E., J. S. Killingley, and W. H. Berger (1980), The Magnetic Epoch-6 carbon shift: A change in the ocean's $^{13}C/^{12}C$ ratio 6.2 million years ago, *Marine Micropaleontology*, *5*(0), 185–203.

Vincent, E., and W. H. Berger (1985), Carbon dioxide and polar cooling in the Miocene: The Monterey hypothesis, in Sundquist E.T., and Broecker W.S. (Eds.), *The Carbon Cycle and Atmospheric CO_2 : Natural Variations, Archean to Present, Geophysics Monograph Series, American Geophysical Union, Washington, D.C.,* vol. 32, pp. 455–468.

von Hillebrandt, A., L. Krystyn, and W. M. Kuerschner (2007), A candidate GSSP for the base of the Jurassic in the Northern Calcareous Alps (Kuhjoch section, Karwendel Mountains, Tyrol, Austria), *ISJS Newsl*, *34*(1), 2–20.

Wang Z. M., D. Zhong, P. R. Zhao, W. S. Xia, S. B. Zhang, J. Y. Yan et al. (2004), Petroleum of geology of outcrops areas in Kuche Foreland Basin. Petroleum Industry Press, Beijing. (In Chinese)

Ward, P. D., J. W. Haggart, E. S. Carter, D. Wilbur, H. W. Tipper, and T. Evans (2001), Sudden Productivity Collapse Associated with the Triassic-Jurassic Boundary Mass Extinction, *Science*, *292*(5519), 1148-1151.

Ward, P. D., G. H. Garrison, K. H. Williford, D. A. Kring, D. Goodwin, M. J. Beattie, and C. A. McRoberts (2007), The organic carbon isotopic and paleontological record across the Triassic–Jurassic boundary at the candidate GSSP section at Ferguson Hill, Muller Canyon, Nevada, USA, *Palaeogeography, Palaeoclimatology, Palaeoecology*, *244*(1–4), 281–289.

Watkins Jr, J. E., and C. L. Cardelús (2012), Ferns in an Angiosperm World: Cretaceous Radiation into the Epiphytic Niche and Diversification on the Forest Floor, *International Journal of Plant Sciences*, *173*(6), 695–710.

Whiteside, J. H., P. E. Olsen, T. Eglinton, M. E. Brookfield, and R. N. Sambrotto (2010), Compound-specific carbon isotopes from Earth's largest flood basalt eruptions directly linked to the end-Triassic mass extinction, *Proceedings of the National Academy of Sciences*, *107*(15), 6721–6725.

Whiteside, J. H., and P. D. Ward (2011), Ammonoid diversity and disparity track episodes of chaotic carbon cycling during the early Mesozoic, *Geology*, *39*(2), 99–102.

Williams, D. F., M. A. SommerIi, and M. L. Bender (1977), Carbon isotopic compositions of Recent planktonic foraminifera of the Indian Ocean, *Earth and Planetary Science Letters*, *36*(3), 391–403.

Williford, K. H., P. D. Ward, G. H. Garrison, and R. Buick (2007), An extended organic carbon-isotope record across the Triassic–Jurassic boundary in the Queen Charlotte Islands, British Columbia, Canada, *Palaeogeography, Palaeoclimatology, Palaeoecology*, *244*(1–4), 290–296.

Windley, B. F., M. B. Allen, C. Zhang, Z. Y. Zhao, and G. R. Wang (1990), Paleozoic accretion and Cenozoic redeformation of the Chinese Tien Shan Range, central Asia, *Geology*, *18*(2), 128–131.

Windley, B. F., D. Alexeiev, W. Xiao, A. Kröner, and G. Badarch (2007), Tectonic models for accretion of the Central Asian Orogenic Belt, *Journal of the Geological Society*, *164*(1), 31–47.

Wolff, J. A., F. C. Ramos, G. L. Hart, J. D. Patterson, and A. D. Brandon, (2008), Columbia River flood basalts from a centralized crustal magmatic system, *Nature Geosciences, 1*(3), 177–180.

Woodruff, F., and S. M. Savin (1985), $\delta^{13}C$ values of Miocene Pacific benthic foraminifera: Correlations with sea level and biological productivity, *Geology, 13*(2), 119–122.

Woodruff, F., and S. M. Savin (1989), Miocene deepwater oceanography, *Paleoceanography*, *4*(1), 87–140.

Woodruff, F., and S. Savin (1991), Mid-Miocene Isotope Stratigraphy in the Deep Sea: High-Resolution Correlations, Paleoclimatic Cycles, and Sediment Preservation, *Paleoceanography*, *6*(6), 755–806.

Wright, J. D., K. G. Miller, and R. G. Fairbanks (1992), Early and Middle Miocene Stable Isotopes: Implications for Deepwater Circulation and Climate, *Paleoceanography*, *7*(3), 357–389.

Wu, S. Z., (1990), Characteristics of Early Jurassic Flora in Xinjiang, *Xinjiang Geology, 8(*2), 119–131.

Xiao, J. X., C. S. Lin, and J. Y. Liu (2005), Depositional Palaeogeography of Cretaceous of Kuqa Depression in the Northern Tarim Basin, *Geosciences, 19*(2), 253–260.

Yang, H., R. Yan, H. Chen, D. H. Lee, and C. Zheng (2007), Characteristics of hemicellulose, cellulose and lignin pyrolysis, *Fuel*, *86*(12–13), 1781–1788.

Yin A. and Harrison M. (Eds.), (1996), The Tectonic Evolution of Asia, Cambridge. Cambridge University Press, pp. 371–400.

Zachos, J. C., M. A. Arthur, and W. E. Dean (1989), Geochemical evidence for suppression of pelagic marine productivity at the Cretaceous/Tertiary boundary, *Nature*, *337*(6202), 61-64.

Zachos, J., M. Pagani, L. Sloan, E. Thomas, and K. Billups (2001), Trends, Rhythms, and Aberrations in Global Climate 65 Ma to Present, *Science*, *292*(5517), 686–693.

Zeebe, R. E., and D. Wolf-Gladrow (2001), CO_2 in Seawater: Equilibrium, Kinetics, Isotopes: Equilibrium, Kinetics, Isotopes. *Elsevier Oceanographic Series, Elsevier, New York,* pp. 9–11 and pp. 170–175.

Zhang, L. J. (1980), Palynological contribution to the chronology and stratigraphy of Xinjiang. *In: 5th International Palynological Conference*, pp. 1–7.

Zhang L. J. (1983), On the Age of Badaowan Formation in Northern Xinjiang, *Scientia Sinica (Series B), 26* (7), 774–781.

Zhang, W. P., and Y. A. Li (1990), Palynological assemblage of the Ahe Fm, Yangxia Fm and Kezilenuer Fm, Baicheng Area, Xinjiang, *Xinjiang Geology, 8* (3), 256–271.

Zhou, Y. Z. (1984), Early stage of Early Jurassic plant fossils, SW Hunan Province, *Chinese Journal of the Paleontological,* vol. 165. Science Press, Beijing.

Ziegler, P. A. (1990), Geological Atlas of Western and Central Europe, *Shell Internationale Petroleum Maatschappij B.V., Den Haag,* pp. 239.

Ziegler, P. A., S. Cloetingh, and J. D. van Wees (1995), Dynamics of intra-plate compressional deformation: the Alpine foreland and other examples, *Tectonophysics*, *252*(1), 7–59.

Zimmerman, M. A., D. F. Williams, and R. Roettger (1983), Symbiont-influenced isotopic disequilibrium in Heterostegina depressa, *The Journal of Foraminiferal Research, 13*(2), 115–121.

Appendix List

Appendix A $\delta^{13}C$ values on Lignin

-Appendix A.1 Text on theoretical study (page 185–212)

-Appendix A.2 Figures-preliminary data (attached DVD)

Appendix B New Jersey (attached DVD)

-Appendix B.1 Published data

-Appendix B.2 Palynofacies data & images, Site29 New Jersey, Density separation (bottom) part

-Appendix B.3 SEM

-Appendix B.4 Images of hand-picked phytoclasts (reflected light microscopy)

Appendix C North Sea Basin (attached DVD)

-Appendix C.1 Carbon-isotope data

-Appendix C.2 SEM-phytoclasts, Rødding well, Denmark

-Appendix C.3 SEM-phytoclasts, Sønder Vium well, Denmark

Appendix D Kuqa Section, Tarim NW China (attached DVD)

-Appendix D.1 Carbon-isotope data

-Appendix D.2 Outcrop photos, Kuqa section, 2011

-Appendix D.3 Images of charcoal and coal (reflected light microscopy)

-Appendix D.4 SEM images-charcoal and coal

Appendix A

Theoretical consideration on why the individual biomarkers in high molecular weight can faithfully maintain the original carbon-isotope signals, regardless of the degree of degradation by bacteria, or other chemical or physical processes during diagenesis.

A modified version of the Appendix A was prepared for a manuscript as: Linhao Fang, Boshen Wu, ***Does carbon isotope remain original in an individual organic compound during diagenesis?*** It is reproduced here in thesis format. This appendix was contributed as follows:

- L. Fang contributed the initial ideas and wrote up the manuscript.
- B. Wu made much contribution to improve ideas, especially, in charge of the accurate usage of knowledge about organic chemistry.
- L. Fang and B. Wu together discussed and modified the manuscript up to current version.

Do carbon isotopes remain original in individual organic compounds during diagenesis?

Abstract

The stable carbon(C)-isotope value ($\delta^{13}C$) from organic matter (OM) is a very useful measurement both for researching carbon cycle perturbations over Earth history and for monitoring modern environmental hydrocarbon contaminants. Widely used $\delta^{13}C$ values of bulk OM are always questionable, as bulk OM is composed of multiple components, which potentially originate from diverse sources and which undergo selective preservation among different components. Logically, concentration on an individual organic compound can eliminate $\delta^{13}C$ values biased by diverse sources and/or selective preservation. However, does C-isotope fractionation occur in individual organic compounds during diagenesis? Empirical data in literature provide conflicting phenomena with absence or presence of $\delta^{13}C$ values changing in individual organic compounds after diagenesis. To address this conflict, a theoretical solution is proposed on basis of combination of the Rayleigh fractionation equation and the Bigeleisen theory of isotopic effects. This theoretical consideration illustrates that C-isotope fractionation will reduce to an undetectable level when molecular weight rises beyond a threshold (specific thresholds subject to the compound types and reaction conditions). Two experienced threshold values are estimated on the basis of empirical data from published literature. Although the theory-based study agrees with all current high-quality empirical reports, further experimental studies are required for verification. Furthermore, implications and predictions are reached that high molecular-weight compounds and natural polymers (e.g. lignin) maintain their original C-isotope values, no matter what percentage has been degraded by bacteria or by other diagenetic processes.

1. Introduction

The stable carbon(C)-isotope value ($\delta^{13}C$) derived from sedimentary organic matter (OM) has been broadly employed to investigate global carbon perturbation (Hesselbo et al., 2000; Peters-Kotting et al., 2006; Sluijs et al., 2007), $\delta^{13}C$ of palaeo-atmospheric carbon dioxide (Arens et al., 2000; Gröcke, 2002; Jahren et al., 2008), vegetation composition and glacial-interglacial evolution (Huang et al., 1999a, 1999b), palaeoenvironmental changes (e.g. temperature, humidity or aribdity, via water-use efficiency of terrestrial plants) (Bechtel et al., 2008), OM provenance (Pancost and Boot, 2006), C-isotope shifts associated with mass extinction (Arinobu et al., 1999), changes of temperature-stratified palaeo-oceans (Schoell et al., 1994), and modern environmental monitors (O'Malley et. al., 1994, 1996). When these applications are examined in-depth studies, it is found that many authors generated $\delta^{13}C$ from various OM, such as bulk OM, fossil wood, charcoal, coal, phytoclasts and individual compounds, including cellulose, lignin monomers, phytane, pristine, long-chain compounds, sterane and hopane, etc.(Table Appendix A.1).

However, there are two primary challenges in use of $\delta^{13}C$ generated from bulk OM to reconstruct reliable ancient information. Firstly, although bulk OM $\delta^{13}C$ data are the most commonly reported due to their relatively simple measurement, bulk OM always consists of components from diverse sources, which are normally registered by different $\delta^{13}C$ signatures. For instance, the bulk OM collected from marine shelf deposits contains OM of both marine plankton and land plant tissues, which are very distinct in the $\delta^{13}C$ values (Sluijs and Dickens, 2012). Even just land plants show very different C-isotope signatures in different photosynthetic types (GrÖcke 2002, and references therein). For example, C3 plants have values ranging between -23 ‰ and -34‰ (averaging -27‰), while C4 plants have values ranging between -8 ‰ and -16‰ (averaging -13‰). Therefore, the uncertainty of

Table Appendix A.1. $\delta^{13}C$ studies from different compositions of organic matter (OM)

Reference	Bulk OM	Wood fossil	Char -coal	Coal	Phytoclasts	specific compounds					Others
						Cellulose	lignin (monomers)	Phytane	pristine	Long-chain compounds	
Bechtel et al., 2008		√		√		√					
Hesselbo et al., 2000	√	√	√	√							Extracted organic matter by organic solvent
Huang et al., 1999 - geology	√						√			n-alkanes	
Huang et al., 1999a- GCA	√									n-alkanes, n-Acids, n-alkanols, Isoprenoid alkenes	
Pagni et al., 1999b -								√	√		
Schoell et al., 1994											sterane and hopane (marine dominantly)
Peters-Kotting et al., 2006	√	√		√							coalified cuticules
Sluijs et al., 2007											Predominantly derived from dinocysts Apectodinium (marine only)
Sluijs and Dickens, 2012	√										
Aren et al., 2000											Various modern plants
GrÖcke, 2002	√	√									
Jahren et al., 2008											Modern plants
Arinobu et al., 1999										n_{29}-alkanes,	
O'Malley et. al., 1994											polycyclic aromatic hydrocarbons (PAHs)
Hasegawa, 1997					√						
Hesselbo and Pieńkowski, 2011					√						

compositions and sources of the bulk OM is an inevitable flaw, which biases the true C-isotope values during data interpretation.

Secondly, even if OM in bulk derives from the same sources, a selective preservation (or alternatively viewed as a selective degradation) can lead to changes in the ratio of each composition in bulk OM. This alteration influences $\delta^{13}C$ values measured from bulk OM, as different compositions are commonly characterized by different $\delta^{13}C$ signatures (Hatcher et al., 1983; Benner et al., 1987; Hedges et al., 1999). Selective preservation can potentially take place during any stage of transportation or diagenesis.

Logically, the two difficulties (diverse sources and selective preservation) can be surmounted by focusing on $\delta^{13}C$ generated from an individual compound, especially when the compound is derived from a definite source, such as lignin, exclusively derived from the land higher plants.

However, even though individual compounds are focused on, a question still arises: does C-isotopic fractionation occur in an individual species of organic compound during diagenesis (including physical, chemical and biological alteration)? The empirical studies in previously published literature have offered a controversial answer. Several reports provide convincing evidence for no C-isotopic fractionation occurring in individual compounds during the processes of diagenesis (Huang et al., 1997; Mazeas et al., 2002), whereas other studies illustrate the unambiguous C-isotopic fractionation of individual compounds during diagenetic processes (Ahad et al., 2000; Masterson et al., 2001). To date, this dispute remains theoretically undefined (Galimov, 2006).

To address the controversy, our present study aims to look into this conflicting phenomenon and to explore underlying mechanisms. The Rayleigh equation and the Bigeleisen theory are used to investigate the mechanisms of isotopic fractionation of individual organic compounds.

Combining these two theories, a possible theoretical explanation is proposed as to why isotopic fractionation of specific compounds in diagenetic processes falls down to an undetectable level when molecular weight is beyond a certain threshold, regardless of what the degree of degradation by bacteria, or any chemical or physical processes during diagenesis. Further implication suggests that some kinds of compound-specific proxies can faithfully record their original $\delta^{13}C$ signatures over immense geological history and complex geological affects.

2. Definition of diagenesis in the present paper

The term 'diagenesis' was initially coined when Von Gümbel studied sedimentary rocks in 1868. He intended to indicate the processes which occur in sediments after deposition without metamorphism, even though his case study actually mistakenly involved metamorphism due to knowledge limits at that age (Segonzac, 1968, developmental details reviewed). Walther (1893-1894), who devoted 18 papers to this concept, was the real founder of the modern understanding of the term, diagenesis. His definition of diagenesis referred to the diagenesis of organic deposits, but the interest was just concentrated on 'carbonization of vegetal matter, silicification of wood, recrystallization and dolomitization of biogenic limestones, etc.'(Segonzac, 1968) without concerning degradation/decomposition of organic deposits, e.g. woody materials, algae, fungi.

Up until the 1950s, sedimentologists particularly paid attention to debating the scope of diagenesis, because of two inconsistent paradigms of using diagenesis on restricted sense or broad sense. Some authors (Krumbein1947; Strakhov 1953, p.12; 1960; Brinkm 1961) narrowly defined diagenesis as only one of sedimentary stages which begins with 'immobilization in the bottom of a basin and continues as long as the series has not been affected by metamorphism'. Many other authors (Blackwelder 1947; Williams et al., 1955)

insisted on a broader meaning of processes involving transportation, deposition and after deposition but prior to metamorphism.

Recently with the introduction to the study of OM in sediments, the concept 'diagenesis' is obliged to be extended on basis of conventional usages. Obviously, it is impossible to obtain explicit discussions and clear thoughts regarding alteration of $\delta^{13}C$ in OM, until an inevitable definition of 'diagenesis' is clarified.

So far, diagenesis is simply defined as 'all the changes that take place in the sediments at low temperature and pressure after deposition (Oxford Dictionary of Earth Sciences, 2008)' or more specifically defined as 'the sum of all those physical, chemical and biological post-depositional processes prior to the onset of metamorphism by which originally sedimentary assemblages and their interstitial pore waters react, and attempt to reach equilibrium with their evolving geochemical environment' (The Encyclopedia of the Solid Earth Sciences, 1993). When diagenesis is extended to OM, potentially ambiguous usage of diagenesis is commonly derived from two wording points: 1) 'all the changes…' or 'the sum of all these…', and 2) 'after deposition' or 'post-depositional processes'.

For point one, if one knows *ANY* kind of (bio)chemical or physical processes affecting to the OM (i.e. the wood is decayed), one can tell that diagenesis took place in OM. In other words, alteration in *ANY* component of OM must mean diagenesis. By contrast, diagenesis doesn't necessarily mean alteration in *ALL* components.

For point two, if diagenesis occurs in OM (e.g. a piece of wood), in light of current definition of diagenesis, the starting point is 'after deposition', which disregards the alteration during transportation (The Encyclopedia of the Solid Earth Sciences, 1993; Oxford Dictionary of Earth Sciences, 2008). If this definition is critically followed, the chemical component and physical situation of OM should be known at the moment immediately following the end of

transportation but before deposition, and then to be compared with that at the moment of the end of deposition but before metamorphism.

However, practically, many authors take a broader meaning of diagenesis when studying $\delta^{13}C$ changes in OM. They make the original fresh OM as a starting point, because much (bio)chemical and physical alteration occurs during transportation. Actually, the (bio)chemical and physical alteration of OM primarily takes places during pre-deposition and shallow burial (< 1-4 m) (Hatcher et al., 1983; Spiker and Hatcher, 1984). Systematic changes in $\delta^{13}C$ values are not normally observed in thermally immature OM due to deeper burial (Sackett, 1964; 1989; Hunt 1970; Dean et al., 1986; Jasper and Gagosian, 1990).

Therefore, in the present account, definition of diagenesis is extended to include: all (bio)chemical and physical alteration occurring previous to finial immobilization during transports and deposits, and occurring during post-deposition but not affected by metamorphism.

3. Paradox of the empirical data

Diagenesis consists of both (bio)chemical and physical changes. The (bio)chemical changes led by bacterial degradation are believed to play important roles in shaping the C-isotope values of OM in the natural world. Thus many empirical field observations and laboratory culture studies are reported regarding the C-isotopic effect derived from bacterial degradation.

Controlled experiments show the absence of C-isotope fractionation for polycyclic aromatic hydrocarbons (PAHs) during aerobic bacterial degradation. Up to 90% PAH compound 2-methylphenanthrene ($C_{15}H_{12}$) has been degraded by bacteria at the end of culture experiments, and at the end the $\delta^{13}C$ values remain stable with a 0.2‰ fluctuation (Mazeas et al., 2002). However, when toluene (C_7H_8), a simple aromatic hydrocarbon, is used as a model

compound in aerobic microbial degradation experiments (Meckenstock, 1999), it shows a significant fractionation with varying α (fractionation factors). The maximum fractionation reaches 10‰ with an α at 1.0026±0.00017 when nearly all toluene materials run out after 25-day experiments. The minimum fractionation is 4‰ with an α at 1.0015±0.00015 at the end of biodegradation (i.e. the end of experiments) where only 80% toluene materials are degraded for 40 days (Meckenstock, 1999). The author ended the later experiment at an arbitrary point that it was adequate to measure the fractionation value and α. If the experiment had been run until nearly all toluene had been degraded, what would the fractionation values have been? One may have found that there seems to be a relationship between fractionation values and fraction of material remaining at the end of biodegradation (i.e. the end of experiments in this example). A full discussion will be made in Section 4 concerning this point.

Similarly, many aromatic compounds demonstrate that C-isotope fractionation is present in some compounds but absent in others during bacterial degradation (O'Malley et al., 1994; Stehmeier et al., 1999; Ahad et al., 2000; Wilkes et al., 2000; Hunkeler et al., 2001; Morasch et al., 2001; Mancini et al., 2003).

Other compounds with different types of chemical bonds and structure have been investigated. Laboratory experiments by culturing bacterial (Chung et al, 1988; Heraty et al., 1999; Boreham et al., 2001; Chan et al., 2012) and field observation (James and Burns, 1984; Pallasser et al., 2000) show large isotopic fractionations of low carbon-number (C1 - ~C5) compounds during biodegradation. Hydrocarbons with intermediate C numbers (~C6 - C9) also show consistent ^{13}C-enrichment in the remaining substrate after the different degrees of biological breakdown (Masterson et al., 2001; George et al., 2002). The C10–C18 n-alkanes show significant or insignificant (Boreham et al., 2001; Sun et al., 2005) carbon-isotope

fractionation. Additionally, laboratory experiments (Mazeas et al., 2002) have demonstrated unchanged carbon isotopic compositions of n-alkanes (≥C19), consistent with field observations under heavy biodegradation (Huang et al., 1997; Mansuy 1997; Sun et al., 2005).

These apparent patterns of C-isotope fractionation presence or absence are critically observed. The possible underlying mechanisms that control the presence or absence of C-isotope fractionation in individual compounds during physical and (bio)chemical processes (i.e. diagenesis) are discussed in the light of Rayleigh's fractionation equation and Bigeleisen's theory on isotope chemistry.

4. The Rayleigh fractionation equation

The C-isotope fractionation caused by biodegradation can be regressed and then predicted by the Rayleigh equation (Meckenstock et al., 1999; Hoefs, 2009), enabling calculation of a fractionation factor. This is because the processes of isotope fractionation*[1], as a result of isotopic effects, fit the physics model of the Rayleigh processes*[2], which can be modelled by the Rayleigh equation.

***[1]The 'isotope fractionation' in the present account is defined as narrow sense of isotope alteration resulted by the isotope effects in one-step physical or chemical reactions. This definition is different with the broad sense of isotope effects involving multi-step reactions, such as photosynthesis of plants (Farquhar et al., 1989; Galimov, 2006).**

***[2]The Rayleigh processes: initially tend to describe the separation of mixture gases by diffusion or similar processes. The ideal physics model is simplified as 'the simple diffusion of a gaseous mixture into a vacuum, with special regard to composition of the residue and corresponding mathematical equations are solved (Rayleigh, 1896). Later, the mathematical equations for the Rayleigh processes are widely applied to all processes whose physical models fit the Rayleigh processes; isotopic fractionation is one of the applications.**

For one substrate converting from its liquid form into its gaseous form (accompanied with isotopic fractionation), Rayleigh's equation is used to quantitatively describe the isotopic fractionation (Hoefs, 2009) is defined as: $\ln(\frac{R_t}{R_0}) = \left(\frac{1}{\alpha} - 1\right)\ln\left(\frac{C_t}{C_0}\right)$ (Equation 1),

where R_0 is the $^{13}C/^{12}C$ ratio of the substrate at initial time and R_t is the $^{13}C/^{12}C$ ratio at observation time t; α is fractionation factor (α is >1when R is defined as ratio of heavy to light isomer); C_0 and C_t are substrate concentrations at the initial time and the observation time t, respectively.

In light of Rayleigh's equation, once R_t, R_0, C_t, C_0 are measured, the fractionation factor α can be determined. In contrast, once α is known, R_t at any given time t is predictable and can be calculated as long as corresponding R_0, C_t, C_0 are measured. According to Equation 1, it is easy to find that R_t/R_0 takes the maximum when C_t/C_0 is reaching the minimum. In a geological context, this means that the maximum isotopic fractionation takes place at the end of biodegradation (Note that an ultimate moment only represents the end of biodegradation, but doesn't necessarily mean all materials are degraded). Thus, Equation 1 is rewritten into $\ln(\frac{R_{end}}{R_0}) = \left(\frac{1}{\alpha} - 1\right)\ln\left(\frac{C_{end}}{C_0}\right)$, where C_{end}/C_0 can be assumed taking a range of degradation percentage, e.g., 0.01, 0.1, 0.2, … 0.9 and 0.99…(Figure1), and $\ln(\frac{R_{end}}{R_0})$ is equal to$\Delta\delta/1000=(\delta_0 - \delta_{end})/1000$. (Due to the definition $\delta_x = \left(\frac{R_x}{R_{st}} - 1\right)x1000(‰)$, thus $\delta_0 = \left(\frac{R_0}{R_{st}} - 1\right)x1000(‰)$, and $\delta_{end} = \left(\frac{R_{end}}{R_{st}} - 1\right)x1000(‰)$; thus, the $\ln\frac{R_{end}}{R_0} = \ln\frac{\delta_{end}+1000}{\delta_0+1000} = \ln\frac{\delta_0+\Delta\delta+1000}{\delta_0+1000} = \ln\left(1+\frac{\Delta\delta}{\delta_0+1000}\right)$. When X<0.01, ln(1+X) ≈ X and δ_0 ranged from -20 to -30, thus, $\ln\frac{R_{end}}{R_0} \approx \frac{\Delta\delta}{\delta_0+1000} \approx \frac{\Delta\delta}{1000}$.)

Most mass spectrometers measuring $\delta^{13}C$ of OM have a ±0.2‰ uncertainty. Thus, if the largest C-isotope fractionation after diagenesis is less than 0.2‰, it would not be detectable.

In practice, $\ln(\frac{R_{end}}{R_0})$ is calculated by $\Delta\delta=\delta_0-\delta_{end}$ whose accuracy would be ±0.4‰. Therefore, the 0.4‰ can be employed to determine the threshold value of α.

Δδ at end / α / Remains	0.2‰	0.4‰	0.5‰
0.1%	1.000029	1.000058	1.000072
1%	1.000043	1.000087	1.000109
10%	1.000087	1.000174	1.000217
20%	1.000124	1.000249	1.000311
30%	1.000166	1.000332	1.000415
40%	1.000218	1.000437	1.000546
50%	1.000289	1.000577	1.000722
60%	1.000392	1.000784	1.00098
70%	1.000561	1.001123	1.001404
80%	1.000897	**1.001796**	1.002246
90%	1.001902	1.003811	1.004768
99%	1.020304	1.041449	1.052354
99.9%	1.249844	1.666111	1.999000

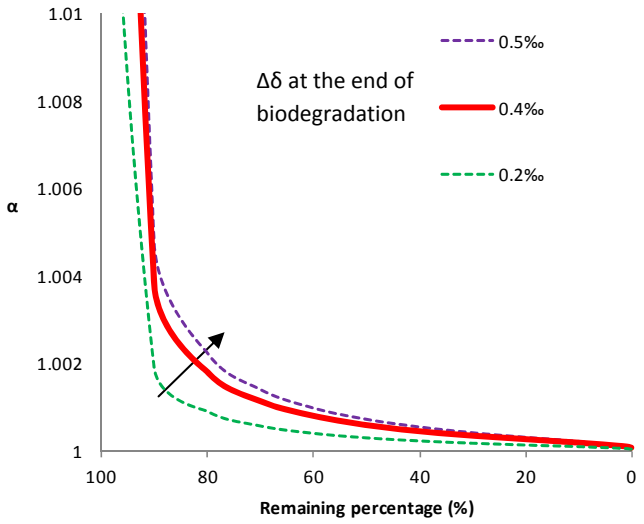

Figure 1 Fractionation factors (α) corresponding with percentages remaining in a given Δδ at the end of degradation. $\Delta\delta=\delta_0-\delta_{end}$ is taken by 0.4‰ which is the measurable extreme value due to the instrumental accuracy where δ ^{13}C is limited to ±0.2‰ (the condition of Δδ=0.2‰ and 0.5‰ are shown as trend references in right plotted graph and left calculated columns). The discrete accurate α values can read from the left calculated columns, once a certain percentage remaining at the end of degradation in a given Δδ value (e.g. 0.2‰, 0.4‰ or 0.5‰) is fixed.

When OM samples are collected after complex geological processes, it is difficult to know what percentage of the original fresh OM remains. However, as inferred in Equation 1, a larger α will lead to larger fractionation, and the largest fractionation occurs at the end of degradation. IfΔδby 0.4‰ assumed as the largest fractionation occurred at the end of degradation, the Δδ0.4‰ serves the boundary value in Equation 1 and all corresponding α at any given remaining percentage can be calculated (Figure 1).

5. The Bigeleisen theory on isotope chemistry

In light of the isotope chemistry theory summarised by Bigeleisen (Urey and Rittenberg, 1933; Bigeleisen and Mayer, 1947; Urey, 1947; Bigeleisen and Wolfsberg, 1958; Bigeleisen, 1965), the isotope fractionation effect (or isotope effect in short) of an individual compound in any chemical transformation is directly determined by the amplitude of the activation energy difference (ΔE_a) between two structurally identical molecules with different levels of isotopic substitutions. An accurate mathematical description can be given, under a set of assumptions by Bigeleisen, including two major factors regarded: a) according to thermal physics, isotopic principles from the gaseous state could be extended into the liquid and solid states, and b) the vibrational frequency of a molecule depends on inversely on the masses of the atoms in the molecule; and three minor factors disregarded: a) the forces in a molecule depend on the electron arrangements, b) the nuclear charges, and c) the positions of the atoms in the molecule. The basic relationship between the isotopic fractionation effects and the molecular weights of a specific compound can be mathematically described (Bigeleisen, 1965) as:

$$\log(\text{isotope effect}) \sim \frac{\Delta m}{mm'} \text{force constant, i.e. } \log \alpha \sim \frac{\Delta m}{mm'} F \quad \text{(Equation 2)}$$

where Δm is the mass difference between two isotopic isomers ($\Delta m = \mid m - m' \mid$), mm' is the mass of one isotopic isomer multiplied by that of the other and F is the force constant measured by the strength of chemical bond.

A rather advanced stage of theoretical development is reached by physics-experiment based equilibrium isotope effects of just the gaseous molecules, whose isotope effects can be theoretically calculated, directly according to the structure and chemical bonding in the molecule. However, an unequivocal solution to gaseous or liquid complex molecules can be

also provided by Equation 2 under equilibrium and dynamics isotope effects, and with or without an inorganic catalyst (Bigeleisen, 1965). This theoretical expression can even extend to kinetic isotope effects under enzymes in biochemical processes (Galimov 2006), as a 'kinetic' process is essentially equivalent to a 'dynamic' process (a reaction taking place driven on energy consuming) and enzymes are essentially organic catalysts (lowering the reaction activation energy, but with no change to enzymes at the end of a reaction).

The biochemical kinetic isotope effects under enzymes have long been thought to be very complicated (e.g. Farquhar et al., 1989), as previous studies were focused on biosynthesis processes rather than (bio)degradation. Biosynthesis is a multiple-step biochemical process. Any single step of biochemical reaction can be modelled by theory, but the overall isotope effect is 'a black box' mystery as parameters such as reaction orders or amplitude currently remain unknown (Summons et al., 1994; Crossman et al., 2001; Chikaraishi, 2003; Galimov 2006).

The essence of biodegradation is a biochemical process. Complex biochemical processes involve the biodegradation from initial substances into other substances, but once any chemical reaction happens to initial substances, the reacted initial substance will be immediately transformed into other substance. Thus, obviously, biodegradation is a one-step process, because the reacted initial substance does not exist anymore after only one-step process. This is the key logical foundation for employing the Rayleigh equation and the Bigeleisen equation to decode the C-isotope fractionation during (bio)degradation processes.

In order to examine isotopic effects between different compounds, each item in Equation 2 should be examined one by one. F varies from bond to bond, but the definite relationship between bond energy and F is unclear to date, making it difficult to precisely calculate F's

effect on α. However, F is constrained by the bond energy that is commonly limited in the range from 50 to 200 kcal/mol which suggests a restricted range of F.

Prior to discussion of item mm' and Δm (molecular-weight effect), it is important to examine a more elementary issue: the probability of different isotopic isomers occurring determines the occurrence probability of molecular weight for a given molecule. In order to estimate the occurrence probability of molecules with various levels of ^{13}C enrichment, we assume that the occurrence of ^{13}C and ^{12}C in a molecule is a simple random event, with the known natural abundance ratio of ^{12}C to ^{13}C as 98.9 to 1.1 [*Craig*, 1957]. For a given compound with n carbon atoms, the occurrence probability (P_i) for compounds containing i ^{13}C atoms is:

$$P_i = C_n^i \left(\frac{1.1}{100}\right)^i \left(\frac{98.9}{100}\right)^{(n-i)} \quad \text{(Equation 3)}$$

where C_n^i means an i-combination of a set with n elements and $C_n^i = \frac{n\cdot(n-1)\cdots(n-i+1)}{i\cdot(i-1)\cdots 1}$. P_i exponentially decreases as the number of ^{13}C atoms increases.

In Equation 2, it is known $F > 0$, based on Bigeleisen's experiments (Bigeleisen 1965). Let $\beta = \frac{\Delta m}{mm'}$, then $\log \alpha \sim \beta F$ (Equation 2.1), since $F > 0$, thus α depends monotonically on β.

For a given compound with *n* carbon atoms, if the ^{13}C composition is *i*, then ^{12}C would have a population of (n-i). If only hydrocarbons considered, two extreme scenarios would be -$(CH_2)_n$- for completely saturated alkanes and -$(C)_n$- for completely unsaturated compounds such as fully fused aromatics. In this case, the molecular weight ranges from 12n to 14n.

Since $\beta = \frac{\Delta m}{mm'}$ β_i varies from $\frac{i}{12n(12n+i)}$ to $\frac{i}{14n(14n+i)}$ (Equation 2.2)

As calculated by Equation 3, for a certain compound with *n* carbon atoms, the occurrence probability P_i for compounds with *i* ^{13}C atoms can be estimated. In order to calculate the

gross isotopic fractionation effect α , the sum β should be known by β_i with the corresponding occurrence probability P_i:

$$\beta = \sum_{i=0}^{n} P_i \beta_i \quad \text{(Equation 4)}$$

The graph for a range of values of *n* in Equation 4 is depicted (Figure 2), for the cases of fully saturated hydrocarbons (in red) and fully unsaturated counterpart (in blue).

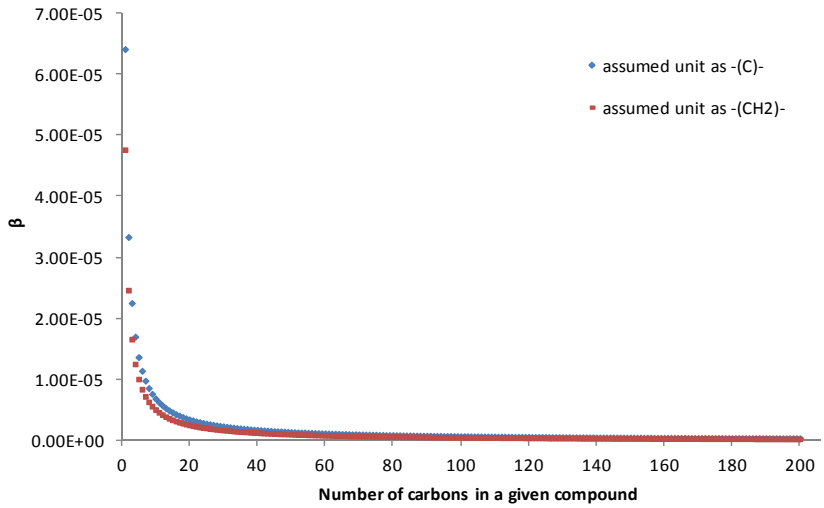

Figure 2 Relationship between β and number of carbon atoms in given compounds (Equation 4 and Equation 2.2), for two extreme cases of fully saturated hydrocarbons (in red) and fully unsaturated counterparts (in blue). Fractionation factor (α) exponentially decreases with increase in C number n in organic compounds, as α exponentially decreases corresponding with the decrease in β value (Equation 2.1) and the β value is power-exponential decreases with the increase in C number n (Equation 2.2).

Sum β exponentially decreases with the increase of the C number n as shown in the Figure 2, and due to $\log \alpha \sim \beta F$, α exponentially decreases with decreasing βF. This indicates that the isotopic fractionation factor α will have a doubly exponential drop when the C number rises (e.g. in long-chain hydrocarbons).

6. Integrated the Rayleigh equation and the Bigeleisen equation

The Rayleigh equation illustrates that α is related with $\ln\left(\frac{C_t}{C_0}\right)$ which represents the percentage remaining at the end of (bio)degradation (i.e. diagenesis) and $\ln(\frac{R_t}{R_0})$ which reflects the result of isotopic fractionation. The Bigeleisen equation illustrates that α is related with the C number of the specific organic compounds. Therefore, for an individual organic compound, the observed α actually is constrained by two factors together: 1) percentage remaining at the end of biodegradation, and 2) the C number of that specific organic compound.

The relationship can be expressed by an integrated mathematic function. For Equation 4, α is the function of C number n and hence Equation 4 can be simply expressed by α = f (n). Then place Equation 4 into Equation 1, it turns out $\ln(\frac{R_t}{R_0}) = \left(\frac{1}{f(n)} - 1\right)\ln\left(\frac{C_t}{C_0}\right)$ (Equation 5).

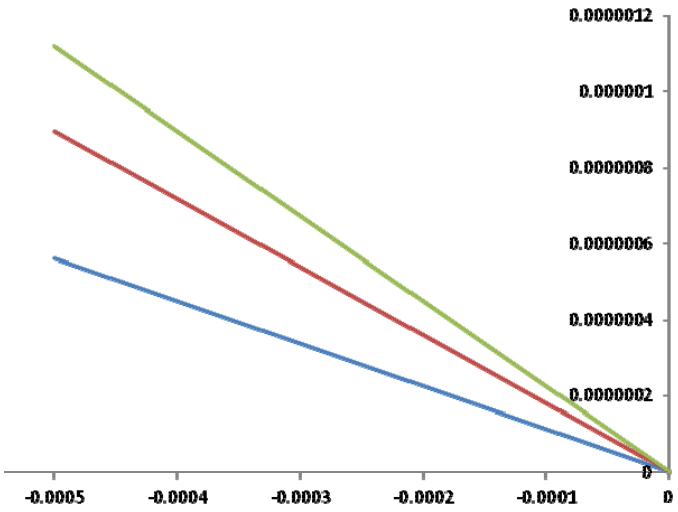

Figure 3 With examples of α1=1.001123, α2=1.001796 and α3=1.002246, i.e. α1< α2< α3, it is shown that with the decrease of α (i.e. increase in C number n (Equation 4 and Equation 2.1)), to reach a given $ln\frac{R_t}{R_0}$, (such as 0.04‰/1000, the horizontal dashed line), the $ln\frac{C_t}{C_0}$ decreases (i.e. C_t/C_0 deceases). Dashed arrow points the α in decreasing trends.

For a given $\ln(\frac{R_t}{R_0})$, when C number n increases, C_t decreases (Figure 3). In geological contexts, the functional relationship means that if the C number in the compounds become larger and larger, the corresponding remaining concentration has to be less and less in order to reach a given level of degradation for a certain organic compound (e.g. the measurable threshold $\Delta\delta$ at ~0.4‰). This understanding provides a good explanation as to why when molecular weight increases (i.e. increasing C number), the individual compounds have to be decomposed (i.e. degraded) by a greater fraction compared with those with lower molecular weight, to reach some same level of C-isotope fractionation.

7. Discussions

7.1. The threshold of undetectable C-isotopic fractionation

As previously shown, once the C number (i.e. molecular weight) of organic compounds is beyond a certain threshold, the fractionation factor will become too small to yield any detectable C-isotope fractionation, even if materials underwent the largest (bio)degradation. So what is the exact threshold? Unfortunately, there is not a general threshold for all organic compounds, because the threshold depends not only molecular weight but also constant force F (Equation 2). F reflects the strength of chemical bonding, varying from bond to bond, subject to specific types of chemical bonding and reaction conditions. In an alternative perspective, F is a kind of experimental parameter, which can be determined by experiments once experimental condition is given. Here a concern arises that a variable F will lead to variable α. Fortunately, F range is constrained by the bond energy that is commonly restricted in the range from 50 to 200 kcal/mol. Therefore, under a certain limited range of F, α ultimately must turn negligible with the constantly increasing molecular weight until beyond a certain threshold.

Some experienced values of threshold can be demonstrated by empirical data from literature. Aromatic-structure compounds are characterised by either C-C σ-bonds or C=C Π bonds. In culture experiments, PAH compound 2-methylphenanthrene ($C_{15}H_{12}$) molecular weight is 192.09 u (u is the symbol of atomic *mass* unit), as assuming that only ^{12}C isotope and ^{1}H exist in both compounds. The $\delta^{13}C$ values remains stable within 0.2‰fluctuation at the end of degradation by bacteria (Mazeas et al., 2002). This empirical example suggests threshold of molecular weight should be below about 190 u for aromatic-structure compounds under these given experimental conditions. Another set of compounds with C-C bonds demonstrate that up to C18 n-alkanes show significant or insignificant (Boreham et al., 2001; Sun et al., 2005) carbon-isotope fractionation. Few C-isotope changes of n-alkanes beyond C19 are consistently recorded with field observations under heavy biodegradation (Huang et al., 1997; Mansuy 1997; Sun et al., 2005). Hence, the threshold of molecular weight should be about 220 u for n-alkanes compounds.

Moreover, a further implication can be reached. Natural organic polymers, such as lignin or cellulose, have large molecular weights (>~5000-10000 u) and they are in solid state. Chemical processes in the solid phase take place much more slowly than liquid or gaseous phases. Together with their large molecular weight, these natural polymers should show negligible C-isotope fractionation. Thus, organic polymers could faithfully document their original stable C-isotope profiles.

7.2. Limited influence by various bacterial types

For a given compound under a given experimental condition, the different bacterial species often result in a different fractionation factor (Meckenstock et al., 1999; Morasch et al., 2002), as the bacterial effect is associated with the efficiency of enzymes and amount of enzymes (bridging the different energy offsets). However, the enzyme only affects F in Equation 2. As

discussed in the section 7.1, the F range has to be limited due to limited strength of chemical bonding and is a certain value under a given condition, whereas constantly increasing the value of molecular weight ultimately leads to a small enough α with negligible C-isotope fractionation. Therefore, although bacterial species can vary, species difference does not overturn our theoretical conclusion. Moreover, the theoretical inference may be expanded to all kinds of organic degradation processes, such as reaction with the organic acid in deposits (not only bacterial degradation), because the inference only relies on basic chemical and physical principles, rather than any requirements to a specific biological process.

7.3. Current and potential applications based on theoretical inference

In light of the proposed theory, polymers or high molecular-weight compounds can safely maintain their original C-isotope records after (bio)degradation (i.e. diagenesis). This C-isotope integrity can be very useful to geological and environmental applications.

7.3.1. Tie points for correlation between marine and terrestrial sedimentary strata

Lignin as a natural polymer can faithfully preserve original $\delta^{13}C$ records after diagenesis. Lignin polymer is uniquely derived from land vascular plants (e.g. Pancost et al., 2006). The $\delta^{13}C$ of lignin can be investigated based on the primary 11 lignin monomers decomposed by CuO oxidation (Hedges and Ertel 1982; Willianms et al., 1998; Carmona et al., 2008). This CuO oxidation technique can extract the $\delta^{13}C$ of lignin from marine siliciclastic deposits where the strata document marine facies and marine fossils. Owing to advantages above, $\delta^{13}C$ values of each lignin monomer extracted from marine deposits can be a tie point for correlation between marine and terrestrial sedimentary strata. The correlation potentially figures out the gap of fossil prototypes between marine and terrestrial strata.

7.3.2. To reconstruct the evolution of atmospheric carbon reservoir

The $\delta^{13}C$ values from wood, fossil wood (Arens et al, 2000; Gröcke 2000; Jahren et al., 2008) and degraded woody materials (Poole et al., 2004) (nearly all woody plants are C3 plants) can be used to reconstruct C-isotopic composition of atmospheric carbon dioxide and then to calibrate paleo-pCO_2 evolution. Analyses of these materials provide a relatively direct approach to reconstruct the evolution of atmospheric carbon reservoir. Moreover, the cellulose or lignin separated from whole wood can individually witness consistent $\delta^{13}C$ values as the whole wood can (Loader et al., 2003), but their $\delta^{13}C$ values compared with that of whole wood keep an nearly constant offset. The three sets of $\delta^{13}C$ values derived from one set of woody samples can make a self-verification, which improves the data quality. Therefore, the C-isotope integrity of cellulose and lignin derived from C3 Plant is a particularly useful proxy in reconstructing the palaeoenvironment and palaeoclimate.

7.3.3. To explore temperature stratification and CO_2 concentration in palaeo-oceans

Sterane and hopane compounds are of high molecular weight and thus in C-isotope integrity, which is another empirical evidence to support the proposed solution in this paper. Sterane compounds primarily originate from plankton and zooplankton in marine or lake environments, but hopane compounds are from bacteriohopane polyls and prokaryotes (Schoell et al., 1994). Combining C-isotope values recorded in these two organic compounds can be used to infer changes of temperature-stratified palaeo-oceans and concentration of carbon dioxide in water mass at the base of the photic zone (Schoell et al., 1994).

7.3.4. To decode coupled evolution of C-isotope between organic and inorganic reservoirs

The coupled evolution of C-isotope between organic and inorganic reservoirs is an important science issue. The knowledge profoundly determines how to interpret the global carbon cycles and $\delta^{13}C$ excursion based on empirical data or modelling (Hays et al., 1999; Kump and Arthur, 1999). For example, the understanding has long stayed puzzled by the organic $\delta^{13}C$ records from mixed resources (Hays et al., 1999), as the complicated variations of organic $\delta^{13}C$ records can be led by change of organic resource and/or selective preservation. Each component in the mixed OM registers different $\delta^{13}C$ signatures. Promisingly, if organic compounds with $\delta^{13}C$ integrity are derived from the known and exclusive resources (e.g. Syringyl phenols monomer of lignin primarily originate from angiosperm lignin), the known provenance is helpful to define the origin of $\delta^{13}C$ changes.

7.3.5. A theoretical perspective of no diagenetic isotopic changes

If $\delta^{13}C$ is generated from the OM which is dominant in components of polymers or high-molecular weight compounds, $\delta^{13}C$ in OM tends to be resistant and to maintain the original $\delta^{13}C$ based on our proposed theoretical explanation. This understanding gives an alternative theoretical insight into the reason why many previous studies on C3 Plant wood-derived materials (Hasegawa, 1997; Arens et al., 2000; Hesselbo et al., 2000, 2007, 2011; Jahren et al., 2008), such as jet, consistently show the reliable $\delta^{13}C$ records. In addition, some critical tests on assumed possible alterations (e.g. test of oil-extraction experiment, Hesselbo et al., 2000) affected by diagenesis had been made and then the results of no influence on C-isotope can be better understood.

7.3.6. Modern environmental monitors

In modern environmental monitors, low-molecular weight molecules are adequate to precisely measure the extent of degradation of the chemically contaminated areas (Meckenstock et al., 1999; Wilkes et al., 2000; Hunkeler et al., 2001; Gray et al., 2002; Morasch et al., 2002; Mancini et al., 2003), as distinguished C-isotope fractionations occur and are thus easy to measure. In contrast, high molecular-weight molecules are capable of revealing the origin and migration trace of contaminants (O'Malley et al., 1994, 1996; Dempster et al., 1997; Mazeas et al., 2002) in that they can preserve the originally characterized C-isotope signatures.

7.3.7. Integrity of other elements' isotopes (i.e. H, O, S, N)

Based on theoretical solution proposed in this paper, other elements' isotopes in high molecular-weight compounds could maintain their originally isotopic signatures after diagenesis as well. Hydrocarbon (even most OM) molecules are constructed by C skeletons. The element H is always necessary part of hydrocarbon molecules. O, S and N are just secondary elements, which are located in internal lattices or minor branches of molecules. Once C skeletons are broken, the molecules would have disappeared. Therefore, for OM built by C skeleton, isotopic effects with molecular-weight dependence must take place to C, likely to H but hardly to O, S and N in most cases.

For instance, hydrogen isotope values derived from sedimentary OM has been particularly useful for the environmental monitoring and the study of hydrological cycles (Hunkeler et al., 2001; Gray et al., 2002; Morasch et al., 2002; Mancini et al., 2003). The application is not only apt for recent days (Englebrecht and Sachs, 2005; Schouten et al., 2006; Ellsworth and Williams, 2007; Van der Meer et al., 2007; Schwab and Sachs, 2011) but also for the remote Earth's history (Jones et al., 2008; Li et al., 2009, 2011).

8. Conclusions

Isotopic fractionation constantly occurs according to Bigeleisen's theory, as zero-point energy difference between different isotopic isomers persistently exists. However, combining Rayleigh's and Bigeleisen's models, a theoretical explanation is apparent for a pattern well illustrated from observation and experiment. The proposed theoretical solution illustrates when molecular weight of organic compounds is beyond a certain threshold (subject to specific types of chemical bonds and reaction conditions), the C-isotope fractionation factor will turn too small to cause any detectable C-isotope fractionation, even if nearly all materials degraded.

The implication are that $\delta^{13}C$ value in high molecular-weight organic compounds (e.g. PAHs and *n*-alkanes) and single species of natural polymer molecules (e.g. lignin and cellulose) will not be affected, regardless of what the degree of degradation led by bacteria or other chemical or physical process during diagenesis. In other words, these kinds of compounds can safely maintain original C-isotope records undergoing complex geological processes over tens of millions of years.

It must be admitted that the theoretical solution is not perfect since some experimental parameters are incomplete in Bigeleisen's equation, but all steps of the theoretical solution can be verified by experiments.

Acknowledgements

First of all, I would like to thank Dr. Boshen Wu. Dr. Wu has made a lot of contribution to discuss on Bigeleisen's theory and contributed part of manuscript on the relevant discussion. I also sincerely thank Dr. Jeremy Roberson and Professor Stephen Hesselbo for constructive suggestion on revising this manuscript in the previous version, Mr. Thomas O'Toole for helping with correcting grammar errors, very beneficial discussion with Dr. Chris Brodie for an explicit academic expression and Ms. Xuan Du for mathematic solutions.

References

Ahad, J. M. E., B. S. Lollar, E. Edwards, G. F. Slater, and B. E. Sleep (2000), Carbon isotope fractionation during anaerobic biodegradation of toluene: implications for intrinsic bioremediation, *Environmental science & technology*, *34*(5), 892–896.

Arens, N. C., A. H. Jahren, and R. Amundson (2000), Can C3 plants faithfully record the carbon isotopic composition of atmospheric carbon dioxide?, *Paleobiology, 26*(1), 137–164.

Benner, R., M. L. Fogel, E. K. Sprague, and R. E. Hodson (1987), Depletion of ^{13}C in lignin and its implications for stable carbon isotope studies, *Nature*, *329*(6141), 708–710.

Bigeleisen, J. (1965), Chemistry of isotopes, *Science*, *147*(3657), 463–471.

Boreham, C.J., L.M. Dowling, and A.P. Murray, (1995), Biodegradation and maturity influences on n-alkane isotopic profiles in terrigenous sequences. *In: Abstracts of 17th International Meeting on Organic eochemistry, San Sebastian, Spain,* 539–541. (abstract)

Boreham, C. J., J. E. Blevin, A. P. Radlinski, and K. R. Trigg (2003), Coal as a source of oil and gas: a case study from the Bass Basin, *Australia APPEA Journal*, *43*(1), 117–148.

Bugna, G. C., J. P. Chanton, C. A. Kelley, T. B. Stauffer, W. G. MacIntyre, and E. L. Libelo, 2004. A field test of $\delta^{13}C$ as a tracer of aerobic hydrocarbon degradation, *Organic geochemistry*, *35*(2), 123–135.

Chan, C. C. H., S. O. C. Mundle, T. Eckert, X. Liang, S. Tang, G. Lacrampe-Couloume, E. A. Edwards, and B. Sherwood Lollar (2012), Large Carbon Isotope Fractionation during Biodegradation of Chloroform by Dehalobacter Cultures, *Environmental science & technology*, *46* (18), 10154–10160.

Chikaraishi, Y. (2003), Carbon and hydrogen isotopic fractionation during lipid biosynthesis of higher plants. In: 13th Goldschmidt Conference, Kurashiki, Japan. *Geochimica et Cosmochimica Acta Special Supplement*, p. G7, 18, AG4 (Abstract).

Chung, H. M., J. R. Gormly, and R. M. Squires (1988), Origin of gaseous hydrocarbons in subsurface environments: Theoretical considerations of carbon isotope distribution, *Chemical geology*, *71*(1–3), 97–104.

Craig, H. (1957), Isotopic standards for carbon and oxygen and correction factors for mass-spectrometric analysis of carbon dioxide, *Geochimica et Cosmochimica Acta*, *12*(1–2), 133–149.

Crossman, Z. M., N. McNamara, N. Parekh, P. Ineson, and R. P. Evershed (2001), A new method for identifying the origins of simple and complex hopanoids in sedimentary materials using stable isotope labelling with $^{13}CH_4$ and compound specific stable isotope analyses, *Organic geochemistry*, *32*(2), 359–364.

Dean, W. E., M. A. Arthur, and G. E. Claypool (1986), Depletion of ^{13}C in Cretaceous marine organic matter: Source, diagenetic, or environmental signal? *Marine Geology*, *70*(1–2), 119–157.

Ellsworth, P. Z., and D. G. Williams (2007), Hydrogen isotope fractionation during water uptake by woody xerophytes, *Plant and Soil, 291*(1–2), 93–107.

Englebrecht, A. C. (2005), Determination of sediment provenance at drift sites using hydrogen isotopes and unsaturation ratios in alkenones, *Geochimica et Cosmochimica Acta*, *69*(17), 4253.

Farquhar G.D., J.R. Ehleringer, K.T. Hubick (1989), Carbon isotope discrimination and photosynthesis. *Annual Review of Plant Physiology and Plant Molecular Biology*, *40*(1), 503–537.

Galimov, E. M. (2006), Isotope organic geochemistry, *Organic geochemistry*, *37*(10), 1200–1262.

Gray J. R., G. L. Couloume, D. Gandhi, K. M. Scow, R. D. Wilson, D. M. Mackay, and B. S. Lollar (2002), Carbon and hydrogen isotopic fractionation during biodegradation of methyl tert-butyl ether. *Environmental science & technology*, *36*(9): 1931–1938.

George, S. C., C. J. Boreham, S. A. Minifie, and S. C. Teerman (2002), The effect of minor to moderate biodegradation on C5 to C9 hydrocarbons in crude oils, *Organic geochemistry*, *33*(12), 1293–1317.

Gröcke, D.R. (2002), The carbon isotope composition of ancient CO_2 based on higher plant organic matter. In Gröcke, D.R., and Kucera, M. (Eds) *Understanding climate change: proxies, chronology, and ocean-atmosphere interactions. London: Royal Society, v. 360*, p. 633–658.

Hasegawa, T. (1997), Cenomanian-Turonian carbon isotope events recorded in terrestrial organic matter from northern Japan, *Palaeogeography, Palaeoclimatology, Palaeoecology*, *130*(1–4), 251–273.

Hatcher, P. G., E. C. Spiker, N. M. Szeverenyi, and G. E. Maciel, 1983. Selective preservation and origin of petroleum-forming aquatic kerogen, *Nature*, *305*(5934), 498–501.

Hayes, J. M., H. Strauss, and A. J. Kaufman (1999), The abundance of ^{13}C in marine organic matter and isotopic fractionation in the global biogeochemical cycle of carbon during the past 800 Ma, *Chemical geology, 161*(1–3), 103–125.

Hedges, J. I. (1999), Sedimentary organic matter preservation; a test for selective degradation under oxic conditions, *Am. J. Sci.*, *299*(7–9), 529–555.

Heraty, L. J., M. E. Fuller, L. Huang, T. Abrajano Jr, and N. C. Sturchio (1999), Isotopic fractionation of carbon and chlorine by microbial degradation of dichloromethane, *Organic geochemistry*, *30*(8, Part 1), 793–799.

Hesselbo, S. P., D. R. Gröcke, H. C. Jenkyns, C. J. Bjerrum, P. Farrimond, H. S. Morgans Bell, and O. R. Green (2000), Massive dissociation of gas hydrate during a Jurassic oceanic anoxic event, *Nature*, *406*(6794), 392–395.

Hesselbo, S. P., H. C. Jenkyns, L. V. Duarte, and L. C. V. Oliveira (2007), Carbon-isotope record of the Early Jurassic (Toarcian) Oceanic Anoxic Event from fossil wood and marine carbonate (Lusitanian Basin, Portugal), *Earth and Planetary Science Letters*, *253*(3–4), 455–470.

Hesselbo, S. P., and G. Pieńkowski (2011), Stepwise atmospheric carbon-isotope excursion during the Toarcian Oceanic Anoxic Event (Early Jurassic, Polish Basin), *Earth and Planetary Science Letters*, *301*(1–2), 365–372.

Hoefs, J. (2009), 'Stable isotope geochemistry', *Springer-Verlag Berlin Heidelberg*.

Huang, Y., G. Eglinton, P. Ineson, P. M. Latter, R. Bol, and D. D. Harkness (1997), Absence of carbon isotope fractionation of individual n-alkanes in a 23-year field decomposition experiment with Calluna vulgaris, *Organic geochemistry*, *26*(7–8), 497–501.

Hunkeler, D., N. Andersen, R. Aravena, S. M. Bernasconi, and B. J. Butler (2001), Hydrogen and Carbon Isotope Fractionation during Aerobic Biodegradation of Benzene, *Environmental science & technology*, *35*(17), 3462–3467.

Hunt, J. M. (1970), The significance of carbon isotope variations in marine sediments, i*n Advances in Organic Geochemistry 1966 (eds G.D. Hobson and G. C. Spears), Pergamon, Oxford*, p. 27–35.

Jahren A. H., N. C. Arens, and S. A. Harbeson (2008), Prediction of atmospheric δ^{13}CO2 using fossil plant tissues: *Reviews of Geophysics, v. 46*, RG1002, doi: 10.1029/2006RG000219

James, A. T., and B. J. Burns (1984), Microbial alteration of subsurface natural gas accumulations, *AAPG Bulletin*, *68*(8), 957–960.

Jasper, J. P., and R. B. Gagosian (1990), The sources and deposition of organic matter in the Late Quaternary Pigmy Basin, Gulf of Mexico, *Geochimica et Cosmochimica Acta*, *54*(4), 1117–1132.

Jones, A. A., A. L. Sessions, B. J. Campbell, C. Li, and D. L. Valentine (2008), D/H ratios of fatty acids from marine particulate organic matter in the California Borderland Basins, *Organic geochemistry*, *39*(5), 485–500.

Kirk, T. K., and R. L. Farrell (1987), Enzymatic' combustion': the microbial degradation of lignin, *Annual review of microbiology*, *41*(1), 465–505.

Kump, L. R., and M. A. Arthur (1999), Interpreting carbon-isotope excursions: carbonates and organic matter, *Chemical geology*, *161*(1–3), 181–198.

Li, C., A. L. Sessions, F. S. Kinnaman, and D. L. Valentine (2009), Hydrogen-isotopic variability in lipids from Santa Barbara Basin sediments, *Geochimica et Cosmochimica Acta, 73(*16), 4803–4823.

Li, C., A. L. Sessions, D. L. Valentine, and N. Thiagarajan (2011), D/H variation in terrestrial lipids from Santa Barbara Basin over the past 1400 years: A preliminary assessment of paleoclimatic relevance, *Organic geochemistry*, *42*(1), 15–24.

Mancini, S. A. (2003), Carbon and hydrogen isotopic fractionation during anaerobic biodegradation of benzene, *Applied and environmental microbiology*, *69*(1), 191–198.

Mansuy, L. (1997), Source identification of oil spills based on the isotopic composition of individual components in weathered oil samples, *Environmental science & technology*, *31*(12), 3417–3425.

Masterson, W. D., L. I. P. Dzou, A. G. Holba, A. L. Fincannon, and L. Ellis (2001), Evidence for biodegradation and evaporative fractionation in West Sak, Kuparuk and Prudhoe Bay field areas, North Slope, Alaska, *Organic geochemistry*, *32*(3), 411–441.

Mazeas, L., H. Budzinski, and N. Raymond (2002), Absence of stable carbon isotope fractionation of saturated and polycyclic aromatic hydrocarbons during aerobic bacterial biodegradation, *Organic geochemistry*, *33*(11), 1259–1272.

Meckenstock, R. U. (1999), $^{13}C/^{12}C$ isotope fractionation of aromatic hydrocarbons during microbial degradation, *Environmental microbiology*, *1*(5), 409–414.

Morasch, B., H. H. Richnow, B. Schink, and R. U. Meckenstock (2001), Stable Hydrogen and Carbon Isotope Fractionation during Microbial Toluene Degradation: Mechanistic and Environmental Aspects, *Applied and environmental microbiology*, *67*(10), 4842–4849.

O'Malley, V. P., T. A. Abrajano Jr, and J. Hellou (1994), Determination of the $^{13}C/^{12}C$ ratios of individual PAH from environmental samples: can PAH sources be apportioned? *Organic geochemistry*, *21*(6–7), 809–822.

O'Malley, V. P. (1996), Stable carbon isotopic apportionment of individual polycyclic aromatic hydrocarbons in St. John's Harbour, Newfoundland, *Environmental science & technology*, *30*(2), 634.

Pallasser, R. J. (2000), Recognising biodegradation in gas/oil accumulations through the $\delta^{13}C$ compositions of gas components, *Organic geochemistry*, *31*(12), 1363–1373.

Pancost, R. D., and C. S. Boot (2004), The palaeoclimatic utility of terrestrial biomarkers in marine sediments, *Marine Chemistry*, *92*(1–4), 239–261.

Peters-Kottig, W., H. Strauss, and H. Kerp (2006), The land plant $\delta^{13}C$ record and plant evolution in the Late Palaeozoic, *Palaeogeography, Palaeoclimatology, Palaeoecology*, *240*(1–2), 23–-252.

Rayleigh, L. (1896), L. Theoretical considerations respecting the separation of gases by diffusion and similar processes, *Philosophical Magazine Series 5*, *42*(259), 493–498.

Sackett, W. M. (1964), The depositional history and isotopic organic carbon composition of marine sediments, *Marine Geology,* 2(3), 173.

Sackett, W.M. (1989), Stable carbon isotope studies on organic matter in the marine environment. In Fritz, P., and Fontes, J.C. (Eds.), *Handbook of Environmental Isotope Geochemistry (Vol. 3): The Marine Environment, A: Amsterdam (Elsevier),* 139–169.

Schoell, M., S. Schouten, J. S. S. Damsté, J. W. d. Leeuw, and R. E. Summons (1994), A Molecular Organic Carbon Isotope Record of Miocene Climate Changes, *Science, 263*(5150), 1122–1125.

Schouten, S. (2006), The effect of temperature, salinity and growth rate on the stable hydrogen isotopic composition of long chain alkenones produced by Emiliania huxleyi and Gephyrocapsa oceanica, *Biogeosciences*, *3*(1), 113.

Schwab, V. F., and J. P. Sachs (2011), Hydrogen isotopes in individual alkenones from the Chesapeake Bay estuary, *Geochimica et Cosmochimica Acta, 75*(23), 7552–7565.

Sluijs, A., and G. R. Dickens (2012), Assessing offsets between the $\delta^{13}C$ of sedimentary components and the global exogenic carbon pool across early Paleogene carbon cycle perturbations, *Global biogeochemical cycles*, *26*(4), DOI: 10.1029/2011GB004224

Spiker, E. C. (1984), Carbon isotope fractionation of sapropelic organic matter during early diagenesis, *Organic geochemistry*, *5*(4), 283–290.

Stehmeier, L. G., M. M. Francis, T. R. Jack, E. Diegor, L. Winsor, and T. A. Abrajano Jr. (1999), Field and in vitro evidence for in-situ bioremediation using compound-specific $^{13}C/^{12}C$ ratio monitoring, *Organic geochemistry*, *30* (8, Part 1), 821–833.

Summons, R. E., L. L. Jahnke, and Z. Roksandic (1994), Carbon isotopic fractionation in lipids from methanotrophic bacteria: Relevance for interpretation of the geochemical record of biomarkers, *Geochimica et Cosmochimica Acta*, *58*(13), 2853–2863.

Sun, Y., Z. Chen, S. Xu, and P. Cai (2005), Stable carbon and hydrogen isotopic fractionation of individual n-alkanes accompanying biodegradation: evidence from a group of progressively biodegraded oils, *Organic geochemistry*, *36*(2), 225–238.

van der Meer, M. T. J., M. Baas, W. I. C. Rijpstra, G. Marino, E. J. Rohling, J. S. Sinninghe Damsté, and S. Schouten (2007), Hydrogen isotopic compositions of long-chain alkenones record freshwater flooding of the Eastern Mediterranean at the onset of sapropel deposition, *Earth and Planetary Science Letters*, 262(3–4), 594–600.

Wilkes, H., C. Boreham, G. Harms, K. Zengler, and R. Rabus (2000), Anaerobic degradation and carbon isotopic fractionation of alkylbenzenes in crude oil by sulphate-reducing bacteria, *Organic geochemistry*, *31*(1), 101–115.